Microbial degradation of organic micropollutants in hyporheic zone sediments

Dissertation

To obtain the Academic Degree

Doctor rerum naturalium

(Dr. rer. nat.)

Submitted to the Faculty of Biology, Chemistry, and Geosciences

of the University of Bayreuth

by

Cyrus Rutere

Bayreuth, May 2020

This doctoral thesis was prepared at the Department of Ecological Microbiology – University of Bayreuth and AG Horn – Institute of Microbiology, Leibniz University Hannover, from August 2015 until April 2020, and was supervised by Prof. Dr. Marcus. A. Horn.

This is a full reprint of the dissertation submitted to obtain the academic degree of Doctor of Natural Sciences (Dr. rer. nat.) and approved by the Faculty of Biology, Chemistry, and Geosciences of the University of Bayreuth.

Date of submission: 11. May 2020

Date of defense: 23. July 2020

Acting dean: Prof. Dr. Matthias Breuning

Doctoral committee:

Prof. Dr. Marcus. A. Horn (reviewer)

Prof. Harold L. Drake, PhD (reviewer)

Prof. Dr. Gerhard Rambold (chairman)

Prof. Dr. Stefan Peiffer

In the battle between the stream and the rock, the stream always wins, not through strength but by perseverance.

Harriett Jackson Brown Jr.

CONTENTS

FIGURES

TABLES

APPENDIX TABLES

EQUATIONS

ABBREVIATIONS

ANOVA	Analysis of variance
ANOSIM	Analysis of similarities
BOD	Biochemical oxygen demand
BBD-PPS	Biocatalysis/Biodegradation database pathway prediction system
BSA	Bovine serum albumin
CEC	Cation exchange capacity
CO_2	Carbon dioxide
COD	Chemical oxygen demand
CTAB	hexadecyltrimethylammonium bromide
DAD	Diode array detector
DOC	Dissolved organic carbon
DT50	Dissipation half-life
EAWAG	Swiss Federal Institute of Aquatic Science and Technology
ESI	Electrospray ionization
$g_{ss}d^{-1}$	Suspended solids (daily discharge in grams)
H_2	Hydrogen
HEF	Hyporheic exchange flow
HPLC	High-performance Liquid Chromatography
IS	Internal standard
K_{biol}	Biodegradation kinetic constant
Kow	Octanol-water partition coefficient
Lat	Latitude

LB	Lysogeny broth
LC-HRMS/MS	Liquid Chromatography high-resolution tandem mass spectrometry
LDA	Linear discriminant analysis
LEfSe	Linear discriminant analysis (LDA) effect size
LOD	Limit of detection
Long	Longitude
LOQ	Limit of quantification
MS	Mass spectrometry
MS/MS	Tandem mass spectrometry
NDIR	nondispersive infrared (sensor)
nm	Nanometer
NSAID	Non-steroidal anti-inflammatory drug
OTU	operational taxonomic unit
PCR	Polymerase chain reaction
PEG	polyethylene glycol
PPCPs	Pharmaceuticals and personal care products
PW	Porewater
qPCR	Quantitative polymerase chain reaction
RPM	Rotations per minute
SD	Standard deviation
SU	Stockholm University
SW	Surface water
TFA	Trifluoroacetic acid
TOC	Total organic carbon

TrOC	Trace organic compound
TP	Transformation product
UHPLC-MS/MS	Ultra-performance liquid chromatography - tandem mass spectrometry
UV	ultraviolet (radiation)
UV-VIS	Ultraviolet–visible
X-Gal	5-bromo-4-chloro-3-indolyl-D-galactopyranoside

1. SUMMARY

The hyporheic zone is the water-saturated streambed sediment layer characterized by the simultaneous occurrence of multiple physical, biological, and chemical processes. The hyporheic zone contributes to the self-purification capacity of streams by removing point and nonpoint source pollutants mainly via microbial activity. However, such potentials, associated microbial communities, and impacts on microbial community structure are largely unknown for specific widely distributed compounds of environmental concern.

Thus, pollutant removal potentials in hyporheic zone sediments were investigated using the non-steroidal anti-inflammatory drug ibuprofen. Ibuprofen biodegradation in oxic sediment microcosms amended with ibuprofen, or ibuprofen and acetate was determined. Unsupplemented and heat-sterilized sediments served as controls. Ibuprofen biotransformation occurred via 1-, 2-, 3-hydroxy and carboxy-ibuprofen as transient primary transformation products. Quantitative PCR analysis revealed a significantly higher 16S rRNA abundance in ibuprofen-amended relative to un-amended incubations. Time-resolved amplicon Illumina MiSeq sequencing targeting 16S rRNA genes and 16S rRNA revealed a clear effect of ibuprofen on the microbial community structure and many new ibuprofen responsive taxa affiliating with Acidobacteria, Actinobacteria, Bacteroidetes, Gemmatimonadetes, Latescibacteria and Proteobacteria. This was confirmed by specific 16S rRNA gene expression analysis of representative taxa. Two strains utilizing ibuprofen as sole carbon and energy source of the genera *Novosphingobium* and *Pseudomonas* were isolated and will serve as model organisms for elucidating ibuprofen degradation pathways.

Redox gradients along the streambed depth profile impact pollutant removal. Microbial removal of the beta-blocker metoprolol, in the redox-delineated hyporheic zones was investigated using oxic and anoxic sediment microcosms. Biotransformation of metoprolol occurred under both incubation conditions. In the oxic microcosms, metoprolol was transformed mainly to metoprolol acid, while under anoxic conditions, metoprolol acid and hydroxy metoprolol were formed, indicating dissimilar metabolic pathways for metoprolol degradation under the contrasting incubation conditions. The transformation products were subsequently completely degraded under both conditions. The responsive taxa associated with metoprolol degradation were affiliated with the Proteobacteria and Bacteroidetes under oxic conditions, and Proteobacteria, Acidobacteria, Chloroflexi, Firmicutes and Gemmatimonadetes under anoxic conditions.

The organic matter content influences multiple biogeochemical reactions. The effect of organic carbon on the fate of 13 trace organic compounds (TrOCs) was investigated using sediments differing in the total organic carbon content (TOC). Oxic sediment microcosms with low and high TOC content differed in the biotransformation and sorption removal efficiencies of the TrOCs. Significantly higher biotic removal efficiencies of compounds such as ibuprofen, ketoprofen and acesulfame were observed in high relative to low TOC sediments. The removal efficiency via biotransformation was generally higher than by sorption for all compounds tested except for propranolol for which complete removal occurred via both mechanisms. Acesulfame removal via sorption was marginal. Quantitative PCR and 16S rRNA gene amplicon Illumina MiSeq sequencing suggested that higher removal efficiencies of most compounds correlated with high bacterial abundance, diversity, and high TOC. The bacterial community in high-TOC sediment samples was more stable to TrOC

additions compared to the community in low TOC sediments. Latter communities were characterized by a decline in the relative abundance of most phyla except Proteobacteria. Bacterial families enriched in the presence of TrOCs relative to unamended controls included Methylophilaceae, Caldilineaceae, Acidimicrobiaceae, Xanthobacteriaceae, Hydrogenophiliaceae, Rhodospirillaceae Gemmatimonadaceae and Rhodocyclaceae, suggesting either resistance to or stimulation by suplemental TrOCs.

Bedform features such as ripples and dunes alter hyporheic exchange fluxes and porewater residence times. The contribution of bedform features and microbial diversity on the attenuation of TrOCs was investigated by measuring the dissipation half-lives (DT50s) of 31 TrOCs (mainly pharmaceuticals) under different combinations of bacterial diversity and bedforms using 20 recirculating flumes in a central composite face factorial design. Using targeted and suspect screening, quantitative PCR and time-resolved amplicon Illumina MiSeq sequencing, a set of DT50s and microbial transformation products were determined. About 20 compounds responded significantly to bacterial diversity and four to both diversity and hyporheic flow. Bacterial taxa abundant in microbial communities supporting biodegradation of the test compounds included Acidobacteria (groups 6, 17, and 22), Actinobacteria (*Nocardioides* and *Illumatobacter*), Bacteroidetes (Terrimonas and Flavobacterium) and diverse Proteobacteria (Pseudomonadaceae, Sphingomonadaceae, and Xanthomonadaceae).

The collective results indicated that the hyporheic zone sustains (i) efficient biotic (trace) organic pollutant degradation of diverse compounds, and (ii) hitherto unknown microbial communities catalyzing (trace) organic pollutant removal. Results further suggest that (iii) TOC content affects removal efficiency of some TrOCs by directly

impacting the microbial community dynamics and associated biotransformation processes, (iv) microbial diversity is the primary driver of biotransformation processes in the hyporheic zone, and (v) the interplay of the physical, biological, and chemical processes contributes to improved attenuation of TrOCs in the hyporheic zone. Thus, the hyporheic zone is a reservoir of hitherto unknown microbial biodiversity providing an essential ecosystem service.

2. ZUSAMMENFASSUNG

Die hyporheische Zone ist der wassergesättigte Bereich von Flussbett Sedimenten, der durch vielfältige gleichzeitig ablaufende physikalische, biologische und chemische Prozesse charakterisiert ist. Die hyporheische Zone trägt zur Selbstreinigungskraft von Fließgewässern über die effiziente Entfernung von Kontaminanten aus klar eingegrenzten und diffusen Quellen, hauptsächlich über mikrobielle Aktivitäten, bei. Jedoch sind solche Potenziale, assoziierte mikrobielle Gemeinschaften und Einflüsse auf die Struktur der mikrobiellen Gemeinschaft für spezifische, weit verbreiteter, umweltrelevanter Substanzen weitestgehend unbekannt.

Daher wurden Schadstoffentfernungspotenziale in Sedimenten aus der hyporheischen Zone mit Hilfe des nicht-steroidalen, entzündungshemmenden Wirkstoffs Ibuprofen untersucht. Biodegradation von Ibuprofen wurde in oxischen Mikrokosmen mit Sediment untersucht, denen Ibuprofen oder Ibuprofen und Acetat zugesetzt war. Nicht-supplementiertes oder hitzesterilisiertes Sediment diente als Kontrolle. Ibuprofen wurde über 1-, 2- und 3-Hydroxy sowie Carboxyibuprofen als transiente primäre Transformationsprodukte biologisch abgebaut. Quantitative PCR Analysen zeigten signifikant höhere 16S rRNA-Abundanzen in Ibuprofen-versetzten im Vergleich zu den nicht-supplementierten Mikrokosmen. Zeitlich aufgelöste Amplikon-Illumina-MiSeq-Sequenzierung der 16S rRNA Gene und der 16S rRNA zeigten einen bedeutenden Effekt von Ibuprofen auf die mikrobielle Gemeinschaftsstruktur und viele neuartige Taxa innerhalb der Acidobacteria, Actinobacteria, Bacteroidetes, Gemmatimonadetes, Latescibacteria und Proteobacteria, die auf Ibuprofen angesprochen haben. Dies wurde mit Hilfe spezifischer 16S rRNA Genexpressionsanalysen anhand repräsentativer Taxa

bestätigt. Zwei Stämme, die Ibuprofen als einzige Kohlenstoff- und Energiequelle nutzen konnten, zwei durch Ibuprofen angereicherte Taxa der Amplikonbliotheken repräsentierten und zu den Genera Novosphingobium sowie Pseudomonas gehörten, konnten isoliert werden und werden als Modellorganismen zur Aufklärung von Ibuprofenabbauwegen dienen.

Redoxgradienten entlang des Flussbetttiefenprofiles beeinflussen die Entfernung von Schadstoffen. Die mikrobielle Entfernung des Betablockers Metoprolol, aus der redoxkompartimentierten hyporheischen Zone wurde mit Hilfe von oxischen und anoxischen Mikrokosmen mit Sediment untersucht. Biotransformation von Metoprolol fand unter beiden Bedingungen statt. In den oxischen Mikrokosmen wurde Metoprolol vorwiegend zu Metoprololsäure transformiert, während unter anoxischen Bedingungen Metoprololsäure und Hydroxymetoprolol gebildet wurden, was auf unterschiedliche mikrobielle Abbauwege oder Aktivitäten unter den kontrastierenden Inkubationsbedingungen in der hyporheischen Zone hinweist. Die Transformationsprodukte wurden unter oxischen und anoxischen Bedingungen anschließend komplett abgebaut. Reagierende Taxa, die mit Metoproloabbau in Verbindung gebracht wurden, gehörten unter oxischen Bedingungen zu den Proteobacteria und Bacteroidetes, sowie zu den Proteobacteria, Acidobacteria, Chloroflexi, Firmicutes und Gemmatimonadetes unter anoxischen Bedingungen.

Der Anteil an organische Substanz beeinflusst vielfältige biogeochemische Reaktionen. Der Einfluss von organischem Kohlenstoff auf den Verbleib von 13 organischen Spurenschadstoffen (TrOCs) wurde mit Hilfe von Sedimenten unterschiedlichen Gehaltes an gesamten organischen Kohlenstoff (TOC) untersucht. Oxische Mikrokosmen mit Sediment, das einen hohen oder niedrigem TOC aufwies, zeigten unterschiedliche Biotransformations- und Sorptions-abhängige

Enfernungseffizienzen der TrOCs. Signifikant höhere biotische Entfernungseffizienzen wurden für Verbindungen wie Ibuprofen, Ketoprofen, und Acesulfam in Sedimentmikrokosmen mit hohem im Vergleich zu niedrigem TOC gefunden. Die Entfernungseffizienz über Biotransformation war für alle Verbindungen generell höher als durch Sorption, mit der Ausnahme von Propanolol, an dessen Entfernung beide Mechanismen gleichermaßen beteiligt waren. Sorption war für die Entfernung von Acesulfam vernachlässigbar. Quantitative PCR und 16S rRNA Gen-Amplikon-Illumina-MiSeq-Sequenzierung legte nahe, dass die Entfernungseffizienzen der meisten Verbindungen mit hohen bakteriellen Zellzahlen und bakterieller Diversität, sowie hohem TOC korrelierten. Die mikrobielle Gemeinschaft der Sedimente mit hohem TOC waren in Bezug auf die Zugabe von TrOC stabiler, als die mikrobielle Gemeinschaft in Sedimenten mit niedrigem TOC. Letztere waren durch einen Rückgang der relativen Abundanzen der meisten Phyla mit der Ausnahme von Proteobacteria charakterisiert. Familien der Bacteria, die in der Anwesenheit von TrOCs im Vergleich zu den nicht-supplementierten Kontrollen angereichert waren, umfassten Methylophilaceae, Caldilineaceae, Acidimicrobiaceae, Xanthobacteriaceae, Hydrogenophiliaceae, Rhodospirillaceae, Gemmatimonadaceae and Rhodocyclaceae, was durch Resistenz gegenüber den supplementierten TrOCs, oder durch Stimulation erklärt werden kann.

Flussbettstrukturen wie Rippel und Dünen verändern den hyporheischen Austauschfluss und damit die Porenwasserverweilzeiten. Der Beitrag von Flußbettstrukturen und mikrobieller Diversität auf die Attenuation organischer Schadstoffe in der hyporheischen Zone wurde durch Messung der Halbwertszeiten (DT50s) von 31 TrOCs (hauptsächlich Pharmazeutika) bei verschiedenen Kombinationen aus bakterieller Diversität und Bettstrukturen mit Hilfe von 20

rezirkulierenden Gerinnen in einem multifaktoriellem Design untersucht. Durch Kombination aus subtanzspezifischer und nicht-zielgerichteter Analytik organischer Verbindungen zusammen mit quantitativer PCR und zeitlich aufgelöster 16S rRNA Gen-Amplikon-Illumina-MiSeq-Sequenzierung wurden DT50s und mikrobiellen Transformationsproduktdynamiken als Funktion der beiden Faktoren ermittelt. Ungefähr 20 Verbindungen reagierten deutlich auf mikrobielle Diversität und vier auf beide, mikrobielle Diversität und hyporheischen Fluss. Bakterielle Taxa, die in mikrobiellen Gemeinschaften abundant waren, die Biodegradation der Testverbindungen unterstützten, umfassten Acidobacteria (groups 6, 17, and 22), Actinobacteria (Nocardioides and Illumatobacter), Bacteroidetes (Terrimonas and Flavobacterium) and diverse Proteobacteria (Pseudomonadaceae, Sphingomonadaceae, und Xanthomonadaceae).

Die gesammelten Ergebnisse zeigen, dass die hyporheische Zone (i) effizienten biotischen (Spuren-)Schadstoffabbau einer Vielzahl unterschiedlichster Verbindungen ermöglicht und (ii) bislang unbekannte mikrobielle Gemeinschaften, die die Entfernung von (Spuren-)Schadstoffen katalysieren, unterstützt. Die Ergebnisse deuten weiterhin daraufhin, dass (iii) der Gehalt an TOC die Entfernungseffizienz einiger TrOCs über direkte Effekte auf die mikrobielle Gemeinschaft und damit verbundene Biotransformationsprozesse beeinflusst, sowie (iv) das Zusammenspiel physikalischer, biologischer und chemischer Prozesse zu einer verbesserten Attenuation von TrOCs in der hyorheischen Zone beiträgt. Daher stellt die hyporheische Zone ein Reservoir bislang unbekannter mikrobieller Diversität dar, die eine essenzielle Ökosystemdienstleistung zur Verfügung stellt.

3. INTRODUCTION

3.1. Emerging pollutants in the environment

3.1.1. Occurrence

The “emerging pollutants” are compounds not currently covered by the existing water-quality regulations but considered a potential threat to the environmental ecosystems, human health and safety (La Farre *et al.* 2008). The compounds are not necessarily new as some have been present in the environment for decades with their “discovery” only attributed to improvements in analytical technics (Barbosa Junior *et al.* 2016). Such compounds include pharmaceutical and personal care products (PPCPs), steroids and hormones, surfactants, nanoparticles, flame retardants, perfluorinated compounds, industrial chemicals, pesticides, and associated transformation products (La Farre *et al.* 2008; Hai *et al.* 2014). Most organic compounds are associated with human use, and their occurrence in the environment depends on the usage and disposal mechanisms. Majority of the compounds are disposed of via municipal and industrial wastewater treatment systems. Others such as agricultural-related wastes, e.g. pesticides and veterinary drugs may reach the environment via terrestrial run-offs and leaching, atmospheric deposition or when liquid manure is sprayed on agricultural fields (Figure 1; La Farre *et al.* 2008). While some of the compounds are eliminated during wastewater treatment or on site in terrestrial systems in case of pesticides, others tend to be removed partially or bypass the treatment processes unchanged, ending as complex mixtures in receiving surface waters (Margot *et al.* 2015; Jaeger *et al.* 2019a;Posselt *et al*. 2020)

The inefficient removal of such compounds during wastewater treatment is attributed to the design of most conventional wastewater treatment plants (WWTPs) whose primary purpose is to rapidly remove nutrients (organic carbon, nitrogen and

phosphorus) (Atashgahi *et al.* 2015). As such, the WWTPs are characterized by short hydraulic and sludge retention times that may be inadequate for elimination of xenobiotics before the discharge of the effluent into receiving rivers. As by design, most synthetic compounds exhibit a degree of stability and persistency (Berkner and Thierbach 2014), the continued discharge of non-degraded parent compounds and active metabolites by the currently existing WWTPs seems inevitable.

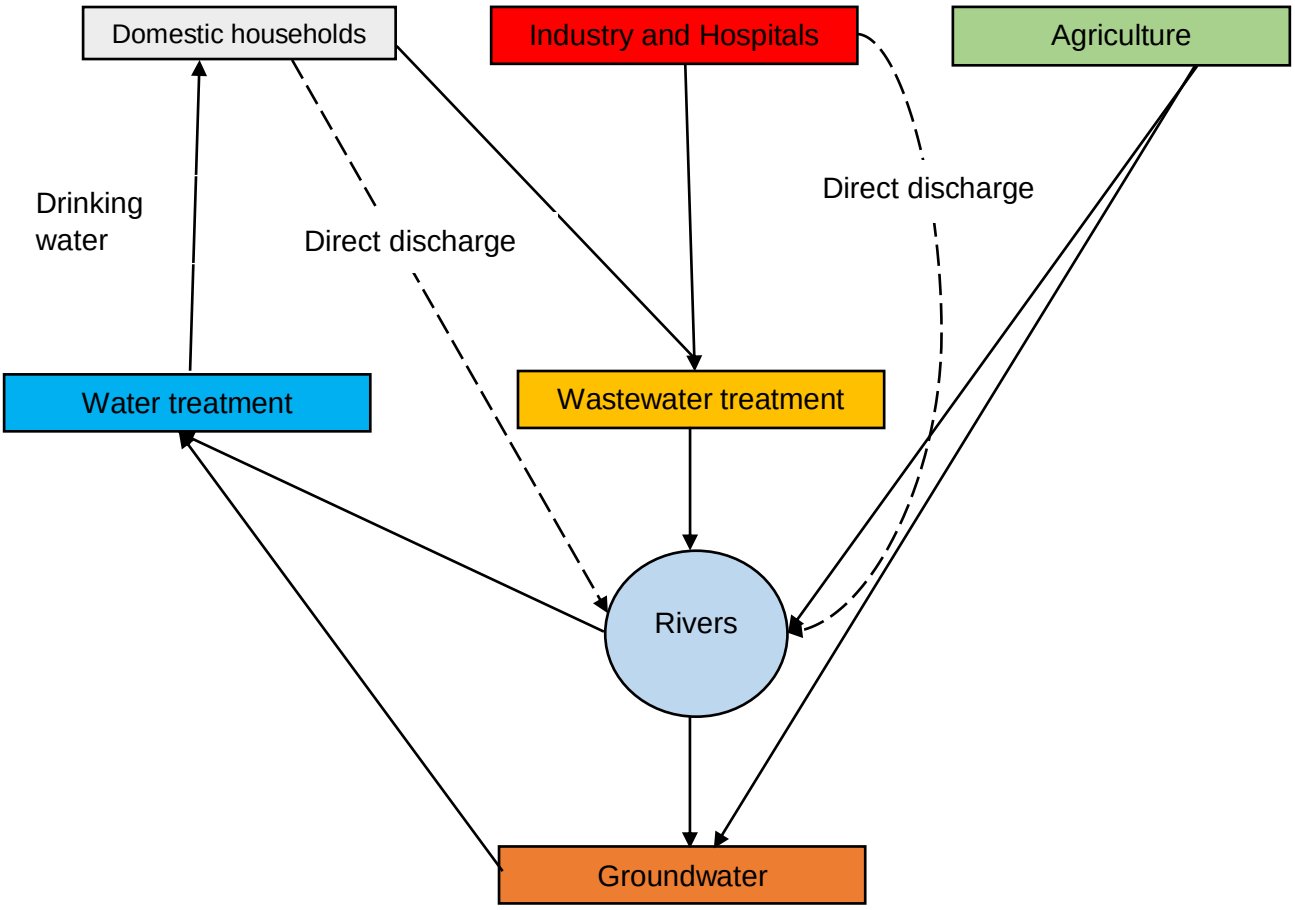

Figure 1. Sources and pathways of organic (micro-) contaminants in the water cycle. Figure was modified after Ellis (2006).

3.1.2. Importance of organic pollutants in the environment

The continued discharge of contaminated effluents results in pseudo-persistence and accumulation of the organic micropollutants in surface waters (Daughton 2003; Lewandowski *et al.* 2011). Though detected within the ng – μgL^{-1} range and christened trace organic contaminants (TrOCs), the compounds remain biologically active thus presenting a threat to the aquatic ecosystem mainly when such receiving systems are used in the production of drinking water (Pal *et al.* 2014). Effects such as acute and chronic toxicity to the aquatic biota, bioaccumulation, potential loss of biodiversity and unforeseen adverse effects on the human health raise concern (Hai *et al.* 2014). Recent studies have reported deleterious effects of some emerging pollutants on different trophic levels (La Farre *et al.* 2008). The occurrence of the contaminants in some cases as complex mixtures amplifies the toxicity due to additive, synergistic or antagonistic effects as well as continual exposure over long periods (Daughton 2003; Lawrence *et al.* 2005).

For example, natural and synthetic estrogens cause endocrine disruption in humans and animals such as aquatic species at the ngL^{-1} range (Clara *et al.* 2005; Matozzo *et al.* 2008; Combalbert and Hernandez-Raquet 2010). Ibuprofen, a non-steroidal anti-inflammatory drug widely consumed globally for its analgesic, anti-inflammatory, and antipyretic properties exhibited an adverse effect on the reproduction of some aquatic organisms such as zebrafish, planktonic crustaceans and the Japanese rice fish (Li *et al.* 2016). Ibuprofen was also detected in the bile of wild fish caught downstream of a WWTP (Brozinski *et al.* 2012) while cytotoxic effects of ibuprofen combined with other pharmaceuticals on human kidney embryonic cells have also been reported (Pomati *et al.* 2006). Potential metoprolol toxicity at μgL^{-1} to mgL^{-1} levels has been reported against all trophic levels from autotrophs (algae) to fish (Rubirola *et al.* 2014). The

antidepressants fluoxetine and sertraline and their metabolites were detected in wild fish, suggesting potential bioaccumulation (Brooks *et al.* 2005). An ecotoxicological risk of acetylsalicylic acid, bezafibrate, carbamazepine, diclofenac, fenofibrate, and paracetamol was predicted based on estimated baseline toxicity with quantitative structure-activity relationships (QSAR) (Lienert *et al.* 2007).

Ibuprofen and carbamazepine reduced bacterial biomass of some riverine biofilm communities while cyanobacteria were suppressed by a mixture of ibuprofen, carbamazepine, furosemide, and caffeine (Lawrence *et al.* 2005). Benzotriazole derivatives are reported as mutagenic in bacteria and cytochrome P-450 inhibitor in addition to demonstrated toxicity against plants (La Farre *et al.* 2008). Perfluorochemicals commonly used in the production of such stain-resistant items as clothing and utensils including perfluorooctanoic acid, perfluorobutanoic acid and perfluorohexane sulfonate have been detected in reclaimed effluents. Perfluorochemicals are toxic, persistent and highly water-soluble, therefore, raising concern over their potential to contaminate drinking water sources (Hai *et al.* 2014). The effect of antibiotics on the emergence of resistant bacterial strains and spread across species via horizontal gene transfer is well documented (Neu 1992; Dzidic and Bedeković 2003). Such findings give rise to concerns on the long-term ecological impact of the micropollutants on aquatic ecosystems as well as the potential effect on the health and safety of higher trophic levels (Posselt *et al.* 2020).

3.1.3. The fate of TrOCs in the environment

Despite the risks mentioned above, attenuation of some pollutants in constructed and natural environments via such removal mechanisms as biodegradation and sorption has been reported (Posselt *et al.* 2018). The removal mechanism involved is majorly

dependent on the interaction of the TrOC's physicochemical status with environmental factors such as pH, temperature, redox conditions, microbial community, operating parameters such as hydraulic and sludge retention time in WWTPs, and organic carbon content (Schwarzenbach 1986; Hai *et al.* 2014; Peralta-Maraver *et al.* 2018b). For example, hydrophobicity of a TrOC may be estimated using the octanol-water partitioning coefficient (K_{ow}) to determine the probability of sorption. However, potential ionization of functional groups depending on the pH of the surrounding media may influence the $K_{ow.}$ Therefore, to account for such an effect of pH, the effective octanol-water partitioning coefficient (log *D*) ought to be considered to predict the actual sorption potential of the compound. Generally, log *D* values ≥ 3 suggest sorption is a vital removal mechanism for a particular TrOC (Hai *et al.* 2014).

Moreover, non-hydrophobic processes such as electrostatic interactions or complexation with metal ions may also contribute to the sorption of TrOCs (Boxall *et al.* 2002; Schaper *et al.* 2019). Anionic and neutral compounds sorb onto organic matter (Tülp *et al.* 2009) and are, therefore, affected by the total organic carbon content (Jaeger *et al.* 2019a). Cationic compounds tend to sorb to negatively charged surfaces and highest retention via sorption of such compounds has been demonstrated in sediment-water matrices (Writer *et al.* 2013; Kodešová *et al.* 2015).

Like sorption, the biodegradability of the TrOCs depends on their physicochemical properties. This biodegradability is based on a kinetic constant k_{biol} L $g_{ss}.d^{-1}$ derived from pseudo first order kinetic models as described in the Equation 1;

Equation 1.

$$\left(\frac{dCw}{dt}\right) = -k_{biol} \text{ X } C_w \text{ X } X_{active}$$

where k_{biol} L $g_{ss}.d^{-1}$is the biodegradation constant; C_w is the concentration of compound in the water phase (μgL^{-1}) and X_{active} is the concentration of active biomass (Tran *et al*. 2018).

A proposal by Joss *et al.* (2006), attempted to classify compounds according to a biodegradation constant (k_{biol}) and identified three TrOC groups whereby compounds with k_{biol} < 0.1L $g_{ss}.d^{-1}$ are removed to < 20%, compounds with k_{biol} < 10L $g_{ss}.d^{-1}$ are transformed by < 90%, while moderate removal is predicted to be in between. The molecular weight is also considered a determinant on the biodegradability of TrOCs (Tadkaew *et al.* 2011). The authors investigated the removal of 40 TrOCs in a membrane bioreactor and identified a correlation between TrOC removal efficiency and their molecular weight. While compounds with molecular weight > 300 $gmol^{-1}$ registered removal efficiencies > 60%, those with molecular weight < 300 $gmol^{-1}$ exhibited variable removal efficiencies ranging from near zero to more than 98%. The authors attributed the trend to the higher molecular weight compounds constituting more functional groups and branches that are a target for different microbial degradation pathways.

Moreover, a correlation between the molecular structure and functional moieties of TrOCs and their biodegradability has been demonstrated (Reemtsma *et al.* 2002; Tadkaew *et al.* 2011). Esters, aromatic alcohols and nitriles contain functional groups enhancing higher biodegradability while compounds with halogen groups and complex structures such as an alkyl chain branch exhibit reduced biodegradability (Corvini *et al.* 2006; Hai *et al.* 2011) Compounds with electron-withdrawing functional groups, exhibit low removal efficiency compared to those with electron-donating groups, e.g. hydroxyl and primary amine groups (Tadkaew *et al.* 2011).This may explain the differences observed in removal efficiencies of compounds such as pharmaceuticals

within a pharmacological class. For example, antiepileptic drugs vastly differ in structure ranging from complex azepines to branched chain carboxylic acids (Onesios *et al.* 2009). Antibiotics such as sulfonamides and macrolides vary markedly in their mechanism of action and structures. For example, the sulfonamide has two rings connected by a sulfur atom and C-N bonds while macrolides have a ring with side chains or sugars. These properties render the sulfonamides more polar and hydrophilic compared to macrolides, subsequently affecting their removal. Variable susceptibility of chiral pharmaceuticals to biodegradation depending on enantiomeric fractionation patterns where the S enantiomers of compounds such as ibuprofen, ketoprofen and naproxen as well as beta-blockers (alprenolol and propranolol) were preferentially degraded compared to their R counterparts (Hashim *et al.* 2010; Hashim *et al.* 2011), suggest that enantiomeric fractionation patterns are important factors in predicting biotransformation potential. Despite the apparent variable removal mechanisms of TrOCs depending on the physicochemical status, it is important to note that in the environment, the processes are not necessarily exclusionary but rather complementary since for instance sorption may impair or enhance the bioavailability of a compound (Findlay and Sobczak 2000; Hai *et al.* 2014).

Biodegradation is considered the most important removal mechanism of TrOCs in the environment (Radke *et al.* 2009; Lewandowski *et al.* 2011; Li *et al.* 2016; Coll *et al.* 2019; Liu *et al.* 2019). In the majority of the cases, however, biotransformation rather than complete mineralization of the parent compounds is observed via the activity of such microorganisms as bacteria, archaea and fungi (Lewandowski *et al.* 2011;Tran *et al.* 2013; Posselt *et al.* 2018)

Though evidence for the capability of such microbes to respond to minute concentrations of organic compounds from biosensor studies suggests concentrations

of organic compounds down to the pg L^{-1} range suffice to induce transcription of catabolic genes and corresponding enzymes for their transformation (Haque *et al.* 2013), their occurrence in low concentrations is considered insufficient to support growth (La Farre *et al.* 2008; Tran *et al.* 2013). Some TrOCs may also exhibit toxicity rendering them unfavorable to enter catabolic pathways of microbial cells (Tran *et al.* 2013). Therefore, many TrOCs are degraded cometabolically in the presence of a primary growth substrate such as organic carbon that maintains the biomass (Tran *et al.* 2013). Studies using higher than typical *in situ* TrOC concentrations have revealed that some bacterial strains can utilize organic pollutants as sole carbon and energy sources (Murdoch and Hay 2013; Marchlewicz *et al.* 2017; Żur *et al.* 2018). Such a metabolic degradation potential is, however, possible if the target compound is non-toxic to the degrader. A tolerance of up to 5000 mgL^{-1} of ibuprofen by a sludge community as well as increased metabolic activity after continued exposure was reported (Davids *et al.* 2017), suggesting resilience against stressor effect of pollutants by microbial communities. Dynamic utilization of a mix of four pharmaceutical compounds; ibuprofen, carbamazepine, furosemide, and caffeine at 10 μgL^{-1} was observed in a riverine biofilm community where both nutrient-like and toxic effects on some fractions of the microbial community were reported (Lawrence *et al.* 2005). Such findings suggest the threshold concentration for pollutants to serve as a sole carbon source is unclear and may vary from compound to compound.

The predominance of biodegradation as a TrOC removal mechanism is attributed to the versatility of microbes whose metabolic pathways and enzyme catalogue is not only diverse but dynamic in responding to emerging compounds (Tran *et al.* 2013). A case in point is the degradation of acesulfame, hitherto considered persistent (Buerge *et al.* 2009) and used as a stable marker of domestic wastewater in groundwater

(Buerge *et al.* 2009; Engelhardt *et al.* 2013), but which has been recently shown to be biodegradable in constructed and natural environments (Castronovo *et al.* 2017; Kahl *et al.* 2018; Jaeger *et al.* 2019a; Schaper *et al.* 2019).The impact of horizontal gene transfer in natural environments including sediments, soil and water is reported (Lorenz and Wackernagel 1996), and is likely associated with such emerging potential to degrade the ever-dynamic array of synthetic micropollutants. Utilization of parent compounds by a subset of the microbial community followed by further degradation of the intermediates or even complete mineralization by other microbes (Tran *et al.* 2013), as well as mixed substrate use among environmental microorganisms (Harder and Dijkhuizen 1982) further promote the efficient environmental removal of TrOCs via microbial activity. Owing to the highlighted inefficient removal of TrOCs in most conventional WWTPs and receiving surface waters (Kunkel and Radke 2008; Peralta-Maraver *et al.* 2018b), research focus has shifted onto the utility of the hyporheic zone to efficiently remove micropollutants bypassing the WWTPs.

3.2. Hyporheic zone

The hyporheic zone is the saturated sediment interface between surface water and groundwater located directly beneath and lateral to streams and river corridors (Wroblicky *et al.* 1998). The zone spatially fluctuates between the surface and groundwater and is characterized by multiple physical, biological and chemical processes simultaneously occurring at several scales (Figure 2; (Ward 2016; Schaper *et al.* 2018a; Galloway *et al.* 2019). Discipline-specific focus on the hyporheic zone processes in the context of its functional relevance within river ecosystems has resulted in variable definitions (Peralta-Maraver *et al.* 2018b). For example, ecologists consider the hyporheic zone as the streambed layer beneath the surface water with a

thickness in the range of centimeters whereas in biology, it's described as the sediment volume hosting a characteristic hyporheic community (Tonina and Buffington 2009). In hydrology, the hyporheic zone comprises the flow paths that begin and end at the sediment-water interface while in biogeochemistry, it constitutes the ecotone where the mixing of surface water and groundwater and where a certain percentage of the surface water is present (Gooseff, 2010; Ward, 2016; Gomez-Velez *et al.* 2017). An integrative definition by Ward (2016) encompassing the cross-disciplinary definitions considers four key criteria of an hyporheic zone: (1) saturated subsurface, (2) flow paths originating from and returning to the surface water, (3) interactions with the stream occurring within a temporal scale, and (4) processes of interest occurring continuously from the stream–subsurface interface to the groundwater continuum.

3.3. Removal of TrOCs in the hyporheic zone

The characteristic interaction of physical (e.g. transport of water and solutes), chemical (e.g. sorption, chemical reactions), and biological processes (e.g. microbial activity, bioturbation) in the hyporheic zone renders it a significant contributor to the self-purification capacity of lotic systems (Krause *et al.* 2009; Lewandowski *et al.* 2011). Considered a natural bioreactor, the turnover and degradation of nutrients (carbon, nitrogen, phosphorus) and organic (micro-)pollutants are among the prominent ecological services the hyporheic zone provides (Zarnetske et al. 2011a; Zarnetske et al. 2011b; Lewandowski *et al.* 2019).

The removal of the ever dynamic array of TrOCs reaching the aquatic ecosystems by the hyporheic zone has gained traction since it is now considered the last line of defense for preventing wastewater-derived organic contaminants from reaching near-surface aquifers that are used for drinking water production (Posselt *et al.* 2020). Of

the active TrOC attenuation processes in this ecotone including dispersion, sorption-desorption, advection and biotransformation (Burke *et al.* 2014; Schaper *et al.* 2018a), microbial mediated degradation is considered the major pathway through which TrOCs are removed in the hyporheic zone. As a biological activity, this attenuation mechanism is influenced strongly by the several parameters that characterize the hyporheic zone. These include hyporheic exchange flows (HEF), subsurface residence time, temperature, redox conditions, organic carbon content and the microbial community structure (Burke *et al.* 2014; Hebig *et al.* 2017; Lewandowski *et al.* 2019; Munz *et al.* 2019).

3.4. Drivers and processes influencing TrOC removal in the hyporheic zone

3.4.1. Hyporheic exchange flow and subsurface residence time

HEF is defined by hydrological processes such as downwelling (recharge) where surface water enters the groundwater reservoir, upwelling (discharge) where groundwater infiltrates the hyporheic zone into the surface water as well as underflow, an advective flow where surface water infiltrates into the bed, travels for some distance across the longitudinal gradient before returning into the stream (White *et al.* 1987; Martone *et al.* 2020). The complex interaction of the water and the streambed features influences the magnitude and intensity of the HEF and residence time of water in the hyporheic zone since the hyporheic exchange may occur over a wide range of spatial and temporal scales ranging from millimeter/second flow paths to kilometer-scale flow paths spanning years (Singh *et al.* 2019). The increased residence time of water in the hyporheic zone allows adequate contact time between nutrients and micropollutants and potential degraders (Peralta-Maraver *et al.* 2018b). The development of slow-growing bacteria is favoured, in turn creating a more diverse microbial community with the enhanced physiological potential to effectively breakdown the more recalcitrant

compounds that bypass the WWTPs (Lewandowski *et al.* 2011; Peralta-Maraver *et al.* 2018).

The dominant drivers of HEF at the regional scale are groundwater and river stage levels while the local scale is impacted more by bed morphology, channel velocity and sediment heterogeneity (Martone *et al.* 2020). Considering the characteristic variability in rivers over short distances and time scales, differences in streambed features such as bedforms and pool-rifles, planform morphology, sediment hydraulic conductivity and porosity can induce fluctuations in physicochemical conditions that directly impact the resident biota and associated processes (Magliozzi *et al.* 2019; Singh *et al.* 2019). Generally, HEFs significantly impact the river ecology by controlling transport of dissolved oxygen, nutrients, dissolved and particulate organic carbon and micropollutants into the hyporheic zone (White *et al.*1987; Triska *et al.* 1989; Lapworth *et al.* 2011; Galloway *et al.* 2019). Moreover, HEFs regulate stream water temperature, an essential factor in the ecological functioning of the hyporheic zone (Magliozzi *et al.* 2019; Singh *et al.* 2019). Transient streamflow events resulting from human activity such as discharge from WWTPs or natural precipitation inputs can have significant effects on the HEF intensity and magnitude by, for example, inducing enhanced surface water infiltration into the sediment. Such waters potentially rich in dissolved oxygen, nutrients and organic matter, in turn, impact biogeochemical processes such as nitrification and denitrification as well as in-stream TrOC removal (Gu *et al.* 2008; Schaper *et al.* 2018; Singh *et al.* 2019).

3.4.2. Temperature gradients

Temperature strongly influences biological activity, and its effect on the microbial removal of some TrOCs in the zone has been demonstrated (Burke *et al.* 2014). The

authors reported an order of magnitude higher removal rates under high temperature (19.7 °C) and oxic than cold (6.5 °C) and oxic conditions for metoprolol, acesulfame, diclofenac and tolytriazole. For phenazone and its associated metabolites acetylaminoantipyrine and formylaminoantipyrine, the removal rate constants decreased by a factor of 3.3, 2.5 and 4.1, respectively with decreasing temperature. In a comparable riverbank filtration, *in situ* degradation rates for diclofenac and sulfamethoxazole varied within an order of magnitude for temperature changes between 5 and 20 °C (Munz *et al.* 2019). These results suggest that under similar redox conditions, seasonal fluctuations in temperature may impact TrOC removal. Temperature also influences the redox conditions. An expanded oxic zone in case of low temperatures while warm temperatures causing a rapid transition from oxic to manganese reducing conditions in the hyporheic zone was reported (Burke *et al.* 2014). A similar observation in an artificial recharge system revealed aerobic conditions prevailed under low temperatures (< 14 °C) while temperatures exceeding 14 °C turned conditions anaerobic (Massmann *et al.* 2006). Such observations are attributed to the fact that redox processes are microbially mediated, hence a variation in temperature influences microbial activity and associated redox gradients.

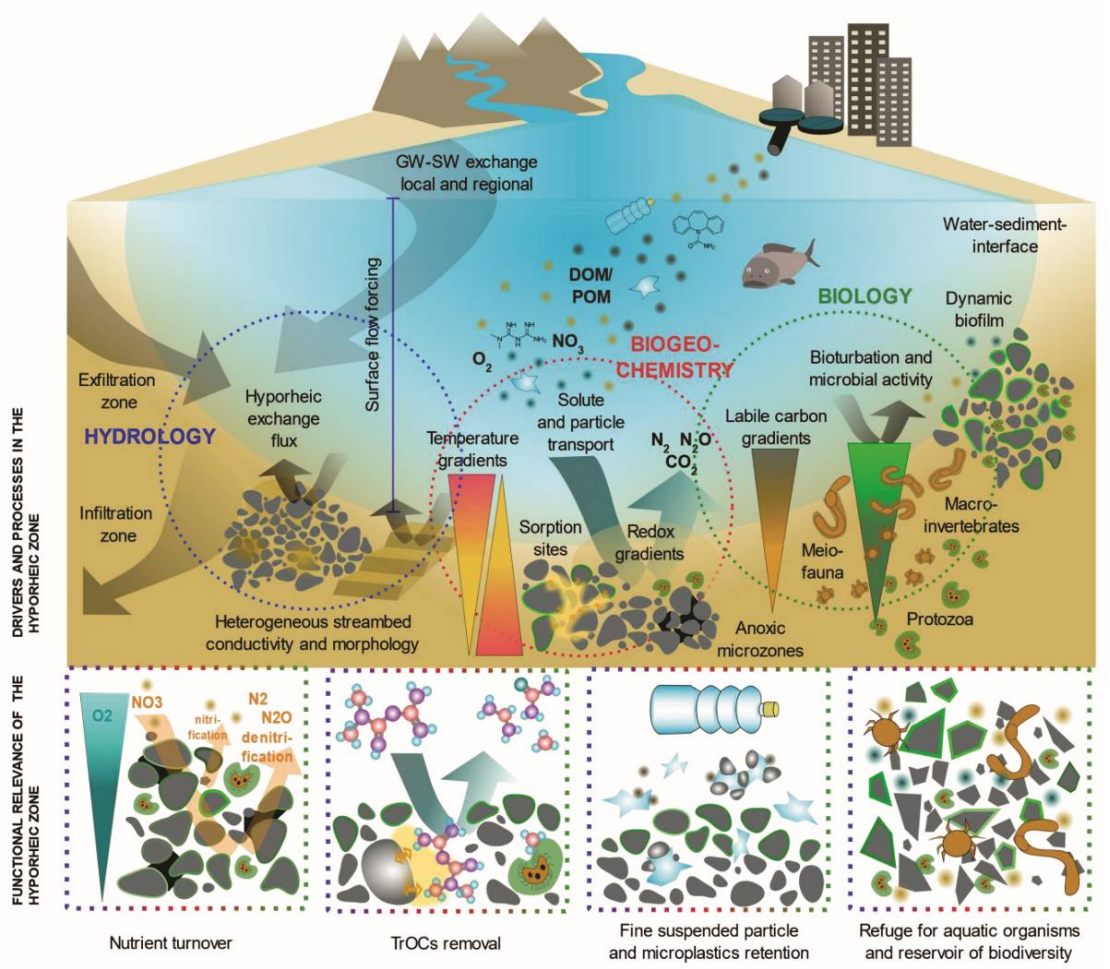

Figure 2. Conceptual model of the major hyporheic zone drivers and processes and functional relevance of the hyporheic zone. Dashed circles indicate the interaction of physical, chemical and biological processes that make hyporheic zone a significant contributor to the self-purification capacity of lotic systems. GW-SW exchange is groundwater-surface water exchange. The figure was modified and used with permission from Lewandowski *et al.* (2019).

3.4.3. Redox gradients

The hyporheic zone is a highly biogeochemically active zone characterized by an exchange of dissolved oxygen, nutrients and organic carbon (Krause *et al.* 2011). A typical redox cascade in the hyporheic zone develops via utilization of available electron acceptors in the presence of non-limiting amounts of electron donor, essentially organic carbon (Lewandowski *et al.* 2019). The effect of this redox delimitation of the hyporheic zone directly affects the resident microbiota dynamics

and associated micropollutant biodegradation pathways. In downwelling zones, dissolved oxygen in the infiltrating surface water is consumed readily via aerobic microbial processes. The heterotrophic microorganisms utilizing organic carbon can under oxic conditions cometabolically degrade TrOCs, where the micropollutants are oxidized by enzymes or cofactors generated during the metabolism of the primary substrate (Tran *et al.* 2013). Moreover, processes such as nitrification carried out by autotrophic ammonia oxidizing microbes have been reported to have a significant impact on the dissolved oxygen concentration and may account for up to 50 % of the BOD in the aerobic hyporheic zone (Storey *et al.*1999). Interestingly, nitrification is associated with the degradation of many TrOCs such as aromatic and halogenated hydrocarbons, methane and steroids (Arp *et al.* 2001; Tran *et al.* 2013). The ammonia monooxygenase in autotrophic ammonia oxidizers exhibits a non-specific enzyme activity and oxidizes a broad substrate range that includes TrOCs in the presence of its main substrate, ammonia (Helbling *et al.* 2012; Tran *et al.* 2013)

Upon depletion of the dissolved oxygen, microbial metabolism relies on alternative electron acceptors such as nitrate/nitrite, manganese, iron oxy/hydroxides, sulfate and organics along the thermodynamic cascade that is normally characterized by a progressive decline in energy yield (Ghattas *et al.* 2017). Essentially, the TrOCs are biodegraded cometabolically by the reductive activity of enzymes or cofactors produced during the primary substrate decomposition (Tran *et al.* 2013). The supply of nitrate in the infiltrating water, as well as the nitrification-denitrification reactions occurring in the anoxic microzones within oxic segments of the streambed, makes denitrification a major contributor to biogeochemical dynamics in the hyporheic zone (Lewandowski *et al.* 2011). Denitrification can account for up to 50 % of organic carbon decomposition (Christensen *et al.* 1990; Triska *et al.* 1993). However, its contribution

to the removal of TrOCs is difficult to determine since most denitrifiers are facultative aerobes that can use aerobic and anaerobic metabolism under denitrifying conditions (Ghattas *et al.* 2017). Biodegradation of TrOCs under denitrifying conditions has only been demonstrated in lab-scale bioreactors as the complete exclusion of oxygen in the environment cannot be guaranteed. Suarez *et al.* (2010), reported variable removal efficiencies of 16 PPCPs under denitrifying conditions. Fragrances (galaxolide, tonalide, celestolide), fluoxetine and natural estrogens were removed to above 70 % while ibuprofen, citalopram, trimethoprim, roxithromycin, sulfamethoxazole, erythromycin, diazepam, carbamazepine, diclofenac, naproxen exhibited less than 40% removal in bioreactors with an SRT of over 20 days.

Manganese and iron reduction have also been associated with the removal of such contaminants as benzene, toluene, ethylbenzene and xylene (BTEX) and halogenated aromatics (Ghattas *et al.* 2017). Microbial-mediated reduction of iron (III) is also linked to the abiotic degradation by iron (II) of sulfamethoxazole, nitroaromatic compounds and dichlorodiphenyltrichloroethane (Tor *et al.* 2000; Li *et al.* 2010; Mohatt *et al.* 2011).

Sulphate is used as an electron acceptor in the degradation of a broad spectrum of organic micropollutants such as BTEX, polycyclic aromatic compounds, i.e. naphthalene and anthracene, alkanes and chlorinated compounds (Ghattas *et al.* 2017). Below the inorganic electron acceptors reducing zone, degradation of some organic compounds under methanogenic conditions occurs. These include aromatics such as phenoxyethanol and 2-sec-butyl-4, 6-dinitrophenol, benzene, toluene, halogenated aromatic compounds and triclosan (Frings and Schink 1994; Hammill and Crawford 1996; Veetil *et al.* 2012; Liang *et al.* 2013; Ghattas *et al.* 2017). The degradation of such complex compounds is postulated to occur from the syntrophic association between methanogens and fermentative and acetogenic bacteria that

supply the electron donors such as formate, acetate and H_2/CO_2 to the methanogens (Stams *et al.* 2005; Ghattas *et al.* 2017). The halorespiring bacteria use H_2 or organic substrates e.g. acetate as electron donor while using a variety of organohalides including benzenes, phenols, and halogenated alkanes as electron acceptors, (Ghattas *et al.* 2017), hence contributing to their removal from the environment. While biodegradation of TrOCs is more widely reported in oxic compared to anoxic conditions, for some compounds such as halogenated aromatic compounds, better degradation occurs under anoxic conditions (Vogel *et al.*1987). Such findings signify the utility of environments with a variety of redox conditions such as the hyporheic zone in the overall removal of TrOCs.

3.4.4. Organic carbon gradients

The bioavailable total organic carbon (TOC) (i.e., dissolved organic carbon (DOC) + particulate organic carbon (POC) in the hyporheic sediments is considered a major factor limiting microbial metabolism (Findlay and Sobczak 2000), thereby directly or indirectly impacting coupled processes such as biotransformation of TrOCs. Most streambed sediments of receiving rivers are characterized by allochthonous-derived organic carbon from wastewater effluents (Gücker *et al.* 2006) as well as autochthonous-derived organic matter from decomposing leaf litter and macrophytes (Romani *et al.* 1998). The surface sediment layer as the primary contact point with these deposits, consequently, has higher concentration of organic carbon compared to subjacent layers. Subsequently, bacterial populations, turnover and metabolism are high in this layer, suggesting high mineralization rates that decrease exponentially with depth (Wellsbury *et al.*1996; Harvey *et al.* 2013; Knapp *et al.* 2017; Schaper *et al.* 2019). As TrOC attenuation is coupled to biogeochemical reactions fuelled by the

organic carbon (Atashgahi *et al.* 2015), a decline in TOC concentration with increasing depth might impair the overall TrOC removal efficiency of the hyporheic zone.

Most studies on hyporheic zone metabolism, however, focus on the DOC (Findlay *et al.* 1993; Schindler and Krabbenhoft 1998; Zarnetske *et al.* 2011a; Stegen *et al.* 2018; Schaper *et al.* 2019), while the processing of POC, a considerable constituent of the TOC has received less attention. This may be due to the consideration that labile DOC reaching the hyporheic zone is supplied as a continuous input by surface or groundwater in case of downwelling or upwelling conditions, while POC is embedded in the sediment and its bioavailability depends on turnover rates (Findlay and Sobczak 2000). However, in comparing DOC transferred into the sediment to the POC degraded in the same volume and based strictly on relative mass, POC would be the predominant carbon source for hyporheic sediment microbial communities while considering controlling factors such as water velocity and POC stock (Findlay and Sobczak 2000). As such, POC supports baseline metabolism, especially in subsurface sediments, while DOC only triggers short-term fluctuations above this baseline (Vervier *et al.*1993). Additionally, DOC and POC pools are intimately connected by biological activity whereby secondary consumption of the DOC contributes to the POC pool via the heterotrophic microbial community (Fisher *et al.* 1998), while POC is transformed into DOC by the hydrolytic activity of bacterial biofilms (Sempéré *et al.* 2000). Though the turnover rates and the extent to which DOC is generated from aggregate POC remains largely unknown, bacterial degradation of up to 87% of the initial amount of POC within 48 hours has been reported in marine samples (Sempéré *et al.* 2000). The interplay between the two organic carbon components makes it difficult to resolve the relative contribution of DOC or POC in the hyporheic sediments, hence the need to consider them cumulatively as TOC.

3.4.5. Microbial community structure

The biodiversity and functions of the microbial community influence and are also influenced by the environmental factors in the hyporheic zone. For instance, most receiving rivers impacted by effluents from upstream WWTPs exhibit high nutrient loads and in extreme cases, eutrophication (Drury *et al.* 2013). The settling and accumulation of organic matter in the hyporheic zone result in rapid depletion of dissolved oxygen via increased chemical oxygen demand (COD) and biochemical oxygen demand (BOD), and a sharp redox gradient may be established creating oxic benthic and anoxic underlying sediment layers (Brunke and Gonser 1997). Such redox gradients in the sediment profile create local niches allowing inhabitation of specific microbial communities. Cumulatively, the redox cascade results in a diverse microbial community with high metabolic versatility that favour enhanced removal of TrOCs (Boulton *et al.* 1998; Peralta-Maraver *et al.* 2018b; Schaper *et al.* 2019). Moreover, the large surface area occupied by the sediment particles, pore spaces and organic matter serves as ideal retention sites for the infiltrating compounds and microbial habitats where complex microbial biofilms consisting of bacteria, archaea, algae, fungi, protozoa and metazoans interact (Battin *et al.* 2016). The combined metabolic activity of these hyporheic zone communities entailing inter and intra-trophic transfer of compounds and metabolites promote the ecological functioning of the hyporheic zone including the transformation of TrOCs (Krause *et al.* 2009; Peralta-Maraver *et al.* 2018). Most studies on stream biofilms have focused on the bacteria and archaea due to rapid developments in high throughput sequencing techniques and databases while little is known about organisms such fungi in the stream ecosystems (Baschien *et al.* 2008; Battin *et al.* 2016). Fungi and other microeukaryotes are part of the microbial community in streams, although rare relative to bacteria, and potentially contribute to

biodegradation processes (Baschien *et al.* 2008). Eukaryotic algae may form biofilms together with bacteria in the benthic zone; however, their occurrence in sediments is highly limited by the low availability of light. Archaea likewise represent only a minor fraction of the stream bed microbial community and are restricted to specialized niches in the hyporheic zone (Posselt *et al.* 2020). Thus, the hyporheic zone biofilms are majorly dominated by bacteria (Baschien *et al.* 2008; Buriánková *et al.* 2013; Battin *et al.* 2016; Lewandowski *et al.* 2019; Posselt *et al.* 2020).

Bacterial taxa, including Proteobacteria, Bacteroidetes, Actinobacteria, Firmicutes, Gemmatimonadetes, Verrucomicrobia, Planctomycetes and Deinococcus–Thermus are most commonly detected in stream biofilms (Battin *et al.* 2016). Within the bacterial phyla are thousands of taxa of lower ranks inhabiting various microhabitats in the hyporheic zone whose diversity and composition is influenced by the prevailing physicochemical conditions, allowing niche differentiation and community composition shifts from the local (millimeter) to reach (kilometer) scales (Battin *et al.* 2016). For example, reduced hydraulic stress allows thicker biofilm formation, less light penetration and a community shift toward heterotrophs (Battin *et al.* 2003). Streambed morphology-induced variation in hydraulics was, for instance, shown to account for almost half of the variation in microbial beta diversity in experimental streams (Besemer *et al.* 2009). At the reach scale, the effects of such factors as catchment geology and altitude were shown to influence microbial diversity as they affect the catchments from where microbial cells reaching the rivers are recruited (Wilhelm *et al.* 2013). The biodiversity dynamics in benthic biofilms may also be influenced by variable source catchments of stream networks (Besemer *et al.* 2013). Changes at the local and reach scales may, therefore, impact the functioning of the biofilms and by extension, the aquatic ecosystem.

The efficiency of the hyporheic zone as a significant sink for TrOCs is partially attributed to higher microbial diversity than WWTPs and surface water, both characterized by low abundance and diversity of microorganisms (Kunkel and Radke 2008; Peralta-Maraver *et al.* 2018; Schaper *et al.* 2018a).Though it is difficult to establish a relationship between bacterial diversity and function in case of complex biofilm communities, studies in engineered environments have suggested such a correlation between bacterial diversity and or abundance and removal efficiency of TrOCs (Johnson *et al.* 2015; Stadler *et al.* 2018). Recently, an artificial river system in a flume study revealed a similar correlation (Jaeger *et al.* 2019b), suggesting that even in the extensively diverse stream biofilms, changes in the bacterial diversity affect the functioning of the hyporheic zone. While functional gene redundancy in the degradation of common substrates such as organic carbon, nitrate and phosphate is still prevalent (Battin *et al.* 2016), the degradation of emerging complex TrOCs may necessitate a broader catalogue of enzymes from different taxa to degrade due to the variable functional groups and intermediates reaching the hyporheic zone (Jaeger *et al.* 2019a).

3.5. Hypotheses and objectives

Hyporheic zones as key compartments for the functioning of aquatic ecosystems contribute to the turnover and degradation of organic matter, nutrients and micropollutants. While extensive knowledge on the retardation and transformation of organic matter and nutrients and on the microorganisms involved exists, the transformation potentials for most emerging organic micropollutants are unknown, and microbial communities associated with their removal in the hyporheic zone are not well resolved. Moreover, the hyporheic zones are characterized by the simultaneous occurrence of multiple physical, biological, and chemical processes that directly or indirectly impact the microbial community dynamics and associated removal of TrOCs. To resolve the micropollutant transformation potential of the hyporheic zone and how the biogeochemical factors therein influence the microbial removal of TrOCs, the following hypotheses were formulated.

1. The sedimentary matrix provides a high surface area that anchors a diverse microbial community with micropollutant degradation potential
2. The microbial pollutant degradation potential is influenced by the prevailing biogeochemical factors in sediments e.g. redox conditions, organic matter content
3. Sediment morphology influence on hyporheic exchange fluxes impacts microbial community dynamics e.g. diversity and coupled processes such as biotransformation of TrOCs.
4. TrOCs serve as both growth substrates and toxicants to different microbial community fractions.

The objectives of this dissertation were to (i) determine organic micropollutant biodegradation potentials as a function of the multiple and transient gradients in the hyporheic zone sediment downstream from a WWTP using microcosm and mesocosm setups, (ii) identify degradation intermediates and hypothetical degradation pathways, (iii) relate microbial community changes to micropollutant exposure and hence to (iv) identify potential degraders. As the current knowledge on degradation-associated genes and metabolic pathways for most emerging micropollutants is limited, identification of micropollutant-responsive taxa was investigated based on analysis of 16S rRNA gene (whole community) and 16S rRNA ("active" fraction of the total community).

4. MATERIALS AND METHODS

4.1. Site description

The sampling site is a section of the River Erpe, a tributary of the Spree River in Brandenburg and Berlin, Germany. As part of the HypoTRAIN project, the site was selected to investigate the fate of TrOCs in the hyporheic zone using multidisciplinary approaches from the hydrology, ecology, microbiology, engineering, environmental physics, contaminant science and modelling disciplines. The site was selected based on the availability of preliminary data from a previous study (Lewandowski *et al.* 2011). The Erpe represents a typical lowland urban stream impacted by municipal wastewater. Located at the eastern edge of the Berlin, River Erpe receives up to 80% of its discharge as wastewater from the Münchehofe WWTP (42,500 m^3 d^1 dry weather capacity) and several other smaller WWTPs. Different sites, depending on the objectives of the various studies within the HypoTRAIN project, were selected (S1-S6) **(Figures 3 and 4).** Regarding this dissertation, the site S5 located approximately 0.7 km downstream of the effluent discharge site at Heidemühle (Lat, 52.478647; Long, 13.635146) was utilized as the sampling location.

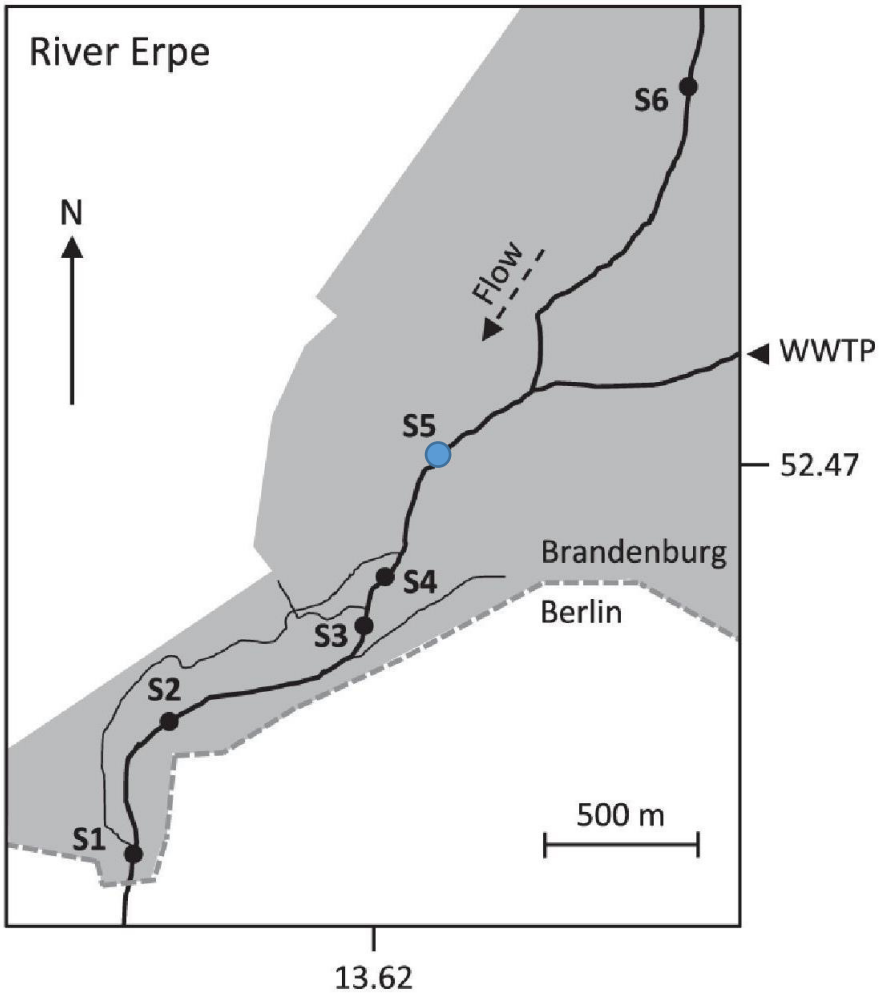

Figure 3. The study sites at the River Erpe, Berlin Germany investigated under the HypoTRAIN project. The sampling site (S5) downstream of the Münchehofe WWTP was used as sampling location for all samples used in this dissertation. The figure was modified and used with permission from Peralta-Maraver *et al.* (2018a).

Figure 4. Image of the sampling site ‘Heidemühle’ on River Erpe
Image was taken by Malte Posselt

Through a sampling campaign in September 2015, using passive samplers, over 300 TrOCs were quantified mainly downstream of the Münchehofe WWTP (Mechelke *et al.* 2019). Out of these, a total of 31 compounds were selected for further characterization on their fate in the hyporheic zone. The selected compounds were mostly pharmaceuticals and covered a wide range of physicochemical properties (Table 1; Figure 5). The compounds were purchased from Sigma-Aldrich (UK) or Toronto Research Chemicals (Canada) at purities ≥ 96%.

Table 1. Test compound investigated in the current study. Compound properties logKOW and logDOW, pH8.3 were predicted from SMILES strings using JChem for Excel (Vers. 19.14.0.500, ChemAxon). Table used with permission from Posselt *et al.* (2020).

Parent compound	Abbreviation	logDow	logKow	Molecular formula	Exact mass	vendor
Acesulfame	ACS	-1.49	-0.55	C4H5NO4S	162.9939	Sigma
Amisulpride	AMI	-0.04	0.25	C17H27N3O4S	369.1722	TRC
Atenolol	ATE	-0.95	0.43	C14H22N2O3	266.1630	Sigma
Benproperine	BENP	4.37	5.19	C21H27NO	309.2093	TRC
Benzotriazole	BNZ	1.19	1.26	C6H5N3	119.0483	Sigma
Bezafibrate	BEZ	0.50	3.99	C19H20ClNO4	361.1081	Sigma
Carbamazepine	CBZ	2.77	2.77	C15H12N2O	236.0950	Sigma
Celiprolol	CEL	0.04	1.50	C20H33N3O4	379.2471	TRC
Citalopram	CIT	2.27	3.76	C20H21FN2O	324.1638	Sigma
Clofibric acid	CFA	-0.61	2.90	C10H11ClO3	214.0397	Sigma
Diclofenac	DIC	0.80	4.26	C14H11Cl2N1O2	295.0167	Sigma
Flecainide	FLEC	1.86	3.19	C17H20F6N2O3	414.1378	Sigma
Fluoxetine	FLX	2.66	4.17	C17H18F3NO	309.1340	Sigma
Furosemide	FUR	-1.68	1.75	C12H11ClN2O5S	330.0077	Sigma
Gemfibrozil	GEM	1.02	4.39	C15H22O3	250.1569	Sigma
Hydrochlorothiazide	HCTZ	-0.64	-0.58	C7H8ClN3O4S2	296.9645	Sigma
Ibuprofen	IBU	0.66	3.84	C13H18O2	206.1307	Sigma
Irbesartan	IRB	3.99	5.39	C25H28N6O	428.2325	TRC
Ketoprofen	KET	0.14	3.61	C16H14O3	254.0943	Sigma
Metaxalone	MTX	2.37	2.37	C12H15NO3	221.1052	TRC
Metformin	METF	-3.66	-1.36	C4H11N5	129.1014	Sigma
Metoprolol	METO	0.38	1.76	C15H25NO3	267.1834	Sigma
Naproxen	NPX	-0.44	2.99	C14H14O3	230.0943	TRC
Paracetamol	PAR	0.88	0.91	C8H9N1O2	151.0633	Sigma
Propranolol	PROP	1.20	2.58	C16H21NO2	259.1572	Sigma
Sitagliptin	SIT	0.65	1.26	C16H15F6N5O	407.1181	Sigma
Sotalol	SOT	-1.28	-0.40	C12H20N2O3S	#N/A	Sigma
Sulfamethoxazole	SMX	-0.13	0.79	C10H11N3O3S1	253.0521	Sigma
Sulpiride	SUL	-0.02	0.22	C15H23N3O4S	341.1409	Sigma
Valsartan	VAL	0.34	5.27	C24H29N5O3	435.2270	Sigma
Venlafaxine	VEN	2.04	2.74	C17H27NO2	277.2042	Sigma

Beta blockers

Atenolol

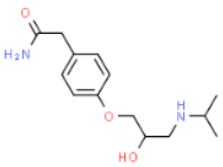

Celiprolol

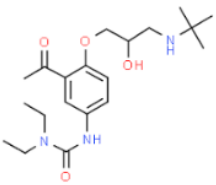

Metoprolol

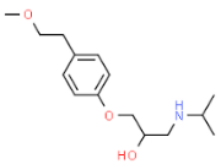

Propranolol

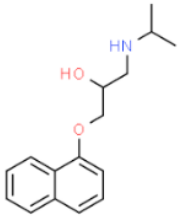

Sotalol

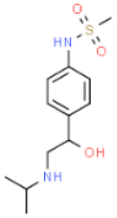

NSAIDs

Diclofenac

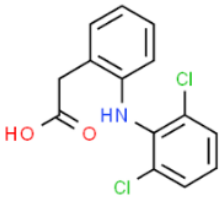

Ibuprofen

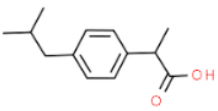

Ketoprofen

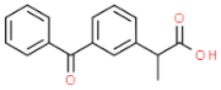

Naproxen

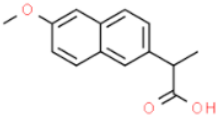

Antihypertensives

Furosemide

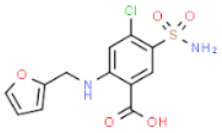

Hydrochlorothiazide

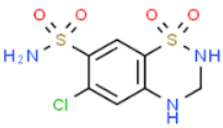

Irbesatan

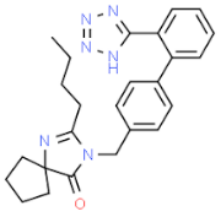

Valsartan

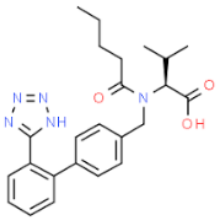

Antihyperlipidaemia

Bezafibrate

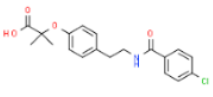

Clofibric acid

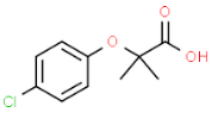

Gemfribrozil

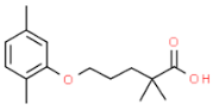

Antidepressants

Citalopram

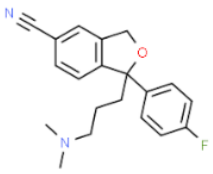

Fluoxetine

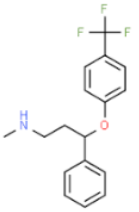

Venlafaxine

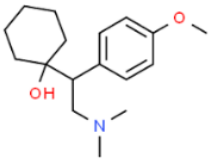

Antidiabetics

Metformin

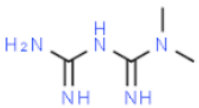

Sitagliptin

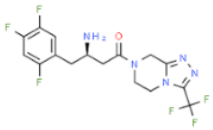

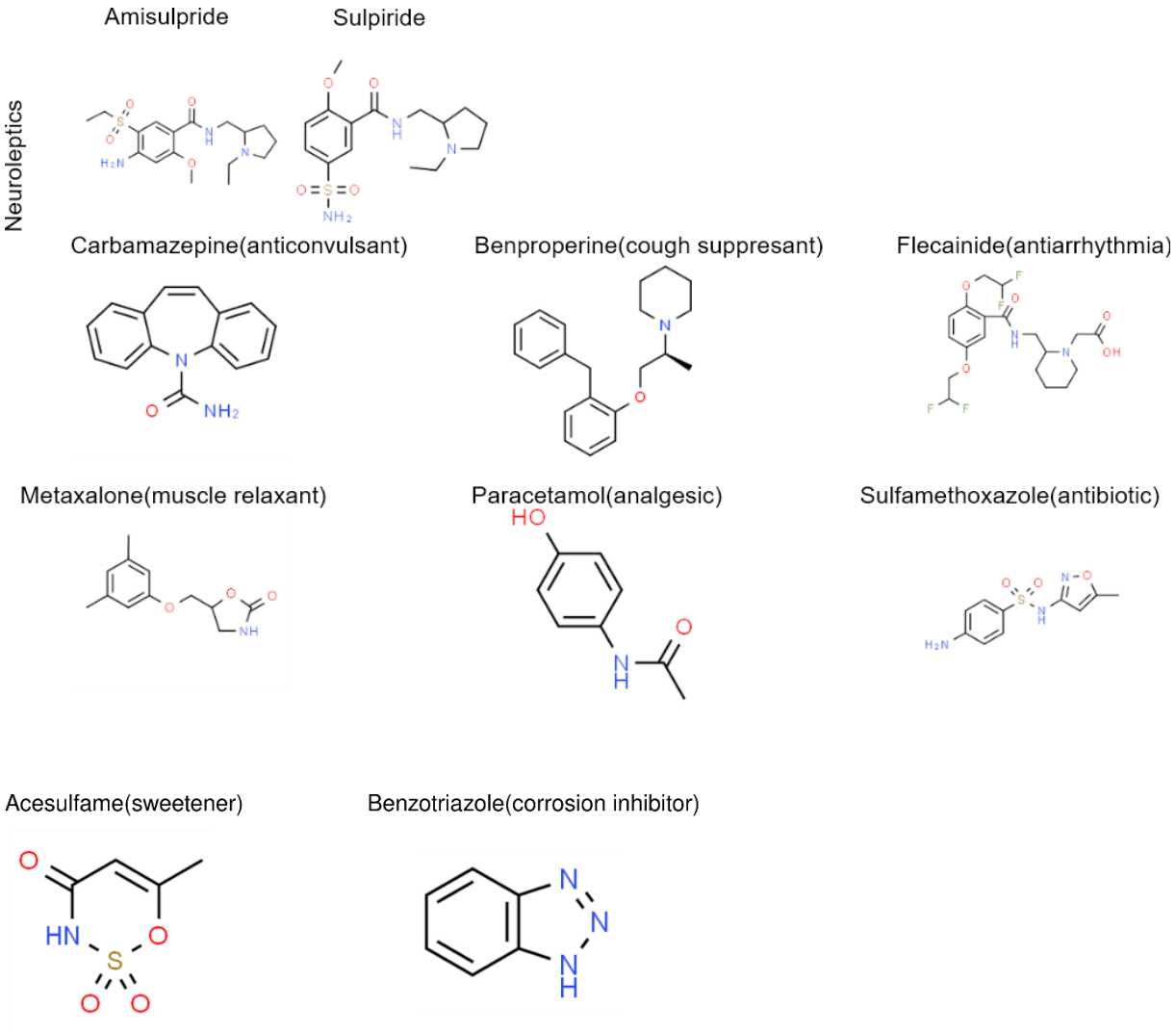

Figure 5. Chemical structures of the test compounds. Source: ChemSpider (Pence and Williams 2010).

4.2. Sampling procedure

Sediment and water samples were collected during four sampling campaigns conducted at the study site. Surface sediment samples (0 – 5 cm depth) were collected from several points on the streambed with a flat hand shovel and stored in sterile Whirl-Pak sampling bags (Merck, Germany). Sediment cores were collected using 6-cm-diameter simple gravity corers (Uwitec, Mondsee, Austria). The corers, essentially open-ended plastic tubings, were pushed into the sediment, sealed at the top with a

rubber stopper and retrieved **(Figure 6).** Surface water samples were obtained from the same site and stored in 2L-screw mouth Duran® bottles (Sigma-Aldrich, Germany). Freshly collected sediment and water samples were transferred to the laboratory in sterile, airtight containers at 4°C for further processing.

Figure 6. Images of the core sampling approach at River Erpe
Images were taken by Muhammad Raza.

4.3. Experimental setups

4.3.1. TrOC removal potential of hyporheic zone sediments

The potential of the hyporheic zone in the removal of micropollutants is attributed mainly to the activity of the indigenous microbial community; particularly bacteria (Battin *et al.* 2016). The sedimentary matrix provides retention sites for the microbial communities and nutrient-rich pore water, factors that enhance the zone's micropollutant-degradation potential. Such potentials were investigated using ibuprofen as a model organic compound.

Grab sediment samples and surface water were collected in September 2015 and transferred to the laboratory. The freshly collected sediment samples were then manually homogenized, and an aliquot stored in the - 80°C freezer for subsequent nucleic acid extraction. The remaining fresh sediment was stored at 4° C and used to set up microcosm experiments within two weeks.

The microcosms were prepared in triplicates using 25 grams fresh sediment and 50 ml natural river water in autoclaved 120 ml conical flasks. A pre-incubation for 10 days to reduce dissolved endogenous carbon was performed. Subsequently, a set of microcosms was supplemented with ibuprofen to achieve final concentrations of 5, 40, 200 and 400 µM, and the second set with 1 mM acetate concomitant to ibuprofen at the same concentrations. Unamended biotic control microcosms and two abiotic controls comprising of autoclave-sterilized sediment (i.e., sorption control), and autoclave-sterilized river water (i.e., hydrolysis control) amended with a final concentration of 200 µM ibuprofen were included. All flasks were sealed with sterilized Steristoppers® (Heinz Herenz, Hamburg, Germany). Microcosms were then incubated in the dark at 15°C with shaking at 100 rotations per minute. Liquid samples were taken under sterile conditions after the first amendment (t0) and at regular intervals following incubation. Ibuprofen or Ibuprofen-acetate were re-fed four times to the same initial concentrations upon complete substrate depletion as determined using the high performance liquid chromatography (HPLC)(4.4.1.2). In total, the microcosms were amended five times. Following the third re-feeding and at the end of the incubation (after the fifth re-feeding), two-gram sediment subsamples were taken from the treatments and biotic controls and stored at - 80°C for future nucleic acid extraction.

4.3.2. Effect of redox conditions on the TrOC removal potential

Dissolved oxygen depletion along the sediment depth profile leads to the establishment of a redox gradient with oxic benthic and underlying anoxic sediments (Brunke and Gonser 1997). Little is known about the impact of such redox zonation on the resident microbiota dynamics and associated processes such biotransformation of TrOCs. This was investigated using metoprolol as a model compound.

Sediment samples were collected from the upper 40-cm riverbed layer at nine random locations within a 10 m stretch of the sampling site in June 2016. Preliminary analysis indicated the upper 30 cm of the hyporheic zone was oxic, with the anoxic zone occurring after 30 cm depth as reported elsewhere (Schaper *et al.* 2019). Sediment samples for oxic and anoxic microcosm incubations were obtained from the upper 10 cm (0 -10 cm) and (30 – 40 cm) depths, respectively. The freshly collected sediment layers were pooled in triplicates corresponding to the sampling depth and manually homogenized.

The microcosms were prepared in triplicate in sterilized 250-ml conical flasks sealed with Steristoppers® (Heinz Herenz, Germany) for the oxic incubations, and in 250-ml glass bottles sealed with rubber septa bound-screw caps (Sigma-Aldrich, Germany) for the anoxic incubations. Each microcosm contained 40 g of sediment (fresh weight) and 120 ml river water. The anoxic microcosms were then purged for one hour with pure nitrogen to remove any residual oxygen in the headspace. All microcosms were pre-incubated statically for 14 days at 20°C in the dark to acclimatize and degrade any residual metoprolol and dissolved organic matter. Following pre-incubation, exogenous metoprolol was added into the microcosms. The metoprolol was first prepared by desalting the analytical grade metoprolol tartrate (Sigma-Aldrich,

Germany), using a reverse phase flash column (BÜCHI Labortechnik AG, Switzerland). The c18 flash column was initially activated with five column volumes methanol followed by five column volumes of water. 1.0 g of metoprolol tartrate was dissolved in 10 ml water and added to the column. The tartrate salt was washed out with three column volumes of water, then the metoprolol was eluted with acidified pure methanol using sulfuric acid in a step gradient (5% to 50% methanol). Metoprolol absorption characteristics were checked at 222 nm using ultraviolet–visible (UV-VIS) spectrophotometry (Shimadzu, Japan). Pure metoprolol was subsequently concentrated *in vacuo* via rotary evaporation of the solvent. The concentrated metoprolol was dissolved in water to make a 1M stock solution.

Following pre-incubation, the exogenous metoprolol was added into the microcosms to initial final concentrations of 15 and 150 µM, hereafter referred to as Low and High metoprolol concentrations, respectively. In parallel, an incubation where no metoprolol was added, i.e. biotic control, as well as abiotic controls constituting of autoclaved sediment and river water to account for losses via sorption and hydrolysis, respectively, were included. The abiotic controls were amended only with the High metoprolol concentration. Slurry samples were drawn from the microcosms at specified days during the experiment duration using syringes. The samples were subsequently centrifuged (13,000 x g, 5 minutes) and filtered using 0.2 µm-regenerated cellulose membrane filters (Agilent Technologies, CA, USA) to determine metoprolol concentration (4.4.1.3). Sediment samples were obtained from experimental microcosms and biotic control at days 0, 65 and 120 and stored in the -80°C freezer for subsequent nucleic acid extraction.

4.3.3. TrOC removal under contrasting organic carbon conditions

The bioavailable TOC in hyporheic sediments is considered a major limiting factor for microbial metabolism (Findlay and Sobczak 2000), thereby directly or indirectly impacting coupled processes such as biotransformation of TrOCs. TOC content varies along the sediment depth profile. However, the impact of such varying TOC conditions on the resident microbial and TrOC removal dynamics are largely unresolved.

Analysis of the sediment TOC content as described (4.3.3.) revealed the surface (0 – 10 cm) and the subjacent layer (10 – 20 cm) contained 8.65 % and 3.21 % TOC, respectively. Three sediment cores were collected in June 2016, transferred to the laboratory and sliced into discrete 10 cm layers (0 –10 cm) and (10 – 20 cm). The sediment segments were immediately manually homogenized and subsamples stored at - 80°C for subsequent nucleic acid extraction. About 2 g of sediment was taken from each layer, placed in 5 ml glass vials and approximately 2 ml of river water amended with a mixture of 13 test compounds added. The test compounds were nonsteroidal anti-inflammatory drugs (NSAIDs) (diclofenac, ibuprofen, ketoprofen and naproxen) beta-blockers (metoprolol, propranolol), cholesterol-lowering agents (bezafibrate, clofibric acid), antihypertensive drugs (furosemide, hydrochlorothiazide), anticonvulsant (carbamazepine), an artificial sweetener (acesulfame) and a corrosion inhibitor (benzotriazole) to yield an initial concentration of approximately 500 µg L^{-1}. The slurry was then thoroughly mixed, and the bottles capped. In total, six replicates were prepared from each sediment layer. A blank control setup consisting of sediment and river water but unamended with the test compounds was included. To account for abiotic losses via sorption onto the sediment or the glass vials, two microcosm setups, one containing sediment and the other only river water were treated with 0.1 % sodium azide to reduce bacterial activity. All setups were incubated statically in the dark at

18°C (the prevailing temperature during sampling). After 15 days of incubation, three replicates from each treatment were sacrificed. The supernatant was withdrawn for analysis of test compounds (4.4.2.), while the sediment from the biotic setups was stored at - 80°C for subsequent nucleic acid extraction. This step was repeated after 65 days of incubation.

4.3.4. Influence of HEF and microbial diversity on TrOC removal

Hyporheic exchange flows (HEFs) facilitate contact between contaminants in surface water and potential microbial degraders. HEF as a function of hydraulic conductivity and sediment morphology (Hester *et al.* 2013) together with the resident microbial community structure (especially diversity)(Peralta-Maraver *et al.* 2019) are therefore potential key controls of the fate of organic contaminants in lotic aquatic environments. Although long hypothesized, such links were never systematically addressed. The influence of bacterial taxonomic diversity and HEF on the dissipation half-lives (DT50s) of organic contaminants detected in surface waters and the associated formation of transformation products was evaluated (Posselt *et al.* 2020).

The experiment was based on a central composite face factorial design and used 20 circulating flume mesocosms (2 × 0.4 m) simulating different river conditions. The sediment volume was 20 L per flume covered with 60 L deionized water (ReAgent Chemicals, Cheshire, England) and every flume was equipped with a pump (NWA 1.6 adj 2.6 W, Newa Wave Industria, Loreggia, Italy) to establish surface water flow velocity of ca. 0.08 m s^{-1} similar to the River Erpe (0.05 to 0.3 m s^{-1}) (Jaeger *et al.* 2019a). Nutrients, such as phosphate and ammonium, and other solutes (inorganic ions in mg L^{-1} range and organic and inorganic micronutrients in µg L^{-1} range (Table 2; 4.5.1) were added, resembling concentrations and composition in the natural River

Erpe (Jaeger *et al.* 2019a). The two experimental variables (i.e. HEF and bacterial diversity) were studied at three levels each. Natural sediment from the River Erpe was collected using grab samplers in May 2017, immediately homogenized and stored at 4 °C until use within one month. The River Erpe sediment was used as inoculum in a dilution-to-extinction approach by mixing with sterilized commercial sand (oven-dried at 120 °C for 24 h). The approach was based on the principle that the least abundant species in a preceding community were eliminated through sequential dilution resulting in a less diverse community compared to the original community (Stadler *et al.* 2018). Sediment samples were collected in May 2017 at River Erpe, immediately homogenized and stored at 4 °C until use within one month while commercial sand (Wickes, Watford, United Kingdom) was washed and oven-dried at 120 °C for 24 h before mixing. The level of bacterial diversity was thus expected to decrease in the order: S1 (1:10 sediment: sand) > S3 (1:10^3 sediment: sand) > S6 (1:10^6 sediment: sand). Additionally, the sediment morphology in the flumes was manipulated to induce different intensities of HEF by varying the number of bedforms (Figure 6).The level of HEF was expected to decrease in the order B6 (three bedforms on each side of the flume) > B3 (3 bedforms on one side) > B0 (no bedforms). The HEF metrics, i.e. (exchange flux [L d^{-1}], exchange volume [L] and residence time [d]) were determined using a salt tracer dilution test (Jaeger *et al.* 2019a). 50 mg NaCl was added to each flume and recessions of the electrical conductivity were measured as surface water with high salt concentration gradually mixed with porewater of lower salt concentration The dilution resulting from the hyporheic exchange was measured using a hand-held electrical conductivity meter or loggers (CTD-Diver, van Essen Instruments, Delft, the Netherlands) for about 7.5 days. Pore water samplers (10 cm length, 0.15 µm pores, RHIZON FLEX, Rhizosphere Research Products, Netherlands) were glued to plastic

holders and thus positioned at equal heights (1.5 cm above the flume bottom) inside the sediment. In B3 and B6 flumes, samplers were placed in the second bedform and a second sampler in the third bedform as a backup in case of clogging. In B0 flumes, pore water samplers were installed at the same position but inside the flat sediment. Due to the small extraction volumes (15 mL per sampling event) relative to the pore water volume exchanged per day (ca. 10 L for 3 and 6 bedforms and about 0.5 L in flat sediment) (Peralta-Maraver *et al.* 2019) and the distribution of water extraction over the entire channel cross-section no substantial disturbance was expected in the flow paths or overall residence times by the sampling regime.

The experimental design encompassed the number of flumes per treatment-combination (S and B) as follows: S1+B6: 2, S3+B6: 2, S6+B6: 2, S1+B3: 2, S3+B3: 4, S6+B3: 2, S1+B0: 2, S3+B0: 2, S6+B0: 2. The flumes were pre-incubated for 12 days to allow regrowth of the bacterial communities in the diluted sediments to similar abundance.

After the 12 days of pre-incubation, the flumes were amended with 10 µg L^{-1} of each of the 31 test compounds (Table 1). This concentration was similar for most test compounds as detected in the river Erpe which we aimed to simulate a; Posselt *et al.* 2018) but also in other streams or WWTP effluents (Kay *et al.* 2017; Schaper *et al.* 2018; Paíga *et al.* 2019). Two unamended flumes (S3+B3) were included as biotic controls and served as a reference for the effect of test compounds on taxa in amended flumes. Surface and pore water were sampled before the amendment and after that on days 1, 2, 3, 7, 14, 21, 28, 42, 47, 56 and 78 for analysis of the test compounds (4.4.2.). Sediment was collected before the amendment, and after 21 and 56 days for subsequent extraction of DNA (4.6.1). Two previous studies provided experimental (Jaeger *et al.* 2019a) and modelled (Betterle; Personal communication)

evidence that a) the two variables, HEF and bacterial diversity, were successfully manipulated at three levels in the central composite face factorial design setup, b) sediment dilutions translated into different levels of bacterial diversity at similar bacterial biomass, and c) HEF increased in the presence of bedforms.

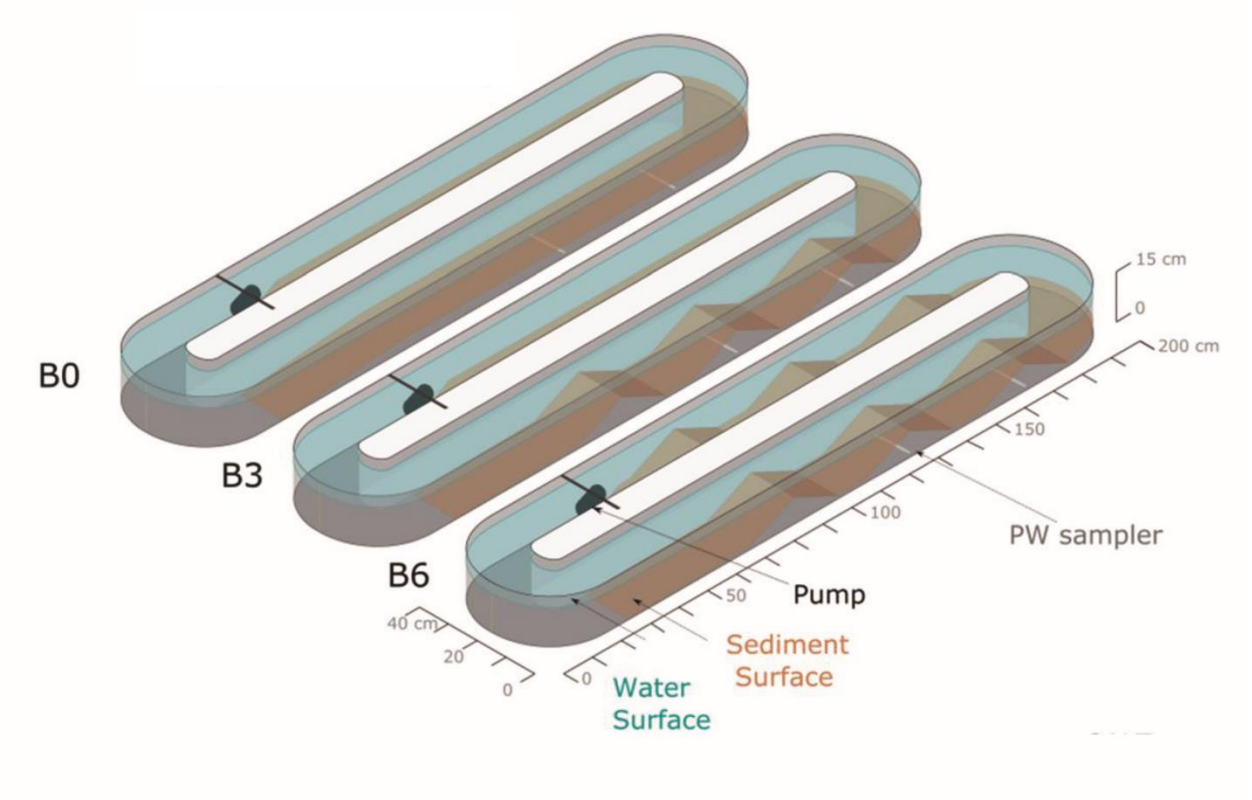

Figure 7. Flume setup scheme showing the three levels of the bedform variable. B6, B3, B0 represent six, three and zero bedforms, respectively. Figure modified and used with permission from Jaeger *et al.* (2019b).

4.4. Analytical methods

4.4.1. High performance liquid chromatography (HPLC)

4.4.1.1. Preparation of liquid samples

Liquid samples from the microcosm setups on ibuprofen (4.3.1) and metoprolol (4.3.2) were analyzed using HPLC at the University of Bayreuth, Department of Ecological Microbiology and the Leibniz University Hannover, Institute of Microbiology. The samples were prepared using a centrifugation step (13,000 *x g*, 5 minutes) and microfiltered (0.22 µm pore diameter, PTFE membrane) directly into 1 ml glass vials (Agilent Technologies, CA, USA).

4.4.1.2 Ibuprofen

Ibuprofen concentration (4.3.1) was quantified using an Agilent 1260 series HPLC fitted with a Zorbax SB-C18 column at 30°C and a diode array detector (Agilent 1260 series, Agilent Technologies, CA, USA) under isocratic conditions. The mobile phase was acetonitrile-20 mM acetate buffer (50:50 v/v), pH 3 at a flow rate of 0.5 ml min^{-1}. Spectra ranging from 200 to 320 nm were used to determine peak purity. The absorbance signal at 225 nm was used for quantification with external standards prepared in deionized water. Data were obtained and processed with ‘ChemStation’ (Agilent Technologies, CA, USA).

4.4.1.3. Metoprolol

Metoprolol concentration (4.3.2) was quantified using an Agilent 1260 series HPLC fitted with a Zorbax SB-C18 column and a diode array detector (Agilent 1260 series, Agilent Technologies, CA, USA). The mobile phase consisted of 0.2 % Trifluoroacetic acid (TFA) in deionized water (solvent A) and 0.16 % TFA in acetonitrile (solvent B).

Analysis was performed under gradient conditions starting with 95 % A / 5 % B for 15 min followed by 50 % A / 50 % B for 5 min, 100 % B for 0.1 min, and finally 15 % A / 85 % B for 4.9 min. The flow rate was 0.5 ml min^{-1}, and the column oven temperature was set at 40°C. Metoprolol eluted after 19.6 min as detected by the diode array detector (DAD) with an absorbance signal at 210 nm. Concentration was determined using external standards prepared in deionized water. Data were obtained and processed with 'ChemStation' (Agilent Technologies, CA, USA).

4.4.2. Mass spectrometry

4.4.2.1. Sample preparation

Analysis of samples for parent compounds and transformation products were analyzed using reversed-phase ultrahigh-performance liquid chromatography electrospray ionization triple quadrupole tandem mass spectrometry (RP-UHPLC-ESI-QqQ) at Stockholm University (SU), Department of Environmental Science. The liquid samples, stored at - 20 degrees for not more than three months, were defrosted at room temperature and thoroughly vortexed before processing. Volumes of 800 µL were combined with 195 µL methanol and the isotope-labelled internal standard mix of the parent compounds (Table 1) and transformation products (Table 2) in 5 µL methanol. The mixture was then vortexed and filtered using syringe filters (Filtropur S 0.45 µm, PES membrane, Sarstedt AGandCo, Germany) into 2 mL micro vials (Thermo Scientific, Germany) as reported in Posselt *et al.* (2018).

A subset of the samples from the flume experimental setup (4.3.4) was prepared and analyzed using reversed-phase liquid chromatography electrospray ionization high resolution tandem mass spectrometry (RP-LC-ESI-HRMS/MS) at the Department of Environmental Chemistry of the The Swiss Federal Institute of Aquatic Science and

Technology (EAWAG). The frozen water samples (-20°C) were equilibrated to room temperature, which was followed by a centrifugation step (2 mL sample, 3,020 g for 30 min at 20°C, Megafuge 1.0R, Heraeus) and the transfer of supernatant aliquots (1 mL) into HPLC sample vials. Isotope-labelled internal standards of the parent compounds and transformation products (Tables 1 and 2) were directly added to the vials (20 ng mL^{-1}). The calibration series was prepared in NANOpure™ water (0, 1, 10, 100, 500, 1000, 2500, 5000 and 10000 ng L^{-1}).

NANOpure water was generated with a lab water purification system (D11911, Barnstead/Thermo Scientific, USA), liquid chromatography–mass spectrometry (LC/MS) grade water was generated with a Milli-Q water purification system (Merck, Germany) or purchased from VWR (Germany). LC/MS grade methanol was purchased from Optima™, Fisher Scientific, Switzerland or Merck KGaA, Germany, analytical grade formic acid (≥ 98%) (Merck, Germany) and acetic acid (≥ 99.7%) (Sigma-Aldrich, Germany). HPLC-grade acetonitrile was purchased from Merck (Germany).

4.4.2.2. Targeted quantification of parent compounds and transformation products

A total of 31 selected parent compounds (Table 1) and 37 target transformation products were analyzed (Table 2). Samples analyzed using the RP-UHPLC-ESI-QqQ followed a recently developed direct-injection method (Posselt *et al.* 2018). The samples (20 µL) were injected into an Ultimate 3000 UHPLC system (Thermo Scientific, MA, USA) equipped with a Waters Acquity UPLC HSS T3 column (1.8 µm, 2.1 mm × 100 mm) (Manchester, UK). The mobile phase consisted of 10 mM acetic acid in deionized water (solvent A) and 10 mM acetic acid in methanol (solvent B). A chromatographic gradient (97% A/3% B to 60% A/40% B in 2.7 min and finally to 3%

A/97% B in 3.3 min) was employed after which the system was returned to starting conditions and equilibrated for 4 min. During the run, a method blank sample and a quality control standard was injected every 15-20 samples. The flow rate was 500 µL min^{-1} during the gradient and 1000 µL min^{-1} for equilibration. The column oven temperature was set to 45 °C. The column was coupled to a Quantiva triple-quadrupole mass spectrometer equipped with a heated electrospray ionization source. (Details on the operational conditions of the MS can be found in Posselt *et al.* (2018). MS data were processed using Thermo Scientific 'Xcalibur 3.1.66.10' and quantified using the internal standards method (Posselt *et al.* 2018).

For the samples prepared at EAWAG (4.4.2.1), a volume of 50 µL of both water samples and calibration standards was injected) into a reversed-phase C18 liquid chromatography column (Atlantis T3, 3 x 150 mm, 3 µm, Waters, USA). Water and methanol, both acidified with 0.1% formic acid, were used as eluents for the chromatographic gradient (0% to 95% methanol in 18.5 min, 95% methanol for 10 min, 95% to 0% methanol in 4 min). The analytical column was coupled to a high-resolution tandem mass spectrometer (QExactive or QExactive Plus, Thermo Scientific, USA) by an electrospray ionization interface (ESI). Mass spectra were acquired in full-scan mode (ESI polarity switching) at a mass resolution of 140,000 (FWHM at m/z 200) with subsequent data-dependent MS2 (Top5, mass resolution 17,500). For the quantification of target analytes (30 parents, 27 TPs), chromatographic peaks were automatically detected (5 ppm mass tolerance) and integrated (minimum three data points) using the ICIS algorithm of TraceFinder (version 4.1 EFS, Thermo Scientific, USA). Peak integrations were reviewed manually. To each target analyte, a matching internal standard (IS) was assigned (internal standard method). If the matching IS was not available, an IS with a similar retention time was selected. Linear 1/x-weighted

calibration curves were generated by fitting the analyte concentration (x) against the Standard-to-IS peak area response ratio (y) without forcing the fit through zero (Posselt *et al.* 2020).

Table 2. Transformation product properties (target analysis). logKOW and logDOW, pH 8.3 were predicted from SMILES strings using JChem for Excel (Vers. 19.14.0.500, ChemAxon). Table used with permission from Posselt *et al.* (2020).

Parent Compound	Transformation product	Abbrev.	logDow	logKow	mol-form	exact-mass
Amisulpride	Amisulpride N-oxide	TP.AMINO	-0.87	-0.87	C17H27N3O5S	385.1671
Atenolol	Atenolol-desisopropyl	TP.ATDP	-1.84	-0.78	C11H16N2O3	224.1161
Bezafibrate	2/4-Chlorobenzoic acid	TP.CBA24	-1.29	2.23	C7H5ClO2	155.9978
	3-[(4-chlorobenzoyl)-amino]propanoic acid	TP.BZCPA	-2.12	1.37	C10H10ClNO3	227.0349
Benzotriazole	1-Methyl-Benzotriazole	TP.BEZM	1.42	1.42	C7H7N3	133.0640
	4-Hydroxy-1H-Benzotriazole	TP.BEZ4H	0.30	1.00	C6H5N3O	135.0433
	1-Hydroxy-Benzotriazole	TP.BEZ1H	-0.75	0.63	C6H5N3O	135.0433
	4/5-Methylbenzotriazole	TP.BEZ5M	1.72	1.78	C7H7N3	133.0640
Carbamazepine	Carbamazepine epoxide	TP.CEPX	1.97	1.97	C15H12N2O2	252.0899
	Carbamazepine-10-11-dihydro-10-11-dihydroxy	TP.CDH	0.81	0.81	C15H14N2O3	270.1004
	Acridine	TP.CAI	3.50	3.51	C13H9N	179.0735
	Acridone	TP.CAO	4.20	4.20	C13H9NO	195.0684
	Iminostilbene	TP.CIMI	3.78	3.78	C14H11N1	193.0891
Citalopram	Citalopram carboxylic acid	TP.CITCA	0.82	0.83	C20H22FNO3	343.1584
	Citalopram didesmethyl	TP.CITDD	1.07	2.95	C18H17FN2O	296.1325
	Desmethyicitalopram	TP.CITDM	1.18	3.38	C19H19FN2O	310.1481
Diclofenac	4-Hydroxydiclofenac	TP.DIC4H	0.30	3.96	C14H11Cl2NO3	311.0116
	Diclofenac amide	TP.DAM	3.80	3.80	C14H9Cl2NO	277.0061
	Homogentisic acid	TP.DICHA	-2.52	1.00	C8H8O4	168.0423
Fluoxetine	4-Trifluoromethylphenol	TP.FLXTM	2.51	2.55	C7H5F3O1	162.0292
Hydrochlorothiazide	Chlorothiazide	TP.CTZ	-0.49	-0.44	C7H6ClN3O4S2	294.9488
	4-Amino-6-chloro-1-3-benzenedisulfonamide	TP.ABS	-1.09	-1.04	C6H8ClN3O4S2	284.9645
Ibuprofen	1-Hydroxyibuprofen	TP.IBU1H	-0.64	2.69	C13H18O3	222.1256
	2/3-Hydroxyibuprofen	TP.IBU23H	-0.92	2.37	C13H18O3	222.1256
	Carboxyibuprofen	TP.IBUC	-3.95	2.78	C13H16O4	236.1049
Metformin	Guanylurea	TP.GU	-3.37	-2.03	C2H6N4O	102.0542
Metoprolol	Atenolol acid (Metoprolol acid)	TP.MEA	-1.26	-1.24	C14H21N1O4	267.1471
	alpha-Hydroxymetoprolol	TP.MEH	-0.54	0.84	C15H25NO4	283.1784
Sulfamethoxazole	Sulfamethoxazole N1-glucuronide	TP.SMXG	-4.59	-1.30	C16H19N3O9S	429.0842
	N4-Acetylsulfamethoxazole	TP.SMXA	-0.07	0.86	C12H13N3O4S	295.0627
Sulpiride	Sulpiride N-oxide	TP.SUNO	-0.79	-0.79	C15H23N3O5S	357.1358
Valsartan	Valsartan acid	TP.VAA	-1.83	3.18	C14H10N4O2	266.0804
Venlafaxine	Venlafaxine O-desmethyl	TP.VOD	1.88	2.29	C16H25N1O2	263.1885
	Venlafaxine N-oxide	TP.VNO	1.61	1.61	C17H27NO3	293.1991
	Venlafaxine N-desmethyl	TP.VND	0.87	2.36	C16H25N1O2	263.1885
	Venlafaxine N-N-didesmethyl	TP.VNND	0.77	1.92	C15H23N1O2	249.1729
	Venlafaxine N-O-didesmethyl	TP.VNOD	0.73	1.74	C15H23N1O2	249.1729

4.4.2.3. Non-target/suspect screening of transformation products

From the experimental setup (3.4.1), identification of suspect transformation products in the absence of reference standards was carried out. The suspect biological transformation products were screened by submitting the raw data obtained by RP-LC-ESI-HRMS/MS to the Compound Discoverer program (version 2.1, Thermo Scientific). This allowed for the automated detection (minimum intensity: 10'000, 30% intensity tolerance) and grouping (ESI adducts, isotope peaks) of peak features (characterized by m/z, retention time and intensity) with the subsequent compound assignment (elemental composition based on predefined maximum elemental counts within a mass tolerance of 5 ppm). Mass spectra acquired in positive and negative ESI polarity mode (contained within the same raw data due to ESI polarity switching) were extracted and processed in separate workflows. The underlying suspect list consisted of biological TPs that were either predicted from the molecular formulas of the parent compounds using an Excel spreadsheet (transformations: oxidation, reduction, cleavage, conjugation) or from the molecular structures of the parent compounds using the Eawag-Biocatalysis/Biodegradation Database Pathway Prediction System (Eawag- BBD PPS), http://eawag-bbd.ethyporheic zone.ch/predict/, settings: relative reasoning, no immediate rules, aerobic and anaerobic transformations allowed, 3 generations). The output of the suspect screening were two lists of assigned compounds (one per ESI mode), from which compound time-series were extracted for every experimental treatment (1.3 M time-series in total, peak areas as average/median among replicate flumes). Time-series were prioritized by two approaches, i.e. (1) by only considering series with MS2 information (0.2 million), and (2) by only considering Eawag-BBD PPS predicted compounds independent of the MS2 information (0.6 million). In subsequent steps, target analytes and IS were

excluded, and time-series only further evaluated if the compound matched the suspect list. Another criterion was the absence/minimal presence (maximum peak area in unspiked flumes / minimum peak area in time-series ≤ 20%) of the suspected TP in unfortified flumes. In the first run, 15 unspiked flume samples were considered for this comparison. Because one unspiked sample appeared cross-contaminated, the respective sample was excluded, and the comparison repeated with 14 unspiked samples (approach 1). This time, the peak area ratio threshold of 20% (see above) was only applied, if the suspected compound was present in 7 or more unspiked samples. The final (prioritized) time-series were assigned to 50 hierarchical clusters using the hclust function in R, and clusters grouped (group 1: increase, 2: increase and decrease, 3: other trends). For parent compounds without tentatively identified suspect TP, literature was surveyed, and potential candidates were looked up in Compound Discoverer (Posselt *et al.* 2020).

4.4.3. Quantification of TOC

Determination of TOC in the sediment samples was performed using a liquiTOC II elemental analyzer (Elementar Analysensysteme GmbH, Germany) at the Technical University of Darmstadt, Institute of Applied Geosciences, Darmstadt, Germany. The sediment samples were air-dried for several days, ground to grain sizes less than 2 mm and then homogenized using a riffle splitter. About 10 g was subjected to catalytic high-temperature combustion (400°C) where TOC was converted into CO_2 and quantitatively determined using a nondispersive infrared sensor (NDIR) detector.

4.4.4. Quantification of Nitrate

The concentration of nitrate was determined colorimetrically by a modified method of (Cataldo *et al.* (1975). Slurry samples were centrifuged (13,000 x g, 5 minutes) and

filtered using 0.2 µm-regenerated cellulose membrane filters. To remove nitrite, 1 µl amidosulfuric acid (10%) was added to a 5 µl sample, mixed thoroughly, and incubated at room temperature for 5 minutes. 20 µl of 5 % salicylic sulfuric acid was added and further incubated for 30 minutes at room temperature, followed by the addition of 167 µl 6 M NaOH. The samples were then cooled, and the developed colour (yellow) was measured at 410 nm using a plate reader (BioTek, Germany).

4.4.5. pH

The pH of the liquid samples was determined using a portable pH meter fitted with a pH electrode (InLab 422; Mettler Toledo GmbH, Gießen, Germany).

4.4.6. Salt tracer dilution test /Electrical conductivity

The surface water-pore water exchange flux Qin (Ld^{-1}) and exchange volume V_s were calculated according to the equations 2 and 3:

Equation 2:

$$V_s = \frac{V_w\ (C_0 - C_{eq})}{C_{eq}}$$

Equation 3

$$Q_{in} = kV_w \frac{C_0 - C_{eq}}{C_0}$$

Where V_s is the volume of pore water affected by hyporheic exchanges, V_w is the surface water volume, C_0 is the electrical conductivity at the beginning of the test and C_{eq} is the electrical conductivity at equilibrium. K represents the rate constant of the

concentration change over time. The average residence time [d] was calculated as the ratio between exchange volume and exchange flux (Jaeger *et al.* 2019b).

4.5. Microbiological methods

4.5.1. Solutions and media

Stock solutions and media were prepared with deionized water (Seralpur Pro CN, Germany). The mineral salts and trace metal stock solutions were added to the deionized water to achieve target concentrations and then sterilized by autoclaving (120 °C, 20 minutes).The vitamin solution was filter-sterilized using cellulose membrane filters (0.2 µm pore size) and added to the autoclaved media components after cooling to room temperature. The pH of freshly prepared media was adjusted with filter-sterilized 1N HCl or NaOH.

4.5.1.1 Defined mineral medium DM 1 (Oxic)

Table 3 Mineral defined media solution DM 1 was prepared to attain mineral concentrations measured in the surface water in the River Erpe (Jaeger *et al.* 2019a).

Mineral salt	**mg L^{-1}**
$CaCl_2$	254.7
$NaHCO_3$	25.0
KCl	45.4
$MgSO_47H_2O$	109.7
Na_2SO_4	114.2
KH_2PO_4	2.1
NH_4Cl	28.6
$C_6H_{12}O_6$	150.0
$MnCl_2•4H_20$	7.9
$NaNO_3$	154.8

Trace elements	**mg L^{-1}**
$CuSO_4$	0.96
Na_2SeO_3	0.38
$Na_2Mo_4 \cdot H_2O$	1.03
$Na_2WO_4 \cdot 2H_2O$	2.97
$NiCl_2$	2.72
H_3BO_3	6
$ZnCl_2$	7.16
$CoCl_2$	5.4

Vitamins	**µg L^{-1}**
ribovlavin	0.5
biotin	5
folic acid	5
nicotinic acid	5
pantothenic acid	5
pyridoxal-HCl	5
thiamine	5
choline chloride	5
myoinositol	10
vitmain B12	0.01
lipoic acid	6.26
p-aminobenzoic acid	6.26

4.5.1.2. Defined mineral medium DM 2 (Oxic)

Table 4. Oxic defined mineral medium DM 2 was prepared modified from Balch *et al.* (1979) and Wüst *et al.* (2009).

Mineral salts	**mg L^{-1}**
NaCl	100
$(NH4)_2SO_4$	25
$CaCl_2 \cdot 2H_2O$	10
$MgCl_2 \cdot 6H_2O$	10
NH_4Cl	50
KH_2PO_4	50

Trace salts	**mg L^{-1}**
$C_6H_6NNa_3O_6 \cdot H_2O$	15
$MnSO_4 \cdot H_2O$	5
$FeSO_4 \cdot 7H_2O$	1
$CoCl_2 \cdot 6H_2O$	1
$CaCl_2 \cdot 2H_2O$	1
$ZnSO_4 \cdot 7H_2O$	1
$AlK(SO_4)_2 \cdot 12H_2O$	0.2
$CuSO_4 \cdot 5H_2O$	0.1
H_3BO_3	0.1
$Na_2MoO_4 \cdot 2H_2O$	0.1

Vitamins	**µg L^{-1}**
Biotin	2

Folic acid	2
Pyridoxine hydrochloride	10
Thiamine hydrochloride	5
Riboflavin	5
Nicotinic acid	5
DL-calcium pantothenate	5
vitamin B12	0.1
p-aminobenzoic acid	5
Lipoic acid	5

The pH was adjusted to the prevailing pH in the surface water during sampling (pH 7.3).

Solidified defined mineral medium DM 2 (Oxic)

Oxic solidified mineral medium DM 2 was prepared as indicated in (4.5.1.2.) with the addition of 15 g agar L^{-1}.

4.5.1.3. LB agar medium

Table 5. LB agar medium was prepared according to Sambrook *et al.* (1989) and comprised of:

Compound	**g L^{-1}**
Tryptone	10
Yeast extract	5
NaCl	5
Agar	15

4.5.1.4. LB agar with ampicillin/IPTG/X-Gal

LB medium was prepared (4.5.1.3), autoclaved, and filter-sterilized solutions of ampicillin (100 mg L^{-1}), isopropyl β-D-1-thiogalactopyranoside (IPTG; 120 mg L^{-1}) and 5-bromo-4-chloro-3-indolyl-β-D-galactopyranoside (X-gal; 40 mg L^{-1}) were added when the media cooled to approximately 55 °C. The pH was adjusted to 7.0 before the media was let to solidify.

LB agar with ampicillin

LB medium was prepared (4.5.1.3) autoclaved, and filter-sterilized ampicillin (100 mg L^{-1}) added when the media was cooled to approximately 55 °C.

4.5.1.5. SOC medium

Table 6. The SOC medium was prepared according to Sambrook et al. (1989) and comprised of:

Compound	g L^{-1}
Tryptone	2
Yeast extract	0.5
NaCl	0.06
KCl	0.02
$MgCl_2$	0.2
$MgSO_4$	0.25
Glucose	0.36

The medium was autoclaved prior to addition of filter-sterilized solutions of $MgCl_2$, $MgSO_4$, and glucose.The pH was adjusted to 7.0.

4.5.2. Enrichment and isolation procedures

A sediment subsample from the microcosm supplemented with 400 µM ibuprofen (4.3.1) was subjected to a serial dilution (1:10 (w/v) in oxic defined mineral medium DM 2 (Table 4). The medium was supplemented with 400 µM ibuprofen as only-carbon and energy source. The sediment dilutions were incubated for 21 days at 15°C in the dark for the enrichment of potential ibuprofen degraders. The 10^{-6} dilution was the highest sediment dilution showing turbidity indicative of growth (4.5.3.), and was streak-plated onto the same medium DM 2 solidified with 1% agar. Isolated colonies were then transferred to liquid mineral medium DM 2 containing 400 µM ibuprofen and tested for ibuprofen degrading capabilities under oxic conditions via HPLC (4.4.1.2.). Ibuprofen-degradation positive colonies were purified via repeated streak-plating, picking of single colonies, and transfer to liquid mineral medium DM 2 supplemented with ibuprofen. The purity of the isolates was indicated by the homogeneous colony and cell morphologies as visualized with the microscopy (4.5.4.). At least 5 colonies from each isolate were subjected to PCR, and the 16S rRNA gene was amplified from genomic DNA using primer set 27F/1492R (Horn *et al.* 2005; Frank *et al.* 2008), and the thermocycler program (Table 9). The PCR products were subjected to Sanger-sequencing reactions at Microsynth Seqlab (Göttingen, Germany) followed by a comparison of the 16S rRNA gene sequences from all respective isolates against the NCBI blast search tool within the GenBank database. Nearly complete 16S rRNA gene sequences of the isolates were aligned with closely cultured relatives as indicated by blastn analysis using the ARB-SILVA aligner tool and phylogenetic tree reconstruction performed (4.7.2.).

4.5.3. Growth measurments

Growth of isolates was determined based on optical density measurements at a wavelength of 600 nm using a UV- VIS spectrophotometer (Shimadzu, Japan).

4.5.4. Microscopy

Cell morphology was examined with a Zeiss Axioskop 2 microscope fitted with an Axiocam MR monochrome (TV 2/3"C 0.63X 1069-414) (ZEISS, Germany) in bright field mode and x40 and x100 magnifications.

4.6. Molecular techniques

4.6.1. Extraction of nucleic acids

Nucleic acids were extracted from sediment samples following a modified rapid method for coextraction of DNA and RNA from natural environments (Griffiths *et al.* 2000). Approximately 0.5 g of sediment was placed in 2 ml screw-capped tubes (VWR International) containing 1 g of zirconia/silica beads (0.5 g of Ø 0.5 mm beads and 0.5 g of Ø 0.1 mm beads; BioSpec, Bartlesvill, OK, USA). Extraction was performed by addition of 0.5 ml CTAB extraction buffer (10% (wt/vol) CTAB, 0.7 M NaCl, 240 mM potassium phosphate buffer, pH 8.0) and 0.5 ml of phenol-chloroform-isoamyl alcohol (25:24:1) (pH 8.0). Bacterial cells were lysed by bead-beating at a speed of 5.5 ms^{-1} for 30 s in a FastPrep FP120 bead beater (Thermo Savant, Holbrook, NY, USA). The liquid phase containing nucleic acids was separated by centrifugation (16,000 × g) for 5 min at 4°C and transferred in a new 2 ml microcentrifuge tube on ice. In cases where the liquid phase was considerably unclear (brownish), the samples were placed on ice for 10 min and re-centrifuged. 0.5 ml chloroform/isoamyl alcohol (24:1) was added to the liquid phase, mixed thoroughly by resuspension with a pipette and centrifuged (16,000 × g) for 5 min at 4°C to separate the nucleic acids from residual phenol and

proteins. The upper phase was transferred into a new 2 ml microcentrifuge tube on ice. Two volumes (about 0.8 ml) of precipitation buffer (1.6 M NaCl 30% (wt/vol) PEG 6000) and 2 µl molecular grade glycogen (10mgml^{-1}) were added and the components gently but thoroughly mixed by resuspension with a pipette. A 2-hour incubation on ice was then performed, followed by centrifugation (18,000 × g) for 30 min at 4°C. The supernatant was discarded, and the pellet washed with 0.5 ml ice-cold ethanol (70%) to remove salts. A centrifugation step (18,000 × g) for 5 min at 4°C to remove ethanol was performed, and the pellet was air-dried at room temperature for approximately 5 min. The dry pellet was subsequently resuspended in 50 µl nuclease-free water.

4.6.2. Separation of DNA and RNA

The coextracted nucleic acids were separated by enzymatic digestion. To obtain RNA, DNA was removed by addition of 1 µL RNase free DNAse (1 U µL^{-1}) and 3 µL 10x reaction buffer (100 mM Tris HCl, pH 7.5, 25 mM $MgCl_2$; 1 mM $CaCl_2$) to 26 µL nucleic acid extractions. The reaction mix was then incubated for 60 min at 37°C. DNA was obtained by removing RNA using 1 µL DNase free RNase (10 mg mL^{-1}) added into 20 µL nucleic acids, and the reaction mix incubated for 45 min at room temperature.

4.6.3. Quantification of nucleic acids

The concentration and purity of extracted nucleic acids were determined using a spectrophotometer (ND 1000; NanoDrop, NC, USA). Nucleic acids absorb at 260 nm; hence this wavelength is used to calculate the concentration. The ratio 260/280 is used to assess purity with a ratio of ~1.8 and ~2.0 considered for “pure“ DNA and RNA, respectively. Lower values of the ratio indicate contamination by proteins. The 260/230 ratio considered a secondary measure of nucleic acid purity ranges between

2.0-2.2 for '"pure" nucleic acids with lower ratio values indicating contamination by such compounds as phenol.

Nucleic acids occurring in low concentration were quantified using a fluorescence-based method. DNA and RNA concentrations were determined with Quant-iT® PicoGreen DNA and RiboGreen RNA assay kits (Invitrogen, Germany), respectively, following the manufacturer's protocol (Invitrogen, CA, USA). Fluorescence was measured on a Multiskan™ FC Microplate Photometer (Thermo Fischer Scientific, Germany) and concentrations determined based on external DNA/RNA standards provided by the manufacturer.

4.6.4. Reverse transcription of RNA

Reverse transcription of RNA into cDNA was performed using the SuperScript® IV Reverse Transcriptase kit (Invitrogen, CA, USA). Up to 11µl RNA template was mixed with 1 µl random hexamers (50 µM) and 1 µl dNTP mix (10 mM). The components were briefly centrifuged and heated at 65 °C for 5 min to anneal the primers to the template RNA, then incubated on ice for 1 min. A reverse transcription reaction mix consisting of 4 µl SSIV buffer (5x), 1 µl DTT (100 mM), 1 µl RNaseOUT™Recombinant RNase Inhibitor and 1 µl SuperScript® IV Reverse Transcriptase (200 U/ µl) was prepared in a reaction tube and briefly centrifuged. The annealed RNA and reverse transcription reaction mix were combined, and the reaction mixture incubated at 23°C for 10 min, then for a further 10 min at 55 °C. The reaction was then inactivated by incubating it at 80 °C for 10 min.

4.6.5. Polymerase chain reaction (PCR)

Amplification of DNA and cDNA templates was performed using PCR (Saiki *et al.* 1988). In this dissertation, all PCR analyses targeted the 16S rRNA gene. Published and newly designed primers (Table 7) were employed to amplify full length or specific regions of the gene depending on the objective. The PCR cycles (denaturation, annealing, and elongation steps) were performed using the SensoQuest labcycler (SensoQuest GmbH, Germany).

Table 7. The primers (and their corresponding sequences) used to amplify the 16S rRNA gene and 16S rRNA transcripts (cDNA).

Target gene/plasmid/taxa	**Primer**	**Primer sequence (*5'-3'*)**	**Reference**
16S rRNA gene (Bacteria and Archaea)	U341F	CCTAYGGGRBGCASCAG	(Sundberg *et al.* 2013)
16S rRNA gene (Bacteria and Archaea)	U806R	GGACTACNNGGGTATCTAAT	
16S rRNA gene (Bacteria)	27F	AGA GTT TGA TCM TGG CTC	(Lane 1991)
16S rRNA gene (Bacteria)	907 R	CCG TCA ATT CMT TTR AGT TT	(Lane 1991)
16S rRNA gene (Bacteria)	1492R	TACCTTGTTACGACTT	(Weisburg *et al.* 1991)
pGEM-T vector	M13F	GTA AAA CGA CGG CCA G	(Messing, 1983)
pGEM-T vector	M13R	CAG GAA ACA GCT ATG ACC	
16S rRNA gene (Bacteria)	Eub 341F	C CTACGGGAGGCAGCAG	(Muyzer *et al.* 1993)
16S rRNA gene (Bacteria)	Eub 534R	ATTACCGCG GCTGCTGG	
Actinobacteria (OTU 28)	HGC236F	GCG GCC TAT CAG CTT GTT	(Warnecke *et al.* 2004)
	HGC664R	AGG AAT TCC AGT CTC CCC	
Sphingomonadaceae (OTU 1)	SPF	AAG TCA GAG GTG AAA GCC CG	This study
	SPR	TTG TCC AGT CAG TCG CCT TC	

Acidobacteria Subgroup17/Unclassified (OTU 39)	S17F	TTG TCC AGT CAG TCG CCT TC	This study
	S17R	TCA AGC CTG CTA GTT TCC CG	
Hydrogenophaga (OTU 9)	HYF	GCC TTC GGG TTG TAA ACT GC	This study
	HYR	AAA CGC CAT TCC CAG GTT GA	
Fodinicola/Streptomyces (OTU 15)	FDF	CCT CTT TCA GCA GGG ACG AA	This study
	FDR	AAG TCT GCC CGT ATC GAG TG	
Chloroflexi/Unclassified (OTU 16)	CHF	TCG GGA ATT TTG CGC AAT GG	This study
	CHR	CCT GCC TTC GAG TCG ATC AG	
Gemmatimonadetes/Unclassified (OTU 32)	GMF	AAA CCA CTG TCG GAA GGG AC	This study
	GMR	CGA GCC TGG CAG TCT AGA AG	

4.6.5.1. 'Control' PCR

The integrity of DNA and cDNA templates was verified using 'control' PCR. The first PCR was performed after enzymatic digestion of DNA to confirm that the RNA samples were DNA-free and the second to confirm efficient reverse transcription of RNA to cDNA. The samples were amplified using the primer pairs 27F/907R and the thermal profile (Table 8).

4.6.5.2. Isolate full-length 16S rRNA PCR

PCR was performed using cell suspension or individual isolate colonies as template. The approach used the universal primer pair 27F and 1492 R and the protocol (Table 9) targeting the near-full length 16S rRNA gene of the isolates enriched with ibuprofen (4.3.1). The PCR products were used in the ligation step of cloning.

4.6.5.3. PCR for representative enriched OTUs (4.3.1)

The 16S rRNA gene fragments of the enriched OTUs were amplified using the designed primers and one primer set targeting the Actinobacteria from (Warnecke *et al.* 2004) following the protocol (Table 10).

4.6.5.4. PCR for Illumina sequencing

The amplification for Illumina sequencing were performed at LGC Genomics GmbH (Berlin, Germany). 16S rRNA genes and 16S rRNA were amplified using the primers 341F and 806R targeting the V3-V4 hypervariable region of the 16S rRNA genes of bacteria and archaea (Sundberg *et al.* 2013). First step PCR amplification directly amplified the DNA and cDNA templates using the reagents and thermal profile (Table 11). The second step PCR used the same protocol but the template was 1µl purified PCR product derived from the first step, and the primers were extended with sample-specific multiplex tags.

Table 8. Reagents and thermal profile of the control PCR

PCR reaction mix		Thermal profile			
Reagent (Stock conc.)	Volume (Final conc.)	Step	Temp°C	Time	Cycles
KAPA Taq Buffer B (10x)[a]	3 (1x)	Initial denaturation	95	3 mn	1
$MgCl_2$ (25 mM)[a]	3 (1.5 mM)	Denaturation	95	30 s	
dNTP mix (10 mM)[a]	0,6 (0.2 mM)	Annealing	50	30 s	35
27F (10 µM)[b]	1,5 (0.4 µM)	Elongation	72	90 s	
907R (10 µM)[b]	1,5 (0.4 µM)	Final elongation	72	5 mn	1
KAPA Taq DNA Polymerase (5 $U \cdot \mu l^{-1}$)[a]	0,15 (0.5U)	Storage	4	∞	
PCR-grade water	14,25				
Template	1				

[a] KAPA HiFi Hotstart PCR Kit (KapaBiosystems, WN, US)

[b] See Table 7.

Table 9. Reagents and thermal profile for full length 16S gene PCR

PCR reaction mix		Thermal profile			
Reagent (Stock conc.)	Volume (µl) (Final conc.)	Step	Temp. °C	Time	Cycles
5 PRIME Mastermix (2.5x)[a]	10 (1X)	Initial denaturation	94	10 min	1
$MgCl_2$ (25 mM)	1 (1 mM)	Denaturation	94	30 s	
27F (10 µM)[b]	1 (0.4 µM)	Annealing	52	40 s	35
1492R (10 µM)[b]	1 (0.4 µM)	Elongation	72	90 s	
PCR-grade water	11	Final elongation	72	7	1
Template	1	Storage	4	∞	

[a]5 PRIME GmbH, Hilden, Germany. [b] See table 7.

Table 10. The primer sets used in amplifying representative OTUs (note annealing temperatures) (A) and the thermal profile for their amplifications (B)

A

Target taxa (representative OTUs from amplicon libraries included in the groups targeted)	Primer name	Primer set	Annealing temperature	Reference
Actinobacteria (OTU 28)	HGC236F	5'-GCG GCC TAT CAG CTT GTT-3'	55.5°C	(Warnecke *et al.* 2004)
	HGC664R	5'-AGG AAT TCC AGT CTC CCC-3'		
Sphingomonadaceae (OTU 1)	SPF	5'-AAG TCA GAG GTG AAA GCC CG-3'	58°C	This study
	SPR	5'-TTG TCC AGT CAG TCG CCT TC-3'		
Acidobacteria Subgroup17/Unclassified (OTU 39)	S17F	5'-TTG TCC AGT CAG TCG CCT TC-3'	58°C	This study
	S17R	5'-TCA AGC CTG CTA GTT TCC CG-3'		
Hydrogenophaga (OTU 9)	HYF	5'-GCC TTC GGG TTG TAA ACT GC-3'	58°C	This study
	HYR	5'-AAA CGC CAT TCC CAG GTT GA-3'		
Fodinicola (OTU 15)	FDF	5'-CCT CTT TCA GCA GGG ACG AA-3'	58°C	This study
	FDR	5'-AAG TCT GCC CGT ATC GAG TG-3'		

Chloroflexi/Unclassified (OTU 16)	CHF	5'-TCG GGA ATT TTG CGC AAT GG-3'	58°C	This study
	CHR	5'-CCT GCC TTC GAG TCG ATC AG-3'		
Gemmatimonadetes/Unclassified (OTU 32)	GMF	5'-AAA CCA CTG TCG GAA GGG AC-3'	58°C	This study
	GMR	5'-CGA GCC TGG CAG TCT AGA AG-3'		

B

PCR reaction mix		Thermal profile			
Reagent (Stock conc.)	Volume (Final conc.)	Step	Temp. °C	Time	Cycles
KAPA Taq Buffer B (10x)[a]	3 (1x)	Initial denaturation	95	3 min	1
$MgCl_2$ (25 mM)[a]	3 (1.5 mM)	Denaturation	94	30 s	
dNTP mix (10 mM)[a]	0,6 (0.2 mM)	Annealing	Refer to A	30 s	35
OTU specific (10 µM)[b]	1,5 (0.4 µM)	Elongation	72	90 s	
OTU specific (10 µM)[b]	1,5 (0.4 µM)	Final elongation	72	7 min	1
KAPA Taq DNA Polymerase (5 $U \cdot \mu l^{-1}$)[a]	0,15 (0.5U)	Storage	4	∞	
PCR-grade water	14,25				
Template	1				

[a] KAPA HiFi Hotstart PCR Kit (KapaBiosystems, WN, US)

[b] See Table 10 A.

Table 11. Reagents and thermal profile of the Illumina sequencing PCR

PCR reaction mix		Thermal profile			
Reagent	Volume (Final conc.)	Step	Temp. °C	Time	Cycles
MyTaq buffer (5x)[a]	5 µl (1x)	Initial denaturation	96	2 min	
MyTaq DNA polymerase (1.5 U)[a]	0.5 µl	Denaturation	96	15 s	
BioStabII PCR Enhancer[b]	2 µl	Annealing	50	30 s	30
U341F (15 pmol)[c]	2.5 µl	Elongation	70	90 s	
U806R (15 pmol)[c]	2.5 µl	Final elongation			
DNA/cDNA (5 ng)	1 µl	Storage	4	∞	
nuclease-free water	6.5 µl				

[a] 5x MyTaq™ Reaction Buffer (Bioline Meridian, TN, US)

[b] BioStabII PCR Enhancer (Merck, Darmstadt, Germany)

[c] see table 7.

4.6.6. Quantitative PCR (qPCR)

Quantitative kinetic PCR (qPCR) was used to estimate the numerical abundance of 16S rRNA gene and 16S rRNA sequences of the total bacterial community (Table 12) as well as of some representative OTUs (Table 13). Quantification was performed using the SensiMix™SYBR® & Fluorescein Kit (Bioline Reagents Ltd, UK) and the Bio-Rad iQ5 optical system software version 2.0. (Bio-Rad Laboratories, Inc, CA, US).The quantification of the target genes is based on the intercalation of a fluorescent dye, in this case, SYBR Green with double-stranded DNA. The amplification of the target gene corresponds with an increasing fluorescence signal of the fluorescent dye. The DNA and cDNA samples were diluted 100- and 50-fold, respectively, to reduce potential inhibition by coextracted PCR-inhibiting compounds. Negative controls containing no template were run alongside the samples to assess potential contamination, and only when no amplification was observed in these controls was the assay considered for further analysis. Each sample was assayed in technical quadruplicates to account for pipetting errors. Gene copy numbers were determined based on external standards. The standards were prepared via cloning of the target gene on the pGEM-T vector (4.6.7.) and amplified using the primer set M13F and M13R (Table 7). The PCR products were subsequently purified (4.6.2) and quantified using the Quant-iT dsDNA PicoGreen Assay (4.6.3) to serve as standards based on their calculated copy numbers (equation. 4).

The copy numbers of standards against which the abundance of the target DNA was calculated were initially quantified based on the concentration of the purified M13 PCR products using the ***Equation 4***:

$$C_{TG} = \frac{C_{ST} \times V}{n_{TG} \times MW_{bp}} \times N_A$$

Where C_{TG} is the copy numbers, C_{ST}; concentration of standard (ngµl^{-1}), V; volume of standard used (µl), n_{TG}; length of target gene in basepairs, MW_{bp}; 660 gmol^{-1}(molecular weight of dsDNA (1basepair) and N_A; the Avogadro constant: 6.23 x 10^{23} molecules mol^{-1}.

Table 12. Reagents and thermal profile for total bacterial community qPCR

PCR reaction mix		Thermal profile			
Reagent (Stock conc.)	Volume (µl) (Final conc.)	Step	Temp. °C	Time	Cycles
SensiMix™SYBR®& Fluorescein (2x)[a]	10 (1X)	Initial denaturation	95	10 min	1
$MgCl_2$ (25 mM)[a]	1 (5 mM)	Denaturation	94	30 s	
EUB 341 F (25 µM)[b]	1 (250 nM)	Annealing	55.7	40 s	35
EUB 534 R (25 µM)[b]	1 (250 nM)	Elongation	72	40 s	
BSA[c]	1 (150 ng/µl)				
PCR-grade water	10	Final elongation	72	5	1
Template	1	Storage	4	∞	

[a]SensiMix™ SYBR® & Fluorescein Kit (Bioline Meridian, TN, US)

[b]See Table 7.

[c] Pierce ™ Bovine Serum Albumin (Thermo Fisher Scientific, Germany).

Table 13. Reagents and thermal profile for specific OTU qPCR

PCR reaction mix		Thermal profile			
Reagent (Stock conc.)	Volume (µl) (Final conc.)	Step	Temp. °C	Time	Cycles
SensiMix™SYBR®& Fluorescein (2x)[a]	10 (1X)	Initial denaturation	95	3 min	1
$MgCl_2$ (25 mM)[a]	1 (5 mM)	Denaturation	94	30 s	
F. primer (25 µM)[b]	1 (250 nM)	Annealing	Variable (Table 11A)	30 s	35
R. primer (25 µM)[b]	1 (250 nM)	Elongation	72	90 s	
BSA[c]	1 (150 ng/µl)				
PCR-grade water	10	Final elongation	72	7	1
Template	1	Storage	4	∞	

[a]SensiMix™ SYBR® & Fluorescein Kit (Bioline Meridian, TN, US)

[b]See Table 10 A.

[c] Pierce ™ Bovine Serum Albumin (Thermo Fisher Scientific, Germany).

4.6.7. Cloning

Purified PCR products for whole bacteria community and OTU-specific taxa analyses were inserted into pGEM®-T vector plasmid (pGEM®-T System, Promega, Germany) via ligation. The ligation reaction consisted of 2.5 µl Rapid ligation buffer, 0.5 µl pGEM®-T vector, 1 µl PCR product, 0.5 µl ligase filled up to 5 µl molecular-grade water. The ligation reaction was first incubated at room temperature for 1 hour and subsequently overnight at 4°C to allow ligation of the DNA fragments into the vector plasmid.

3 µl of the ligated vector plasmids were mixed with 50 µl cultures of competent *E.coli* JM 109 cells (Promega) and incubated for 30 min on ice. The transformation was conducted through a heat shock at 42°C for 50 sec in a water bath. The cells were immediately placed back on ice following the heat shock. The cells were added to 950 µl SOC medium (4.5.1.5.) and incubated for 1 hour at 37°C on a shaker at 150 rpm. The cell suspension was centrifuged for 5 min at 5000x g and approximately 800 µl supernatant discarded. The remaining cell suspension was resuspended and then streaked on LB Agar plates with Ampicillin, IPTG and XGAL (4.5.1.4.). The agar plates were incubated overnight at 37 °C and blue/white screening of the colonies performed. The ampicillin inhibited the growth of plasmid-free cells since the vector plasmids encode for β-lactamase, which hydrolyzes ampicillin. Additionally, cells containing vector plasmids lacking the inserts formed blue colonies since the *lacZ*-encoded β-galactosidase that catalyzes the conversion of colourless X-Gal to a blue product was functional as the *lacZ* remained intact. In contrast, cells harbouring the insert within the multiple cloning site located within *lacZ* interrupt expression of the β-galactosidase by *lacZ,* hence such colonies remain white.

The white colonies were picked, resuspended in 30 µl PCR-water and used as the template for M13-PCR (Table 14) to assess insert length and amplification for subsequent Sanger sequencing.

Table 14. Reagents and thermal profile for M13 PCR

PCR reaction mix		Thermal profile			
Reagent (Stock conc.)	Volume (µl) (Final conc.)	Step	Temp. °C	Time	Cycles
KAPA Taq Buffer B (10x)[a]	2 (1X)	Initial denaturation	95	5 min	1
$MgCl_2$ (25 mM)[a]	2 (2.5 mM)	Denaturation	95	60 s	
dNTP mix[a]	2 (0.2 mM)				35
M13 uniF (10 µM)[b]	0.4 (0.2 µM)	Annealing	54	45 s	
M13 uniR (10 µM)[b]	0.4 (0.2 µM)	Elongation	72	90 s	
KAPA Taq DNA Polymerase (5 $U \cdot \mu l^{-1}$)[a]	0.1 (0.025 $U \cdot \mu l^{-1}$)				
PCR-grade water	10	Final elongation	72	5	1
Template	1	Storage	4	∞	

[a] KAPA HiFi Hotstart PCR Kit (KapaBiosystems, WN, US)

[b] See Table 7.

4.6.1. Agarose gel electrophoresis

PCR products were visualized by agarose gel electrophoresis using 1% agarose gel prepared with TAE buffer (40 mM Tris, 20 mM acetate, 1 mM EDTA, pH 8.5, AppliChem GmbH, Darmstadt, Germany) and 10% SYBR Safe DNA Gel Stain

(Invitrogen, Germany). Samples mixed with gel loading dye (4:1) and molecular weight markers (Biovendis, Germany) were loaded into the wells and subjected to an electric current (70 mV for 30 min) to drag them through the gel. Separated fragments were visualized with a UV transilluminator (Herolab, Germany).

4.6.2. Purification of PCR products

PCR products were purified using the MinElute PCR Purification Kit (Qiagen, Germany) following the manufacturer's instructions. 5 volumes of Buffer PB was mixed with 1 volume of the PCR reaction, applied to the MinElute column and centrifuged for 1 min (17,900 x g). The flow-through was discarded, the MinElute column washed with 750 µl Buffer PE and centrifuged for 1 min (17,900 x g). DNA was subsequently eluted from the MinElute column after the addition of 10 µl Buffer EB (10 mM Tris.Cl, pH 8.5) and centrifuged for 1 min (17,900 x g).

4.7. Bioinformatics

4.7.1. Primer design and specificity assessment

Specific primers targeting the OTU sequences (Table 10) were designed using the Primer-Blast tool (https://www.ncbi.nlm.nih.gov/tools/primer-blast/) using default settings (Ye *et al.* 2012). The tool consists of a module (Primer3) to generate candidate primer pairs and another (BLAST) to check the target specificity of the designed primers against the target sequences *in silico*. Synthesis of the designed primers was performed at Seqlab (Microsynth, Germany) and their specificity was assessed with genomic DNA and cDNA from representative samples using PCR (Table 10 B) and gel electrophoresis. The amplified amplicons were subsequently cloned using standard methods (4.6.7.) followed by Sanger-sequencing to ascertain identity as well as specificity of amplification, and to generate the qPCR standards (4.6.6.).

4.7.2. Isolate sequence processing and phylotype assignment

Isolate sequences (4.6.7.) obtained from the Sanger-sequencing reactions were processed with MEGA7 (Kumar *et al.* 2016) and SINA (Pruesse *et al.* 2012) softwares, in addition to the NCBI VecScreen and Blast functions. First, the sequences of vector origin were removed using the VecScreen tool (https://www.ncbi.nlm.nih.gov/tools/vecscreen/) followed by the editing of any sequencing errors in the generated chromatograms using the Trace editor function in MEGA7. The sequences were assigned to novel species based on a similarity threshold of 97 % (Yarza *et al.* 2008). The 16S rRNA gene sequences were aligned with closely cultured relatives as indicated by blastn analysis against GeneBank using the SINA web aligner (www.arb-silva.de/aligner). Subsequently, phylogenetic tree reconstruction was

performed with MEGA7 using the neighbour-joining method (Saitou and Nei 1987) and 1000 bootstrap replications.

4.7.3. Processing of Illumina amplicon sequence data

Raw 16S rRNA gene and 16S rRNA sequences were pre-processed by demultiplexing all libraries using the Illumina bcl2fastq 1.8.4 software. The reads were then sorted by amplicon inline barcodes corresponding to independent samples. The barcode sequences were clipped from sequences after sorting, followed by clipping of sequencing adapter remnants from all reads. Reads with final length < 100 bases were discarded. Primer sequences were removed, the sequence fragments turned into forward-reverse orientation and merged using BBMerge 34.38. 16S pre-processing and Operational Taxonomic Unit (OTU) picking from amplicons was performed with Mothur 1.35.1 (Schloss *et al.* 2009). The sequences containing ambiguous bases (Ns), with homopolymer stretches of more than 8 bases or with an average Phred quality score below 33 were removed. Remaining sequences were aligned against the 16S Mothur-Silva SEED r119 reference alignment. Sequencing error reduction was achieved through preclustering, and elimination of chimera carried out with the uchime algorithm. This was followed by taxonomical classification of the sequences (against the Silva reference classification) and the removal of sequences from domains of life other than Bacteria and Archaea. Single replicates with less than 1000 reads were excluded from further analysis. OTU picking by clustering at the 97 % identity level (using the cluster.split method) and OTU consensus taxonomical calling integrating the taxonomical classification of the cluster member sequences was then performed. The representative sequences of each OTU (with at least 2 observed sequences) were queried against a filtered (unknown and unclassified sequences were removed) version of the ribosomal database project release 11.4 reference. A summary table

with taxonomy and alignment details for each OTU representative sequence was generated. The OTU relative abundance data filtered for low-abundance OTUs was subsequently generated with QIIME 1.9.0 from rarified data based on the sample with the minimum number of sequences or variance filtered and normalized (total sum scaling resulting in relative abundances) according to default settings in the Microbiome Analyst pipeline (Dhariwal *et al.* 2017). Please note that the Silva r119 used in this dissertation classifies the “Betaproteobacteria” as “Betaproteobacteriales”, an order of the Gammaproteobacteria. Thus, genera and higher taxonomic ranks that formerly represented “Betaproteobacteria” now belong to “Gammaprotobacteria”.

4.7.4. Accession numbers

Illumina and Sanger sequence data were deposited in the NCBI Sequence Read Archive (SRA) and GenBank nucleotide sequence databases, respectively.

Table 15. Accession numbers of sequences obtained in this dissertation

Sample/Experiment	**Accession number**	**Repository**
Ibuprofen degradation (4.3.1)	PRJNA529686	SRA
Metoprolol degradation (4.3.2)	PRJNA587738	SRA
TOC impact on TrOC degradation (4.3.3)	PRJNA633609	SRA
Flume study (4.3.4)	PRJNA531245	SRA
Novosphingobium sp. strain CR1	MK910996	GenBank
Pseudomonas thivervalensis strain MAH1	MN317372	GenBank
Uncultured Gemmatimonadetes	MK732967	GenBank
Uncultured Chloroflexi	MK732966	GenBank
Uncultured *Fodinicola*	MK732965	GenBank
Uncultured *Hydrogenophaga*	MK732964	GenBank
Uncultured Acidobacterium	MK732963	GenBank
Uncultured Sphingomonadaceae	MK732962	GenBank

4.8. Calculations and Statistical analyses

4.8.1. Concentration of solutions

Stock solutions were prepared to desired concentration (mol L^{-1}) by adding a defined mass of the target compound (g) into a defined volume (L) of solvent i.e. water based on the molar mass of the compound ($gmol^{-1}$):

$$m = cMV$$

Where m is the amount of compound in g; c, concentration of the compound in solvent; M, molar mass of the compound; V, the volume of the solvent in Liters.

The stock solutions were added to the microcosms and media to achieve a final working concentration depending on the total volume of the water or media used in the setups based on the ***Equation 5***:

$$V_{st} = \frac{c_w V_w}{c_{st}}$$

Where V_{st} is the volume of the stock solution; c_w, working concentration; V_w, working volume; c_{st}, concentration of stock solution.

4.8.2. Removal efficiency

The removal efficiency of test compounds was calculated as a percentage of the initial concentration amended into the microcosms using the ***Equation 6***:

$$R_E = \frac{C_0 - C_f}{C_0} \times 100$$

where R_E is the removal efficiency; C_0 and C_f are initial and equilibrium concentrations (μgL^{-1}), respectively.

4.8.3. Sample mean and Standard deviation

Sample means and standard deviations were calculated from values obtained from all replicates in a biological sample using the equations.

Equation 7*:* Mean

$$\bar{x} = \left(\frac{\sum_{i=1}^{n} x_i}{n}\right)$$

Where $\bar{x}$ represents the mean; *n*, number of replicates; *i*, number running from 1 to n. *xi*, actual values measured in each of the replicates in the sample.

Equation 8*:* Standard deviation (SD)

$$SD = \sqrt{\frac{\sum_{i=1}^{n}(x_i - \bar{x})^2}{n-1}}$$

4.8.4. Analysis of Variance (ANOVA)

In estimating differences between means of more than two sample groups, analysis of variance (ANOVA) was used. The output was based on the variance between and within sampling groups. ANOVA was implemented in SigmaPlot and PAST 3 software (Hammer *et al.* 2001).

4.8.5. ANalysis Of SIMilarity (ANOSIM)

The ANOSIM test was applied to assess if there were significant differences in the microbial community composition among sample groups. The test is the equivalent of ANOVA-like hypothesis test in evaluating non-parametric multivariate data and compares the mean of ranked dissimilarities between groups to the mean of ranked dissimilarities within groups. The ANOSIM R statistic is used to assess the statistical

significance An R value close to "1.0" suggests dissimilarity between groups while an R value close to "0" suggests an even distribution within and between groups. An R value below "0" suggests that dissimilarities within groups are greater than between groups (Clarke and Gorley 2001).

4.8.6. DESeq2

DESeq2 (Love *et al.* 2014) is a package in R (R Core Team 2013) used in differential gene expression analysis based on a model using the negative binomial distribution. In this dissertation, DESeq2 was used to evaluate significant differential abundance in OTUs in treated relative to untreated samples (controls) based on the log2Foldchange value. A log2Foldchange value greater than “0” suggested the OTUs were enriched while a log2Foldchange value lower than “0” suggested the OTUs were inhibited/eliminated by the treatment. The differential abundance was considered significant at adj. $p < 0.01$ or $p < 0.05$ using the Benjamin-Hochberg correction.

4.8.7. Linear discriminant analysis effect size analysis

Linear discriminant analysis (LDA) effect size (LEfSe) algorithm (Segata *et al.* 2011) as implemented in the Microbiome Analyst pipeline (Dhariwal *et al.* 2017) was used to identify specific taxa whose relative abundance changed significantly based on 16S rRNA gene and 16S rRNA sequences analysis as evaluated based on Kruskal-Wallis test ($p \leq 0.05$). Moreover, the significant taxa were ranked according to the effect sizes.

4.8.8. Alpha and beta diversity

Within-sample (alpha diversity) and between sample (beta diversity) diversity analyses were evaluated in PAST 3 (Hammer *et al.* 2001). Alpha diversity was determined based on species richness, Shannon diversity and Shannon evenness indices using

rarefied sequence data based on OTUs defined at 97% similarity level and applying post-hoc Tukey test. Species richness accounts for the number of species in a sample without taking their abundances into account. The Shannon diversity index combines measures of richness and abundance while evenness accounts for the spread of individuals among species with low values indicating dominance of one or few species and high value indicating relatively equal distribution of individuals across all present species (Morris *et al.* 2014; Posselt *et al.* 2020).

Beta diversity analysis based on the abundance of OTUs defined at 97% similarity level and the Bray-Curtis distance metric was visualized on a principal coordinate analysis plot (PCoA). Samples exhibiting smaller dissimilarity values in their microbial community composition clustered together compared to those with significantly dissimilar values, with the variation in the dissimilarity matrix observable along the PCoA axes.

4.8.9. Correlation analysis

Spearman's rank correlation coefficient was implemented in SigmaPlot 13 to assess strength and direction of the relationship between different treatments and bacterial diversity indices in (4.3.4). The statistical significance of the coefficient *Rs* value was determined based on *p* value = 0.05.

4.9. Contribution of coworkers

Unless otherwise stated below, sampling, experimental setups, measurements, data analyses and interpretation were performed by me. Most of the data in this dissertation forms components of published papers and manuscripts submitted or in preparation (9) and is presented herein similarly.

4.9.1. Degradation of ibuprofen

Experimental design was conceptualized by Marcus A. Horn and I. Anna Jaeger (Department Ecohydrology, Leibniz-Institute of Freshwater Ecology and Inland Fisheries and Geography Department, Humboldt University Berlin, Berlin, Germany) collected sediment and water samples from the sampling site, Berlin. Kirsten Knoop and Adrian Ho (Institute of Microbiology, Leibniz University of Hannover, Hannover, Germany) assisted with primer design and cloning. Frank Schaarschmidt (Institute of Biostatistics Leibniz University of Hannover, Hannover, Germany) performed preliminary Illumina sequence data analysis. Malte Posselt (Department of Environmental Science, Stockholm University, Stockholm, Sweden) performed HPLC-MS data analysis.

4.9.2. Degradation of metoprolol under oxic and anoxic conditions

Experimental design was conceptualized by me together with Marcus A. Horn. Malte Posselt performed HPLC-MS data analysis.

4.9.3. Impact of TOC on micopollutant removal

Experimental design was conceptualized by Malte Posselt and I. Malte Posselt performed HPLC-MS data analysis. Muhammad Raza (Institute of Applied

Geosciences, Technical University of Darmstadt, Darmstadt and IWW Water Centre, Mülheim an der Ruhr, Germany) analyzed TOC.

4.9.4. Effect of HEF and Bacterial diversity on micropollutant DT50s

This experiment was conducted as part of the “Joint Experiments” within the Marie Skłodowska-Curie Innovative Training Network-HypoTRAIN. The experimental design was carried out by select members within the consortium. These were: Marcus A Horn, Cyrus Rutere (Department of Ecological Microbiology, University of Bayreuth, Bayreuth and Institute of Microbiology, Leibniz University of Hannover, Hannover, Germany). Jonathan P. Benskin, Anna Sobek, Claudia Coll, Malte Posselt (Department of Environmental Science, Stockholm University, Stockholm, Sweden). Anna Jaeger, Karin Meinikmann, Jorg Lewandowski (Department Ecohydrology, Leibniz-Institute of Freshwater Ecology and Inland Fisheries and Geography Department, Humboldt University Berlin, Berlin, Germany). Muhammad Raza (Institute of Applied Geosciences, Technical University of Darmstadt, Darmstadt and IWW Water Centre, Mülheim an der Ruhr, Germany). Jonas Mechelke, Juliane Hollender (Swiss Federal Institute of Aquatic Science and Technology, Eawag, Dubendorf and Institute of Biogeochemistry and Pollutant Dynamics, ETH Zürich, Zürich, Switzerland. Phillip Blaen, Stefan Krause (School of Geography, Earth and Environmental Sciences, University of Birmingham, Birmingham, UK).

Experimental set up and sampling was performed by Malte Posselt, Jonas Mechelke, Anna Jaeger, Claudia Coll, Muhammad Raza, Karin Meinikmann and me.

Measurements, data analyses and interpretation were performed by Malte Posselt, Jonas Mechelke, Anna Jaeger, Claudia Coll (physicochemical data) and me (Microbiological data).

5. RESULTS

5.1. Micropollutant removal potential in the hyporheic zone

5.1.1. Transformation of ibuprofen in hyporheic zone sediments

Degradation of ibuprofen in ibuprofen amended sediments occurred without significant delay except for the 400 µM treatment that exhibited an initial nine-day lag phase (Figure 8 A-D). Ibuprofen was depleted within 11 days for 5 and 40 µM treatments, and within 16 days for 200 and 400 µM treatments. In the presence of acetate, the degradation of ibuprofen tended to be delayed across most concentrations after the first amendment with ibuprofen and acetate (Figure 8 E-H). The initial time for the depletion of ibuprofen depended on the initial ibuprofen concentration as well as acetate supplementation and ranged from 11 – 34 days (Figure 8). After subsequent re-feedings, ibuprofen was degraded entirely within 1-3 days in the presence and absence of acetate, indicating enrichment of ibuprofen degraders. Ibuprofen concentrations were essentially constant in control microcosms containing autoclaved sediment and river water, while ibuprofen was below the detection limit in the unamended microcosms (Figure 9).

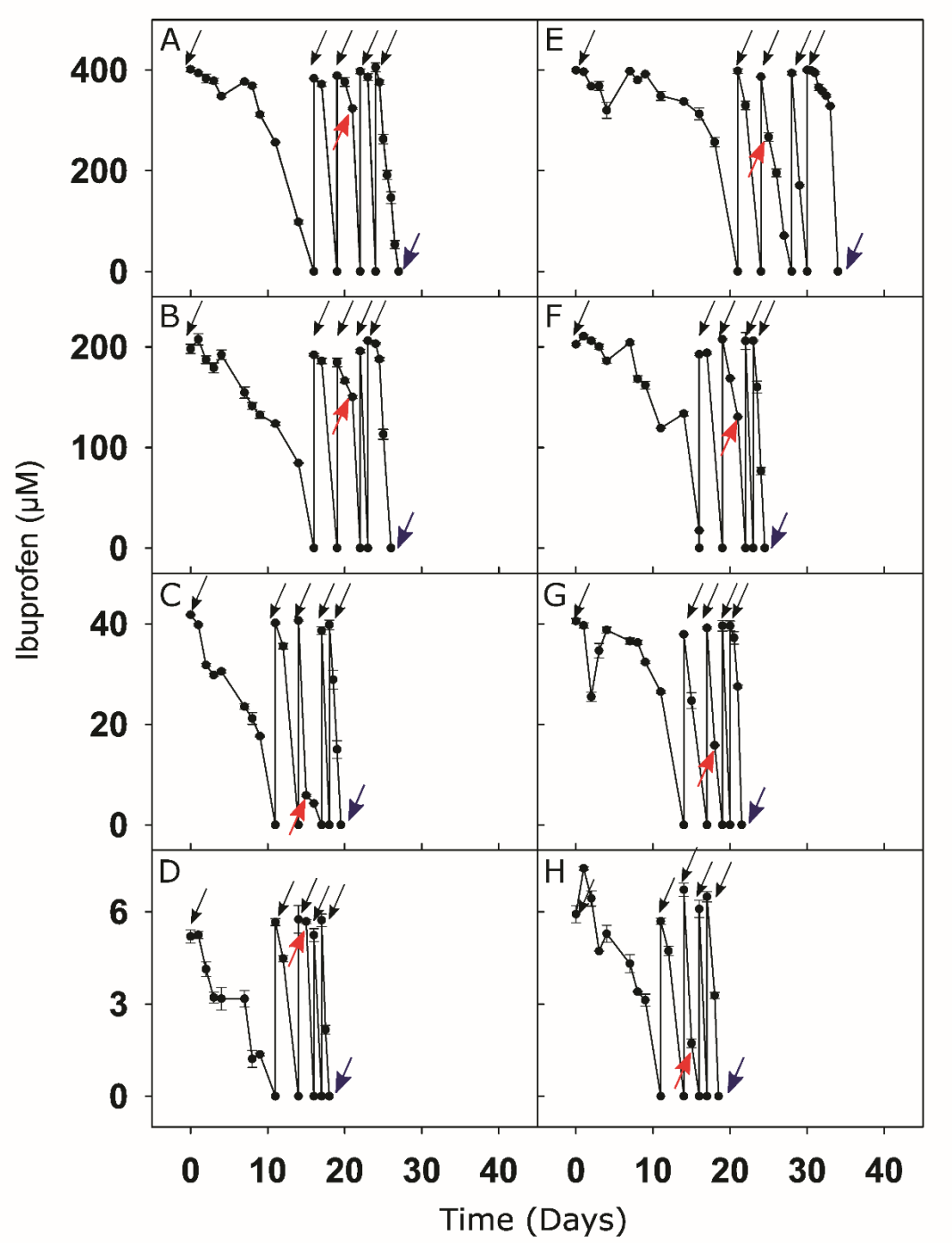

Figure 8. Apparent degradation of ibuprofen in oxic hyporheic zone sediment microcosms. Plots A - D correspond to sediment amended with ibuprofen concentrations of 5 µM, 40 µM, 200 µM and 400 µM, respectively. Plots E- H correspond to sediment amended with both 1 mM acetate and ibuprofen concentrations of 5 µM, 40 µM, 200 µM and 400 µM, respectively. Values are the arithmetic means of triplicate oxic incubations. Error bars indicate standard deviations. Some standard deviations are smaller than the symbol size and therefore not apparent. Arrows indicate the time of refeeding of microcosms with ibuprofen (A - D) and acetate and ibuprofen (E- H), respectively. Red and blue arrows indicate sampling of the sediment for nucleic acid extraction after the third and fifth refeeding, respectively. Figure used with permission from Rutere *et al.* 2020.

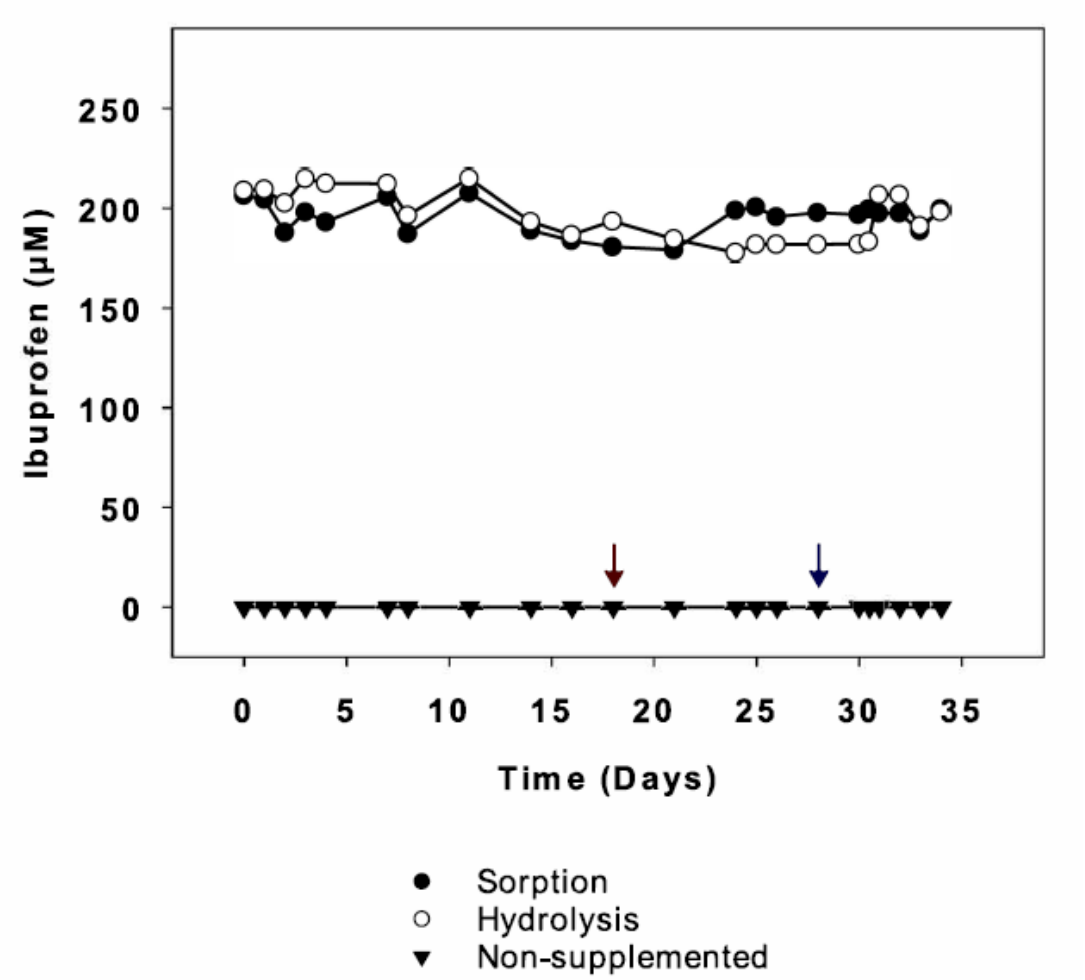

Figure 9. Control microcosms for the ibuprofen degradation experiment (Figure 8). 'Non-supplemented' represents the unamended sediment. The abiotic controls 'Sorption' and 'Hydrolysis' contained autoclaved sediment and river water, respectively, and were amended with 200 µM ibuprofen. Value s are the arithmetic means of three replicate incubations. Red and blue arrows indicate sampling of the sediment for nucleic acids extraction after third and fifth re-spiking, respectively. Error bars indicating standard deviations are smaller than the size of the symbols and therefore not apparent. Figure used with permission from Rutere *et al.* 2020.

Microcosms amended with 200 µM ibuprofen were representative treatments with the highest initial ibuprofen concentration that showed ibuprofen degradation without appreciable delay as well as a quick ibuprofen degradation after the fourth re-feeding and were thus chosen for in-depth transformation product analysis. 1-Hydroxyibuprofen, 2-hydroxyibuprofen, 3-hydroxyibuprofen and carboxyibuprofen

were transiently detected, suggesting that such compounds were transformation intermediates (Figure 10). 2-hydroxyibuprofen was the main transformation intermediate and was likewise rapidly removed.

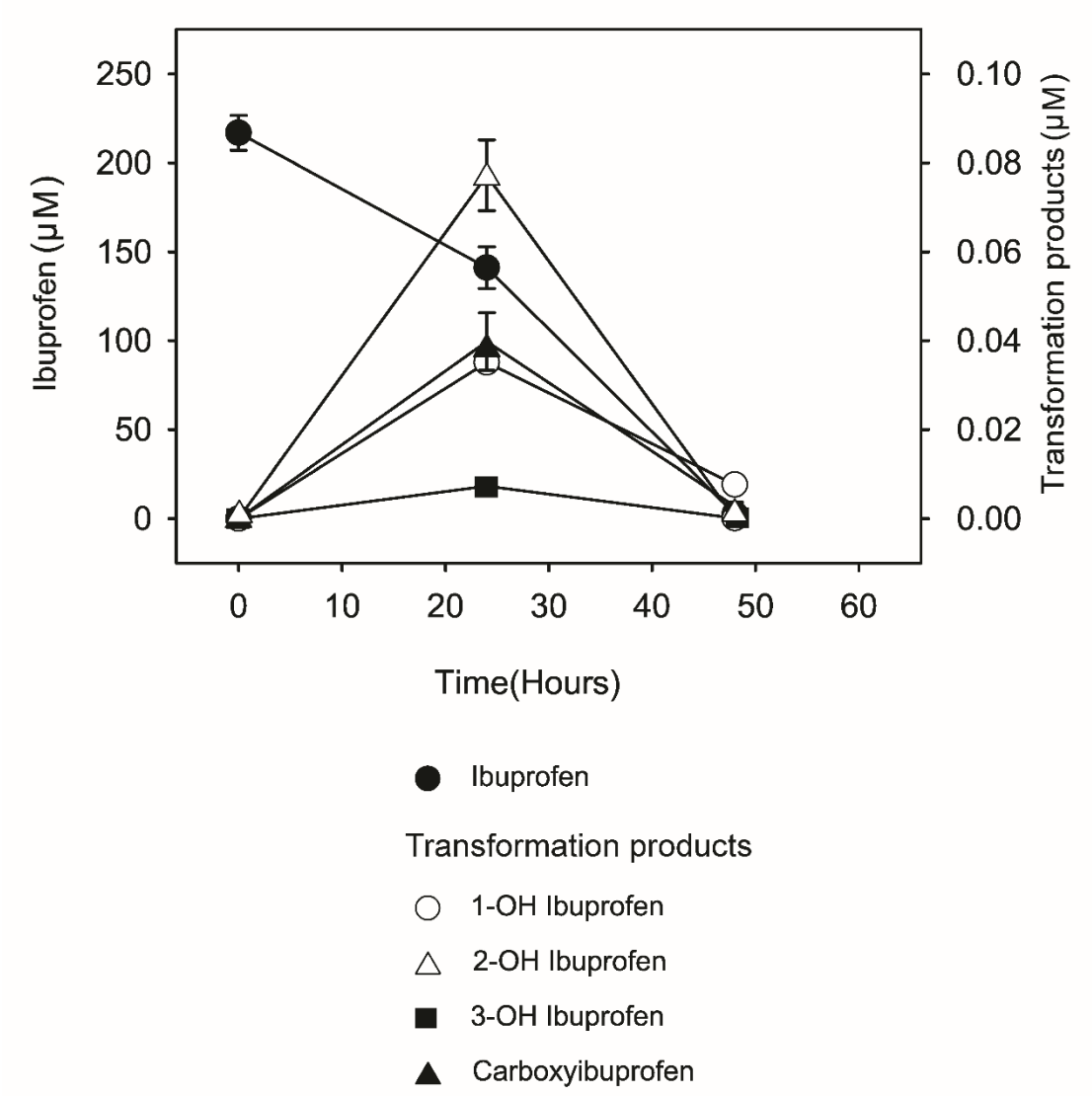

Figure 10. Ibuprofen transformation products in oxic hyporheic zone sediment microcosms amended with 200 µM of ibuprofen (4th respike; see Figure 8B). Values are the arithmetic mean of three replicate incu bations, and error bars indicate standard deviations. Some standard deviations are smaller than the symbol size and therefore not apparent. Figure used with permission from Rutere *et al.* 2020.

5.1.2. Effect of treatments on total bacterial abundance by qPCR analysis

Total bacterial 16S rRNA gene abundance tended to be lower in ibuprofen treatments than in controls based on samples assessed after the third and fifth refeeding (Figure 11). However, such a difference was not significant (ANOVA, $p > 0.05$). The 16S rRNA copy numbers were significantly higher in treatments relative to unamended controls after the third refeeding, but lower than the unamended controls after the fifth refeeding **(**Figure 11) (ANOVA, $p < 0.05$).

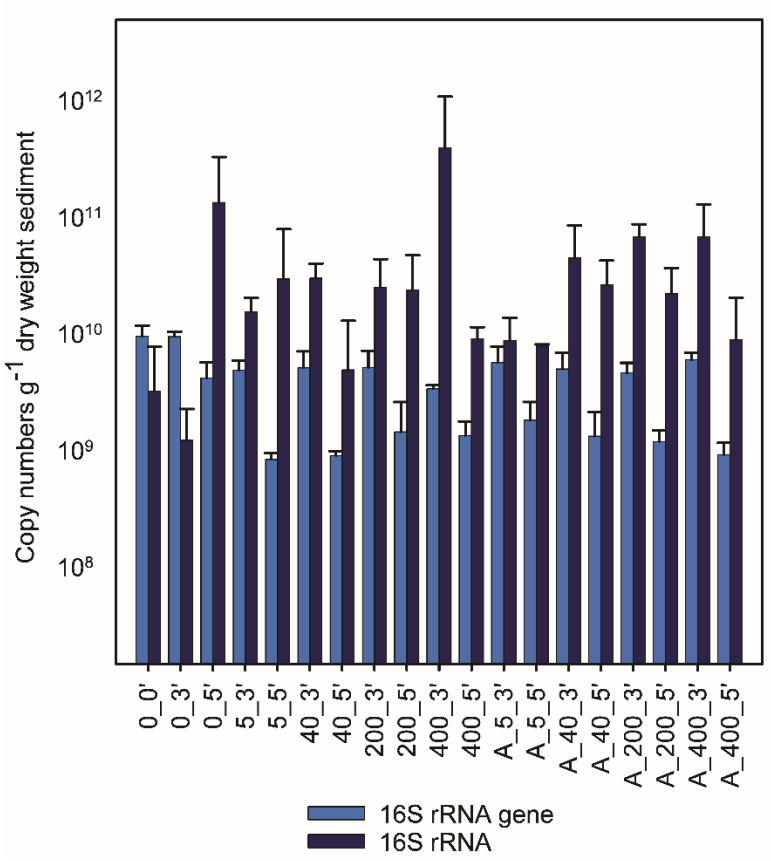

Figure 11. Copy numbers of the 16S rRNA gene and 16S rRNA detected in total bacterial community. Sample code: A, amended with 1 mM acetate and ibuprofen perfeeding; 0, 5, 40, 200, and 400, indicate supplemental ibuprofen concentrations of 0 µM, 5 µM, 40 µM, 200 µM and 400 µM, respectively, given per feeding; 0', 3', and 5', correspond to samples obtained at the start of the incubation, and after the third and fifth refeeding, respectively (see figure 8). Sampling times for unamended controls were according to those of the 400 µM ibuprofen treatment. Values are the arithmetic average of three replicates. Error bars indicate standard deviation values. Figure used with permission from Rutere *et al.* 2020.

5.1.3. Effect of treatments on alpha and beta diversity

The resultant number of 16S rRNA gene and 16S rRNA sequences per sample ranged from 10,767 to 19,244 and 11,616 to 19,397, respectively. The datasets were normalized to a uniform sequencing depth based on the sample with the lowest sequences for diversity analyses. Alpha diversity from samples taken after the third and fifth refeeding revealed significantly lower Shannon diversity (ANOVA, $p \leq 0.05$) at the OTU level in samples amended exclusively with ibuprofen or ibuprofen-acetate relative to unamended controls (Figure 12). Species richness tended to follow the same trend; however, differences were not significant (ANOVA, $p > 0.05$) (Figure 12).

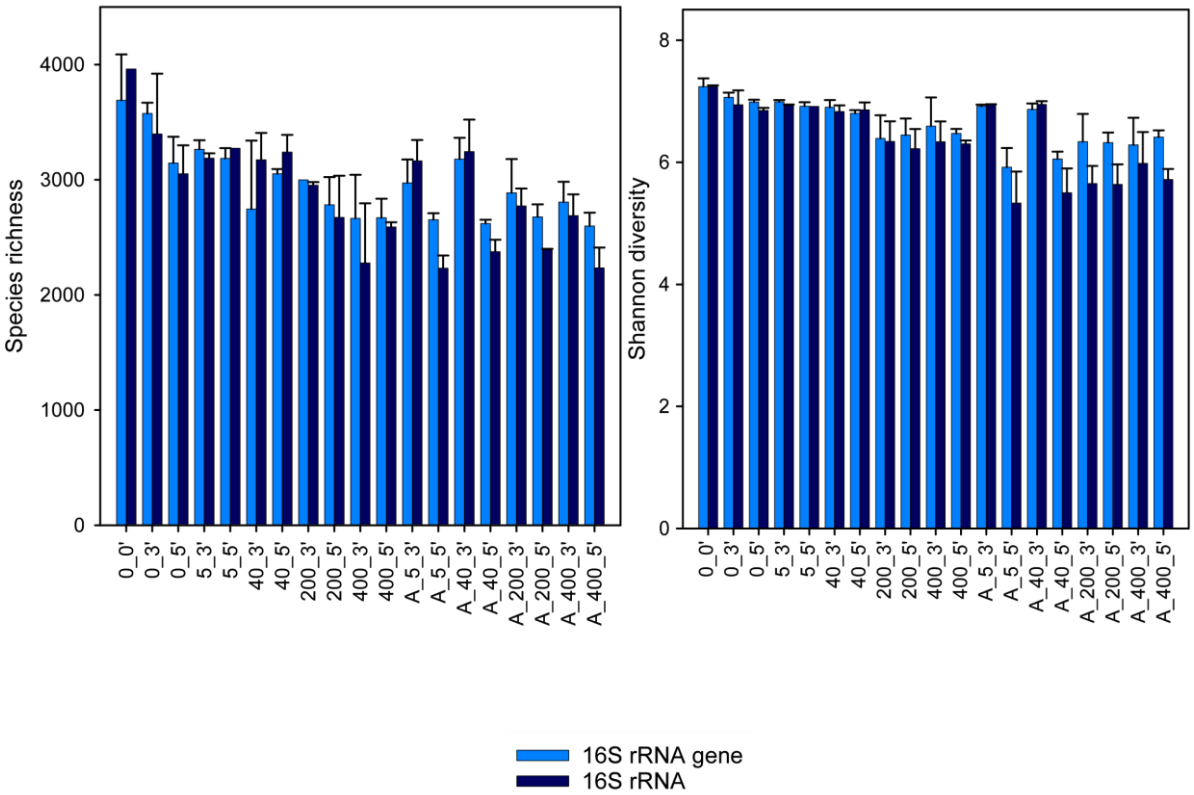

Figure 12. Alpha diversity and richness estimators of 16S rRNA gene and 16S rRNA obtained from Illumina amplicon sequencing. Sample code: A, amended with 1 mM acetate and ibuprofen per feeding; 0, 5, 40, 200, and 400, indicate supplemental ibuprofen concentrations of 0 µM, 5 µM, 40 µM, 200 µM and 400 µM, respectively, given per feeding; 0', 3', and 5', correspond to samples obtained at the start of the incubation, and after the third and fifth refeeding, respectively. Sampling times for unamended controls were according to those of the 400 µM ibuprofen treatment. Values are the arithmetic average of three replicates. Error bars indicate standard deviation values. Figure modified and used with permission from Rutere *et al.* 2020.

Beta diversity visualization using Principal Coordinate Analysis (PCoA) based on Bray-Curtis distances indicated that microbial communities in ibuprofen and ibuprofen-acetate treatments were distinct from the unamended controls and original sediment before incubation based on 16S rRNA gene and 16S rRNA sequences, respectively (Figure 13 A and B). Consistently, two-way ANOSIM tests indicated that in samples amended exclusively with ibuprofen, both ibuprofen treatment (DNA: $R = 0.7$, RNA: $R = 0.63$, $p < 0.0001$) and incubation time (DNA: $R = 0.98$, RNA: $R = 0.98$, $p < 0.0001$) contributed significantly to the differences in the microbial community composition among the samples. Similarly, ibuprofen-acetate treatment (DNA: $R = 0.75$, RNA: $R = 0.72$, $p < 0.0001$) and incubation time (DNA: $R = 1$, RNA: $R = 0.99$, $p < 0.0001$) also contributed significantly to the differences in the microbial community composition of the corresponding samples. The R-values greater than 0.6 indicated a rather strong dissimilarity between microbial communities from different treatments and time points. Communities from treatments amended with low and high ibuprofen concentrations (i.e., 5-40 and 200-400 µM, respectively) formed clusters separated along axis 1, suggesting a dose-dependent effect of ibuprofen (Figure 13 A and B).

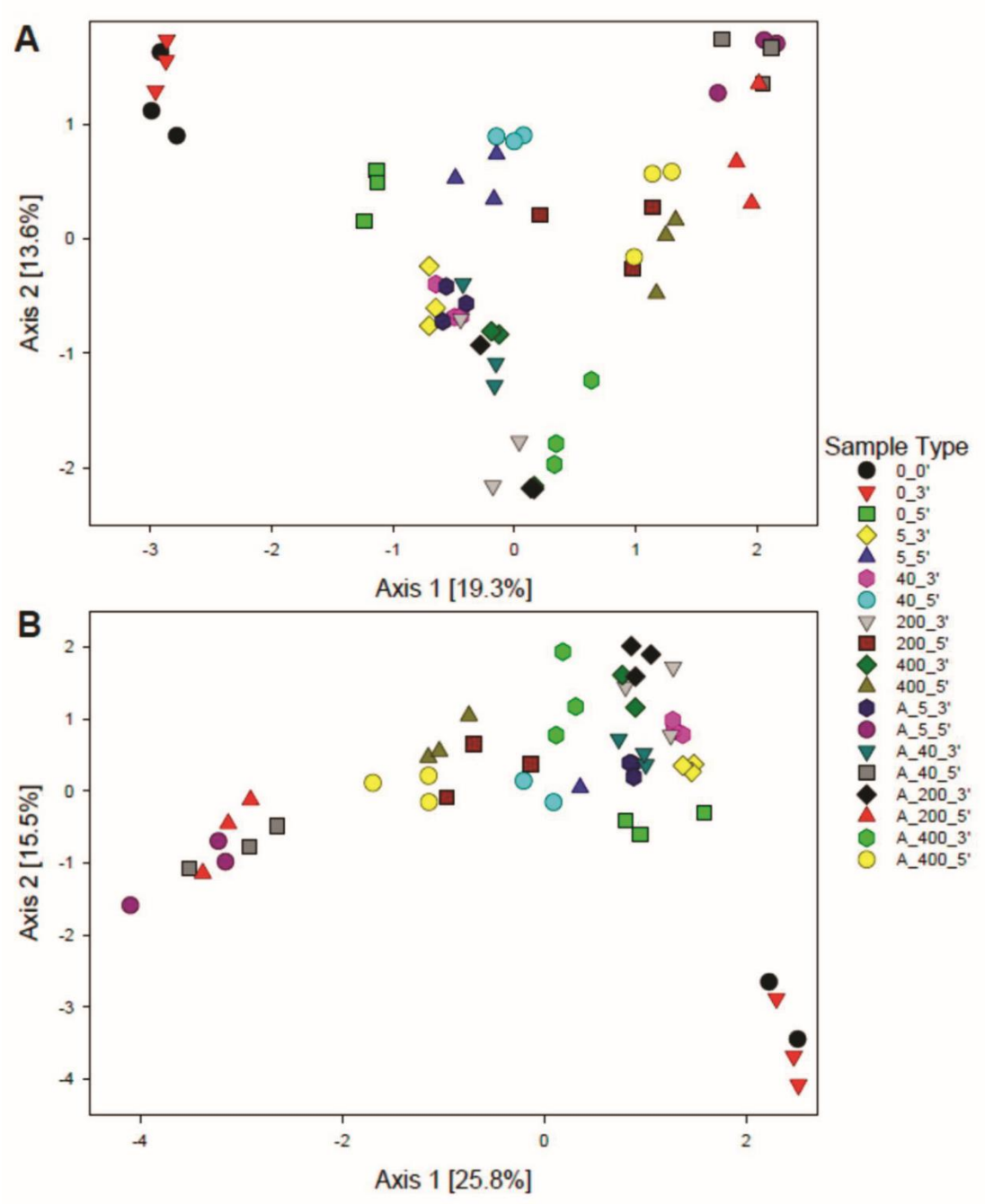

Figure 13. Principal coordinate analysis of the Bray Curtis dissimilarity metric showing the effect of ibuprofen and ibuprofen/acetate treatments on the bacterial community composition based on OTUs from 16S rRNA gene (panel A) and 16S rRNA (panel B). Sample code: A, amended with 1 mM acetate and ibuprofen per feeding; 0, 5, 40, 200, and 400, indicate supplemental ibuprofen concentrations of 0 µM, 5 µM, 40 µM, 200 µM and 400 µM, respectively, given per feeding; 0', 3', and 5', correspond to samples obtained at the start of the incubation, and after the third and fifth refeeding, respectively. Sampling times for unamended controls were according to those of the 400 µM ibuprofen treatment. Figure used with permission from Rutere *et al.* 2020.

5.1.4. Effect of treatments on general phylum-level taxonomic composition

The dominant phyla (>1% relative abundance) on both DNA and RNA levels were Proteobacteria, Chloroflexi, Acidobacteria, and Actinobacteria, followed by Firmicutes, Bacteroidetes, Gemmatimonadetes, Latescibacteria, and Nitrospirae (Figure 14 A and B). Such phyla were among the top ten based on linear discriminant analysis (LDA) score on DNA and RNA level, explaining differences among treatments (Figure 14 C). Proteobacteria, Acidobacteria, Bacteroidetes, Gemmatimonadetes and Latescibacteria tended to be stimulated by ibuprofen or ibuprofen and acetate (Figure 14). Actinobacteria and Chlorobi showed a variable response to the treatments when DNA and RNA levels were compared. Interestingly, Acidobacteria, Gemmatimonadetes and Latescibacteria appeared to be stimulated in treatments with low concentrations of ibuprofen (5-40 µM) in the absence of supplemental acetate on DNA and RNA level. Proteobacteria were most abundant in amplicon libraries of treatments with acetate and high concentrations of ibuprofen (200-400 µM). Such a finding was attributed primarily to the Gammaproteobacteria (data not shown). Bacteroidetes responded to all ibuprofen concentrations with a high relative abundance in amplicon libraries. Such a high relative abundance was particularly prominent on RNA level in treatments with high concentrations of ibuprofen (200-400 µM). Chloroflexi, Firmicutes and Nitrospirae tended to decrease on average in relative abundance in response to ibuprofen. Archaeal sequences were generally less abundant than bacterial sequences in amplicon libraries, affiliated primarily with Thaumarchaeota and Euryarchaeota. Likewise, they tended to decrease in response to ibuprofen treatments on DNA and RNA level except for Thaumarchaeota that tended to be stimulated on RNA level with low ibuprofen concentrations.

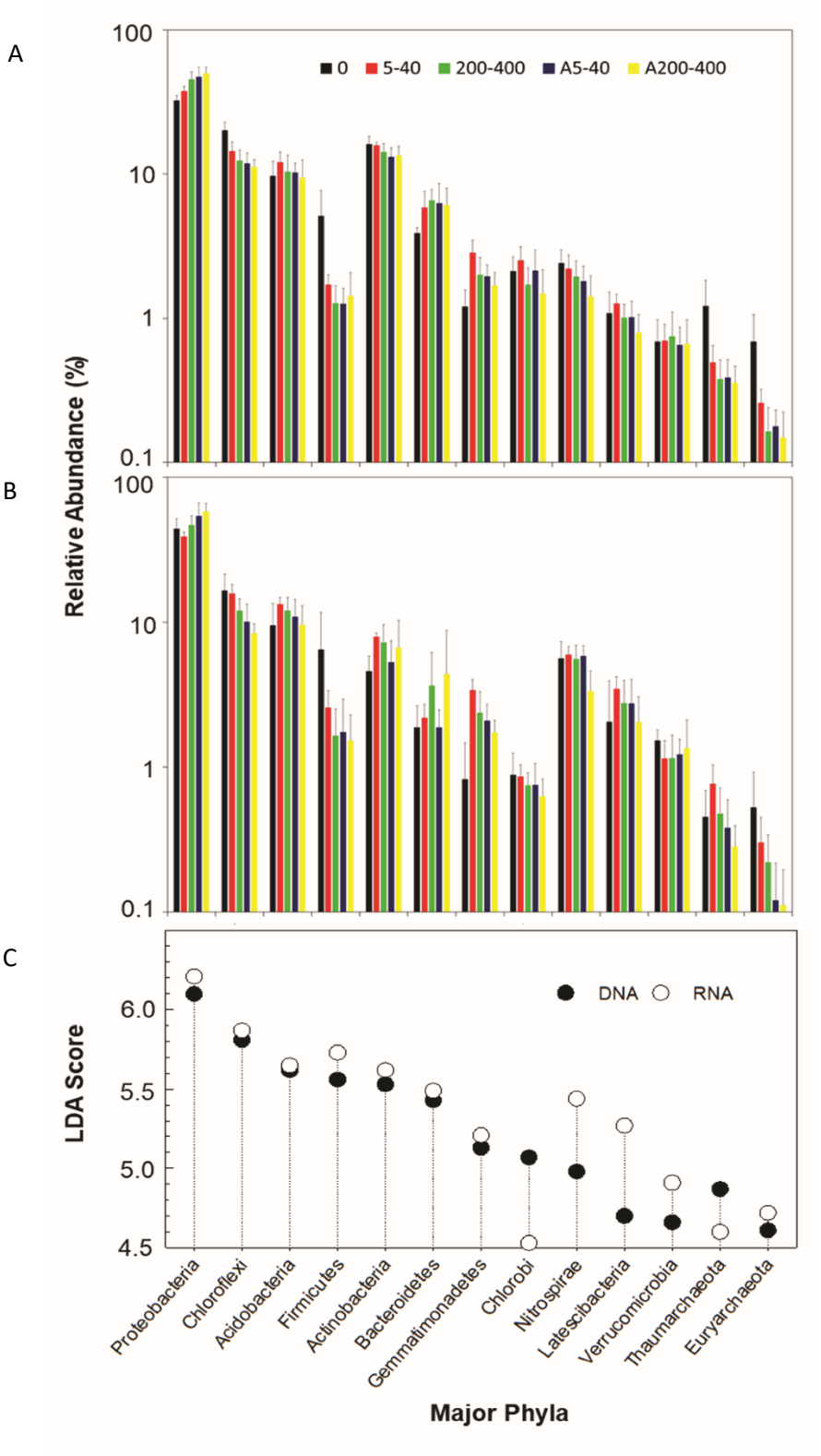

Figure 14. Relative abundance of major bacterial (greater than 1% relative abundance) and archaeal phyla on DNA (A) and RNA (cDNA, B) level, as well as corresponding LDA scores (C). Archaea are indicated by the grey box. Values and error bars represent means from all time points per treatment (see Figures 8, 9) of up to 12 samples and standard deviation, respectively. 0, unamended controls; 5-40, 'low ibuprofen treatments' with 5 and 40 µM ibuprofen; 200-400, 'high ibuprofen treatments'

with 200 and 400 µM ibuprofen; A5-40, ‘low ibuprofen treatments’ with supplemental 1 mM acetate; A200-400, ‘high ibuprofen treatments’ with supplemental 1 mM acetate. Filled and open circles, DNA and RNA (cDNA) level, respectively. Figure used with permission from Rutere *et al.* 2020.

5.1.5. Effect of treatments on family-level taxonomic composition

Pseudomonadaceae, Sphingomonadaceae, and Commamonadaceae were the families with the highest LDA scores that had on average higher relative abundances in ibuprofen treatments compared to non-supplemented controls on DNA and RNA level (Figure 15), which was likewise reflected in the OTU based analysis (Figures 16 and 17) and following phylum level analysis. Notably, such families were consistently crucial in ibuprofen and ibuprofen-acetate treatments. Other families that had high LDA scores and higher relative abundances in amplicon libraries from ibuprofen treatments compared to non-supplemented controls on DNA and RNA level included Gemmatimonadaceae, Xanthomonadaceae, Nocardioidaceae, Flavobacteriaceae, Sandaracinaceae and Cytophagaceae (Figure 15 A), suggesting that members of these families were stimulated in ibuprofen treatments. Bdellovibrionaceae were likewise stimulated. In contrast, LDA scores of family-level taxa that had lower relative abundances in ibuprofen treatments compared to non-supplemented controls on DNA and RNA level suggested a negative impact of ibuprofen (Figure 15 B). Many well-known anaerobes (e.g., Caldilineaceae, Peptostreptococcaceae, Desulfobacteraceae and Syntrophaceae) as well as aerobic nitrifiers of the Nitrospiraceae and uncultured families met such a criterion, suggesting that anaerobic processes such as primary, and secondary syntrophic, fermentations and nitrification might be impaired by ibuprofen.

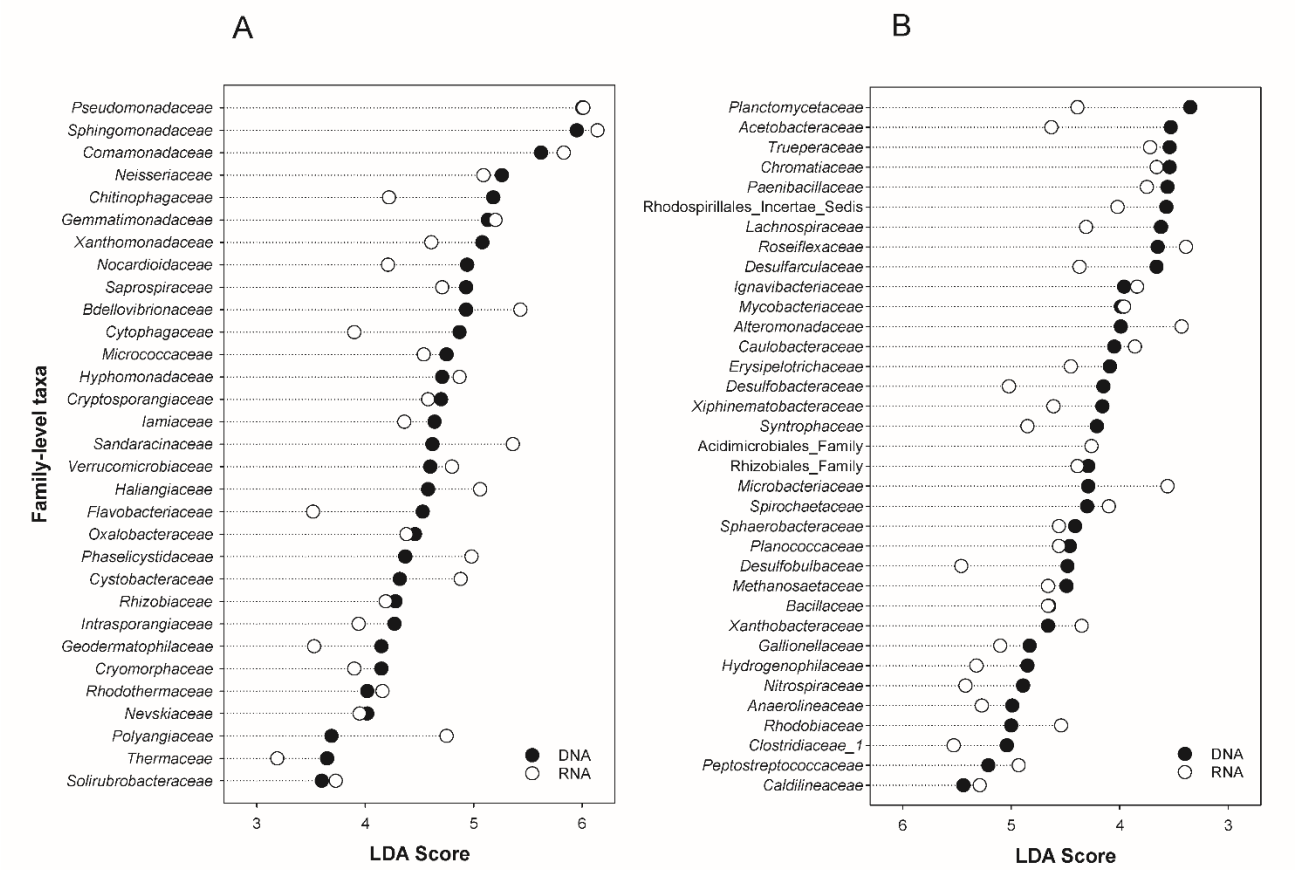

Figure 15. Linear discriminant analysis (LDA) scores on DNA and RNA level for families that were more (A) or less (B) abundant in treatments with ibuprofen relative to non-supplemented controls and displayed a consistent response on DNA and RNA level. Figure used with permission from Rutere *et al.* 2020.

5.1.6. OTU-level taxa associated with ibuprofen degradation

Differential abundance analysis was performed to identify ibuprofen responsive OTU-level taxa. Taxa whose abundances significantly changed in ibuprofen treatments relative to unamended controls (log2foldchange > 0.5; $p < 0.05$) were considered enriched and thus candidate taxa for representing ibuprofen degraders. Many OTUs (78 to 92) were enriched in ibuprofen treatments representative for high and low ibuprofen amendments (400 and 40 µM, respectively; Table A1). Consistent with analyses on phylum and family levels, OTUs enriched in response to ibuprofen affiliated primarily with Acidobacteria, Alpha-, Gamma-, and Deltaproteobacteria,

Bacteroidetes, Gemmatimonadetes and Latescibacteria. Cumulated log2fold change values in response to ibuprofen relative to unamended controls suggest a preferential enrichment of OTUs affiliating with Acidobacteria, Chloroflexi, Deltaproteobacteria, Gemmatimonadetes, Latescibacteria and Saccharibacteria with low ibuprofen concentrations of 40 µM on DNA level (Figure 16; Table A1). In contrast, OTUs affiliating with Alpha- and Gammaproteobacteria, Actinobacteria, Bacteroidetes and Verrucomicrobia were more enriched with high ibuprofen concentrations of 400 µM (Figure 16). OTUs affiliating with Alpha-, Gamma-, and Deltaproteobacteria, Actinobacteria and Chlorobi tended to be stimulated by supplemental acetate.

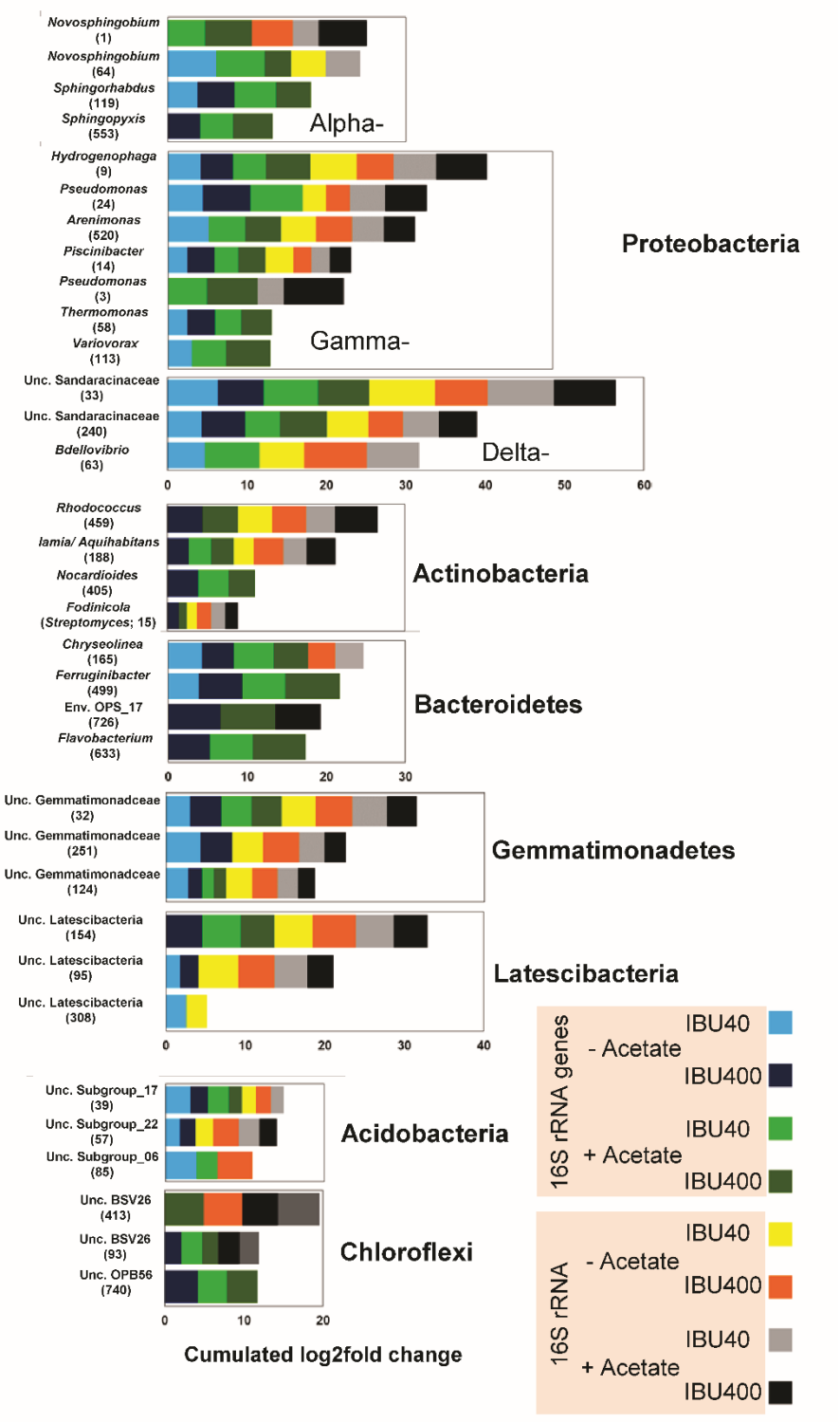

Figure 16. Log2fold change of ibuprofen responsive OTUs summed up for all OTUs affiliating with the same (sub-) phylum (based on data from Table S2). A, DNA; B, RNA (cDNA). OTUs significantly enriched by ibuprofen relative to unamended controls sampled at the same time point had a Log2-fold change > 0 at p-adj < 0.05. IBU40 and IBU400, ibuprofen amendment with 40 and 400 µM ibuprofen, respectively. IBA40 and IBA400, ibuprofen amendment with 40 and 400 µM ibuprofen, respectively, together with 1 mM acetate. Figure used with permission from Rutere *et al.* 2020.

Proteobacteria OTUs dominated ibuprofen responsive taxa in general. Such taxa included alphaproteobacterial *Novosphingobium*, *Sphingomonas*, *Hyphomicrobium* and *Woodsholea* affiliated OTUs, gammaproteobacterial (Betaproteobacteriales affiliating) OTUs related to *Hydrogenophaga*, *Piscinibacter* and *Vogesella*, gammaproteobacterial OTUs related to *Pseudomonas* and *Arenimonas*, as well as OTUs affiliating with *Bdellovibrio* and distantly related to *Sandaracinus*. *Rhodococcus, Lamia/Aquihabitans, Nocardioides* and *Fodinicola* related OTUs along with uncultured taxa were prominent among the Actinobacteria. Ibuprofen enriched important taxa of the Bacteroidetes included *Chryseolinea, Ferruginibacter, Flavobacterium* and uncultured taxa. Ibuprofen enriched OTUs of the Gemmatimonadaceae and Latescibacteria were distantly related to *Gemmatimonas* sp. and to uncultured organisms, respectively. OTUs affiliating with subgroups 6, 17, and 22 within the Acidobacteria were enriched in response to ibuprofen. Notably, some phyla that showed on average a generally variable or even negative response to ibuprofen nevertheless contained OTUs that were enriched in response to ibuprofen (Table A1), demonstrating the need for high taxonomic resolution on OTU level. Such phyla were Chloroflexi (Figure 16; Table A1), Chlorobi (e. g., OTUs 93 and 740), Nitrospirae (e. g., OTU 7 related to *Nitrospira moscoviensis*), and Verrucomicrobia (e.g., OTU 162 related to *Prosthecobacter* sp.). Hitherto uncultured groups (e.g., NS9_marine_group, env. OPS_17, KD4-96; Table A1), enriched by ibuprofen indicate new potential ibuprofen degraders in hyporheic zone sediments. Most of the OTUs enriched in ibuprofen treatments following incubation were detected in the original community and/ or the unamended controls (Table A2). OTUs 1, 15, 32, 95, 39, and 93, indicative of Novosphingobium sp. (Alphaproteobacteria), Fodinicola sp. (Actinobacteria), uncultured Gemmatimonadetes, uncultured Latescibacteria, Acidobacterial subgroup 17, and uncultured Chloroflexi of the BSV26 group, respectively, had relative

abundances of greater than 0.1% in the original community on the DNA level in the non-rarified datasets.

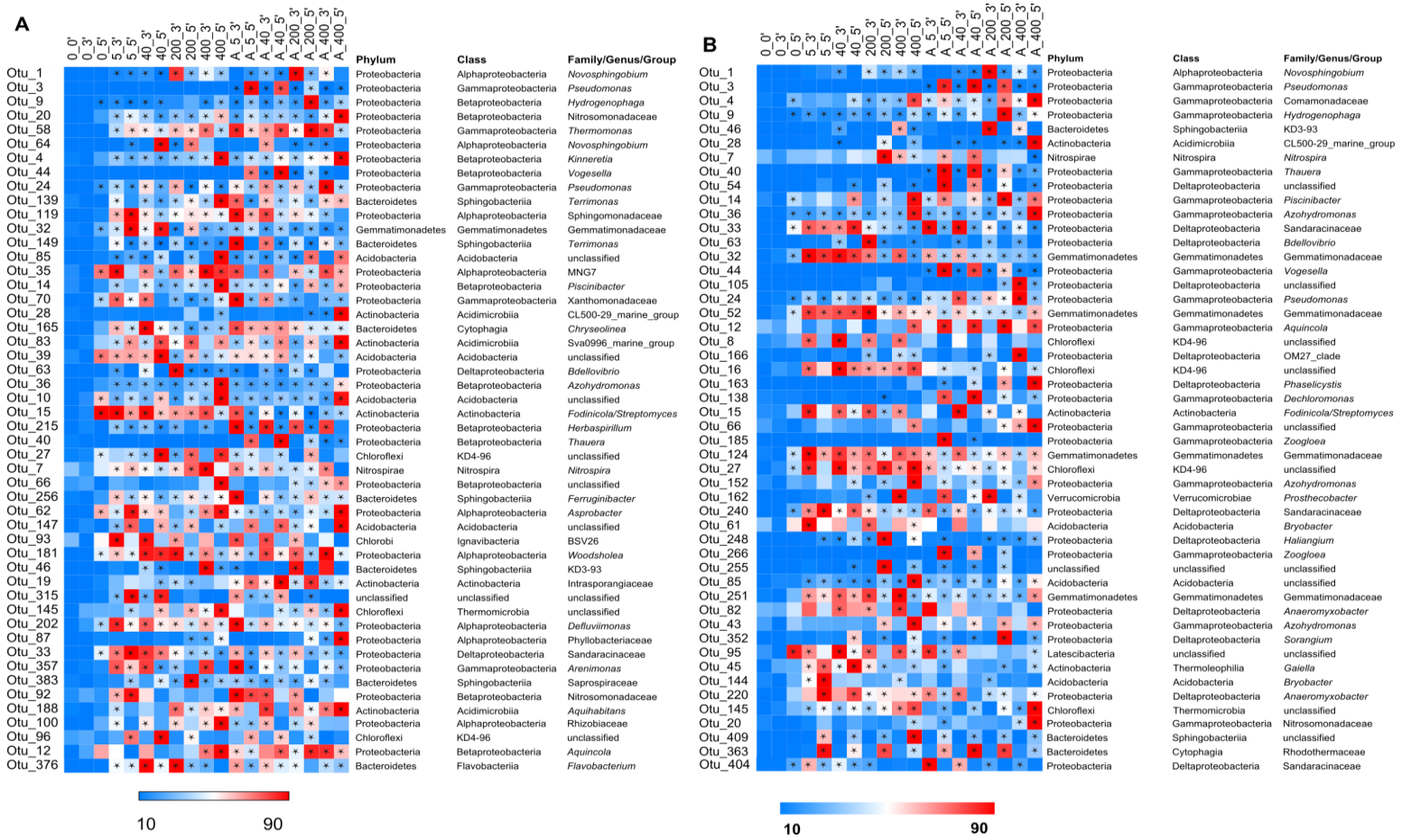

Figure 17. Heat map of LEfSe identified top 50 most differentially abundant taxa based on 16S rRNA gene (A) and 16S rRNA (cDNA; B) amplicon analysis after the third and fifth refeeding (Fig. 1). OTUs are sorted according to the difference in their mean read counts in ibuprofen amended and unamended samples. OTUs with a linear discriminant analysis score of ≥ 4 and their phylogenetic affiliation are shown. The color code reflects median, as well as upper and lower quantiles of read counts normalized to the total number of reads per OTU from all samples. Sample code: A, amended with 1 mM acetate and ibuprofen per feeding; 0, 5, 40, 200, and 400 indicate supplemental ibuprofen concentrations in µM given per feeding; 0', 3', and 5' correspond to samples obtained at the start of the incubation, and after the third and fifth refeeding, respectively. Sampling times for unamended controls were according to those of the 400 µM ibuprofen treatment. *, Samples with significant differential relative abundance compared to the start of the incubation based on DESeq2 (adj p < 0.1). Figure used with permission from Rutere *et al.* 2020.

5.1.7. Quantification of representative ibuprofen enriched OTUs

An increase in relative abundance in amplicon libraries does not necessarily indicate stimulation. Thus, qPCR was utilized to verify representative ibuprofen-stimulated taxa as indicated by relative abundance data using 16S rRNA (cDNA) to 16S rRNA gene ratios as an indicator of taxon-specific activity. Expression of 16S rRNA genes of representative OTUs was significantly higher (ANOVA, $p \leq 0.05$) in 400 µM ibuprofen treatments relative to unamended controls (Figure 18), which agreed with the Deseq2 differential abundance data analysis. This highlighted the reliability of the differential abundance approach to identify potential ibuprofen-responsive taxa in hyporheic zone sediment microcosms.

5.1.8. Ibuprofen degrading strains CN1 and MAH1

Growth of the isolates CN1 and MAH1 under oxic conditions as determined by optical density measurements (data not shown) and degradation of ibuprofen (Figure 19), indicated the ability of the isolates to utilize ibuprofen as carbon and energy source to support their growth.The two strains affiliated with ibuprofen-responsive OTUs 1 (*Novosphingobium* related) and 24 (*Pseudomonas* related) (Figure 19; Table A1), respectively with the 16S rRNA gene similarities of CN1 and MAH1 to representative sequences of OTUs 1 and 24, > 97%. CN1 had a 16S rRNA gene similarity of 96.8% and 96.3% to *Novosphingobium flavum* strain UCM-28 (Acc. Nr. NR_152007) and *N. aromaticivorans* strain IFO 16084 (Acc. Nr. NR_112090), respectively, and clustered with other organisms of the genus *Novosphingobium* (Figure 20 A), suggesting that strain CN1 represents a new ibuprofen degrader of the genus. A 16S rRNA gene similarity of 99.9% of MAH1 to *Pseudomonas thivervalensis* (Acc. Nr. KF528727) and clustering with *P. thivervalensis* (Figure 20 B) suggests MAH1 as an ibuprofen degrading strain of this species.

Consistent with the phylogenetic affiliations, the two isolates were rod-shaped similar to the closest cultured members of their respective genera. The closely related ibuprofen-responsive OTUs 1 and 24 of the isolates were also present in the original hyporheic zone community prior to incubation at a relative abundance of approximately 0.01 – 0.1% (Table A2), suggesting their relevance in ibuprofen degradation in situ. The OTUs were further stimulated by ibuprofen on the DNA and RNA level following amendment of the sediment microcosms with exogenous ibuprofen (Figures 17 and 19; Table A1).The stimulation of OTU 1 generally resulted in higher relative abundances than OTU 24 and tended to be most prominent in treatments with low ibuprofen concentrations (Figure 19). The ibuprofen degradation kinetics of *Novosphingobium* strain CN1 (approximately 400 µM of ibuprofen within 2 days; Figure 19 A), showed a high capacity to quickly degrade ibuprofen and were in the range of ibuprofen degradation rates observed after the fifth refeeding of ibuprofen in hyporheic zone sediments (Figure 8). The high relative abundance of CN1 representing OTU 1 in treatments with low rather than with high concentrations of ibuprofen (Figure 19), suggest that the *Novosphingobium* strain CN1 represents a copiotrophic organism whose growth is impaired in situ in the presence of high ibuprofen concentrations. The relative abundance of OTU 24 indicative of the strain MAH1 was essentially similar in all ibuprofen treatments, although ibuprofen degradation of MAH1 was rather slow (approximately 300 µM of ibuprofen within 8 days; Figure 19B). Such data suggest that *Pseudomonas thivervalensis* MAH1 represents an oligotrophic organism with a high ibuprofen tolerance.

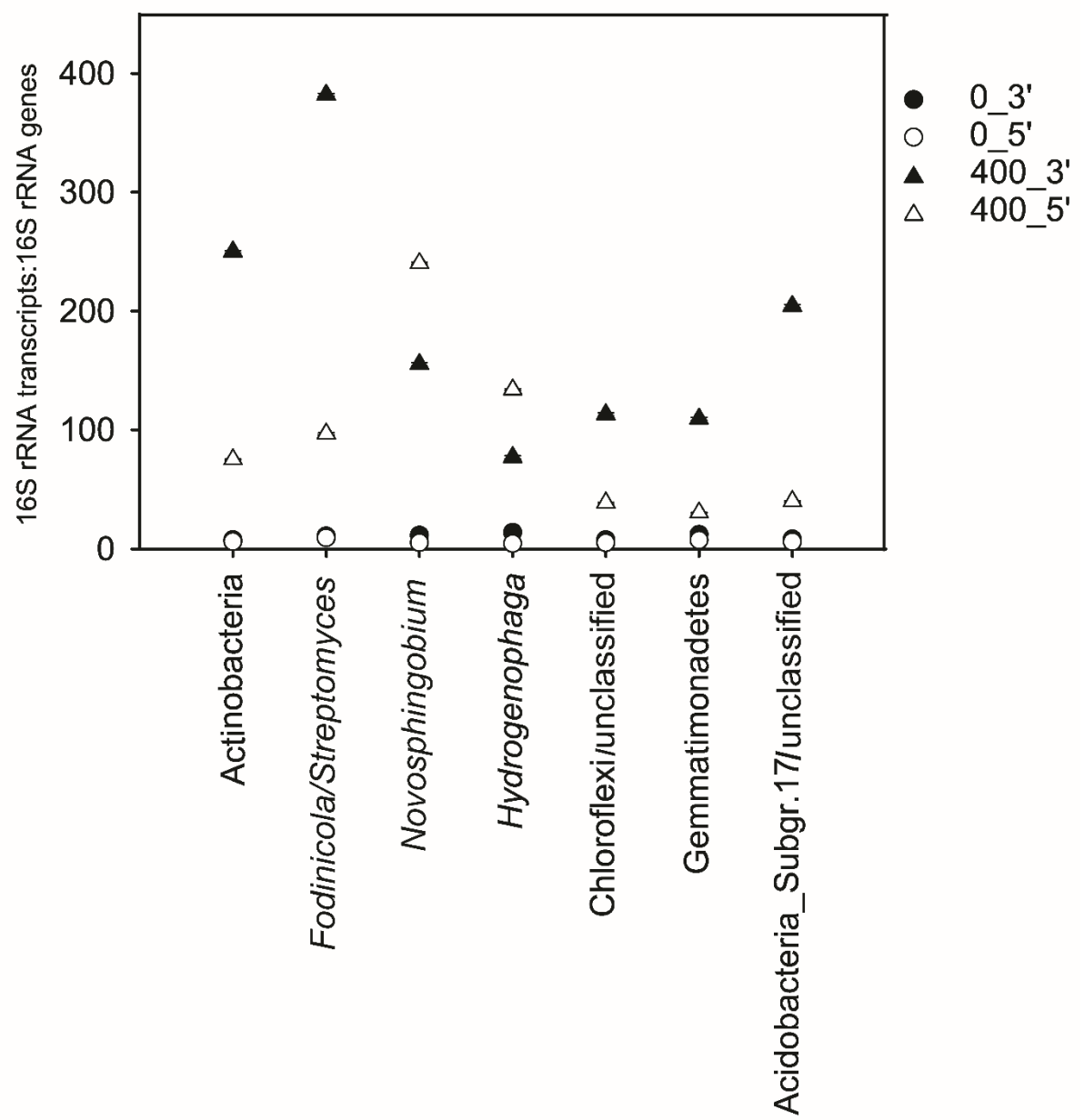

Figure 18. 16S rRNA (cDNA) to 16S rRNA gene ratios determined by qPCR for selected taxa stimulated by ibuprofen in the 400 µM treatment (Figs. 1, 2, and 3) as an indicator of taxon specific activity. Values are the arithmetic means of triplicate incubations. Error bars indicate standard deviation but are smaller than the symbol size and therefore not apparent. Sample code: 0 and 400 indicate supplemental ibuprofen concentrations in µM given per feeding; 3' and 5' correspond to samples obtained after the third and fifth refeeding, respectively. Sampling times for unamended controls were according to those of the 400 µM ibuprofen treatment. Figure used with permission from Rutere *et al.* 2020.

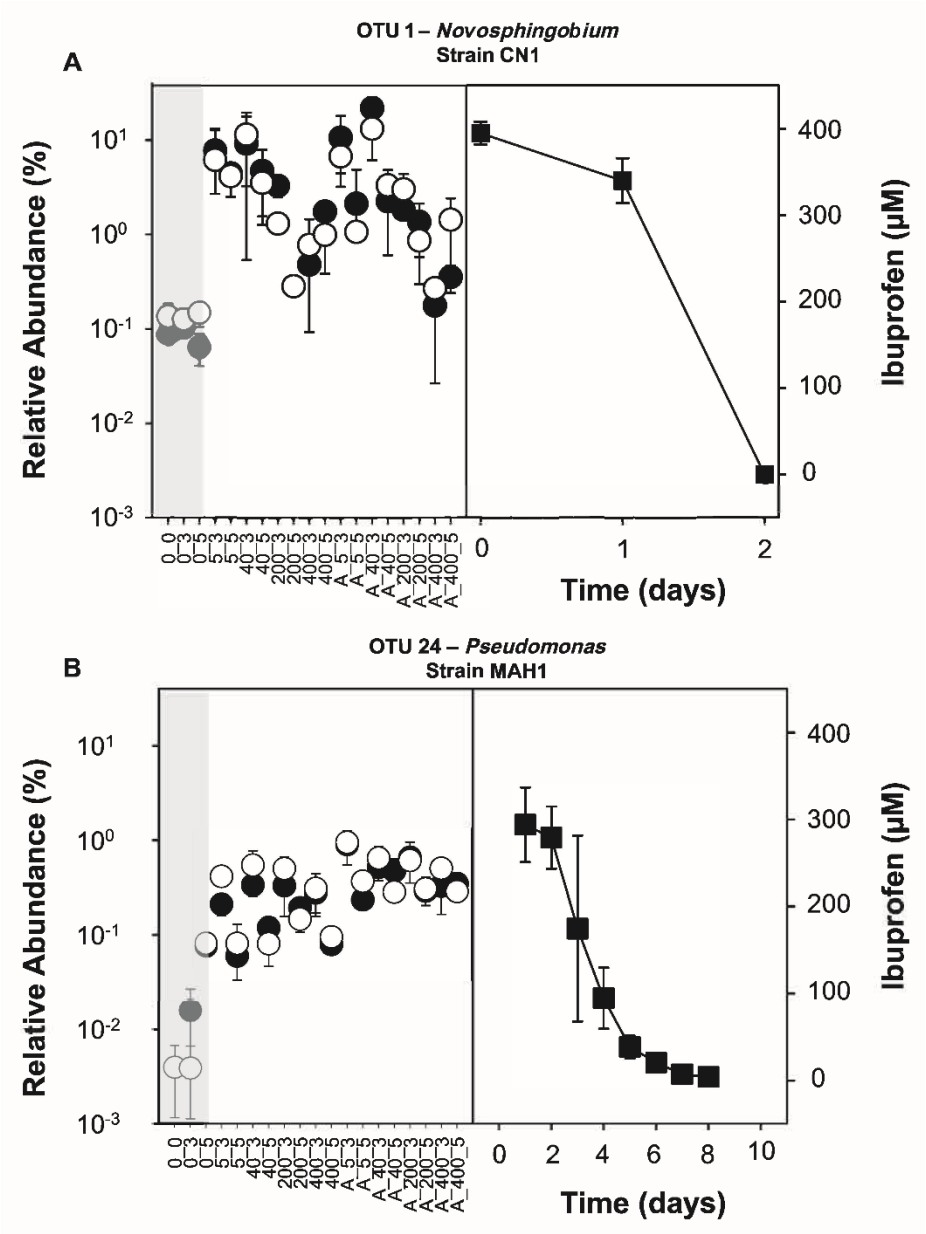

Figure 19. Effect of ibuprofen on the relative abundance of OTUs in 16S rRNA gene (DNA) and 16S rRNA (RNA or cDNA) derived amplicon librararies from oxic hyporheic zone sediment microcosms (Figure 8) affiliating with ibuprofen degrading strains *Novosphingobium* CN1 (A) and *Pseudomonas* MAH1 (B), and the capacity of both strains to degrade ibuprofen under oxic conditions. The grey box indicates unsupplemented oxic control microcosms. Values represent arithmetic means of triplicates, and error bars indicate standard deviations. Filled and open circles, DNA and RNA (cDNA) level, respectively; filled squares, ibuprofen concentration. Sample code: A, amended with 1 mM acetate and ibuprofen per feeding; 0, 5, 40, 200, and 400 indicate supplemental ibuprofen concentrations in µM given per feeding; 0', 3', and 5' correspond to samples obtained at the start of the incubation, and after the third and fifth refeeding, respectively. Sampling times for unamended controls were according to those of the 400 µM ibuprofen treatment. Figure used with permission from Rutere *et al.* 2020.

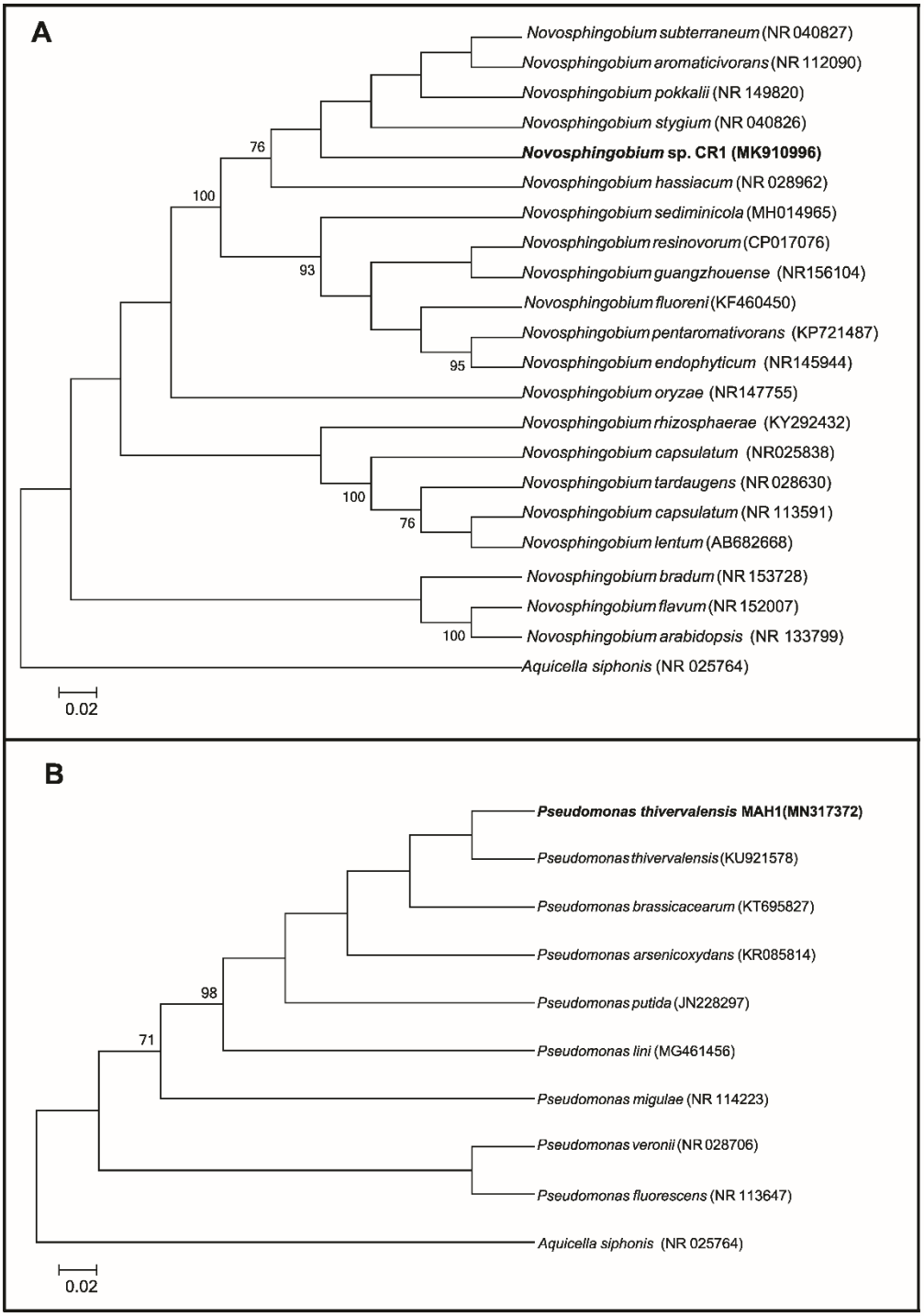

Figure 20. Phylogenetic tree reconstructed with the neighbour-joining method based on 16S rRNA gene sequences of strain CR1 and other *Novosphingobium* species (panel A) and strain MAH1 and other *Pseudomonas* species (panel B), showing their position among phylogenetic neighbours. Aquicella siphonis strain SGT-108 was used as an outgroup. Bootstrap values (based on 1000 replications) above 70 % are shown at branch nodes. Figure used with permission from Rutere *et al.* 2020.

5.2. Impact of redox gradients on the removal of micropollutants

5.2.1. Transformation of metoprolol in the oxic and anoxic hyporheic zone sediments

Complete removal of metoprolol in the 15 and 150 µM treatments occurred within 65 and 72 days, respectively, after an initial lag phase of approximately 40 days under oxic conditions (Figure 21 A). Following the second and third re-feeding of metoprolol, however, immediate degradation resulting in complete removal within 35 days irrespective of initial metoprolol concentration was observed (Figure 21 A). Under anoxic conditions, complete degradation irrespective of spiked metoprolol concentration initially occurred within 72 days following a lag phase of about 55 days (Figure 21 B). Degradation after the second re-feeding occurred within 35 days in both treatments without a significant lag phase observed. However, after the third re-feeding, complete removal was only observed in the 15 µM treatment and the 150 µM treatment exhibiting incomplete removal (Figure 21 B). In the abiotic control, approximately 21 % of the initial metoprolol concentration was removed by sorption. However, metoprolol concentration remained mostly unchanged in the hydrolysis control during the entire incubation (170 days: Figure 21 C).

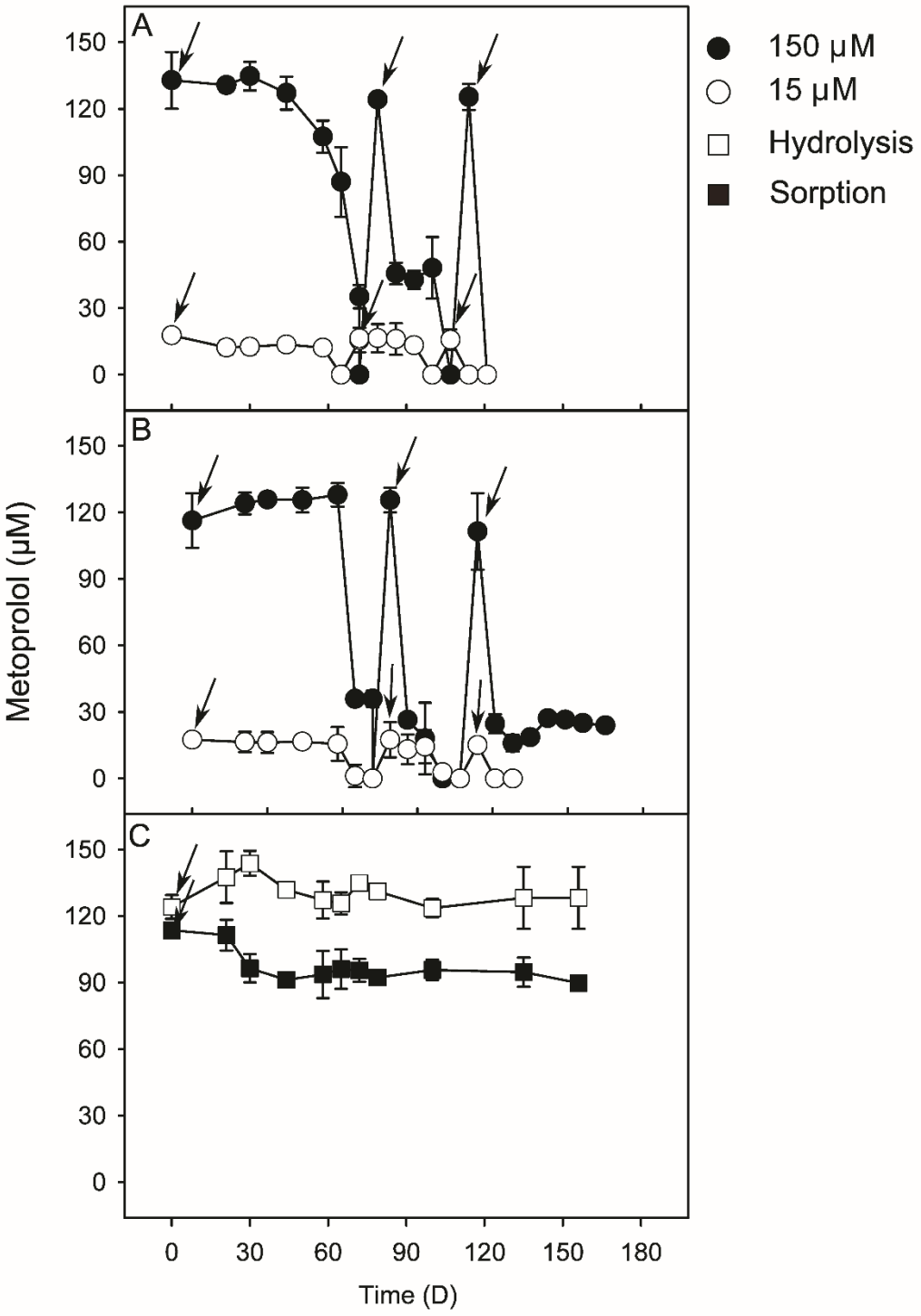

Figure 21. Apparent degradation of metoprolol in hyporheic zone sediment microcosms. Panels A and B represent sediment amended with 15 µM and 150 µM metoprolol under oxic and anoxic conditions, respectively. Panel C represents abiotic controls (sorption and hydrolysis) that were amended with 150 µM metoprolol and consisted of autoclaved sediment and river water, respectively. Values are the arithmetic means of triplicate incubations. Error bars represent standard deviations. Some standard deviations are smaller than the symbol size and therefore not apparent. Arrows indicate the time of refeeding of microcosms with metoprolol.

Analysis of the transformation products revealed metoprolol was transformed mainly to MTPA under oxic conditions (Figure 22 A). Under anoxic conditions, MTPA and α-HMTP were identified, with α-HMTP the major transformation product (Figure 22 B). The transformation products were subsequently completely removed under both incubation conditions (Figure 22 A and B).

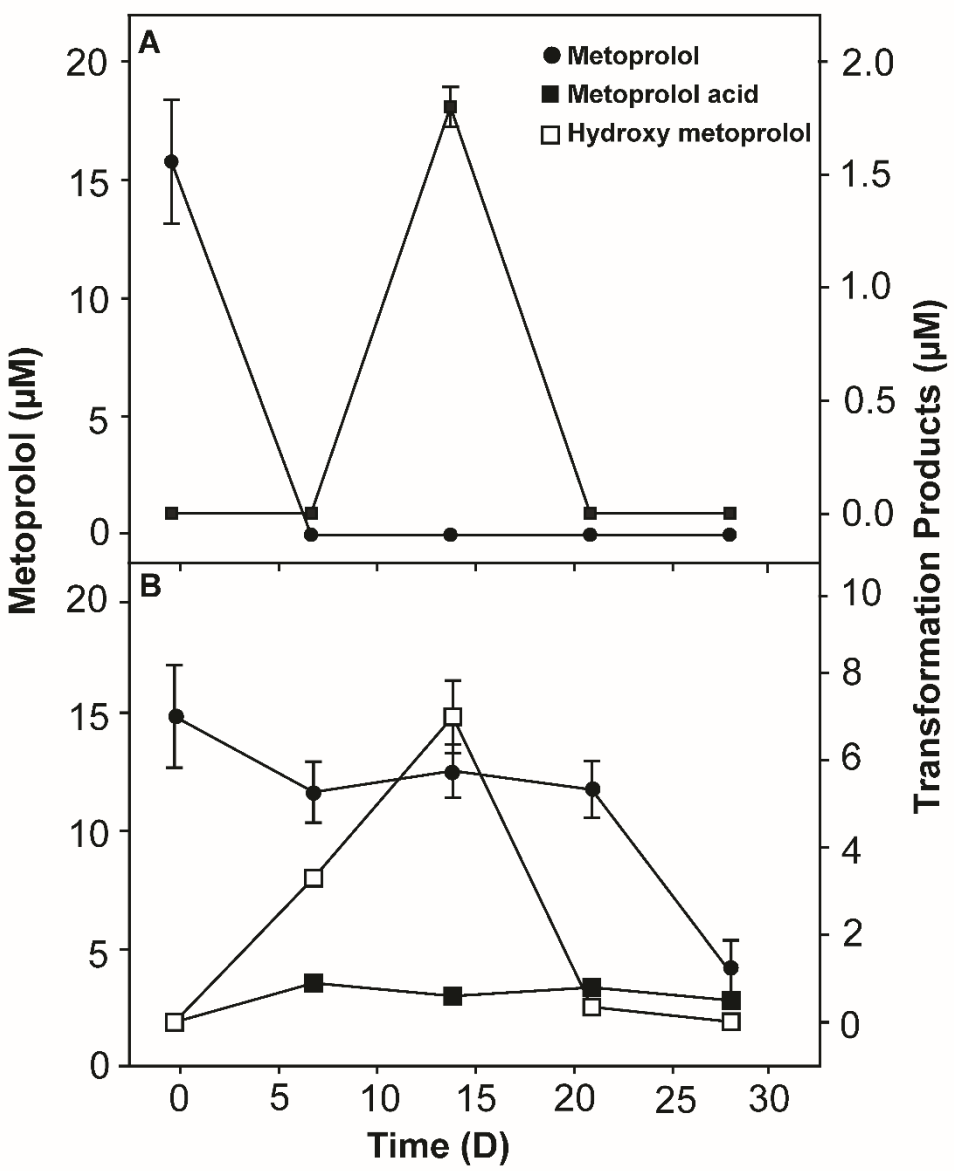

Figure 22. Metoprolol transformation products in hyporheic zone sediment microcosms under oxic (panel A) and anoxic conditions (panel B) subsampled from the 15µM metoprolol treatment (following 2nd refeeding, see Fig. 8 A and B). Values are the arithmetic means of triplicate incubations. Error bars represent standard deviations. Some standard deviations are smaller than the symbol size and therefore not apparent. Note different scales for the secondary axes.

5.2.2. Sediment properties and Redox zonation

A relatively similar GSD characterized the sediment through the depth profile with sand accounting for approximately 60 – 70 %. Gravel and silt accounted for about 20 % and 10 % in the oxic layer and 10 % and 30 % in the anoxic layer, respectively, as reported in (Peralta-Maraver *et al.* 2018a). Following incubation in oxic conditions, the endogenous nitrate concentration in treatments and biotic controls declined from approximately 0.6 - 0.8 mM to about 0.3 - 0.4 mM during the first 60 days; values fluctuated within 0.4 – 0.6 mM range after that (Figure 23 A). In anoxic conditions, nitrate concentration decreased rapidly within the first 20 days from approximately 0.4 - 0.6 mM to about 0.37 mM and remained constant after that (Figure 23 B). A constant nitrate concentration characterized the sorption control for the significant part of the incubation (Figure 23 C). The pH in the microcosms ranged between 6.4 - 6.7 throughout the incubation period.

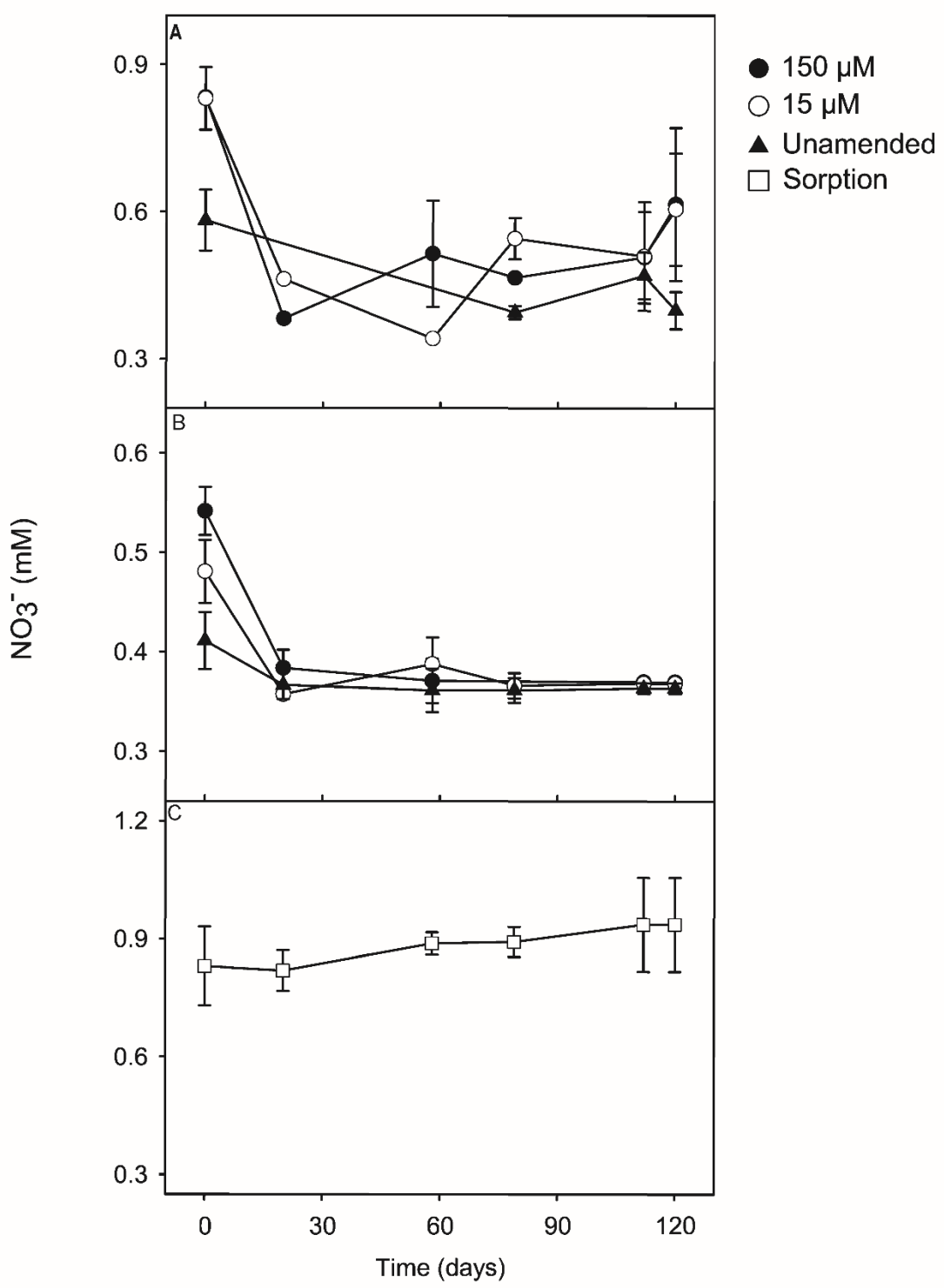

Figure 23. Evolution of Nitrate (NO_3^-) concentration during incubation. Panels A and B represent $NO3^-$ concentrations in metoprolol-amended (15 µM and 150 µM) and unamended sediment microcosms under oxic and anoxic conditions, respectively. Panel C represents $NO3^-$ concentration in the abiotic (sorption) control amended only with 150 µM metoprolol under anoxic conditions. Values are the arithmetic means of triplicate incubations. Error bars represent standard deviations.Some standard deviations are smaller than the symbol size and therefore not apparent.

5.2.3. Effect of metoprolol treatment on alpha and beta diversity

16S rRNA gene and 16S rRNA sequences in samples from the oxic treatments ranged from 11,435 to 49,428 and 15,253 to 49,921, respectively. Samples from the anoxic treatments had 16S rRNA gene and 16S rRNA sequences ranging from 14,063 to 49,943 and 30,672 to 49,963, respectively. The datasets were normalized to a uniform sequencing depth of the respective group sample with the lowest sequences for diversity analyses. 16S rRNA gene-based species richness, Shannon diversity and evenness tended to decrease in both metoprolol-amended and unamended control incubations, but compared to the original community, this decrease was not significant under oxic conditions (ANOVA, $p > 0.05$) (Figure 24 A-C). Likewise, no significant differences were observed in any of the diversity indices between the treatments, corresponding controls, or the original community at any timepoints under anoxic conditions (Figure 24 D-F). In contrast, at the 16S rRNA level, diversity indices tended to be higher following oxic incubation than in the original community (Figure 24 A-C). However, the differences were not significant as was for anoxic incubations (ANOVA, $p > 0.05$) (Figure 24). The difference in the indices between the 15 µM treatment and respective controls at days 65 and 120 was also not significant under oxic and anoxic conditions (ANOVA, $p > 0.05$). In the 150 µM treatment, a significant decline in the 16S rRNA level-based indices occurred compared to the controls at day 120 (ANOVA, $p < 0.05$) under oxic and anoxic conditions (Figure 24).

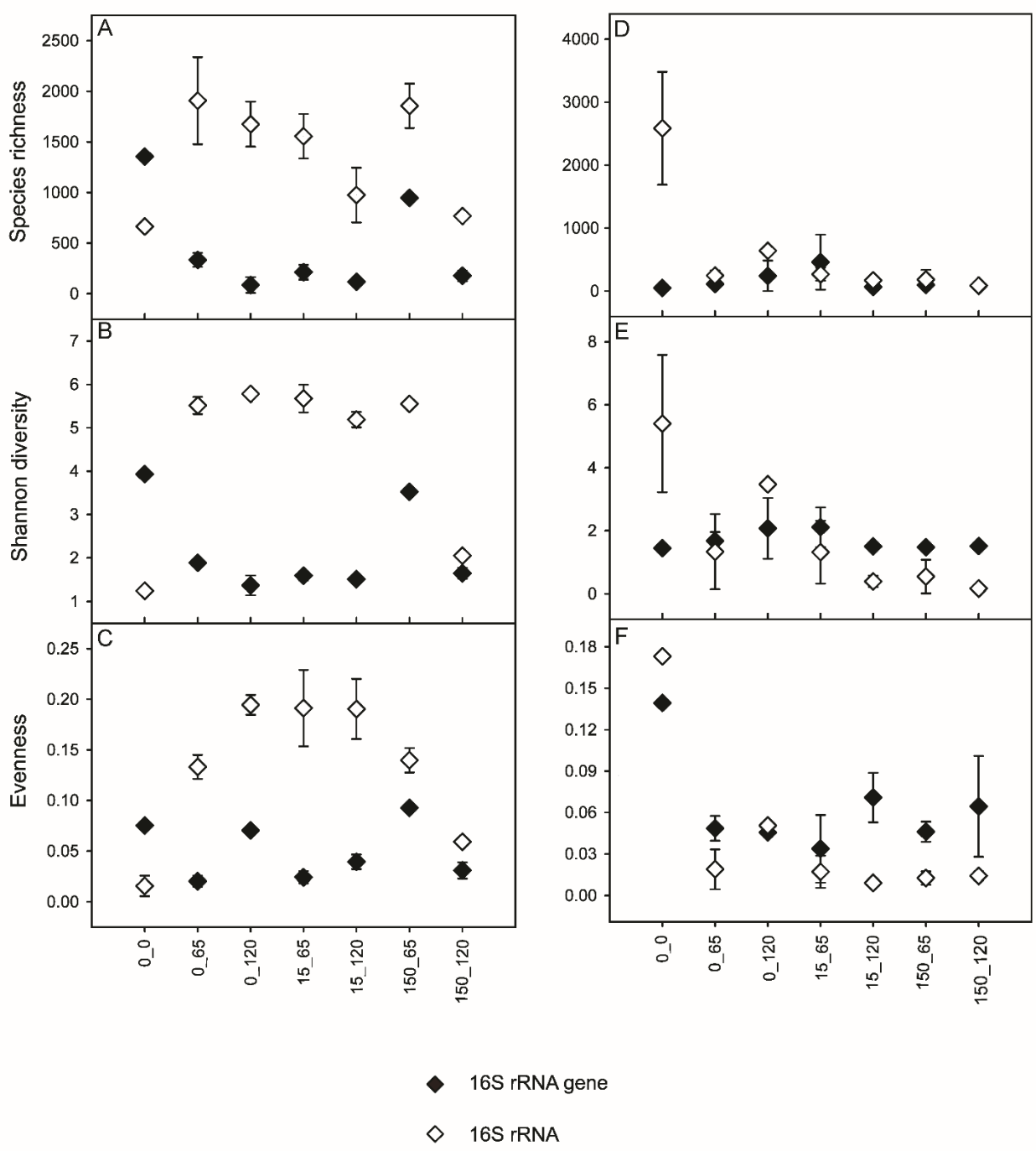

Figure 24. Alpha diversity indices based on 16S rRNA gene and 16S rRNA sequences. Panels A, B and C represent species richness (A), Shannon index (B) and evenness index (C) for microcosms incubated under oxic conditions. Panels D, E and F represent species richness (A), Shannon index (B) and evenness index (C) for microcosms incubated under anoxic conditions. Values are the arithmetic means of triplicate incubations. Error bars represent standard deviations. Some standard deviations are smaller than the symbol size and therefore not apparent. Sample code: 0, 15 and 150 indicate metoprolol concentration (µM). 0, 65, and 120 at the last position in the code indicate day of sampling.

PCoA revealed no apparent clustering of the samples based on metoprolol treatment or incubation duration under oxic conditions based on 16S rRNA gene sequences due to high variability observed among replicates (Figure 25 A). Consistent with these observations, the two-way ANOSIM test revealed no significant dissimilarity among the samples due to metoprolol amendment ($R = 0.04$, $p = 0.2$) or incubation time ($R = 0.08$, $p = 0.1$). At the 16S rRNA level, clustering patterns concomitant to metoprolol amendment but not incubation time were observed under oxic conditions (Figure 25 B). The corresponding two-way ANOSIM test revealed a stronger contribution to the overall dissimilarity among the samples was indeed a factor of metoprolol amendment ($R = 0.5$, $p = 0.002$), while incubation time had only a minimal impact ($R = 0.2$, $p = 0.1$). The R-values greater than 0.6 suggest a rather strong dissimilarity between microbial communities from different treatments and time points.

Under anoxic conditions, samples clustered as a function of metoprolol treatment at the DNA and RNA levels (Figure 25 C and D) but of incubation time only at the DNA level (Figure 25 C). The corresponding two-way ANOSIM test indicated that metoprolol treatment caused a significant dissimilarity among samples ($R = 0.65$, $p = 0.0006$) whereas incubation time resulted in a fairly strong dissimilarity among the samples ($R = 0.4$, $p = 0.02$). At the RNA level, a minor effect on dissimilarity among the samples as a function of metoprolol treatment was detected ($R = 0.3$, $p = 0.001$) but a non-significant effect of incubation time ($R = 0.03$, $p = 0.4$) was observed.

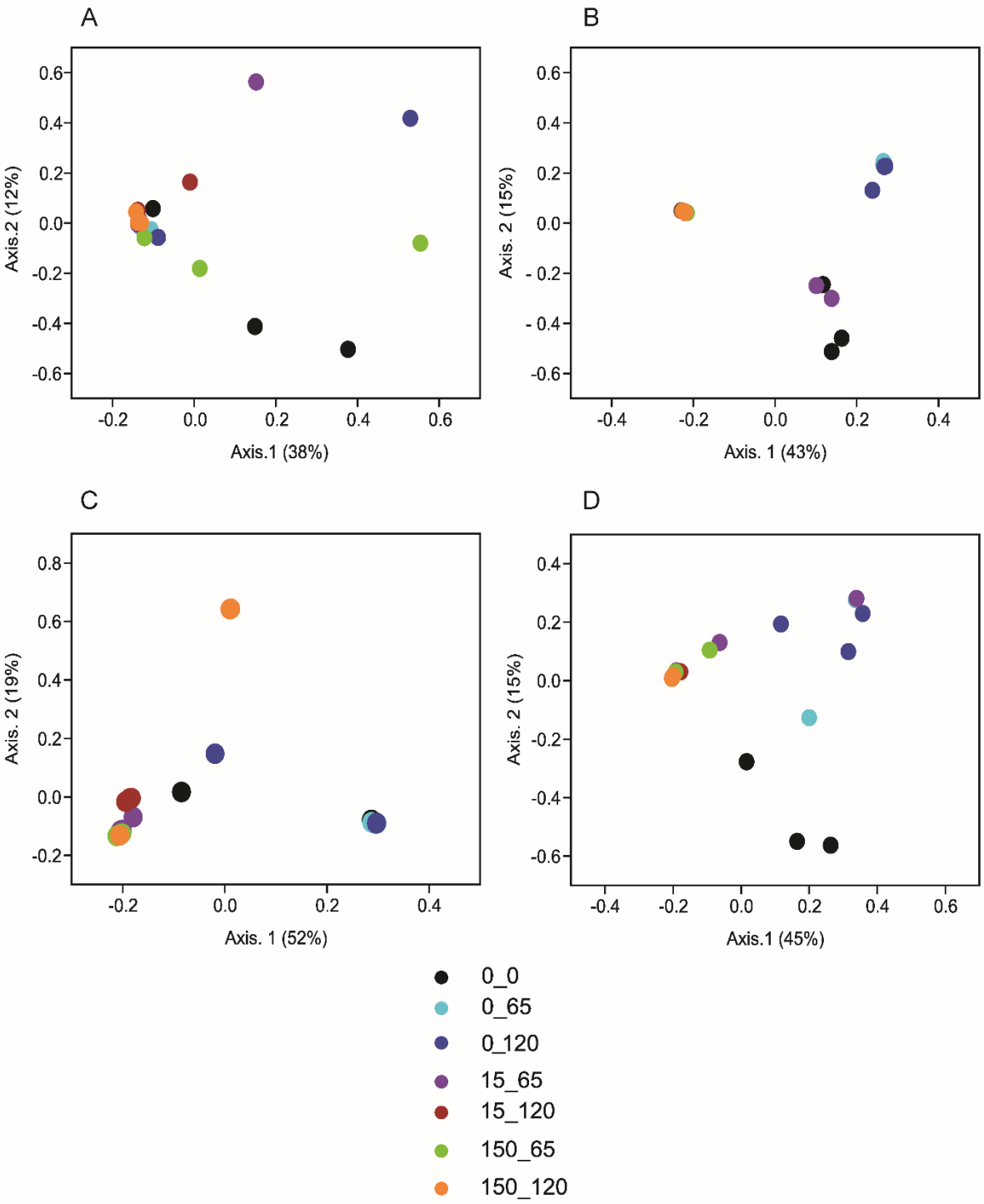

Figure 25. Principal coordinate analysis based on Bray Curtis dissimilarity metric showing the effect of metoprolol treatment on the bacterial community composition on OTU level from 16S rRNA gene and 16S rRNA level. Panel A and B correspond to 16S rRNA gene (A) and 16S rRNA (B) for samples incubated under oxic conditions. Panel C and D correspond to 16S rRNA gene (A) and 16S rRNA (B) for samples incubated under anoxic conditions. Sample code: 0, 15 and 150 indicate metoprolol concentration (µM). 0, 65, and 120 at the last position in the code indicate day of sampling.

5.2.4. Effect of treatments on the Phylum-level taxonomic composition

16S rRNA gene sequence analysis revealed 12 phyla (> 1% relative abundance) in the original sediment bacterial community while the 16S rRNA sequences revealed Proteobacteria and Bacteroidetes as the key phyla accounting for up to 99% of the sequences under oxic conditions (Figure 26 A and B). Following incubation, a shift in the community composition characterized by the predominance of Proteobacteria and Bacteroidetes at both DNA and RNA levels was observed. Bacteroidetes and Actinobacteria seemed to be stimulated in the 15 and 150 µM metoprolol treatments at the DNA level at day 65, respectively (Figure 26 A). However, 16S rRNA sequences indicated a strong stimulation of Proteobacteria, Chloroflexi and Acidobacteria in the 15 µM treatment at day 65 (Figure 26 A). Other phyla detected in the original community at the DNA level including Gemmatimonadetes, Nitrospirae, Chlorobi, Latescibacteria and Firmicutes declined in relative abundance in most control and treatment samples following oxic incubation (Figure 26 A).

Under anoxic conditions, a change in the community composition relative to the original sediment was evident in incubated samples with phyla such Chloroflexi, Acidobacteria, Actinobacteria, Gemmatimonadetes, Nitrospirae, Firmicutes and Latescibacteria present in low relative abundance in the unincubated sediment seemingly increasing in abundance at the DNA level in both controls and metoprolol treatments (Figure 26 C). Relative to controls, however, metoprolol amended samples at day 65 revealed higher relative abundances in the phyla Chloroflexi, Acidobacteria and Actinobacteria. The phylum Firmicutes was also relatively higher in abundance in the 15 µM treatment at day 65 compared to the unamended control or 150 µM treatment, suggesting preferential stimulation at low metoprolol concentration of this phylum. Overall, Proteobacteria was the dominant phylum at DNA and RNA levels under anoxic

conditions (Figure 26 C and D). However, RNA-based analysis revealed a more dramatic change in the microbial community composition, whereby Proteobacteria formed the dominant community members, particularly in the 150 µM treatment (Figure 26 D).

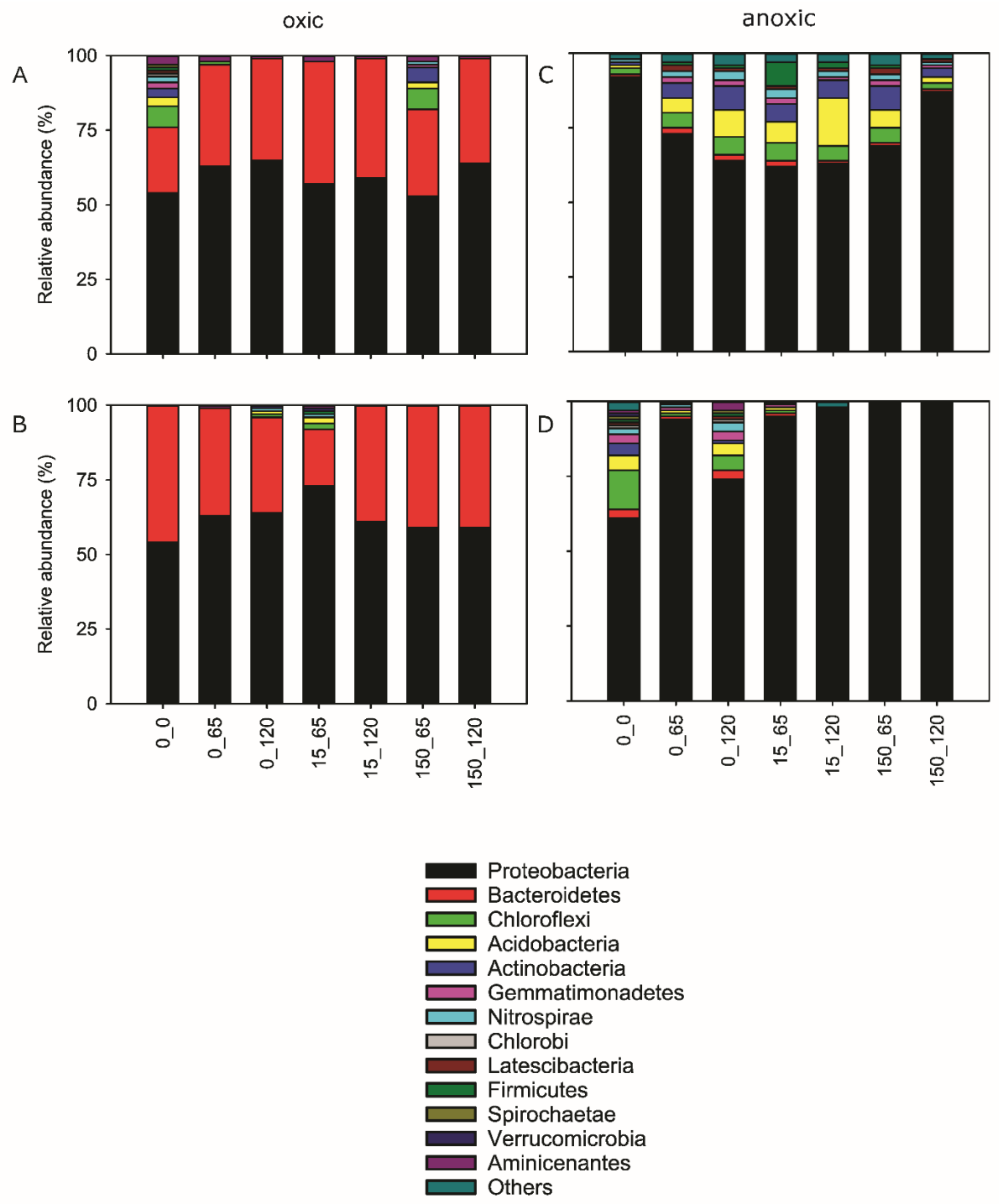

Figure 26. Mean relative abundance of major bacterial phyla (> 1% relative abundance) on 16S rRNA gene and 16S rRNA level. Panel A and B correspond to 16S rRNA gene

(A) and 16S rRNA (B) for samples incubated under oxic conditions. Panel C and D correspond to 16S rRNA gene (A) and 16S rRNA (B) for samples incubated under anoxic conditions. Phyla accounting for less than 1% of all sequences are grouped as ''others''. Sample code: 0, 15 and 150 indicate metoprolol concentration (µM). 0, 65, and 120 at the last position in the code indicate day of sampling.

5.2.5. Effect of treatments on family-level taxonomic composition

As per the phylum-level taxonomic composition, the dominant families (> 3% relative abundance) at both DNA and RNA level under oxic conditions were affiliated to Proteobacteria and Bacteroidetes under oxic conditions (Figure 27 A and B). At the DNA level, the relative abundance of the Proteobacteria affiliated family Chromatiaceae increased in the unamended control compared to metoprolol treatments following incubation. Other families, namely Moraxellaceae, Pseudomonadaceae, Comamonadaceae, and Hydrogenophilaceae, increased in abundance in both the controls and treatments (Figure 27 A). Bacteroidetes-affiliated Flavobacteriaceae exhibited marginally higher relative abundance in the 15 µM treatment compared to controls sampled at the respective time points. At the RNA level, relatively similar community composition was observed across most samples except in the 15 µM treatment sampled at day 65 where the family Acidithiobacillaceae dominated the community in addition to the strong stimulation of Desulfobulbaceae (Figure 27 B).

Under anoxic conditions, Proteobacteria affiliated families dominated the original sediment community with Enterobacteriaceae prominent at the DNA level while Gallionellaceae and Hydrogenophilaceae were additionally detected at the RNA level (Figure 27 C and D). After treatment and incubation, other families occurring in low relative abundance (< 3 %) in the original community at the DNA level exhibited an increase in their relative abundance (> 3 %). These included Hyphomicrobiaceae,

Ectothiorhodospiraceae, Hydrogenophilaceae, Neisseriaceae, unclassified families affiliated with Acidobacteria subgroups 6 and 17, Micrococcaceae and Lactobacillaceae (Figure 27 C). The potentially active fraction captured by RNA analysis revealed Enterobacteriaceae, Desulfobulbaceae and Acidithiobacillaceae as dominant families in the 15 µM treatments, with depletion of metoprolol in the 15 µM treatment at day 120 revealing a decline in the relative abundance of Desulfobulbaceae and Acidithiobacillaceae while Enterobacteriaceae remained dominant (Figure 27 D). Preferential stimulation of the Enterobacteriaceae was evident in the 150 µM treatment under anoxic conditions (Figure 27 D).

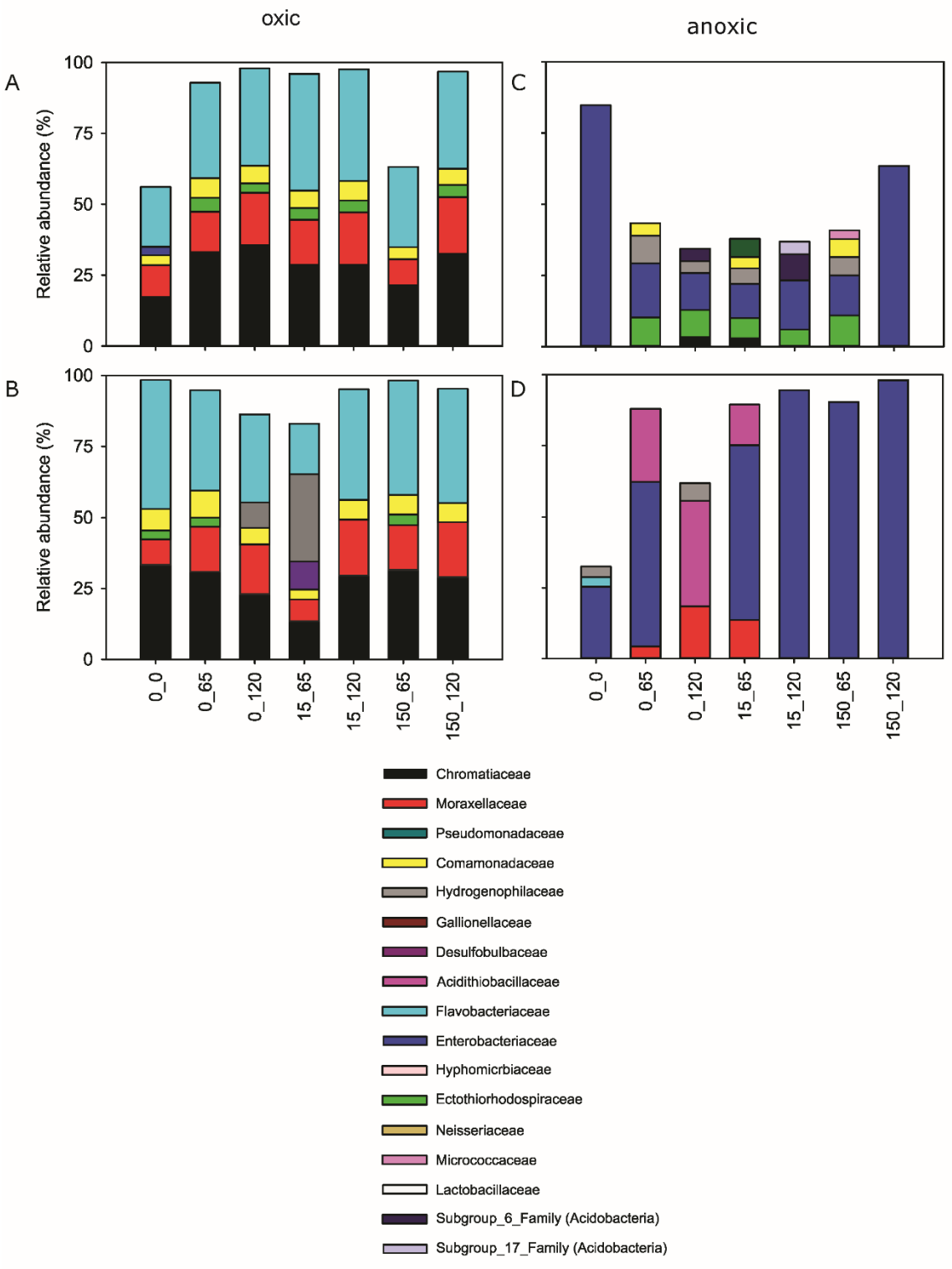

Figure 27. Mean relative abundance of major bacterial families (> 3 % relative abundance) on 16S rRNA gene and 16S rRNA level. Panel A and B correspond to 16S rRNA gene (A) and 16S rRNA (B) for samples incubated under oxic conditions. Panel C and D correspond to 16S rRNA gene (A) and 16S rRNA (B) for samples incubated under anoxic conditions. Sample code: 0, 15 and 150 indicate metoprolol concentration (µM). 0, 65, and 120 at the last position in the code indicate day of sampling.

5.2.6. Taxa associated with metoprolol degrading communities

OTU-level taxa identified under oxic conditions using the differential abundance analysis and considered important in the biotransformation of metoprolol exhibited concentration-dependent response with higher Log2FoldChange values observed in the 150 compared to 15 µM treatments (Table A3). Majority of the OTUs affiliated with Proteobacteria including alphaproteobacteria-affiliated *Phenylobacterium, Caulobacter, Sphingopyxis, Sphingomonas* and *Sphingobium,* gammaproteobacterial OTUs such as *Acinetobacter, Pseudomonas, Rheinheimera* including the betaproteobacteriales affiliating OTUs *Aquabacterium, Limnobacter, Ralstonia, Pelomonas, Albidiferax* and *Thiomonas*. Others were OTUs affiliating with Bacteroidetes (*Flavobacterium* and *Hydrotalea*). These OTUs were also detected in the original sediment at variable relative abundances, suggesting their importance in metoprolol degradation in situ (Table A4).

Under anoxic conditions, most metoprolol responsive OTUs were enriched in the 15 compared to 150 µM treatment (Table A5). Such taxa included alphaproteobacteria-affiliated *Rhodomicrobium, Pedomicrobium, Rhodobium, Rhodoplanes,* deltaproteobacteria affiliated *Byssovorax, Haliangium, Desulfobacca, Sandaracinus, Sorangium* and gammaproteobacteria-affiliated *Acidiferrobacter, Pseudomonas*, *Escherichia* and *Enhydrobacter.* An array of unclassified OTUs affiliated with Subgroups 6, 9 and 17 in the phylum Acidobacteria while *Cellulosimicrobium* (Actinobacteria) was stimulated in the high metoprolol treatment (Table A5). OTUs affiliated with Chloroflexi classes KD4-96, Anaeroliniae, Ardenticatenia, the Firmicutes-affiliated *Bacillus*, and Gemmatimonadaceae (Gemmatimonadetes) were also enriched in metoprolol treatments, with Chloroflexi-affiliated OTUs preferentially stimulated in the low metoprolol treatment (Table A5). These OTUs were also detected

in the original sediment at variable relative abundances, suggesting their importance in metoprolol degradation in situ (Table A6).

5.3. Impact of TOC gradients on micropollutant removal

5.3.1. Depletion of TrOCs under varying TOC concentrations

Depletion of TrOCs in the biotic microcosm setups with initially high (8.7%) and low (3.2%) TOC concentrations varied considerably within and among test compound classes (Figure 28 A). Among the NSAIDs, ibuprofen and ketoprofen removal efficiency was almost two-fold in the surface relative to subsurface samples compared to the marginal difference observed for diclofenac. On the other hand, naproxen was removed entirely under both TOC conditions. The cholesterol-lowering agents bezafibrate and clofibric acid removal correlated with the TOC concentration with higher removal efficiency observed in the surface sediment layer. Clofibric acid was, however, characteristically persistent with less than 50 % removed in all the tested sediment samples. Complete removal of acesulfame occurred in the surface layer compared to only 17 % in the subsurface samples. Marginally higher removal efficiency was also observed in the surface relative to subsurface sediment samples for furosemide, hydrochlorothiazide, carbamazepine and benzotriazole. Among the beta-blockers, complete removal of propranolol was observed under both TOC conditions while metoprolol removal was only marginally higher in the surface relative to subsurface layer samples.

In the abiotic setup, most TrOCs exhibited a correlation with the initial sediment TOC concentration (Figure 28 B). Removal via sorption of the NSAIDs was higher in the surface relative to subsurface samples. Diclofenac removal efficiency (> 55 %), was the highest among NSAIDs tested, followed by ibuprofen. Naproxen and ketoprofen exhibited < 30 % removal efficiency in the surface and only negligible removal in the subsurface samples. Similar to the biotic setups, the removal of the beta-blockers metoprolol and propranolol was relatively high under both TOC conditions. Propranolol

was removed entirely while metoprolol removal exceeded 80 % under both high and low TOC conditions. Though characterized by minimal differences, the removal efficiency of bezafibrate, clofibric acid, carbamazepine and benzotriazole was higher in the surface relative to subsurface samples. Furosemide exhibited a reversed removal pattern with higher removal occurring in the subsurface relative to surface samples. Acesulfame concentration remained unchanged in abiotic setups under both high and low TOC conditions indicating no sorption of the compound occurred.

Taken together, an apparent effect on the removal efficiency of TrOCs by the TOC concentration was evident with a higher removal efficiency of most test compounds occurring in the surface relative to subsurface sediment samples (Figure 28). Moreover, biotransformation was the predominant removal mechanism of TrOCs in the hyporheic zone sediments. The interaction of the microbial community dynamics with TOC and TrOC removal efficiency was, therefore, further interrogated.

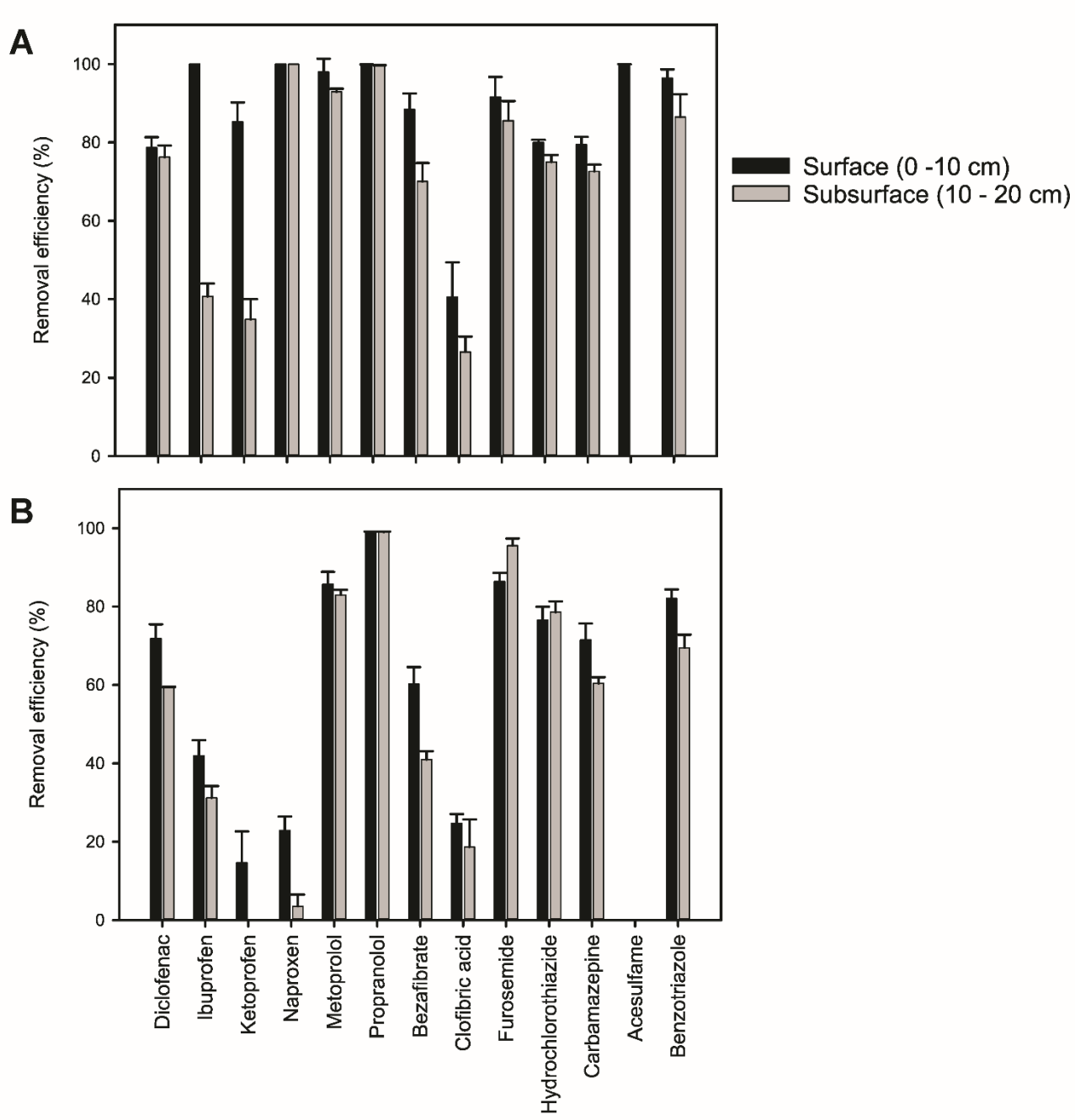

Figure 28. Relative removal efficiency of test compounds in the A) biotic and B) abiotic (sorption) batch microcosms containing surface and subsurface sediment samples. The incubation ran for 65 days with samples taken after 15 and 65 days.

5.3.2. Abundance of the total bacterial community

The unincubated sediment samples (t0 samples) from the two layers reached approximately 10^9 16S rRNA gene and 16S rRNA copies per gram sediment (Figure 29). Following incubation, the 16S rRNA gene copies in the subsurface sediment were significantly lower than in the surface sediment samples (ANOVA, $p < 0.05$). The 16S rRNA copies, however, varied considerably between treatments. With reference to the corresponding t0 samples from each layer, the 16S rRNA gene copies declined in both amended and unamended surface (marginally) and subsurface samples (significantly) (ANOVA, $p < 0.05$) following incubation. A comparison between the incubated unamended and amended samples from each layer revealed higher 16S rRNA gene and 16S rRNA copies in the amended relative to unamended surface sediment samples obtained at days 15 and 65 (Figure 29 A). On the other hand, the 16S rRNA gene copies in the subsurface samples were lower in amended relative to unamended samples on day 15 but higher at day 65 (Figure 29 B). The 16S rRNA copies were, however, generally higher in the amended than unamended samples at both days 15.

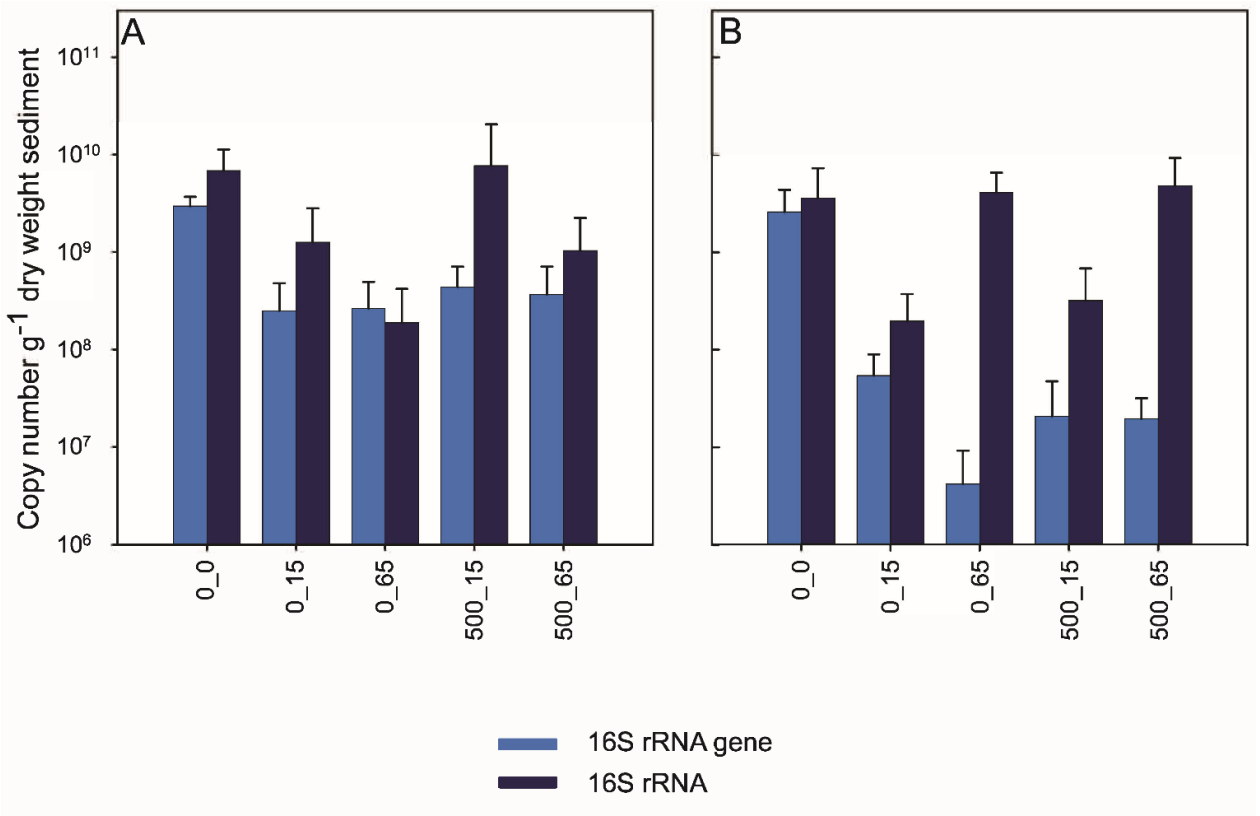

Figure 29. Abundance (copy numbers) of bacterial 16S rRNA genes and 16S rRNA (cDNA) detected in oxic hyporheic zone microcosms containing A) surface and B) subsurface sediment samples. Sample code: 0, 500 indicate supplemental TrOC concentrations in μgL^{-1}. 0, 15, 65 represent sampling days. Values are the arithmetic average of three replicates. Error bars indicate standard deviation values.

5.3.3. Bacterial community alpha and beta diversity

The resultant number of 16S rRNA gene and 16S rRNA sequences per sample ranged from 12,805 to 31,177and 12,805 to 36,649, respectively. The datasets were normalized to a uniform sequencing depth of 12,805 per sample for diversity analyses. The t0 samples revealed higher species richness in the subsurface than surface samples (Figure 30 A) (ANOVA; $p < 0.05$) but similar Shannon diversity across the two sample sets (Figure 30 C) (ANOVA; $p > 0.05$) based on 16S rRNA gene sequences. Following incubation, however, significantly higher species richness was observed in the surface compared to subsurface samples in amended and unamended samples at day 15. The Shannon diversity followed the same trend for samples obtained at days

15 and 65. Moreover, the amended samples from each layer had significantly higher species richness and diversity than the corresponding unamended samples on day 65. Based on 16S rRNA, no significant differences in species richness were observed in the samples as a function of depth, amendment or incubation time (Figure 30 B) (ANOVA; $p > 0.05$). However, diversity was significantly higher in the surface compared to subsurface samples in both amended and unamended samples at day 15 (Figure 30 D) (ANOVA; $p < 0.05$).

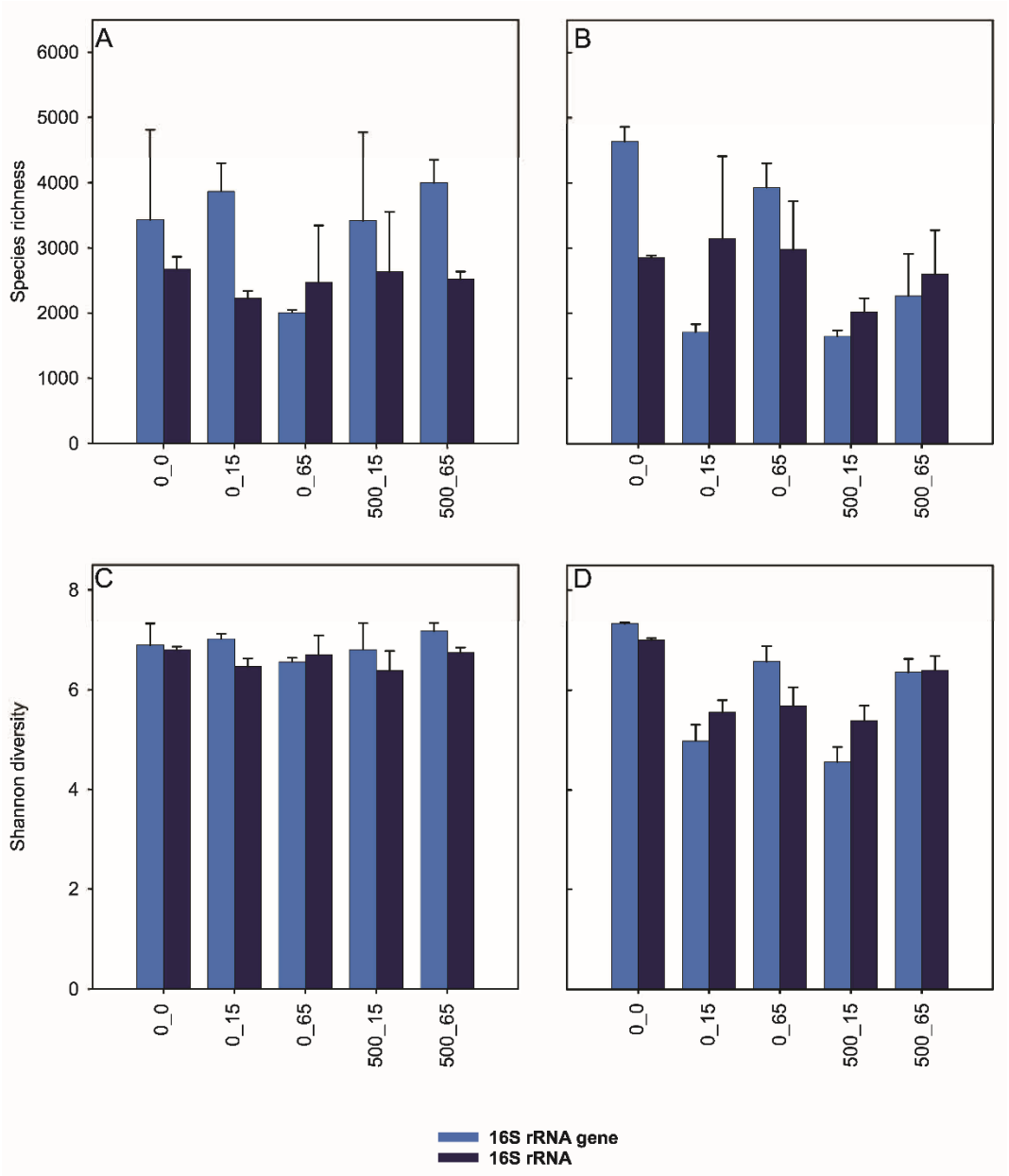

Figure 30. Taxa richness (A, B) and Shannon diversity (C, D) of the total bacterial community in surface and subsurface sediment samples, respectively. Sample code: 0, 500 indicate supplemental TrOC concentrations in μgL^{-1}. 0, 15, 65 represent sampling days. Values are the arithmetic average of three replicates. Error bars indicate standard deviation values.

Beta diversity visualization on PCoA plots based on 16S rRNA gene and 16S rRNA sequence data revealed distinct clustering of the bacterial community in the surface samples according to incubation time but no apparent effect of treatment with the test compounds (Figure 31 A and B). Consistent with these findings, the two-way ANOSIM

test indicated that in the surface samples, incubation time (DNA: R = 0.7, RNA: R = 0.7, $p < 0.02$) accounted significantly for the variation in the bacterial community composition while the effect of treatments was not apparent (DNA: R = 0.3, RNA: R = 0.2, $p < 0.22$). For the subsurface samples, the clustering strongly separated along axis 1, depicting a stronger influence of incubation time than treatment (Figure 31 C and D). The ANOSIM test further revealed the stronger effect of incubation time (DNA: R = 0.9, RNA: R = 0.9, $p < 0.02$) compared to treatment (DNA: R = 0.7, RNA: R = 0.7, $p < 0.01$). Nevertheless, both factors contributed significantly to the differences in the bacterial community composition distribution in the subsurface sediments. The R-values greater than 0.6 indicated a rather strong dissimilarity between microbial communities from different treatments and time points.

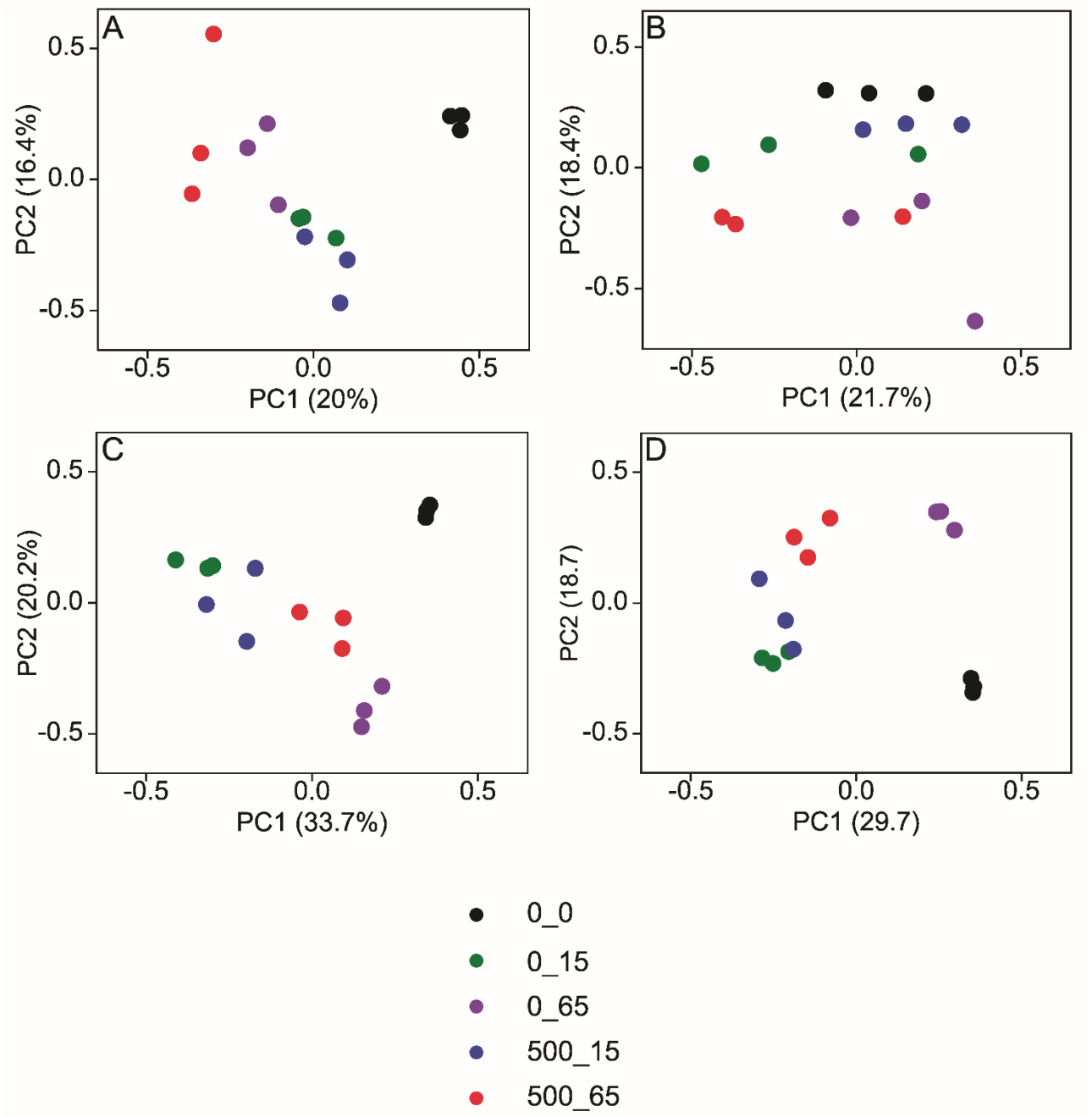

Figure 31. Principal coordinate analysis based on Bray Curtis dissimilarity metric showing the effect of TrOCs on the bacterial community composition on OTU-level from 16S rRNA gene and 16S rRNA data for surface (A,B) and subsurface sediment samples (C,D), respectively. Sample code: 0, 500 indicate supplemental TrOC concentrations in μgL^{-1}. 0, 15, 65 represent sampling days.

5.3.4. Phylum-level taxonomic composition

The predominant phyla in the sediment samples from the two layers on DNA and RNA levels were Proteobacteria, Chloroflexi, Actinobacteria, Acidobacteria, Bacteroidetes and Firmicutes (Figure 32). Other phyla identified (> 1% relative abundance) included Nitrospirae, Gemmatimonadetes and Chlorobi. The t0 samples indicated that only the relative abundance of the predominant phylum Proteobacteria was higher in the surface (38%) compared to the subsurface layer (32%) while other phyla were comparable in terms of relative abundance in the two layers.

Following incubation, changes in the relative abundance of some phyla in amended relative to unamended samples were observed. In surface sediment samples, the phyla whose relative abundance increased concomitant to TrOC amendment included Proteobacteria (DNA: 37 to 41 %, RNA: 40 to 44 %), Bacteroidetes (DNA: 4.5 to 5.5 %, RNA: 3 to 6 %) and Firmicutes (DNA: 4 to 5 %; RNA: 5 to 10 %) at day 15. In the subsurface samples, an increase in the relative abundance of Proteobacteria (DNA: 41 to 62 %, RNA: 49 to 55 %) and a decline in Chloroflexi (DNA: 18 to 14 %, RNA: 15 to 11 %) and Firmicutes (DNA: 11 to 4 %, RNA: 13 to 11 %) was observed in amended relative to unamended samples at day 15.

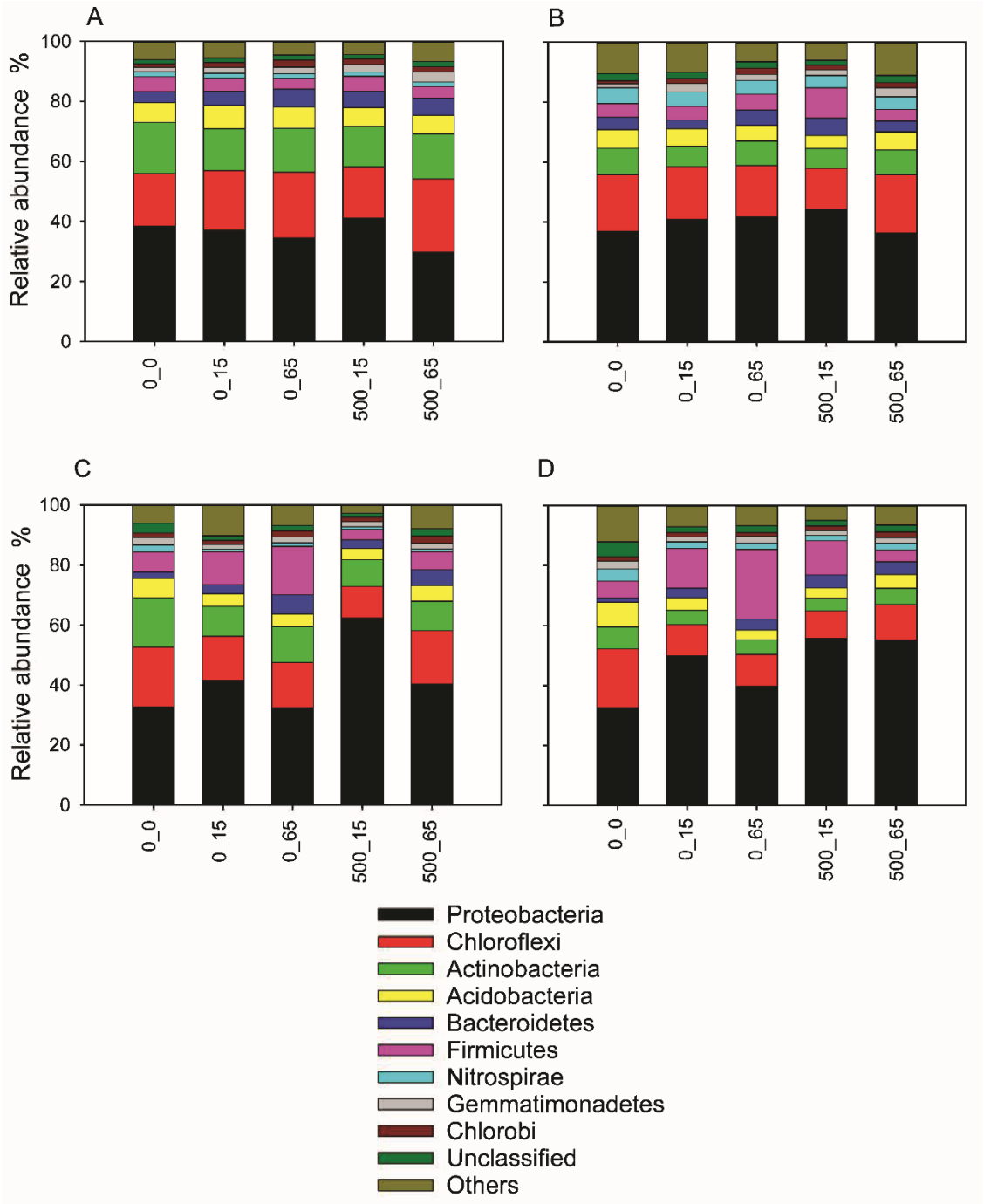

Figure 32. Mean relative abundance of major bacterial phyla (> 1 % relative abundance) on 16S rRNA gene and 16S rRNA level. Panel A and B correspond to 16S rRNA gene (A) and 16S rRNA (B) for surface sediment samples. Panel C and D correspond to 16S rRNA gene (A) and 16S rRNA (B) for subsurface sediment samples. Phyla accounting for less than 1% of all sequences are grouped as “others”. Sample code: 0, 500 indicate supplemental TrOC concentrations in μgL^{-1}. 0, 15, 65 represent sampling days.

5.3.5. Family-level taxonomic composition of bacteria

The t0 surface sediment samples exhibited a higher number of dominant bacterial families (> 3 % relative abundance) than subsurface sediment samples, though only at the RNA level (Figure 33). These included Proteobacteria affiliated Hyphomicrobiaceae, Comamonadaceae, Caldilineaceae, Chloroflexi affiliated unclassified families JG30-KF-CM66, KD4-96, TK10, JG30-KF-CM45, an Acidobacterial Subgroup 6 family and Nitrospiraceae (Nitrospirae). In contrast, the family Anaerolineaceae exhibited higher relative abundances in the subsurface than in surface sediment at the DNA and RNA levels. The relative abundance of Rhodobiaceae was also higher in the subsurface than surface sediment at the DNA level while Gemmatimonadaceae exhibited a similar pattern at the RNA level.

In the incubated samples, the amendment with TrOCs resulted in increased relative abundance in the surface sediment samples of the families Methylophilaceae, Caldilineaceae, unclassified KD4-96 family, Acidimicrobiaceae and Gemmatimonadaceae at the DNA level while at the RNA level Methylophilaceae, Comamonadaceae, Anaerolineaceae, unclassified JG30-KF-CM45, Acidobacteria Subgroup 6 family and Eubacteriaceae were stimulated by the TrOCs (Figure 33 A and B). The amended subsurface sediment samples exhibited higher relative abundance in the families Xanthobacteriaceae, Hydrogenophiliaceae, Rhodospirillaceae, Methylophilaceae, Rhodocyclaceae, and an unclassified KD4-96 family at both DNA and RNA levels, Hyphomicrobiaceae, Caldilineaceae, Acidobacteria Subgroup 6 family only at the DNA level and Comamonadaceae, Anaerolineaceae, and Peptococcaceae at the RNA level, respectively (Figure 33 C and D).

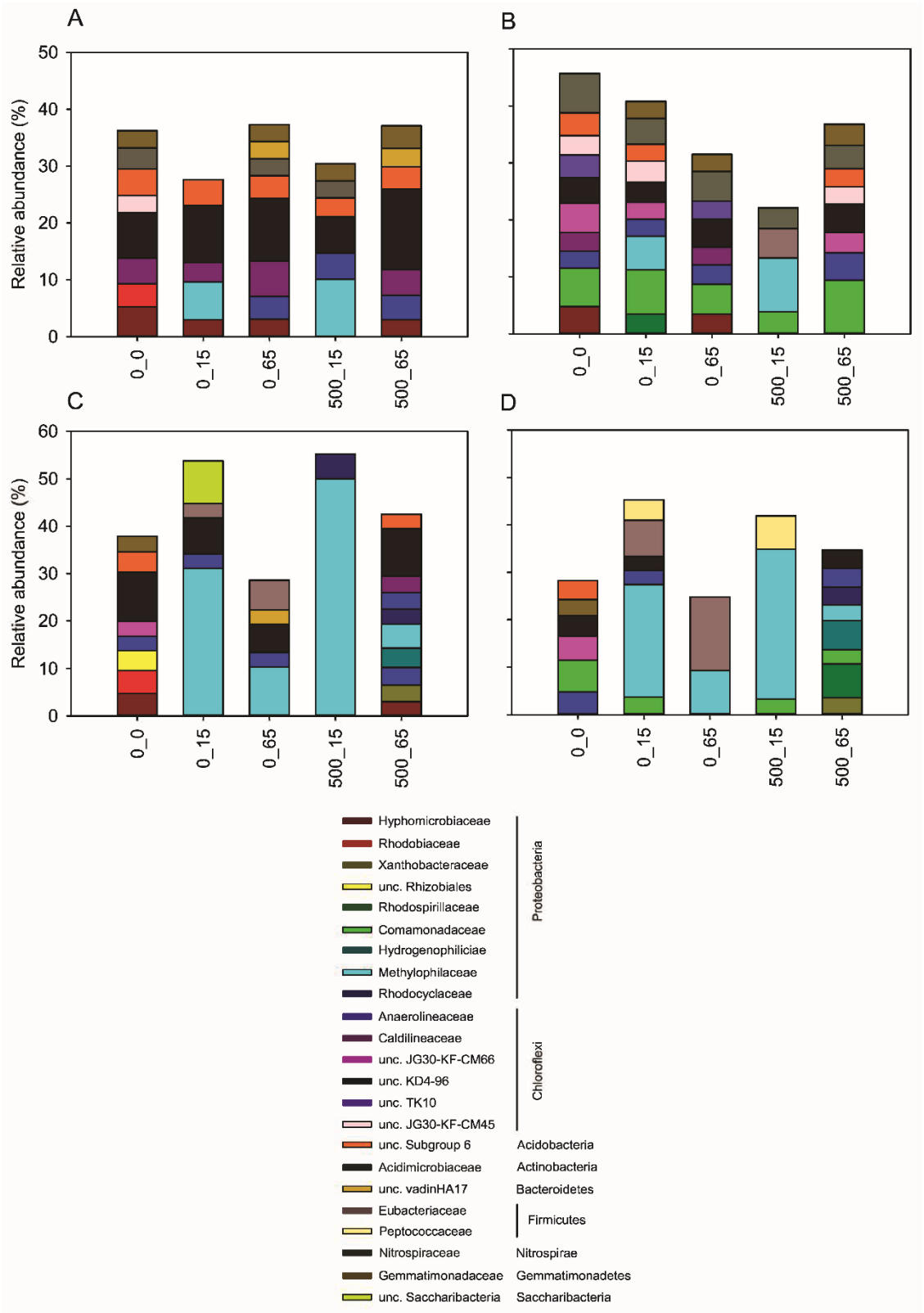

Figure 33. Mean relative abundance of major bacterial families (> 3 % relative abundance) on 16S rRNA gene and 16S rRNA level. Panel A and B correspond to 16S rRNA gene (A) and 16S rRNA (B) for surface sediment samples. Panel C and D correspond to 16S rRNA gene (A) and 16S rRNA (B) for subsurface sediment samples. Sample code: 0, 500 indicate supplemental TrOC concentrations in μgL^{-1}. 0, 15, 65 represent sampling days.

5.3.6. Microbial communities and taxa associated with degradation of the test compounds

Relative to unamended controls, some specific taxa were considered enriched by the test compounds based on the significant differential abundance as determined by Log2foldchange values (Table A7). Based on the 16S rRNA gene and 16S rRNA analyses, enriched taxa including known and unknown genera were only identified in the subsurface samples and affiliated with the phylum Proteobacteria (alpha-, delta-, gamma) and Bacteroidetes (Sphingobacteriia and Cytophagia) (Table A7).

5.4. Effects of bacterial diversity and hyporheic exchange flow on micropollutant removal

5.4.1. Effect of sediment dilution and bedforms on bacterial abundance and diversity

Sediment samples collected after 12 days of pre-incubation reached approximately 1.2 x 10^6 16S rRNA gene copy numbers per gram sediment dry weight (Figure 34) with no significant differences observed across the sediment dilution levels or bedform numbers (ANOVA, $p > 0.05$). Since bacterial abundance was similar among the treatments after the pre-incubation phase, any differences between treatments were attributed to differences in bacterial diversity rather than overall bacterial abundance for this period (Posselt et *al.* 2020). The number of 16S rRNA gene sequences per sample ranged from 12,512 to 37,293. The datasets were normalized to a uniform sequencing depth of 12,512 per sample for diversity analyses.

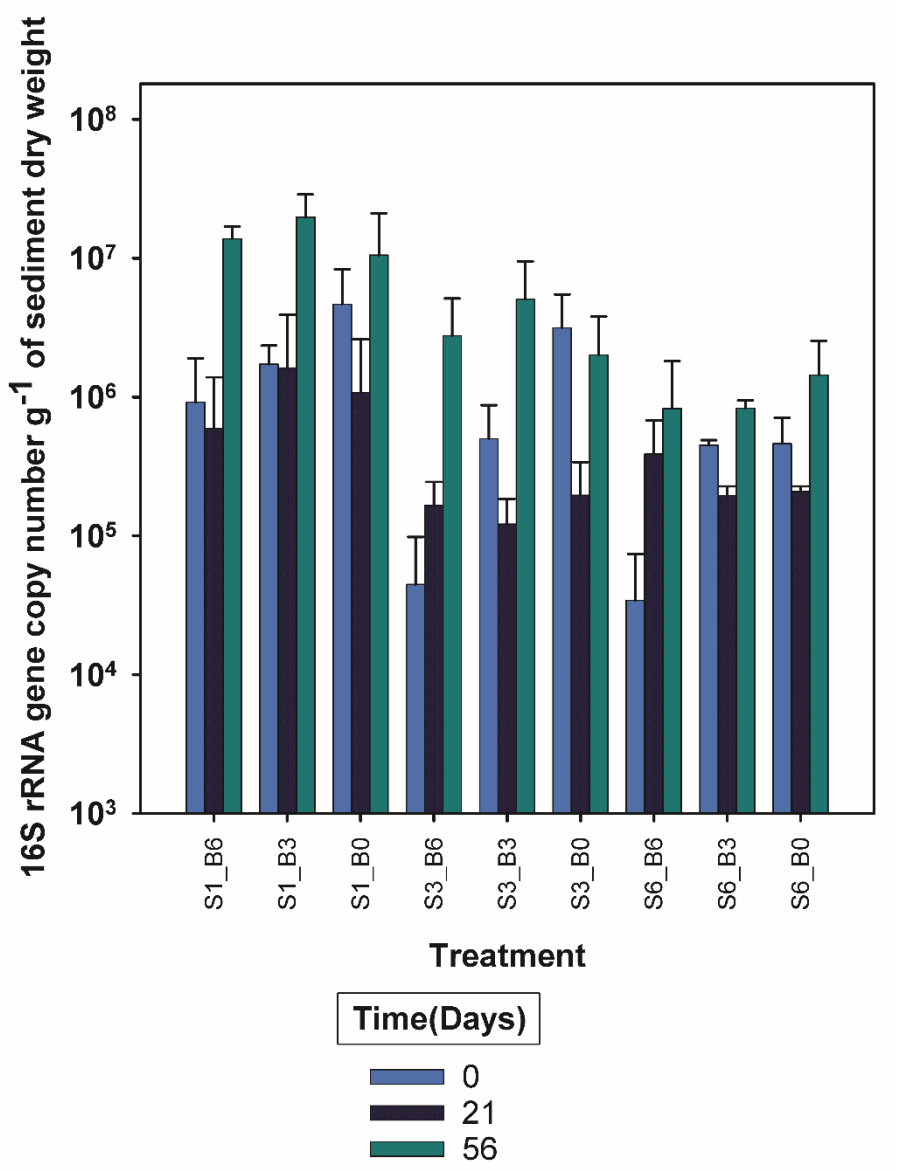

Figure 34. Copy number of 16S rRNA genes per g of dry sediment obtained from real-time PCR at sampling days 0, 21 and 56 of the attenuation phase. S1, S3 and S6 correspond to a sediment: sand dilution of 1:10, $1:10^3$, and $1:10^6$, respectively; B6, B3 and B0 correspond to 6, 3 and 0 bedforms, respectively.

The sediment dilution resulted in a significant decrease in species richness and diversity (Shannon) in S3 and S6 compared to S1 at days 0, 21 and 56 (ANOVA, $p < 0.05$) and between S6 and S3, at day 56 (Figure 35). Furthermore, a significant decrease in evenness was also observed in S3 and S6 compared to S1 at day 56 (ANOVA, $p < 0.05$, Figure 35). The bedform elements did not significantly affect any of the diversity indices measured at any of the sampling time points (ANOVA, $p > 0.05$,

Figure 35) with electrical conductivity data from the salt dilution analysis showing the bedform features did not significantly affect HEF (ANOVA, $p > 0.05$) (Jaeger *et al.* 2019b).

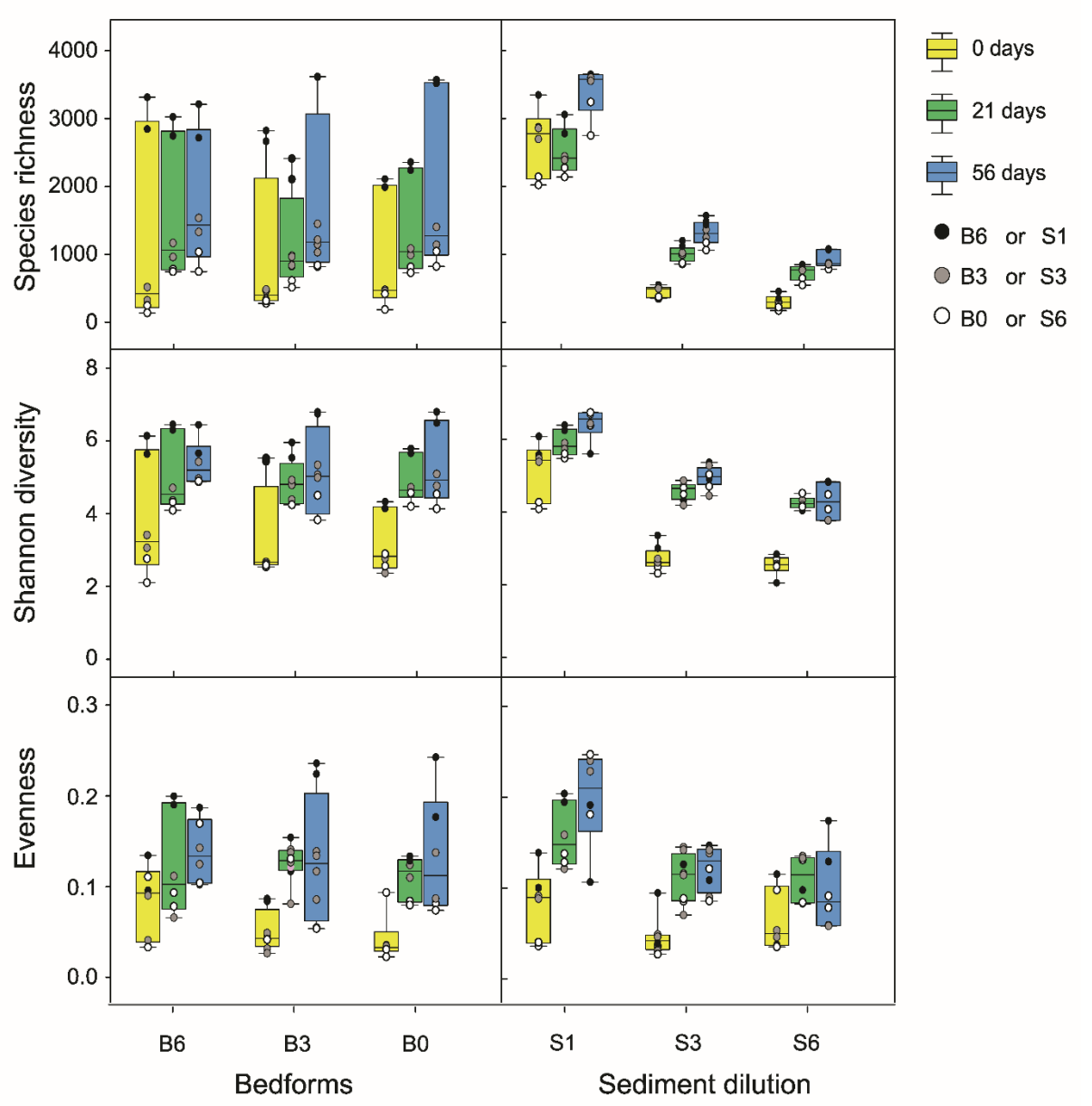

Figure 35. Boxplots of alpha diversity indices based on 16S rRNA gene sequence analysis as a function of bedform number and sediment dilution. B6, B3 and B0 correspond to 6, 3 and 0 bedforms; S1, S3 and S6 correspond to a sediment: sand dilution of 1:10, $1:10^3$, and $1:10^6$, respectively, respectively. Samples were collected before fortification (day 0) and at days 21 and 56 of the attenuation phase. The diversity indices, species richness and Shannon diversity as a function of sediment dilution were significantly different between the least dilute sediment and the subsequent dilutions at all sampling time points while evenness was only significantly different between the least diluted sediment and the subsequent dilutions at day 56 ($p \leq 0.05$). Diversity indices among treatments as a function of the bedform number were similar ($p > 0.05$).Figure modified and used with permission from Posselt *et al.* (2020).

5.4.2. Dissipation half-lives of organic contaminants

The DT50s of the 31 test compounds ranged from 0.5 (fluoxetine) to 306 days (carbamazepine) (Table 16). The most persistent compounds (median DT50s >20 days across all flumes) were carbamazepine (306 days), clofibric acid (223 days), gemfibrozil (67 days), metaxalone (43 days), benzotriazole (39 days), hydrochlorothiazide (30 days), celiprolol (29 days), and naproxen (26 days). In contrast, diclofenac, furosemide, paracetamol and sulfamethoxazole dissipated in less than one day in the majority of the flumes. For these short-lived substances, DT50s could not be determined, and instead DT50s of 0.5 days were assumed. Parent compounds with noticeably short DT50s were fluoxetine (0.5 days), sitagliptin (1.0 day), and citalopram (1.3 days). Among the spiked substances were five beta-blockers (atenolol, celiprolol, metoprolol, propranolol and sotalol), of which four had similar DT50s (2.0 to 3.2 days), while the DT50 for celiprolol was an order of magnitude higher (29 days).

Table 16. Overview minimum DT50 (days) among treatments. Table used with permission from Posselt *et al.* (2020).

Sed. dilution		**S1**			**S3**			**S6**	
Bedforms	**B6**	**B3**	**B0**	**B6**	**B3**	**B0**	**B6**	**B3**	**B0**
Acesulfame	2.3	2.1	2.3	11.0	13.6	12.8	12.7	12.7	21.2
Amisulpride	3.8	4.2	5.1	4.6	7.1	10.3	7.0	5.9	4.3
Atenolol	0.2	0.3	0.3	2.9	2.5	2.9	6.3	6.2	4.4
Benproperine	1.8	1.5	1.7	1.8	2.3	1.2	3.4	2.2	2.4
Bezafibrate	2.6	2.3	3.2	11.0	9.2	5.7	12.7	10.4	9.0
Benzotriazole	32.8	29.6	32.3	44.9	64.9	76.2	21.4	34.0	24.9
Carbamazepine	64.7	81.7	76.3	210.1	170.7	322.5	289.7	338.5	286.9
Celiprolol	9.0	9.0	10.5	32.9	35.1	33.0	15.3	25.4	21.9
Clofibric acid	67.2	69.9	68.5	128.1	203.8	140.7	242.1	317.5	274.0
Citalopram	1.9	1.5	1.3	1.0	1.1	1.1	1.5	1.0	1.0
Diclofenac	10.7	9.2	10.2	NA	NA	NA	NA	NA	NA
Flecainide	7.1	8.0	7.2	7.1	2.8	1.1	2.5	3.6	2.7
Fluoxetine	0.5	0.5	0.5	0.4	0.4	0.3	0.4	0.4	0.5
Furosemide	6.3	7.0	6.4	NA	NA	NA	NA	NA	NA
Gemfibrozil	17.1	18.2	24.4	54.1	37.3	65.9	71.8	131.5	53.6
Hydrochlorothiazide	20.1	20.3	21.9	29.0	31.2	29.4	28.4	33.6	28.9
Ibuprofen	1.4	1.3	2.0	10.4	9.4	9.5	13.9	10.9	10.3
Irbesartan	6.6	5.6	5.6	5.3	0.5	1.5	3.1	8.4	4.8
Ketoprofen	4.3	4.4	5.3	8.5	9.1	9.1	10.7	10.8	10.1
Metformin	3.6	4.3	4.0	5.8	7.1	6.8	21.1	19.6	23.7
Metoprolol	0.5	0.5	0.5	2.3	2.1	2.1	4.4	6.5	3.6
Metaxalone	14.4	16.2	19.2	38.1	42.8	34.7	62.1	50.2	42.7
Naproxen	7.6	6.9	7.6	26.8	21.8	33.8	36.7	30.1	38.9
Paracetamol	1.0	1.0	1.0	1.0	1.0	1.0	1.0	1.0	1.0
Propranolol	0.5	0.5	0.5	2.5	1.3	1.7	3.2	4.9	2.9
Sitagliptin	2.7	2.1	1.7	0.5	0.5	0.4	0.5	0.5	0.5

Sulfamethoxazole	13.2	14.5	13.3	NA	NA	NA	NA	NA	NA
Sotalol	0.5	0.7	0.8	4.4	2.7	2.3	4.6	6.4	4.1
Sulpiride	1.6	1.5	1.9	8.8	10.1	12.4	9.9	10.5	9.8
Valsartan	3.3	3.0	2.9	8.2	6.3	7.1	10.4	11.7	8.2
Venlafaxine	4.9	5.0	5.0	3.6	3.1	4.4	4.7	4.3	3.9

5.4.3. Transformation products formation

In total, we determined 32 TPs in at least one pore water or surface water sample using targeted methods (confidence level: 1) (Table 17) and an additional 25 suspected TPs (confidence level: 3-4) (Table 18) in surface water via the suspect screening workflow (4.6.5). For six parent compounds (acesulfame, flecainide, gemfibrozil, naproxen, paracetamol, sitagliptin) no TPs were included in our target list and suspects were not found. Exclusively target TPs were detected for benzotriazole, carbamazepine, citalopram, diclofenac, hydrochlorothiazide, ibuprofen, sulfamethoxazole, sulpiride, valsartan and venlafaxine, while only suspect TPs were found for benproperine, celiprolol, clofibric acid, furosemide, ketoprofen, metaxalone, propranolol and sotalol. Substances to which we could associate with both suspect and target TPs were amisulpride, atenolol, bezafibrate, fluoxetine, irbesartan, metformin and, metoprolol. Only five out of the 32 TPs on our target list could not be quantified in any sample: 4-hydroxy-1H-benzotriazole, acridone, homogentisic acid, carboxyibuprofen and alpha-hydroxymetoprolol. Three TPs were exclusively detected in pore water (acridine, diclofenac amide and 1-hydroxyibuprofen) whereas two were specific for surface water (1-hydroxy-benzotriazole and 3-[(4-chlorobenzoyl)-amino]propanoic acid) but all were infrequently detected (<7%; Figure 36).

Among all target TPs, valsartan acid (valsartan acid 20.1 µg L^{-1} pore water, 16.4 µg L^{-1} surface water) and metoprolol acid (15.3 µg L surface water, 14.9 µg L^{-1} pore water) occurred at the highest concentrations. The most abundant TP formed exclusively from a single parent compound (metformin) was guanylurea with 9 µg L^{-1} in surface and 7.1

µg L^{-1} in pore water. Several benzotriazole TPs occurred in high abundance (1.1-5.6 µg L^{-1}), including 1-hydroxybenzotriazole, 1-methylbenzotriazole and 4/5-methylbenzotriazole but were at the same time almost exclusively formed in S1 treatments (low dilution, high diversity) and therefore overall, not very frequently detected. Seven TPs were detected in more than 50% of all analyzed samples: N-desmethylvenlafaxine (77%), 4-amino-6-chloro-1-3-benzenedisulfonamide (75%), metoprolol acid (metoprolol acid, 68%), chlorothiazide (66%), valsartan acid (62%), carbamazepine-10, 11-epoxide (56%) and venlafaxine N-oxide (54%).

Table 17. Target transformation products (TPs): Minimum, maximum and average concentrations (ng L^{-1}) in pore water (PW) and surface water samples (SW) from the 20 spiked flumes systems. Table used with permission from Posselt *et al.* (2020).

	Porewater			Surface water		
Transformation product	MAX	MIN	AVG	MAX	MIN	AVG
4-Amino-6-chloro-1-3-benzenedisulfonamide	3535	0	1031	3305	0	1328
Amisulpride N-oxide	24	0	1	110	0	15
Atenolol-desisopropyl	3995	0	59	3045	0	93
1-Hydroxy-Benzotriazole	1105	0	17	0	0	0
4/5-Methylbenzotriazole	1170	0	189	555	0	136
3-[(4-chlorobenzoyl)-amino]propanoic acid	16	0	0	0	0	0
Iminostilbene	47	0	1	6	0	0
Citalopram carboxylic acid	96	0	11	125	0	19
Citalopram didesmethyl	140	0	26	125	0	27
Desmethyicitalopram	77	0	4	84	0	4
4-Trifluoromethylphenol	3	0	0	20	0	1
N4-Acetylsulfamethoxazole	945	0	69	1075	0	130
Sulpiride N-oxide	15	0	0	83	0	11
Venlafaxine N-desmethyl	295	0	28	155	0	50
Venlafaxine N-N-didesmethyl	20	0	0	24	0	0
Venlafaxine N-oxide	61	0	8	160	0	31
Venlafaxine N-O-didesmethyl	125	0	14	81	0	4
1-Hydroxyibuprofen	0	0	0	883	0	4
2/3-Hydroxyibuprofen	7259	0	162	3437	0	84
2/4-Chlorobenzoic acid	1534	0	70	1878	0	126
Acridine	0	0	0	208	0	3
Diclofenac amide	0	0	0	219	0	2
1-Methyl-Benzotriazole	4692	0	163	1363	0	6
Carbamazepine-10-11-dihydro-10-11-dihydroxy	696	0	24	188	0	15
Carbamazepine epoxide	189	0	27	142	0	47
Chlorothiazide	778	0	205	769	0	213
4-Hydroxydiclofenac	583	0	51	643	0	36
Guanylurea	7060	0	580	8976	0	480
Atenolol acid (Metoprolol acid)	14905	0	1828	15273	0	1760
Sulfamethoxazole N1-glucuronide	673	0	3	498	0	4
Valsartan acid	20125	0	4510	16428	0	4182
Venlafaxine O-desmethyl	604	0	66	220	0	29

Table 18. Detected transformation product properties (suspects). logKOW and logDOW, pH 8.3 were predicted from SMILES strings using JChem for Excel (Vers. 19.14.0.500, ChemAxon). Major species at pH 8.3 (average pH across flumes) were calculcated using the ChemAxon's Calculator (cxcalc) in batch mode. RT.m: measured retention time (RT). RT.p: RT predicted from logDOW, pH 3, i.e. at mobile phase pH, with the following formula: RT.p = (logDOW, pH 3+5.4)/0.42 min. Please note that measured and predicted RTs of amisulpride.sTP127, celiprolol.sTP381, metoprolol.sTP237 and metoprolol.sTP239 were relatively large (> 5 min) Table used with permission from Posselt *et al.* (2020).

Parent comp.	sTP(ESI)	Spec	logDow	logKow	SumF	exact-mass	RT.m	RT.p
Amisulpride	sTP127(+)	C	0.23	0.48	C7H13NO	127.0997	*16.5*	*5.7*
Benproperine	sTP325(+)	C	3.23	3.66	C21H27NO2	325.2042	18.0	13.2
Bezafibrate	sTP327(+)	A	-0.10	3.38	C19H21NO4	327.1471	21.0	20.8
Celiprolol	sTP161(+)	Z	-2.62	-2.61	C7H15NO3	161.1052	4.1	5.7
Celiprolol	sTP381(+)	C	0.12	1.59	C20H35N3O4	381.2628	*14.0*	*8.9*
Celiprolol	sTP210(+)	A	-3.01	0.55	C10H10O5	210.0528	15.3	13.5
Celiprolol	sTP248(+)	N	1.32	1.32	C13H16N2O3	248.1161	11.6	15.9
Celiprolol	sTP250(+)	N	1.87	1.94	C13H18N2O3	250.1317	18.4	17.5
Clofibric acid	sTP104(-)	A	-3.51	-0.04	C4H8O3	104.0473	8.1	12.7
Fluoxetine	sTP409(+)	A	0.15	3.61	C21H22F3NO4	409.1501	21.5	21.4
Furosemide	sTP250(-)	A	-2.73	0.66	C7H7ClN2O4S	249.9815	11.6	14.4
I Irbesartan	sTP446(+)	A	3.34	4.84	C25H30N6O2	446.2430	19.9	24.4
Irbesartan	sTP213(+)	A	-1.59	1.84	C11H19NO3	213.1365	18.6	17.2
Ketoprofen	sTP210(+)	N	4.39	4.39	C15H14O	210.1045	22.4	23.3
Metoprolol	sTP226(-)	N	0.66	0.66	C12H18O4	226.1205	17.1	14.4
Metoprolol	sTP210(-)	A	-2.38	1.05	C11H14O4	210.0892	16.5	15.3
Metoprolol	sTP225a(+)	Z	-2.27	-2.24	C11H15NO4	225.1001	10.5	6.5
Metoprolol	sTP225b(+)	C	-0.08	0.80	C12H19NO3	225.1365	12.6	8.2
Metoprolol	sTP237(+)	C	-0.06	1.31	C13H19NO3	237.1365	*19.0*	*8.2*
Metoprolol	sTP239(+)	C	-0.55	0.83	C13H21NO3	239.1521	*18.9*	*7.1*
Metoprolol	sTP253(+)	Z	-1.24	-1.22	C13H19NO4	253.1314	11.3	8.3
Metformin	sTP103(+)	N	-1.71	-1.71	C2H5N3O2	103.0382	5.5	8.8
Metaxalone	sTP251(-)	A	-1.97	1.52	C12H13NO5	251.0794	15.4	16.3
Propranolol	sTP202(-)	A	-1.18	2.28	C12H10O3	202.0630	19.0	18.2
Sotalol	sTP189(+)	Z	-2.53	-2.52	C8H15NO4	189.1001	9.2	6.1

5.4.4. Association between bacterial diversity and DT50s

Species richness, Shannon diversity and evenness as a function of sediment dilution significantly correlated with 21, 22 and nine out of the 31 biotransformed compounds, respectively, compared to 3, 6 and 6 as a function of the bedform number (Table 19, Spearman, $p < 0.05$).

Table 19. Correlation analysis of alpha diversity indices and individual parent compound DT50. Each value represents r (Spearman rank correlation coefficients) with the p value in parenthesis: * Correlations significant at $p < 0.05$. Table used with permission from Posselt *et al.* (2020).

	Sediment dilution						Bedforms					
	Species richness		Shannon diversity H'		Shannon evenness		Species richness		Shannon diversity H'		Shannon evenness	
Acesulfame	-0.76	(0.00)*	-0.73	(0.00)*	-0.48	(0.03)*	-0.76	(0.00)*	-0.73	(0.00)*	-0.48	(0.03)*
Amisulpride	-0.44	(0.05)	-0.63	(0.00)*	-0.60	(0.01)*	-0.13	(0.59)	-0.51	(0.02)*	-0.66	(0.00)*
Atenolol	-0.79	(0.00)*	-0.70	(0.00)*	-0.41	(0.07)	-0.79	(0.00)*	-0.70	(0.00)*	-0.41	(0.07)
Benproperine	-0.38	(0.09)	-0.44	(0.05)	-0.30	(0.20)	0.19	(0.41)	0.30	(0.19)	0.08	(0.72)
Bezafibrate	-0.57	(0.01)*	-0.55	(0.01)*	-0.43	(0.06)	0.09	(0.71)	-0.03	(0.91)	-0.23	(0.33)
Benzotriazole	-0.32	(0.16)	-0.39	(0.09)	-0.33	(0.15)	0.04	(0.86)	-0.38	(0.10)	-0.47	(0.04)*
Carbamazepine	-0.62	(0.00)*	-0.68	(0.00)*	-0.59	(0.01)*	-0.62	(0.00)*	-0.68	(0.00)*	-0.59	(0.01)*
Celiprolol	-0.61	(0.00)*	-0.65	(0.00)*	-0.49	(0.03)*	-0.09	(0.71)	-0.40	(0.08)	-0.46	(0.04)*
Clofibric acid	-0.56	(0.01)*	-0.63	(0.00)*	-0.36	(0.12)	0.05	(0.82)	0.17	(0.46)	-0.05	(0.85)
Citalopram	0.56	(0.01)*	0.57	(0.01)*	0.36	(0.12)	0.35	(0.13)	0.55	(0.01)*	0.32	(0.16)
Diclofenac	0.31	(0.56)	0.31	(0.56)	0.31	(0.56)	0.37	(0.50)	0.43	(0.42)	0.54	(0.30)
Flecainide	0.08	(0.72)	0.14	(0.56)	0.08	(0.72)	-0.05	(0.82)	-0.33	(0.16)	-0.34	(0.14)
Fluoxetine	0.20	(0.40)*	0.59	(0.01)*	0.61	(0.00)*	-0.09	(0.70)	0.20	(0.39)	0.37	(0.10)
Furosemide	-0.09	(0.92)	-0.09	(0.92)	-0.09	(0.92)	-0.14	(0.80)	0.03	(1.00)	-0.03	(1.00)
Gemfibrozil	-0.60	(0.01)*	-0.71	(0.00)*	-0.39	(0.09)	-0.08	(0.73)	0.07	(0.77)	-0.03	(0.89)
Hydrochlorothiazide	-0.56	(0.01)*	-0.64	(0.00)*	-0.33	(0.15)	-0.09	(0.69)	-0.03	(0.91)	-0.22	(0.34)
Ibuprofen	-0.65	(0.00)*	-0.53	(0.02)*	-0.40	(0.08)	-0.04	(0.88)	0.02	(0.93)	-0.22	(0.35)
Irbesartan	0.05	(0.82)	0.10	(0.66)	-0.05	(0.85)	0.00	(0.98)	-0.18	(0.44)	-0.35	(0.13)
Ketoprofen	-0.69	(0.00)*	-0.83	(0.00)*	-0.60	(0.01)*	-0.28	(0.23)	0.25	(0.14)	-0.36	(0.12)
Metformin	-0.68	(0.00)*	-0.67	(0.00)*	-0.40	(0.08)	-0.27	(0.25)	-0.20	(0.39)	-0.25	(0.28)
Metoprolol	-0.71	(0.00)*	-0.62	(0.00)*	-0.38	(0.10)	-0.17	(0.47)	-0.18	(0.45)	-0.29	(0.22)
Metaxalone	-0.50	(0.02)*	-0.76	(0.00)*	-0.61	(0.00)*	-0.13	(0.58)	-0.22	(0.35)	-0.36	(0.12)
Naproxen	-0.78	(0.00)*	-0.82	(0.00)*	-0.34	(0.14)	-0.17	(0.47)	-0.03	(0.88)	0.04	(0.87)
Paracetamol	NA	NA	NA	NA	NA	NA	NA	NA	NA	NA	NA	NA
Propranolol	-0.75	(0.00)*	-0.61	(0.00)*	-0.29	(0.21)	-0.19	(0.41)	-0.13	(0.59)	-0.15	(0.53)
Sitagliptin	0.65	(0.00)*	0.84	(0.00)*	0.71	(0.00)*	0.18	(0.44)	0.41	(0.07)	0.51	(0.02)*
Sulfamethoxazole	-0.43	(0.42)	-0.43	(0.42)	-0.43	(0.42)	-0.54	(0.30)	-0.26	(0.66)	-0.26	(0.66)
Sotalol	-0.63	(0.00)*	-0.50	(0.02)*	-0.35	(0.12)	-0.10	(0.68)	-0.14	(0.55)	-0.29	(0.21)
Sulpiride	-0.74	(0.00)*	-0.71	(0.00)*	-0.42	(0.06)	-0.27	(0.25)	-0.46	(0.04)*	-0.45	(0.05)
Valsartan	-0.70	(0.00)*	-0.64	(0.00)*	-0.29	(0.21)	-0.12	(0.62)	-0.19	(0.42)	-0.22	(0.34)

Venlafaxine	0.45	(0.05)	0.22	(0.37)	-0.12	(0.63)	0.40	(0.08)	0.17	(0.46)	-0.19	(0.41)

5.4.5. Transformation product dynamics at different levels of bacterial diversity and hyporheic exchange flow

In total, 21 of the detected TPs (11 confidence level 1, 12 confidence level 3-4) displayed increasing or constant concentrations in surface water in at least one of the three diversity levels throughout the experiment (i.e. no signs of degradation) and were therefore considered potentially persistent (Figure 36). 11 target TPs showed latter behavior in pore water and 7 of those were accumulating or constant in both pore water and surface water (4-amino-6-chloro-1-3-benzenedisulfonamide, amisulpride N-oxide, carbamazepine-10-11-dihydro-10-11-dihydroxy,carbamazepine-epoxide, chlorothiazide, N4-acetylsulfamethoxazole, venlafaxine N-desmethyl). In these counts, we included TPs with increasing trends leveling off towards the end of the experiment which can be due to depletion of the parent molecules (e.g. carbamazepine epoxide). In several cases, increasing TP concentrations were observed in dilution levels S3 and/or S6 only (medium and low diversity), while higher bacterial diversity in S1 treatments seemed to enable their degradation (e.g. amisulpride N-oxide). Remarkably, venlafaxine N-desmethyl was the only TP with increasing or constant concentrations across all diversity levels in both pore water and surface water throughout the experiment, despite the low DT50 of its parent compound (venlafaxine). Accordingly, ~80% of enlafaxine was removed from the water phase in all flumes as early as day 21. Since venlafaxine N-desmethyl was also the most frequently detected TP along with another abundant venlafaxine TP (venlafaxine N-oxide), we consider both as environmentally relevant. For majority of the target TPs, the effect of HEF due to variable number of bedforms was not apparent (Table 20) while for suspect TPs the bedform variable was not resolved (Table 21).

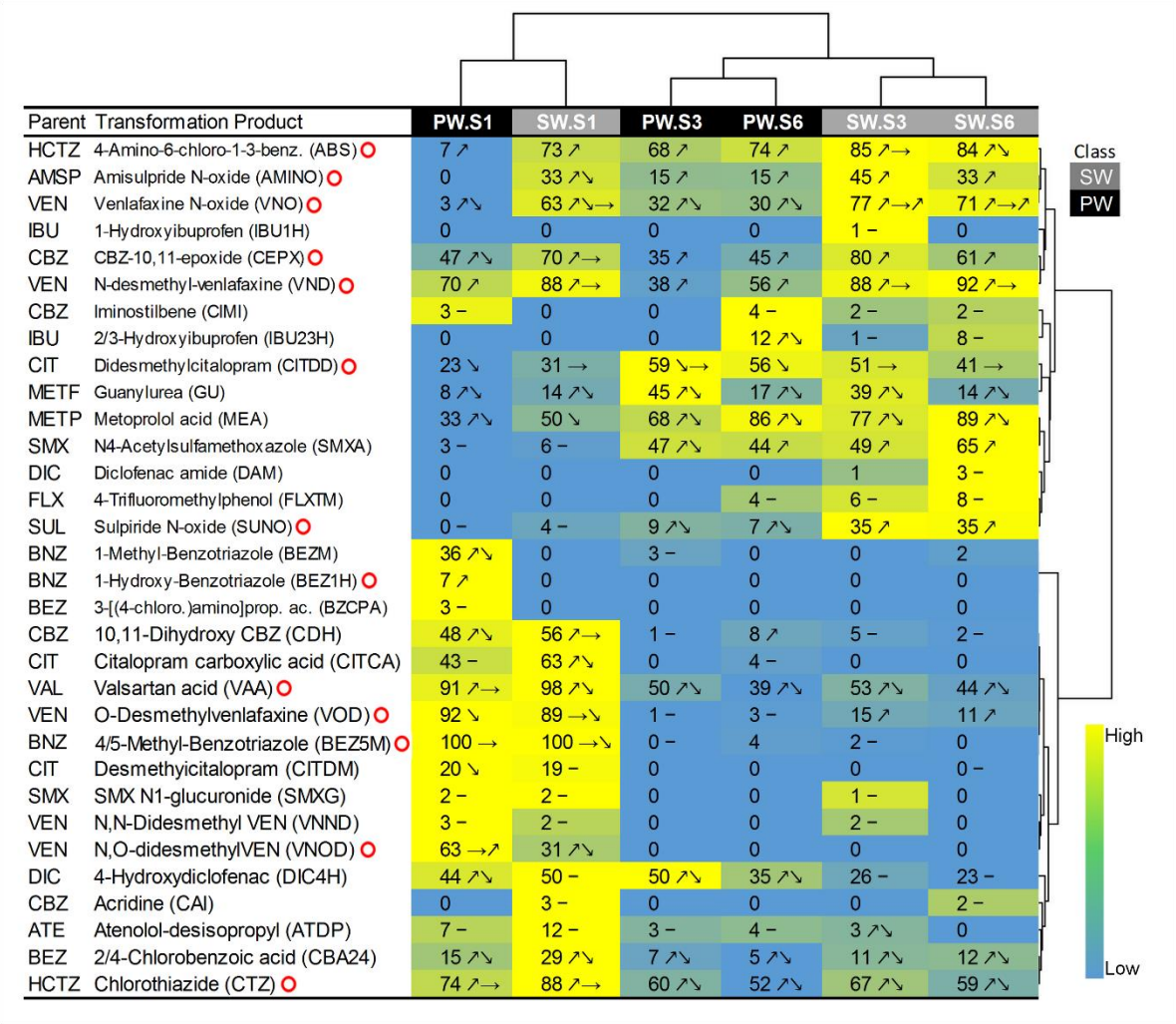

Parent	Transformation Product	PW.S1	SW.S1	PW.S3	PW.S6	SW.S3	SW.S6
HCTZ	4-Amino-6-chloro-1-3-benz. (ABS) ○	7 ↗	73 ↗	68 ↗	74 ↗	85 ↗→	84 ↗↘
AMSP	Amisulpride N-oxide (AMINO) ○	0	33 ↗↘	15 ↗	15 ↗	45 ↗	33 ↗
VEN	Venlafaxine N-oxide (VNO) ○	3 ↗↘	63 ↗↘→	32 ↗↘	30 ↗↘	77 ↗→↗	71 ↗→↗
IBU	1-Hydroxyibuprofen (IBU1H)	0	0	0	0	1 –	0
CBZ	CBZ-10,11-epoxide (CEPX) ○	47 ↗↘	70 ↗→	35 ↗	45 ↗	80 ↗	61 ↗
VEN	N-desmethyl-venlafaxine (VND) ○	70 ↗	88 ↗→	38 ↗	56 ↗	88 ↗→	92 ↗→
CBZ	Iminostilbene (CIMI)	3 –	0	0	4 –	2 –	2 –
IBU	2/3-Hydroxyibuprofen (IBU23H)	0	0	0	12 ↗↘	1 –	8 –
CIT	Didesmethylcitalopram (CITDD) ○	23 ↘	31 →	59 ↘→	56 ↘	51 →	41 →
METF	Guanylurea (GU)	8 ↗↘	14 ↗↘	45 ↗↘	17 ↗↘	39 ↗↘	14 ↗↘
METP	Metoprolol acid (MEA)	33 ↗↘	50 ↘	68 ↗↘	86 ↗↘	77 ↗↘	89 ↗↘
SMX	N4-Acetylsulfamethoxazole (SMXA)	3 –	6 –	47 ↗↘	44 ↗	49 ↗	65 ↗
DIC	Diclofenac amide (DAM)	0	0	0	0	1	3 –
FLX	4-Trifluoromethylphenol (FLXTM)	0	0	0	4 –	6 –	8 –
SUL	Sulpiride N-oxide (SUNO) ○	0 –	4 –	9 ↗↘	7 ↗↘	35 ↗	35 ↗
BNZ	1-Methyl-Benzotriazole (BEZM)	36 ↗↘	0	3 –	0	0	2
BNZ	1-Hydroxy-Benzotriazole (BEZ1H) ○	7 ↗	0	0	0	0	0
BEZ	3-[(4-chloro.)amino]prop. ac. (BZCPA)	3 –	0	0	0	0	0
CBZ	10,11-Dihydroxy CBZ (CDH)	48 ↗↘	56 ↗→	1 –	8 ↗	5 –	2 –
CIT	Citalopram carboxylic acid (CITCA)	43 –	63 ↗↘	0	4 –	0	0
VAL	Valsartan acid (VAA) ○	91 ↗→	98 ↗↘	50 ↗↘	39 ↗↘	53 ↗↘	44 ↗↘
VEN	O-Desmethylvenlafaxine (VOD) ○	92 ↘	89 →↘	1 –	3 –	15 ↗	11 ↗
BNZ	4/5-Methyl-Benzotriazole (BEZ5M) ○	100 →	100 →↘	0 –	4	2 –	0
CIT	Desmethyicitalopram (CITDM)	20 ↘	19 –	0	0	0	0 –
SMX	SMX N1-glucuronide (SMXG)	2 –	2 –	0	0	1 –	0
VEN	N,N-Didesmethyl VEN (VNND)	3 –	2 –	0	0	2 –	0
VEN	N,O-didesmethylVEN (VNOD) ○	63 →↗	31 ↗↘	0	0	0	0
DIC	4-Hydroxydiclofenac (DIC4H)	44 ↗↘	50 –	50 ↗↘	35 ↗↘	26 –	23 –
CBZ	Acridine (CAI)	0	3 –	0	0	0	2 –
ATE	Atenolol-desisopropyl (ATDP)	7 –	12 –	3 –	4 –	3 ↗↘	0
BEZ	2/4-Chlorobenzoic acid (CBA24)	15 ↗↘	29 ↗↘	7 ↗↘	5 ↗↘	11 ↗↘	12 ↗↘
HCTZ	Chlorothiazide (CTZ) ○	74 ↗→	88 ↗→	60 ↗↘	52 ↗↘	67 ↗↘	59 ↗↘

Figure 36. The heat map shows a two-way cluster analysis using Euclidean distance measures with respect to detection rates (expressed as % of all analyzed samples within the respective class with concentrations above the limit of quantification (LOQ); fields were color coded with yellow = high detection rates and blue = low detection rates) of target transformation products (TPs). Hierarchical clusters were generated for TPs and average detection rates of the six sample classes (pore water (PW) or surface water (SW) for each of the three diversity levels as a function of sediment dilution: S1 (low dilution, high diversity), S3 (medium dilution/diversity), S6 (high dilution, low diversity)). Observed TP concentration dynamics in surface water and pore water across the different bacterial diversities (S) are depicted as arrows: upward (↗), downward (↘), stable (→) concentration trends; groups of arrows indicate cases in which changing trends were observed during the experiment; dashes indicate cases where no clear trend was observed. Red circles indicate TPs that were identified as persistent in at least one of the classes. Five TPs were not detected in any sample and are therefore not shown: 4-hydroxy-1H-benzotriazole, acridone, diclofenac amide, carboxyibuprofen, alpha-hydroxymetoprolol. Full names of parent compounds can be found in table 1. Figure used with permission from Posselt *et al.* (2020).

Table 20. Observed concentration dynamics of target transformation products(confirmed with reference standard) in surface water (SW) and pore water (PW) across the different levels of hyporheic exchange flow (B0 plain sediment, B3 three bedforms, B6 six bedforms) are depicted as arrows (upward, downward, stable); dashes indicate cases where no clear trend was observed. “n.d.” indicates that compounds could not be quantified or were not detected. Table used with permission from Posselt *et al.* (2020).

Parent	Transformation product	PW			SW		
		B0	B3	B6	B0	B3	B6
Hydrochlorothiazide	4-Amino-6-chloro-1-3-benzenedisulfonamide	↗→	↗→	↗	↗↘	↗→	↗↘
Hydrochlorothiazide	Chlorothiazide	↗↘	↗↘	↗↘	↗↘	↗↘	↗↘
Amisulpride	Amisulpride N-oxide	–	–	↗	↗	↗	↗
Atenolol	Atenolol-desisopropyl	–	n.d.	–	–	–	–
Benzotriazole	1-Hydroxy-Benzotriazole	–	n.d.	–	n.d.	n.d.	n.d.
Benzotriazole	1-Methyl-Benzotriazole	↗↘	↗↘	↗↘	n.d.	n.d.	n.d.
Benzotriazole	4-Hydroxy-1H-Benzotriazole	n.d.	n.d.	n.d.	n.d.	n.d.	n.d.
Benzotriazole	4/5-Methylbenzotriazole	↗	↗	→	→	↗	→
Bezafibrate	2/4-Chlorobenzoic acid	–	–	–	↗↘	↗↘	↗↘
Bezafibrate	3-[(4-chlorobenzoyl)-amino]propanoic acid	–	n.d.	n.d.	n.d.	n.d.	n.d.
Carbamazepine	Acridine	n.d.	n.d.	n.d.	n.d.	–	–
Carbamazepine	Acridone	n.d.	n.d.	n.d.	n.d.	n.d.	n.d.
Carbamazepine	Carbamazepine-10-11-dihydro-10-11-dihydroxy	↗	–	↗→	↗→	↗→	↗↘
Carbamazepine	Carbamazepine epoxide	↗	↗	↗	↗	↗	↗
Carbamazepine	Iminostilbene	n.d.	–	–	–	–	n.d.
Citalopram	Citalopram carboxylic acid	–	–	–	–	–	–
Citalopram	Citalopram didesmethyl	↘	↘	→	–	↘	↘
Citalopram	Desmethyicitalopram	↘	↘	↘	–	–	–
Diclofenac	Diclofenac amide	n.d.	n.d.	n.d.	–	–	n.d.
Diclofenac	4-Hydroxydiclofenac	↗↘	↗↘	↗↘	–	–	–
Diclofenac	Homogentisic acid	n.d.	n.d.	n.d.	n.d.	n.d.	n.d.
Fluoxetine	4-Trifluoromethylphenol	n.d.	n.d.	–	–	–	–
Metformin	Guanylurea	↗↘	↗↘	↗↘	↗↘	↗↘	↗↘

Ibuprofen	1-Hydroxyibuprofen	n.d.	n.d.	n.d.	n.d.	−	n.d.
Ibuprofen	2/3-Hydroxyibuprofen	↗↘	↗↘	↗↘	−	−	−
Ibuprofen	Carboxyibuprofen	n.d.	n.d.	n.d.	n.d.	n.d.	n.d.
Metoprolol	Atenolol acid (Metoprolol acid)	↗↘	↗↘	↗↘	↗↘	↗↘	↗↘
Metoprolol	alpha-Hydroxymetoprolol	n.d.	n.d.	n.d.	n.d.	n.d.	n.d.
Sulfamethoxazole	N4-Acetylsulfamethoxazole	↗↘	↗↘	↗	↗→	↗	↗
Sulfamethoxazole	Sulfamethoxazole N1-glucuronide	−	n.d.	−	n.d.	−	n.d.
Sulpiride	Sulpiride N-oxide	−	−	−	−	↗	↗
Valsartan	Valsartan acid	↗→	↗→	↗→	↗↘	↗↘	↗↘
Venlafaxine	Venlafaxine N-desmethyl	↗	↗	↗	↗→	↗→	↗→
Venlafaxine	Venlafaxine N-N-didesmethyl	−	n.d.	n.d.	−	−	n.d.
Venlafaxine	Venlafaxine N-oxide	↗↘	↗↘	↗↘	↗→	↗	↗→
Venlafaxine	Venlafaxine N-O-didesmethyl	↗	↘	↘	↘	↘	↘
Venlafaxine	Venlafaxine O-desmethyl	↘	↘	↘	↗↘↗	↗↘↗	↗↘↗

Table 21. Concentration dynamics of suspect transformation products (TPs) across the different levels of bacterial diversity (S1, S3 and S6).The bedform variable is not resolved. Table used with permission from Posselt *et al*. (2020).

Parent	TP	SumF	S1	S3	S6
Amisulpride	sTP127(+)	C7H13NO	−	↗↘	↗↘
BEN	sTP325(+)	C21H27NO2	↗→(↘)	↗	(↗)
Bezafibrate	sTP327(+)	C19H21NO4	↗→	↗	↗
Celiprolol	sTP161(+)	C7H15NO3	−	↘	↘
	sTP381(+)	C20H35N3O4	↗	↗	↗
	sTP210(+)	C10H10O5	↗	↗	↗
	sTP248(+)	C13H16N2O3	↗	↗	↗
	sTP250(+)	C13H18N2O3	↗↘	−	−
Clofibric acid	sTP104(-)	C4H8O3	↓	↘	↓
Fluoxetine	sTP409(+)	C21H22F3NO4	↕	↕	↕
Furosemide	sTP250(-)	C7H7ClN2O4S	↗	↗	↗
Irbesartan	sTP213(+)	C11H19NO3	−	↗↘	↗↘
	sTP446(+)	C25H30N6O2	↗↘	↗↘	↗↘
Ketoprofen	sTP210(+)	C15H14O	↗↘	↗↘	↗↘
Metformin	sTP103(+)	C2H5N3O2	↗↘	−	−
Metoprolol	sTP210(+)	C11H14O4	↗→	↗	↗
	sTP226(-)	C12H18O4	−	↗↘	↗
	sTP225a(+)	C11H15NO4	↘	↗↘	−
	sTP225b(+)	C12H19NO3	↘	↗↘	−
	sTP237(+)	C13H19NO3	↗→(↘)	↗	↗
	sTP239(+)	C13H21NO3	↗↘	↗↘	↗↘
	sTP253(+)	C13H19NO4	−	−	↗↘
Metaxalone	sTP251(-)	C12H13NO5	↗	↗	↗
Propranolol	sTP202(-)	C12H10O3	↗↘	↗→↘	↗
Sotalol	sTP189(+)	C8H15NO4	↗↘	↗→↘	↗

5.4.6. Bacterial community structure and taxa associated with test compound biotransformation supporting communities

The bacterial community composition across treatments was visualized at the phylum level using relative abundance values (n/N) (n, the number of sequences for each OTU and N, the total number of sequences in the sample).The unamended flumes with intermediate S and B levels were used as representative samples to investigate the effect of TrOCs on the taxa impacted by the presence of test compounds in comparable amended flumes. The DESeq2 multifactorial design in R was employed to determine genera whose abundance changed significantly between amended and unamended controls with incubation time as a covariate.

17 known phyla were detected in S1 compared to 13 known phyla in the S3 and S6 dilution levels (Figure 37). This shows that the dilution-to-extinction approach successfully removed some of the rare occurring phyla such as Saccharibacteria, Latescibacteria and Nitrospirae detected in the S1 sediment bacterial community. Within the remaining phyla, specific taxa impacted by the presence of test compounds were identified on the basis of a significant change in abundance relative to unamended controls using the *DESeq2* function (Table A8). The taxa associated with the collective biotransformation of the test compounds were considered enriched in case of log2foldchange > 0 in comparison to unamended samples. These included OTUs affilated with the phylum Acidobacteria such as Holophagae and subgroups 6, 17, and 22. *Nocardioides* and *Illumatobacter* (Actinobacteria), *Terrimonas* and *Flavobacterium* (Bacteroidetes) and *Sphingomonas, Sphingobium* and *Novosphingobium, Arenimonas*, *Pseudomonas and Mesorhizobium* (Proteobacteria).

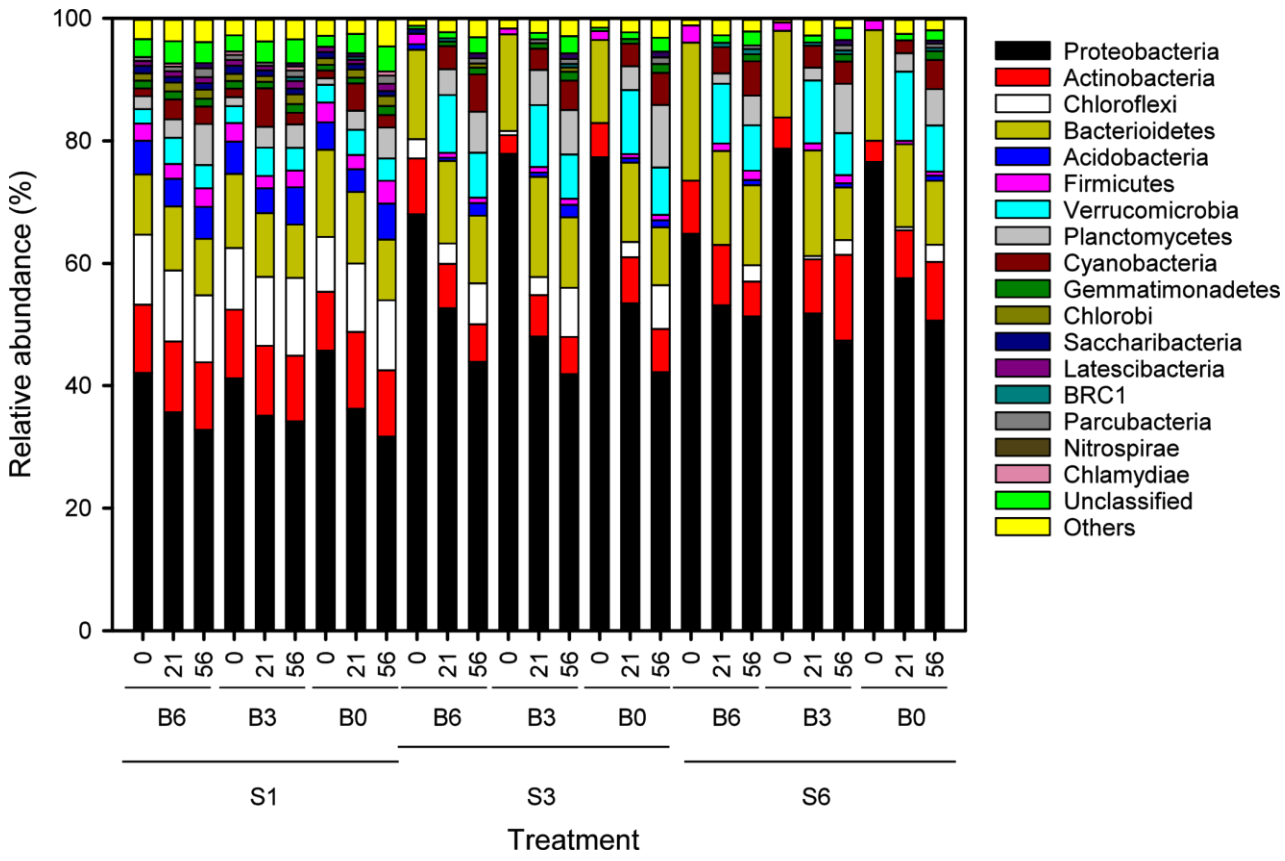

Figure 37. Bacterial community composition at the phylum level in relative abundance values (%) in the respective treatments sampled at days 0, 21 and 56. “Others” represents all phyla whose relative abundance was below 0.5 %. Figure modified and used with permission from Posselt *et al.* (2020).

6. DiSCUSSION

6.1. Biodegradation of ibuprofen: Mineralization potential in the hyporheic zone?

The widely consumed non-steroidal anti-inflammatory drug ibuprofen is an ideal model compound to study the fate of emerging micropollutants in the hyporheic zone as it is frequently detected in many rivers. The large surface area occupied by the sediment particles, pore spaces and organic matter represents an ideal habitat for the proliferation of a diverse microbial community with high metabolic versatility (Boulton *et al.* 1998). The potential to effectively remove ibuprofen, therefore, provides the basis for highlighting that the hyporheic zone sustains efficient biotic (micro-)pollutant degradation, and hitherto unknown microbial diversity associated with (micro-)pollutant removal, a valuable ecosystem service.

The apparent degradation of ibuprofen without appreciable delay was demonstrated in the hyporheic zone sediments (Figure 8). Ibuprofen concentration was observed to influence the rate of degradation after the first feeding. The 400 µM ibuprofen treatment exhibited a nine-day lag phase in contrast to lower concentrations whose disappearance exhibited no significant delay. This is likely attributable to an inhibitory effect on the microbial activity as has been reported for ibuprofen concentration exceeding 50 mg L^{-1} (242 µM) by a decline in oxygen respiration and microbial diversity in activated sludge (Davids *et al.* 2017). Subsequent rapid depletion of ibuprofen following re-feeding irrespective of initial concentration (Figure 8 A-D) suggests a rapid enrichment of microbes capable of ibuprofen degradation and thus adaption of the microbial community. Adaption of an activated sludge microbial community to high concentrations of ibuprofen (5000 mg L^{-1}; 24 mM) after long term exposure shows a rather high limit for ibuprofen tolerance (Davids *et al.* 2017).

Microcosms containing supplemental acetate exhibited a delayed onset of ibuprofen degradation following initial spiking (Figure 8). This might be due to ibuprofen oxidation by enzymes activated during initial degradation of acetate rather than ibuprofen, a phenomenon associated with cometabolic degradation (Tran *et al.* 2013). It may also be due to preferential consumption of acetate by the indigenous hyporheic zone bacteria capable of ibuprofen consumption considering that acetate is a more easily degradable substrate than ibuprofen. In the latter case, ibuprofen is likely degraded upon acetate depletion (Rutere *et al.* 2020). Refeeding the microcosms with ibuprofen-acetate, however, exhibited a rapid ibuprofen degradation similar to ibuprofen-only microcosms, suggesting that ibuprofen degraders were enriched in the absence and presence of supplemental acetate. Ibuprofen stimulated similar taxa in treatments with ibuprofen only and acetate/ ibuprofen (Figure 17), supporting the view that metabolic degradation of ibuprofen was significant in the sediments and that many taxa in the hyporheic zone are prone to respond to ibuprofen. Consistent with previous studies, abiotic losses due to sorption and hydrolysis played a marginal role in total ibuprofen removal, demonstrating that ibuprofen removal was indeed mainly due to biodegradation (Figure 9; (Winkler *et al.* 2001; Kunkel and Radke 2008).

While previous studies in engineered and other natural environments reported biotransformation of ibuprofen (Zwiener *et al.* 2002; Xu *et al.* 2009; Radke *et al.* 2010; Tran *et al.* 2013; Verlicchi and Zambello 2014; Li *et al.* 2016), the different transformation intermediates 1-, 2-, 3-hydroxy- and carboxyibuprofen observed in this study were transiently detected, an indicator for further metabolism and potentially mineralization (Figures 10 and 38). Moreover, the variable intermediates detected suggested utilization of different metabolic pathways characteristic of a diverse bacterial community. As previously demonstrated in pure culture studies, unrelated

taxa exhibited variable biodegradation pathways for ibuprofen (Żur *et al.* 2018). For example, the ibuprofen degrader *Sphingomonas* Ibu-2 hydroxylates ibuprofen to isobutylocatechol following CoA ligation, which is then cleaved to 5-formyl-2-hydroxy-7-methylocta-2, 4-dienoic acid, before oxidation to 2-hydroxy-5-isobutylhexa-2, 4-dienedioic acid (Murdoch and Hay 2005; Murdoch and Hay 2013). *Variovorax* Ibu-1 degrades ibuprofen via ring-hydroxylated ibuprofen (Murdoch and Hay 2015). However, such degradation intermediates were only detected when further metabolism was inhibited by 3-fluorocatechol, suggesting that such intermediates are subject to rapid turnover and may escape detection during routine analyses. Thus, the absence of detected hydroxylated ring structures in our microcosms or the environment does not allow for conclusions on the importance of such ibuprofen degradation pathways (Rutere *et al.* 2020).

Bacillus thuringiensis B1 generates 2-hydroxyibuprofen through the aliphatic monooxygenase activity followed by a series of other enzymes leading to the eventual production of 3-hydroxy-cis,cis-muconic acid that enters the tricarboxylic acid cycle (Marchlewicz *et al.* 2017). *Nocardia* NRRL 5646 was shown to employ a carboxylic acid reductase enzyme system that reduces the carboxylic functional group of ibuprofen to the corresponding alcohol, which is then acetylated (Chen and Rosazza 1994). In this study, 2-hydroxyibuprofen was the primary intermediate identified (Figure 10). Thus, one of the initial reactions of ibuprofen utilization in the microcosms was the transformation of the aliphatic chain as observed with isolates and other environmental samples (Zwiener *et al.* 2002; Quintana *et al.* 2005).

All of the biodegradation pathways named above converge in the tricarboxylic acid cycle, allowing for assimilation of ibuprofen carbon and mineralization of ibuprofen to CO_2. 1,2-dihydroxyibuprofen is a probable dead-end product of fungal ibuprofen

metabolism, which was not detected in our microcosms (Figure 10; (Marco-Urrea *et al.* 2009). Enrichment of ibuprofen degraders, lack of inhibitory effects on ibuprofen degradation after 5 refeedings (Figure 8), and ibuprofen degradation by hyporheic zone isolates with ibuprofen as the only carbon and energy source (Figure 19) along with growth support, and the absence of detected accumulating ibuprofen transformation products (Figure 10) argue in favour of mineralization and assimilation of ibuprofen carbon by hyporheic zone sediment microorganisms potentially via the hypothesized biodegradation pathways (Figure 38);(Rutere *et al.* 2020).

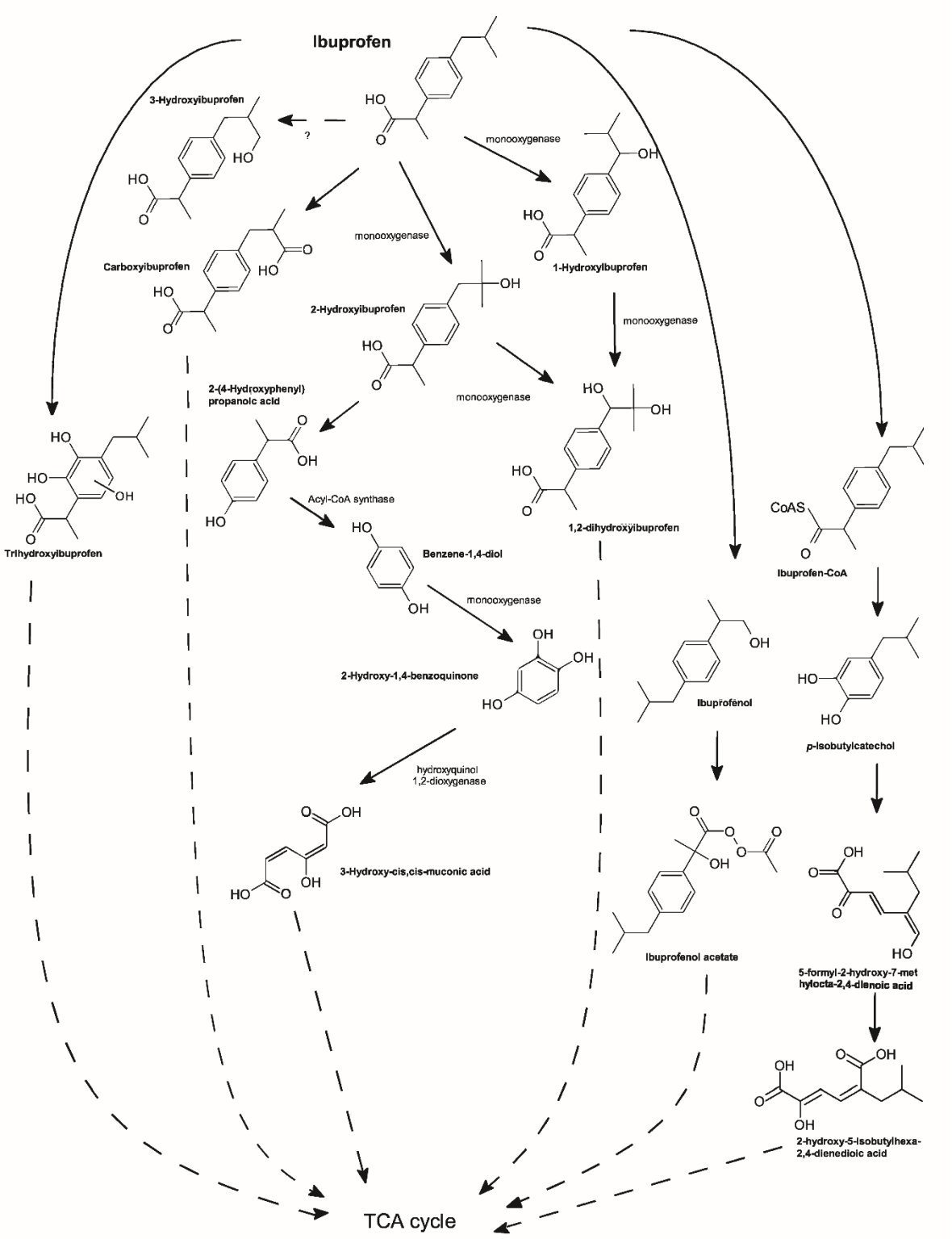

Figure 38. Hypothetical ibuprofen degradation pathway in oxic hyporheic zone sediments based on transformation products identified in this study and previous studies as compiled in Żur *et al.* (2018). Figure used with permission from Rutere *et al.* (2020).

6.1.1. Microbial community dynamics under ibuprofen stressor effect

The higher 16S rRNA copy numbers in ibuprofen treatments compared to unamended controls following the third refeeding (Figure 11), suggest a strong stimulation of the microbial community in the presence of ibuprofen since rRNA abundance serves as a proxy for activity (Herzog *et al.* 2015). Moreover, the identified taxa suggested the hyporheic zone of river Erpe hosted a diverse microbial community (Figures 12, 14; Table A1). Although there was a significant decrease in the Shannon diversity (ANOVA, $p < 0.05$), the species richness was similar in the treatments and controls at the RNA level (ANOVA, $p > 0.05$). Accumulating evidence suggests a positive correlation between species richness and some specific microbially-mediated processes such as micropollutant degradation (Stadler *et al.* 2018; Jaeger *et al.* 2019b; Posselt *et al.* 2020). The decline in Shannon diversity is likely due to selective pressure of ibuprofen on some members of the indigenous sediment microbiota as earlier observed in indigenous riverine biofilms exposed to pharmaceuticals (Lawrence *et al.* 2005).

6.1.2. Generalized ecological niches of ibuprofen-responsive phyla

OTUs affiliating with the phyla Proteobacteria, Bacteroidetes, Chloroflexi, Acidobacteria, Actinobacteria and Gemmatimonadetes were particularly shown to positively respond to ibuprofen amendment (Figures 14, 16, 17). Proteobacteria and Bacteroidetes were primarily observed in a study on a subsurface flow constructed wetland system treating ibuprofen contaminated wastewater and in oxic ibuprofen amended microcosms with activated sludge (Li *et al.* 2016; Davids *et al.* 2017), indicating the presence and response of members belonging to these key phyla in diverse environments to ibuprofen. Proteobacteria were most responsive to high ibuprofen concentrations (Figure 16 and (Davids *et al.* 2017). Their response may be

attributed to their general functional traits as aromatic compound degradation and capability to quickly respond to substrate availability (Seo *et al.* 2009; Ho *et al.* 2017). Microcosms with acetate as a primary substrate exhibited similar patterns relative to ibuprofen-only treatments in terms of relative phylum abundance (Figure 14). However, the relative abundance of Proteobacteria of the Class Gammaproteobacteria was significantly higher (ANOVA, $p < 0.05$) in ibuprofen-acetate-containing than in ibuprofen only microcosms. This would indicate that the Gammaproteobacteria stimulated here by ibuprofen are likewise capable of acetate utilization (Rutere *et al.* 2020).

The variable response to the different ibuprofen concentrations by members of the different phyla such as Acidobacteria, Gemmatimonadetes, and Latescibacteria that positively responded to lower ibuprofen concentrations (5 and 40 µM) and less to higher concentrations (200 and 400 µM; Figure 14), suggests that some bacteria can use micropollutants as a substrate within a specific range of concentration above which it turns toxic or inhibitory (Rutere *et al.* 2020). Thus, our study suggests distinct ecological niches for Proteobacteria that reflect lifestyles of r-strategists and Acidobacteria, Gemmatimonadetes as well as Latescibacteria that reflect lifestyles of K-strategists.

6.1.3. Putative taxa associated with degradation of ibuprofen

New and known bacteria enriched in ibuprofen-amended microcosms relative to unamended controls were associated with degradation of ibuprofen (Figures 14, 17; Table A1). Using the 40 and 400 µM ibuprofen concentrations as representative concentrations for low and high ibuprofen concentrations, diverse families and genera from many phyla were shown to be enriched. Some of these bacteria were also

observed in microcosms with intermediate ibuprofen concentrations and in the original sediment microbial community (Figure 17; Table A2).

Stimulation of Proteobacteria by ibuprofen was most prominent (Figures 16, 17; Table A1). Enrichment of Alphaproteobacteria-affiliated taxa of the Sphingomonadaceae and Hyphomonadaceae in ibuprofen treatments was prominent and corresponded to previous studies in which genera belonging to these families were associated with degradation of xenobiotics (Dallinger and Horn 2014; Braga *et al.* 2015; Bryant *et al.* 2016). Moreover, *Hyphomicrobium*, a genus from the family Hyphomicrobiaceae, has been previously associated with assimilation of 2,4-dichlorophenol, a soil and groundwater contaminant (Dallinger and Horn 2014). Genera closely related to *Sphingopyxis*, *Sphingorhabdus* and *Novosphingobium* affiliating with the ibuprofen-enriched family Sphingomonadaceae have been isolated from a wide variety of environments including freshwater and marine sediments and were associated with the degradation of a wide variety of natural aromatic compounds and xenobiotics (Ghosal *et al.* 2016; Silva *et al.* 2018). The ibuprofen degrading *Sphingomonas* IBU-2 (Murdoch and Hay 2013) and the isolation of the ibuprofen degrading *Novosphingobium* strain CR1 in the study (Rutere *et al.* 2020), extend previous observations to hyporheic zones, consolidate correlations, and emphasizes the biodegradation potential associated with Sphingomonadaceae.

New and known members of the Betaproteobacteriales family Comamonadaceae exhibited a positive association with ibuprofen. Comamonadaceae is among families with members previously reported to aerobically degrade aromatic compounds (Dallinger and Horn 2014). Of the characterized ibuprofen degraders belonging to this family is *Variovorax* Ibu-1 (Murdoch and Hay 2015). In a study exploring co-occurrence patterns between organic micropollutants and bacterial community structure, the

ibuprofen-enriched genus *Hydrogenophaga* (Comamonadaceae) was among bacteria significantly correlated to micropollutants and believed to host enzymes for biotransformation of specific micropollutants (Gao *et al.* 2019). The ibuprofen-enriched genus *Piscinibacter*, whose closest cultivated relative *Piscinibacter aquaticus* (basonym: *Methylibium aquaticum*) was isolated from a eutrophic freshwater pond (Song and Cho 2007), and the family Oxalobacteraceae were hitherto unassociated with the degradation of aromatic compounds (Figures 16,17; Table A1). However, these taxa belong to the order Burkholderiales, whose other families, including Comamonadaceae, are associated with such potentials. It is therefore likely that members Burkholderiales previously not associated with biodegradation may be linked to ibuprofen biotransformation. Enrichment of unknown genera belonging to the family Nitrosomonadaceae by ibuprofen corroborates reported potential of members of this family such as *Nitrosomonas* in bioremediation. Through the activity of ammonia monooxygenase, most ammonia-oxidizing bacteria in this family can co-metabolize micropollutants, thus minimizing potential toxic effects (Tran *et al.* 2013). Potential indirect effects like enhanced ammonia release from biomass turnover due to ibuprofen-stimulated microbial predation (see below) and ammonification might even allow for enhanced growth of certain nitrifiers in the presence of ibuprofen (Rutere *et al.* 2020).

Significant enrichment of Gammaproteobacterial families Pseudomonadaceae and Xanthomonadaceae in ibuprofen treatments is in congruence with previous findings, where Pseudomonadaceae is reported to be involved in biodegradation of polyaromatic compounds such as naphthalene (Ghosal *et al.* 2016). The genus *Pseudomonas* accommodates many isolates capable of aromatic compound degradation (Seo *et al.* 2009). Our isolate *Pseudomonas thivervalensis* MAH1 grew

with ibuprofen as sole carbon and energy source, demonstrating ibuprofen degradation capabilities of this genus (Figure 19)(Rutere *et al.* 2020). The ibuprofen-enriched genus *Arenimonas* (Xanthomonadaceae) has been previously associated with degradation of drugs such as penicillin and carbamazepine in activated sludge and contaminated soils (Cydzik-Kwiatkowska and Zielińska 2018). The genus *Thermomonas* (Xanthomonadaceae) was closely related to the aerobic *Thermomonas carbonis*, isolated from a coal mine (Wang *et al.* 2014), potentially indicating an association of these strains with the degradation of aromatic organic compounds.

The ibuprofen-enriched Deltaproteobacteria were from the orders Myxococcales and Bdellovibionales (Figures 16, 17; Table A1). Myxococcales are associated with degrading complex organic substances, complex secondary metabolism, and a predatory lifestyle (Reichenbach 2001; Livingstone *et al.* 2017). Ibuprofen-stimulated *Sandaracinus* like taxa were related to the cultivated starch-degrading *Sandaracinus amylolyticus* (Mohr *et al.* 2012). *Bdellovibiro* sp. enriched in response to ibuprofen indicated the stimulation of a group recognized as predatory organisms feeding on gram-negative bacteria (Pasternak *et al.* 2014). Predation on gram-negative ibuprofen degraders might likewise increase microbial biomass turnover and thus represent a source of variation in the data set, limiting ibuprofen-dependent stimulation. Thus, we suggest that the enrichment of Deltaproteobacteria in ibuprofen treatments is due to indirect effects, i.e. stimulation of ibuprofen degrading gram negatives serving as prey, rather than due to direct ibuprofen degradation capabilities of this group (Rutere *et al.* 2020).

Taxa affiliated with Actinobacteria, a phylum known to accommodate many species involved in the degradation of complex compounds including phenol, diesel oil, n-alkanes and polycyclic aromatic hydrocarbons (Seo *et al.* 2009; Zhang *et al.* 2012;

Alvarez *et al.* 2017), were also enriched in response to ibuprofen (Figures 15,16,17; Table A1). Such taxa included *Rhodococcus* sp. and *Nocardioides* related OTUs. Both genera are well known for their capabilities to degrade aromatic compounds (Seo *et al.* 2009). Previously, *Nocardia* strain NRRL 5646 of the Actinobacteria that transformed ibuprofen using the carboxylic acid reductase enzyme system has been characterized (Chen and Rosazza 1994); see the previous section). *Fodinicola* sp., closely related to the pesticide-degrading genus *Streptomyces* (Briceño *et al.* 2018), new *Lamia* related and *Illumatobacter* sp. were further examples for ibuprofen-enriched taxa. *Ilumatobacter* sp. was among Actinobacteria affiliated taxa previously considered as potential indicators for exposure to organic pollutants (Rodríguez *et al.* 2018), further highlighting the importance of known and hitherto undetected taxa of the Actinobacteria for biodegradation in the environment.

Ibuprofen-enriched genera affiliating with the phylum Bacteroidetes include *Terrimonas* and *Ferruginibacter* (family Chitinophagaceae, order Sphingobacteriales; Figures 15, 16, 17; Table A1). *Terrimonas* has been shown to degrade benzo[a]pyrene, a polycyclic aromatic hydrocarbon (PAH) (Song *et al.* 2015). The genes encoding the PAH-ring hydroxylating dioxygenase enzymes involved in the first hydroxylation steps of benzo[a]pyrene and other PAHs under aerobic conditions may predictably be involved in ibuprofen degradation. *Ferruginibacter* (Chitinophagaceae) related taxa were found in a fluidized bed reactor fed with alkyl benzene sulfonate (Braga *et al.* 2015). Though an ibuprofen degradation potential has not been previously reported, and members of the family Chitinophagaceae are primarily associated with the degradation of complex polymers including cellulose (Chung *et al.* 2012), ibuprofen degradation potential of *Ferruginibacter* related taxa cannot be excluded. *Flavobacterium*, a genus in the family Flavobacteriaceae, was also stimulated in

ibuprofen treatments as also previously reported (Li *et al.* 2016). Members of this genus have been isolated on 2,4-dichlorophenol (Männistö *et al.* 1999) and also associated with the transformation of pharmaceuticals (Stadler *et al.* 2018), suggesting capabilities for aromatic compound degradation. Bacteroidetes affiliated genera like *Chryseolinea* and other unclassified genera in the family env. OPS_17 (order Sphingobacteriales) were positively associated with ibuprofen amendment extending the reported association of the phylum with the degradation of high molecular weight organic compounds including petroleum hydrocarbons (Gargouri *et al.* 2014) and supporting the view that Bacteroidetes include environmentally relevant aerobic pollutant degraders (Rutere *et al.* 2020).

Few uncultured taxa from low abundance phyla whose ecophysiology is not well characterized were also enriched in ibuprofen treatments suggesting their potential contribution to the degradation of ibuprofen. Enrichment of hitherto unclassified families belonging to Subgroups 6, 17, 22 and other Acidobacterial families in the phylum Acidobacteria in response to ibuprofen extends previous reports on the association of members of this phylum with the degradation of contaminants like polychlorinated biphenyls (Nogales *et al.* 1999), petroleum compounds, metals and radionuclides (George *et al.* 2009). Taxa of the phyla Gemmatimonadetes and Latescibacteria responded to ibuprofen treatments. *Gemmatimonas aurantiaca* is capable of utilizing benzoate as sole carbon and energy source, and the genus *Gemmatimonas* was related to linear alkylbenzene sulfonate degradation in a bioreactor (Braga *et al.* 2015). Thus, there is some support for the hypothesis that such uncultured taxa are likewise involved in ibuprofen degradation (Zhang *et al.* 2003). However, even less information is available for other ibuprofen-stimulated, uncultured taxa of the Armatimonadetes, Chloroflexi, Chlorobi, and some Candidate divisions

(Table A1), demonstrating the need for further research to consolidate a role of such taxa for biodegradation.

6.2. Redox gradients favour enhanced degradation of micropollutants

Effluents impact most receiving rivers from upstream WWTPs with high nutrient loading and in extreme cases, eutrophication (Drury *et al.* 2013). The settling and accumulation of organic matter in the hyporheic zone results in rapid depletion of dissolved oxygen and a sharp redox gradient may be established creating oxic benthic and underlying anoxic sediments (Brunke and Gonser 1997). The effect of this redox delimitation on the pollutant removal capacity of the hyporheic zone cannot be underestimated as it directly affects the resident microbiota dynamics and associated micropollutant biodegradation pathways. The removal of metoprolol, a top 200 drug prescribed in the US, Canada and Germany (Scheurer *et al.* 2010), and ubiquitously detectable in the wastewater effluents (Rubirola *et al.* 2014) due to incomplete removal WWTPs (Souchier *et al.* 2016), provides insights into the potential of the hyporheic zone to remove micropollutants under such dynamic redox conditions.

6.2.1. Metoprolol removal under oxic and anoxic conditions: Dissimilar biotransformation pathways

The removal of metoprolol in the sediment microcosms was primarily attributed to biodegradation and a lesser extent to sorption (Figure 21). Biodegradation was the dominant mechanism accounting for the total removal of metoprolol compared to about 21 % observed in sorption (Figure 21), extending previous studies conducted *in situ* on the same river that reported both, biodegradation and sorption, as the critical attenuation mechanisms for metoprolol in the hyporheic zone (Posselt *et al.* 2018; Schaper *et al.* 2019). Our findings are likewise consistent with previous reports demonstrating the significant contribution of biodegradation in the removal of metoprolol in diverse environments including riverbank filtration systems, WWTPs,

subsurface flow constructed wetlands, biological activated carbon systems and surface water (Schmidt *et al.* 2007; Rubirola *et al.* 2014; Rühmland *et al.* 2015; Abromaitis *et al.* 2016; Li and McLachlan, 2019).

The extended lag phase before metoprolol depletion occurred following initial feeding compared to the immediate onset of degradation in subsequent refeeding (Figure 21 A and B) may be attributed to expression of enzymes involved in its degradation or to the enrichment of the metoprolol-degraders to sufficient abundances for metoprolol degradation to be detectable over time. Indeed, the short hydraulic retention time (6 - 18 h) characteristic of most modern WWTPs (Maurer *et al.* 2007) is considered a contributing factor to their low efficiency in removing most emerging micropollutants (Peralta-Maraver *et al.* 2018b) Our findings, therefore, demonstrate that longer residence time in the sediment matrix may result in enhanced degradation of compounds otherwise considered less or non-biodegradable in conventional WWTPs.

In addition to the residence time, the underlying redox conditions influence the ecological functioning of the hyporheic zone. In a comparable riverbank filtration system, redox conditions were shown to have a more pronounced effect on the removal of micropollutants such as metoprolol than residence times of the water (Schmidt *et al.* 2007). Overall, metoprolol removal rates were comparable under oxic and anoxic conditions (Figure 21 A and B). Though incomplete metoprolol removal under anoxic conditions was observed in the 150 µM treatment after the third refeeding, the complete removal in the 15 µM treatment suggests the anticipated environmental relevant concentrations are amenable to complete removal. Our findings are comparable to the reported riverbank filtration system where metoprolol removal of over 80% occurred under oxic, suboxic, and anoxic conditions (Schmidt *et*

al. 2007), and highlight the potential for complete metoprolol removal under the dynamic redox conditions characteristic of the hyporheic zone.

The biotransformation of metoprolol via different transformation products under oxic and anoxic conditions (Figure 22), suggested the utilization of different metabolic pathways (Figure 39) by the different bacterial communities inhabiting the redox-delineated segments of the hyporheic zone. Under oxic conditions, MTPA was detected only upon depletion of metoprolol (Figure 22 A) suggesting formation via the o-desmethylmetoprolol intermediate as previously reported in open-water wetland microcosms (Svan *et al.* 2016). Moreover, as shown in Figure 22 A, the concentration of MTPA was higher than the initial metoprolol concentration spiked in the third refeeding further suggesting additional MTPA accrued from the oxidation of o-desmethylmetoprolol generated from the preceding (second) re-feeding regime (Figure 21 A). Formation of MTPA directly from metoprolol through CYP450-mediated dealkylation during aerobic microbial biotransformation was also hypothesized in the current study (Figure 39), as previously reported (Kern *et al.* 2010; Posselt *et al.* 2020). In a previous study using batch experiments with activated sludge, MTPA, α-HMTP and O-DMTP were identified as metoprolol transformation products. The latter two transformation products, however, accounted for less than 5% of the initial metoprolol concentration (Rubirola *et al.* 2014), suggesting that α-HMTP may have been formed in the current setup under oxic conditions but was below the detection limit.

Accumulation of MTPA concomitant to metoprolol degradation under anoxic conditions (Figure 22 B), indicated formation via anaerobic o-demethylation. O-demethylation is the initial step in the biodegradation of most methoxylated aromatic compounds by anaerobic bacteria (DeWeerd *et al.* 1988; Liu and Suflita 1993). Moreover, the formation of α-HMTP likely occurred via the oxygen-independent hydroxylase activity,

a universally ubiquitous mechanism for attacking recalcitrant substrates in the absence of oxygen, where water is the source of the hydroxyl group (Heider *et al.* 2016; Rabus *et al.* 2016). The disappearance of the transformation products (Figure 22) under both conditions points to further biotransformation via the intermediates shown (Figure 39) as predicted using the EAWAG-BBD Pathway Prediction System (http://eawag-bbd.ethyporheic zone.ch/predict/aboutPPS.html) or may suggest potential mineralization of metoprolol by the hyporheic zone microbial communities. Taken together, it is evident that redox-delimitations promote variable biodegradation pathways probably from the different bacterial taxa occupying specific niches in the hyporheic zone which is eventually beneficial to the complete degradation of metoprolol particularly in case of downwelling conditions where metoprolol-containing surface water enters the deeper oxygen-depleted hyporheic zones.

The contribution of sorption to the overall removal of metoprolol in the hyporheic zone cannot be underestimated though minor compared to biodegradation. Previous studies conducted *in situ* on River Erpe also reported biodegradation and sorption as the most relevant attenuation mechanisms for metoprolol in the hyporheic zone (Posselt *et al.* 2018; Schaper *et al.* 2019) Sorption of metoprolol onto sediments may vary due to factors influencing its interaction with sediments such as pH and the organic matter content (Schaper *et al.* 2019). In this study, the observed sorption of metoprolol to the sediment was likely influenced by the ambient pH 6.6 measured in the microcosms. Beta-blockers occur in the cationic form at pH 6.5/6.6 as a result of the protonation of the amino moiety of the side chain (Ramil *et al.* 2010). Therefore, sorption to the sediment was likely due to cationic exchange processes. The concentration of metoprolol remained relatively constant throughout the incubation in the water serving

as hydrolysis control, suggesting hydrolysis plays no significant role in attenuation of metoprolol.

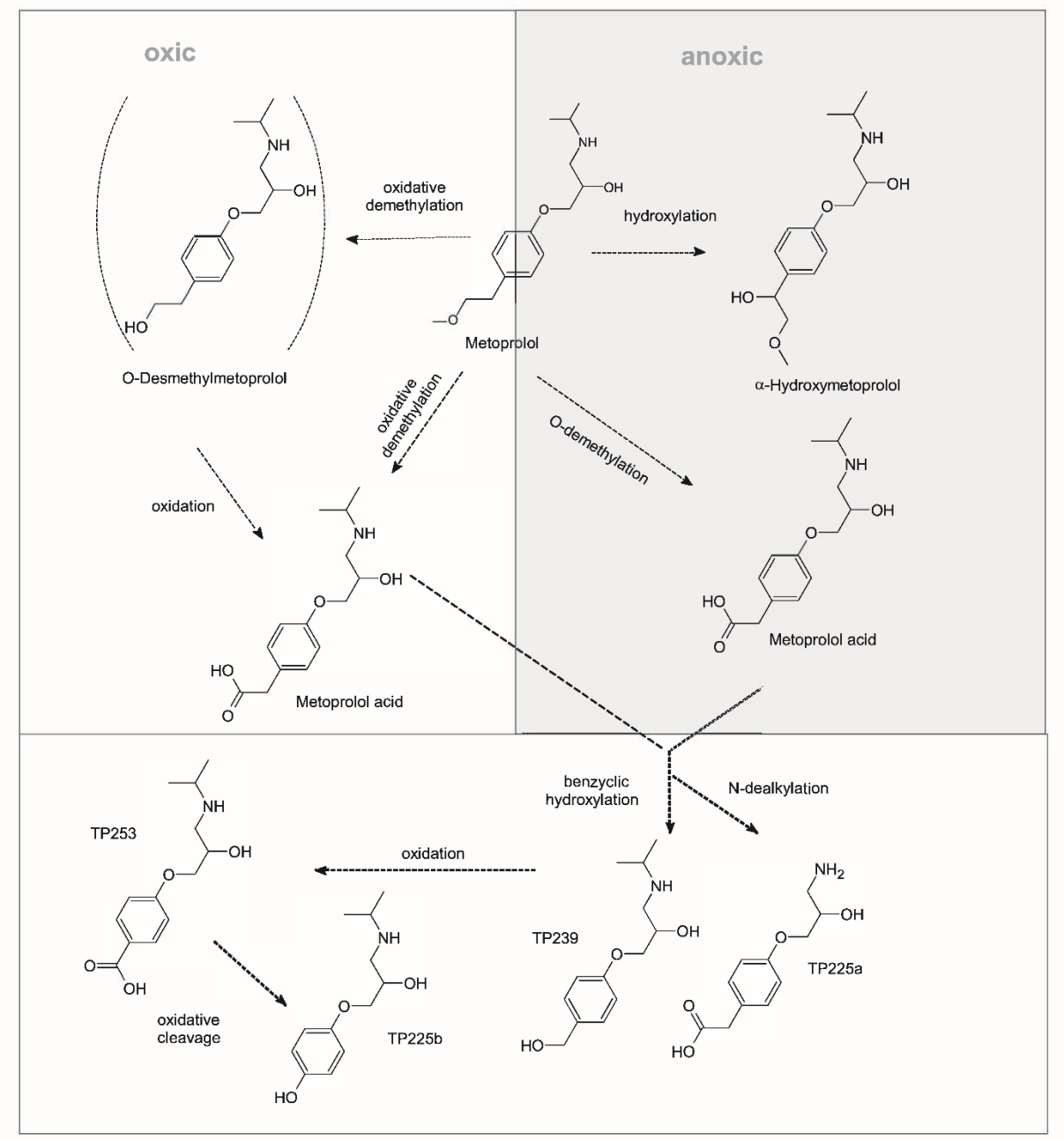

Figure 39. Hypothetical metoprolol biotransformation pathways in hyporheic zone sediments under oxic and anoxic conditions based on transformation products identified in this study and predicted further intermediates.

6.2.2. Bacterial community structure and composition dynamics in metoprolol-impacted oxic hyporheic zone sediments

Samples amended with metoprolol did not differ significantly in terms of bacterial diversity and richness relative to controls likely due to other prevailing edaphic factors cancelling out any apparent effects of metoprolol amendment or resilience of the resident bacterial community against stressors. The decline in the diversity indices at the RNA level following depletion of metoprolol at day 120 (Figure 24 A-C; 21), however, suggests a substantial fraction of the enriched bacterial community actively relied on metoprolol for energy metabolism.

The predominance of Proteobacteria and Bacteroidetes in the sediment samples was as previously reported in other hyporheic zone studies (Marti *et al.* 2017; Kim and Lee 2019). As broadly diverse phyla with complex substrate degradation capabilities (Seo *et al.* 2009; Thomas *et al.* 2011), their prevalence in metoprolol treatments suggests their likely involvement in its removal. Chloroflexi, Acidobacteria and Actinobacteria also exhibited stimulation in metoprolol treatments (Figure 26 A and B). These phyla have also been previously associated with degradation of xenobiotics including polycyclic aromatic hydrocarbons (George *et al.* 2009; Seo *et al.* 2009; Zhang *et al.* 2012; Shahi *et al.* 2016), suggesting some members within these phyla may hold metoprolol degradation potential.

6.2.3. Putative taxa associated with degradation of metoprolol in oxic hyporheic zone sediments

Taxa enriched by metoprolol were identified based on the significant differential abundance relative to non-supplemented controls. Such potential degraders were classified to known or Candidatus genera and families (Figure 27 A and B; Table A3

and A4). Proteobacteria comprised the largest proportion of such responders to metoprolol treatment. Alphaproteobacteria-affiliated OTUs belonging to the family Caulobacteraceae included *Phenylobacterium* previously identified among specific genera in a core microbial community associated with degradation of compounds including metoprolol (Wolff *et al.* 2018). *Caulobacter,* linked to 4-chlorophenol degradation in addition to reported capability to degrade aromatic hydrocarbons (Zhao *et al.* 2016) was also enriched by metoprolol. The Sphingomonadaceae-affiliated *Sphingopyxis, Sphingomonas* and *Sphingobium* are widely reported xenobiotic degraders, in particular of aromatic compounds (Balkwill *et al.* 2003). Their potential involvement in metoprolol degradation further highlights the importance of the family Sphingomonadaceae in micropollutant removal in diverse environmental matrices.

The gammaproteobacterial *Acinetobacter*, belonging to the family Moraxellaceae is an established genus with many species harbouring dynamic metabolic potentials such as degradation of long-chain dicarboxylic acids, aromatic and hydroxylated aromatic compounds (Jung and Park, 2015). Besides, the enriched *Pseudomonas* was closely related to the cultivated *Pseudomonas stutzeri,* a naphthalene degrader (Shimada *et al.* 2012). The two genera belong to families affiliated with the order Pseudomonadales indicating the potential for taxa in this order to degrade polycyclic hydrocarbons. Though the metoprolol enriched *Rheinheimera* has not previously been linked to metoprolol degradation, it belongs to the family Chromatiaceae whose capability to degrade complex aromatic compounds such as naphthalene has been reported (Rochman *et al.* 2017). This suggests a high likelihood that this genus possesses the metabolic capacity to degrade metoprolol. The enrichment by metoprolol of *Limnobacter* (Burkholderiaceae), *Ralstonia* (Ralstoniaceae)*, Pelomonas, Albidiferax, Aquabacterium, Thiomonas* (Comamonadaceae) belonging to the order

Burkholderiales provides further evidence on the relevance of this order in the degradation of a wide spectrum of aromatic compounds including organic pollutants as highlighted through genomic analysis in (Pérez-Pantoja *et al.* 2012). Metoprolol-enriched taxa affiliated with the phylum Bacteroidetes were *Flavobacterium* and *Hydrotalea.* The aromatic hydrocarbon degradation potential of *Flavobacterium* is reported (Hemalatha and VeeraManikandan 2011). Their association with metoprolol enrichment, therefore, highlights the environmental relevance of the Bacteroidetes in organic micropollutant removal.

6.2.4. Bacterial community structure and composition dynamics in metoprolol-impacted anoxic hyporheic zone sediments

The microbial community alpha diversity at RNA level declined significantly following incubation, but the DNA-based diversity remained relatively similar to the original community (Figure 24 D, E, F). This suggests that while the metoprolol amendment may have negatively affected the activity of the community in terms of RNA gene expression, the basal microbial community remained resilient against the stressor effect of metoprolol. Moreover, a decline in richness and diversity while maintaining the functionality (removal of metoprolol) (Figure 21B) indicates the degradation of metoprolol was a function of a broad spectrum as opposed to a specific taxa range within the community.

Proteobacteria dominated metoprolol amended samples at both DNA and RNA levels (Figure 26 C and D) suggesting a quicker response of this phylum to metoprolol compared to other phyla. The broad metabolic diversity and quick response to substrate availability are characteristics of Proteobacteria (Ho *et al.* 2017), which may explain this phenomenon. Despite a decline in relative abundance at RNA level of some phyla including Chloroflexi, Acidobacteria, Actinobacteria and Bacteroidetes,

their contribution to metoprolol degradation cannot be overlooked as previous studies identified them among most abundant in sediment samples contaminated with more than 25 different micropollutants including metoprolol (Nega *et al.* 2019; Posselt *et al.* 2020).

6.2.5. Putative taxa associated with degradation of metoprolol in anoxic hyporheic zone sediments

In congruence with phyla relative abundances (Figure 26 C and D), most of the families and genera impacted by metoprolol affiliated with Proteobacteria (Figure 27 C and D; Table A5 and A6). The alphaproteobacterial family Hyphomicrobiaceae whose affiliated genera *Rhodomicrobium* and *Pedomicrobium* were enriched in metoprolol treatments has been associated with degradation of xenobiotics such as naphthenic acid found in oil sands process affected waters (Islam *et al.* 2016), suggesting a likelihood of these genera to have similar metabolic potential for metoprolol degradation. The genera *Rhodobium* (Hyphomicrobiaceae), *Rhodoplanes* (Rhodobiaceae), and an unclassified Rhizobiales OTU enriched in metoprolol treatments provide further evidence associated with the order Rhizobiales to degrade xenobiotics. Some members belonging to this order are reported degraders of toluene, xylene, benzene, phenol, halogenated aromatic compounds, hydroxyl benzoates and anthracene (Zhang *et al.* 2012). Metoprolol-enriched taxa belonging to the order Desulfobacterales including *Desulfobacca* (Desulfoarculaceae), phylogenetically related to the acetate-degrading sulfate reducer *Desulfobacca acetoxidans* (Elferink *et al.* 1999), have been shown to degrade benzene under similar conditions (Kleinsteuber *et al.* 2008). Moreover, Desulfobulbaceae affiliated OTUs were enriched by metoprolol extending previous association of these families with degradation of aromatic hydrocarbons (Rabus *et al.* 2016).

The gammaproteobacterial facultative anaerobic iron- and sulfur-oxidizing *Acidiferrobacter* enriched in metoprolol treatments has been previously associated with polychlorinated biphenyls contaminated sediments (Matturro *et al.* 2016), and its capability to degrade metoprolol can, therefore, be hypothesized. The enrichment of the family Neisseriaceae in metoprolol treatments (Figure 26 C), primarily associated with human and non-human commensal and pathogenic attributes extends on numerous reports where free-living Neisseria species have been found in different environmental matrices such as soil, contaminated water and sediment, oil-polluted soil and biofilter packing material (Carrillo-Pérez *et al.* 2004; Xu *et al.* 2014; Liu *et al.* 2015).The environmental *Neisseria* were reported to degrade complex TrOCs such as dichlorodiphenyltrichloroethane, benzene, crude oil, naphthalene, and xylene (Carrillo-Pérez *et al.* 2004; Borin *et al.* 2006; Xu *et al.* 2014).

The metoprolol-enriched facultative anaerobe *Enhydrobacter* belongs to the family Vibrionaceae established to have functional genes for polycyclic aromatic hydrocarbon degradation (Zhang *et al.* 2019), strong evidence of its affiliated genera potential to degrade metoprolol. Numerous other unclassified gammaproteobacteria affiliated OTUs (Table A5) enriched in metoprolol treatments highlight the association of this class with the degradation of metoprolol in the hyporheic zone sediments. Unclassified Acidobacterial taxa affiliating with Subgroups 6, 9 and 17 enriched in metoprolol treatments signify the role of members within this phylum in the removal of organic micropollutants as previously reported for pharmaceuticals (Posselt *et al.* 2020), polychlorinated biphenyls (Nogales *et al.* 1999) and petroleum compounds (George *et al.* 2009). Unclassified OTUs affiliated with KD4-96, S085, Anaerolineaceae and Ardenticatenia in the phylum Chloroflexi were also enriched in metoprolol treatments. Presence of KD4-96 in contaminated soils and peatlands treating mining-affected

waters has been reported (Kujala *et al.* 2018), suggesting the probability of Chloroflexi affiliated taxa in the removal of such contaminants as metoprolol in the environment. While Firmicutes-affiliated *Bacillus* has been previously shown to degrade complex compounds such as crude oil in oxic conditions (Xu *et al.* 2018), such activity under anoxic conditions has not been reported. The facultative anaerobic lifestyle exhibited by some *Bacillus* species, however, suggests probable xenobiotic catabolic pathways under anoxic conditions and the enrichment of this genus in the metoprolol treatments, therefore, offers strong evidence for such a potential. While *Gemmatimonas* was previously reported among potential degraders of pyrene in an aerobic bioslurry reactor (Yu *et al.* 2019), the enrichment by metoprolol of an unclassified Gemmatimonadaceae genus phylogenetically related to the facultatively aerobic *Gemmatimonas aurantiaca* (Takaichi *et al.* 2010) under anoxic conditions is another example of potential degradation of complex xenobiotics hitherto reported only under oxic conditions.

Taken together, the microbial removal of metoprolol in the oxic and anoxic segments of the hyporheic zone highlights the potential of aerobic and anaerobic degradation mechanisms in the removal of contaminants in the aquatic environment. Coupled with increased residence time in the sediment matrix, redox zonation contributed to enhanced metoprolol removal by the indigenous microbiota in the hyporheic zone through promoting diverse bacterial taxa occupying the specialized niches and employing varied biodegradation pathways.

6.3. Influence of TOC on organic micropollutant removal in the hyporheic zone

The bioavailable total organic carbon (TOC) (i.e., dissolved organic carbon (DOC) + particulate organic carbon (POC) in hyporheic sediments is considered a major limiting factor for microbial metabolism (Findlay and Sobczak 2000), thereby directly or indirectly impacting coupled processes such as biotransformation of TrOCs. Most streambed sediments of receiving rivers are characterised by allochthonous-derived organic carbon from wastewater effluents (Gücker *et al.* 2006) as well as autochthonous-derived organic matter from decomposing leaf litter and macrophytes (Romani *et al.* 1998). The surface sediment layer as the primary contact point with these deposits, consequently, has a higher concentration of organic carbon compared to subjacent layers. Subsequently, bacterial populations, turnover and metabolism are high in this layer, suggesting high mineralisation rates that decrease exponentially with depth (Wellsbury *et al.*1996; Harvey *et al.* 2013; Knapp *et al.* 2017; Schaper *et al.* 2019). As TrOC attenuation is coupled to biogeochemical reactions fuelled by the organic carbon (Atashgahi *et al.* 2015), a decline in TOC concentration with increasing depth might impair the TrOC removal efficiency of the hyporheic zone. Cognizant of the simultaneous occurrence of numerous micropollutants in the hyporheic zone, the removal efficiency of a set of 13 TrOCs routinely discharged by the Muenchehofe WWTP was investigated using impacted hyporheic zone sediments differing in initial TOC content obtained from the River Erpe.

6.3.1. The interplay between TOC, microbial community and micropollutant removal

Overall, higher removal efficiency of most test compounds via biotransformation in the surface relative to subsurface sediment samples was observed (Figure 28 A). This was

likely due to high bacterial turnover and metabolism associated with the high organic carbon content in the surface sediments. Microbial productivity in the hyporheic sediments is correlated to the organic matter content (Marxsen 1996; Findlay and Sobczak 2000) since organic carbon in the sediment serves as a nutrient source for heterotrophic microorganisms and promotes bacterial colonization (Romani *et al.* 1998). The decrease in bacterial abundance in the incubated samples with increasing depth was, therefore, a response to the organic carbon concentration gradient between the two sediment layers (Figure 29). Though the species richness was higher in the subsurface sediments at t0, the higher TOC concentration in the surface layer correlated with the significantly higher bacterial diversity (Figure 30) and corresponding TrOC removal efficiency (Figure 28). This finding extends previously reported a positive association between high bacterial diversity and increased biotransformation efficiency of some organic micropollutants (Johnson *et al.* 2015; Stadler *et al.* 2018; Jaeger *et al.* 2019b; Posselt *et al.* 2020).

Up to six-fold removal efficiency for acesulfame and two-fold for ibuprofen and ketoprofen in the surface compared to the subsurface layer, exemplifies the significance of the organic matter content in the removal of some micropollutants reaching the hyporheic zone. The trend on a lower margin was reflected in the removal of other compounds such as bezafibrate, clofibric acid, carbamazepine and benzotriazole. The biotransformation of acesulfame occurred only in the surface sediment suggesting the compound is likely degraded by specific taxa that were part of the larger diversity supported by the high TOC content in this layer compared to the subjacent layer. Acesulfame, hitherto considered persistent (Buerge *et al.* 2009), has been recently reported to be amenable to biodegradation in constructed and natural environments (Kahl *et al.* 2018; Jaeger *et al.* 2019b; Schaper *et al.* 2019).The

environmental parameters associated with these recent findings are not yet established, and our current findings hint that the organic carbon content likely plays a significant role in its removal in the aquatic environment. Benzotriazole, considered less biodegradable in WWTPs (Giger *et al.* 2006), was almost completely removed in the sediment samples. This may be attributed to the retention of high organic matter content in sediments that support higher bacterial diversity capable of the transformation of benzotriazole. Moreover, the increased residence time in the hyporheic zone compared to WWTPs may have promoted the slow-growing microorganisms to express the necessary enzymes involved in the degradation of such compounds otherwise considered recalcitrant (Tran *et al.* 2013).

Removal of furosemide, hydrochlorothiazide and carbamazepine was only marginally higher in the surface relative to subsurface sediment samples. Nevertheless, the high removal efficiency observed for the three compounds was unexpected in the first place. Furosemide was only recently shown to be amenable to biotransformation in sediments (Liu *et al.* 2019) with hydrolysis and photolysis earlier considered as the only removal mechanisms (Yagi *et al.* 1991; Katsura *et al.* 2015). Biotransformation as the process responsible for the >70 % hydrochlorothiazide removal in the current study is only speculative as previously, only photolysis (Brigante *et al.* 2005) and hydrolysis (Li *et al.* 2014) have been reported as removal mechanisms. While photolysis can be excluded in the current study, the contribution of hydrolysis to its removal cannot be ruled out, and further investigations would be required. Although degradation of up to 60 % carbamazepine in mixed bacterial culture studies has been reported (Ha *et al.* 2016), removal of up to 69 - 77 % in environmental samples is unprecedented. Majority of previous studies reported the compound as relatively persistent (Burke *et al.* 2018; Posselt *et al.* 2018; Coll *et al.* 2019; Jaeger *et al.* 2019; Liu *et al.* 2019; Schaper *et al.*

2019). Only fungi have been reported to be more prolific degraders of the compound in lab-based experimental setups (Nasir *et al.* 2018). It is, therefore, probable that the degradative role was played by fungi, a component in the sediment microbial community (Findlay and Sobczak 2000) not considered in the current study. Clofibric acid removal was still low (< 40%) under both TOC conditions suggesting the persistence of the compound in water-sediment matrices as reported in previous studies (Löffler *et al.* 2005; Kunkel and Radke 2008).

The complete and near-complete removal of propranolol and metoprolol, respectively, under both TOC concentrations, matches previously reported pattern in two sediment types differing in TOC content (Ramil *et al.* 2010). Their closely related structures may have influenced their similar interaction with TOC and bacterial catabolic pathways. On the other hand, naproxen, ibuprofen and ketoprofen (NSAIDs) exhibited variable interaction with TOC where the latter two were strongly impacted by TOC content while naproxen was not. This may be attributed to the difference in their physical-chemical properties. While the three compounds contain the carboxyl and alkyl functional groups, naproxen differs markedly from the rest by having an ether group which is a weak electron donating group and may account for its varied interaction with TOC or resident microbial communities.

6.3.2. Taxonomic composition dynamics

The taxonomic composition of the bacterial community at the phylum level remained relatively constant throughout the incubation in the surface sediment samples (Figure 32 A and B). A stable supply of carbon and energy from the organic-rich sediment likely contributed to this observation. The corresponding high removal efficiency of the TrOCs suggests cometabolism played a significant role in their removal. The

prevalence of cometabolism in organic-rich matrices, such as the benthic biolayer, was previously demonstrated (Schaper *et al.* 2019). In cases where the concentration of the TrOCs is too low to support biomass growth or where they exhibit apparent toxicity rendering them unfavourable to enter catabolic pathways of microbial cells (Tran *et al.* 2013), the bacteria may use the organic matter as the sole source of carbon and energy while transforming the TrOCs as a non-growth substrate (Arp *et al.* 2001). In some cases, however, the cometabolism initiates a reaction to transform persistent compounds into their more biodegradable forms before they enter the central metabolic pathways (Tran *et al.* 2013). The recorded marginal increase in the relative abundances of Proteobacteria, Bacteroidetes, Firmicutes, Acidobacteria, Chloroflexi and Gemmatimonadetes (Figure 32 A and B), in amended relative to unamended samples may suggest such potential utilization of some TrOCs as a carbon source by these phyla. Indeed, members belonging to these phyla have been associated with degradation of xenobiotics (Nogales *et al.* 1999; Seo *et al.* 2009; Gargouri *et al.* 2014; Braga *et al.* 2015; Ghosal *et al.* 2016; Nega *et al.* 2019; Posselt *et al.* 2020), and their likely involvement in the current study can be hypothesized.

In the subsurface samples, a shift in the bacterial community composition in the amended samples relative to unamended controls at day 15 of incubation (Figure 32 C and D), in which the relative abundance of Proteobacteria increased while other phyla including Chloroflexi, Firmicutes and Actinobacteria declined suggested a possible change in carbon utilization dynamics. Proteobacteria as relatively rapid responders to substrates (Ho *et al.* 2017) and a characteristic broad physiological and metabolic diversity (Harichová *et al.* 2012), may have easily adapted to utilizing the TrOCs as an additional carbon and energy source, hence outcompeting other taxa. Nevertheless, analysis at the family and genus level revealed that even within phyla

that declined in abundance were members potentially utilizing the TrOCs as their abundance seemed to increase in amended relative to unamended samples (Figure 33 C and D; Table A4). This phenomenon has been reported in riverine samples exposed to micropollutants, where nutrient-like or toxic-like effects on different fractions of microbial communities were observed (Lawrence *et al.* 2005).

Putative taxa associated with degradation of the test compounds

Proteobacteria affiliated families responsive to TrOC amendment included Methylophilaceae, whose members are obligate methylotrophs but also associated with degradation of TrOCs such as ketoprofen, formononetin, ibuprofen, primidone, ametrine and naproxen (Phan *et al.* 2016). The enrichment of the family Comamonadaceae corresponds to previous reports on affiliated members associated with the degradation of aromatic compounds (Dallinger and Horn 2014). Though originally associated with anaerobic hydrocarbon degradation, Rhodocyclaceae affiliated members capable of aerobic hydrocarbon degradation have been recently reported (Táncsics *et al.* 2018). Rhodocyclaceae was also found central in the degradation of toluene under oxygen-limiting conditions (Táncsics *et al.* 2018), highlighting potential resilience in the hyporheic zone under changing oxygen availability regimes.This may explain its flourishing in the subsurface sediment samples where oxygen availability may be limited (Figure 33 C and D). The potential of Rhodospirillaceae and Xanthomonadaceae in the degradation of aromatic organic compounds is widely reported (Gibson and Harwood 1995; Wang *et al.* 2014; Brzeszcz and Kaszycki 2018), and their enrichment by TrOCs in the present study extends this observation.

Among the enriched taxa at the genus level included the toluene-degrading *Xanthobacter* (Tay *et al.* 1999), *Hyphomicrobium* previously associated with assimilation of 2, 4-Dichlorophenol, a soil and groundwater contaminant (Dallinger and Horn 2014) and *Novosphingobium* associated with a broad array of natural aromatic compounds (Ghosal *et al.* 2016). Other Proteobacteria affiliated genera hitherto unassociated with xenobiotic degradation but enriched in the amended samples included *Phaselicystis, Leeia, Ferritrophicum, Crenothrix, Magnetospirillum, Reyranella, Prosthecomicrobium Geothermobacter*, suggesting their involvement in the biotransformation of the test compounds and highlighting the hyporheic zone as a reservoir of higher bacterial diversity with organic micropollutant degradation potential. The Bacteroidetes affiliated genus *Terrimonas* previously associated with degradation of dibutyl phthalate (Jin *et al.* 2013) and benzo[a]pyrene (Song *et al.* 2015) was also enriched by the test compounds suggesting its contribution to the removal of the micropollutants.

Increase in the relative abundance of Chloroflexi affiliated Caldilinaceae and Anaerolineaceae following TrOC amendment corresponds to the previous association of these families with TrOC removal (Phan *et al.* 2016; Miettinen *et al.* 2019). The Caldilinaceae affiliated genus *Caldilinea* was associated with TrOC removal in an anoxic-aerobic membrane bioreactor (Phan *et al.* 2016) while Anaerolineaceae representatives were associated with degradation of organic pollutants, aromatics and n-alkanes albeit under anaerobic conditions (Kümmel *et al.* 2015; Chen *et al.* 2016; Miettinen *et al.* 2019). Although considered strictly anaerobic (Zhang *et al.* 2018), a surprisingly considerable abundance of Anaerolineaceae members was detected in aerobic WWTP water samples (Chen *et al.* 2016). The authors attributed the observation to the presence of anoxic microzones within aerated wastewater flocs.

Their prevalence in the current study may also be attributed to similar anoxic microzones reported within the aerobic hyporheic zones (Lewandowski *et al.* 2019). The enrichment of the unclassified KD4-96 and JG30-KF-CM45 families, hitherto unassociated with the degradation of TrOCs suggests their participation in the removal of TrOCs in this study. An unclassified Acidobacteria Subgroup 6 family also enriched in the presence of TrOCs extends further the reported association of members within this phylum with the degradation of such contaminants as polychlorinated biphenyls, petroleum compounds, metals and radionuclides (Nogales *et al.* 1999)(George *et al.* 2009). Though members of the family Acidimicrobiaceae were not shown to harbour genes involved in the degradation of aliphatic and aromatic hydrocarbons in a crude oil field soil metagenomic data analysis (Abbasian *et al.* 2016), their presence in the oil field soil and detection in this study may indicate such potential. Moreover, other taxa affiliated with the phylum Actinobacteria have been associated with degradation of such compounds as phenol, diesel oil, n-alkanes and polycyclic aromatic hydrocarbons (Seo *et al.* 2009; Zhang *et al.* 2012; Alvarez *et al.* 2017).The increase in the relative abundance of Gemmatimonadaceae in amended relative to unamended sediment samples suggests the potential to utilize the TrOCs. Members of this family have been associated with degradation of complex compounds, e.g. the benzoate-degrading *Gemmatimonas aurantiaca* and an uncultured *Gemmatimonas* species associated with alkylbenzene sulfonate (Braga *et al.* 2015).

The enrichment of firmicutes affiliated Eubacteriaceae and Peptococcaceae belonging to Clostridia corresponds to previous studies. Eubacteriaceae was among soil microorganisms associated with soils historically contaminated by heavy metals and hydrocarbons (Vivas *et al.* 2008). Though Peptococcaceae were only previously reported in the anaerobic degradation of aromatic compounds (Kuppardt *et al.* 2014),

the transcription of genes encoding enzymes involved in oxygenase-mediated aerobic benzene degradation in a denitrifying continuous culture in the family Peptococcaceae were recently reported (Atashgahi *et al.* 2018). The potential oxygen production in the culture was hypothesized to be formed via a recently identified nitric oxide dismutase to enable aerobic microbes to thrive in nitrate-containing and oxygen-depleted environments contaminated with hydrocarbons (Atashgahi *et al.* 2018).

6.3.3. Sorptive removal under variable TOC concentration

The higher removal of the NSAIDs (diclofenac, ibuprofen, ketoprofen, and naproxen), cholesterol-lowering agents (bezafibrate, clofibric acid), carbamazepine and benzotriazole in the surface sediment relative to subsurface sediment indicates sorptive removal of these compounds is influenced by organic matter concentration in the sediments. The influence on sorption as a removal mechanism for some organic micropollutants in sediments by the organic matter content was reported (Jaeger *et al.* 2019a; Liu *et al.* 2019; Schaper *et al.* 2019). For some other compounds such as the beta-blockers (metoprolol, propranolol), furosemide and hydrochlorothiazide, no correlation with TOC concentration was observed suggesting other factors or processes contributed to their removal. Indeed, processes such as hydrolysis have been reported as significant removal mechanisms for such compounds as furosemide (Yagi *et al.* 1991) and hydrochlorothiazide (Li *et al.* 2014) and their contribution to their removal in the current study are hypothesized. Moreover, the occurrence of TrOCs in neutral and ionizable forms further determine the type of interaction with the sediment materials due to the influence of external factors such as pH (Schwarzenbach 1986). At the prevailing pH in the microcosms (pH 7.5 - 8), the test compounds potentially exhibited different physicochemical properties and their interaction with the sediment was expected to be driven by different processes such as hydrophobic partitioning for

neutral TrOCs, e.g. carbamazepine and electrostatic interactions and surface complexation for the ionizable TrOCs, e.g. ibuprofen, naproxen, ketoprofen, and diclofenac (Fujioka *et al.* 2015; Schaper *et al.* 2019). In the same way, desorption of the TrOCs from the sediment into the aqueous phase may be driven by the same factors leading to a counteractive effect on the sorption as a TrOC removal mechanism.

The notable differences in the removal of some TrOCs with increasing depth and along a TOC gradient may be associated with the change in bacterial community composition caused by the change in concentration of organic carbon. However, in some cases, low concentration of organic carbon can boost TrOC removal, since, in high concentration, the carbon may also serve as a competitive substrate that inhibits preferential degradation of TrOCs. Biotransformation is the most critical micropollutant removal mechanism in the hyporheic zone. The contribution of sorption also plays a significant role in influencing the fate of organic micropollutants in sediment-water systems. The contribution of the two processes is not exclusionary but rather complementary since, for example, sorption may impair or enhance the bioavailability of a compound.

6.4. Impact of bacterial diversity and hyporheic exchange flow on the transformation of organic micropollutants

The microbial community structure (especially diversity) (Peralta-Maraver *et al.* 2019), and HEF are key controls of the fate of organic contaminants in lotic aquatic environments (Posselt *et al.* 2020). Despite limited information on the functional diversity of most bacterial pollutant degraders, the positive correlation between taxonomic and functional diversity (Stadler *et al.* 2018), allows predicting the biodegradation capacity of the resident bacterial community in the hyporheic zone (Posselt *et al*. 2020). Such a correlation is not universal and functional redundancy, whereby different bacterial species perform a similar function such as degradation of organic carbon is common in bacterial communities (Battin *et al.* 2016). However, for most emerging compounds, degradation is performed by consortia rather than single bacterial strains. The different bacteria may produce different enzymes involved in the different degradation reactions of the same catabolic pathway leading to biotransformation or mineralization of a compound (Tran *et al.* 2013). In other cases, toxic compounds may only be initially degraded cometabolically while their less toxic intermediates enter the catabolic pathways of other bacteria (Tran *et al.* 2013). In the current study, the alpha diversity gradient created following the sediment dilution (Figure 35) correlated strongly with the DT50 of most compounds suggesting that bacterial communities with higher species richness and diversity were more efficient at transforming a larger number of individual test compounds (Table 19; Posselt *et al.* 2020). Our findings, therefore, extend previously reported correlations between bacterial diversity and organic compound biodegradation (Johnson *et al.* 2015; Stadler *et al.* 2018; Jaeger *et al.* 2019b).

Moreover, TPs were least often detected in pore water of the high diversity systems (S1) where most diverse bacterial communities and well-functioning transformation pathways were expected (Figure 36). The higher detection rates, concentrations and longevity of TPs in S6 flumes, on the other hand, may be attributed to inadequate catabolic transformation pathways requiring several types of bacteria found in the original undiluted sediment or S1 dilution level, i.e. a less diverse microbial community has a lower probability of hosting elements of such pathways, leading to enrichment of certain intermediates. Taken together, the data demonstrate the importance of microbial diversity and by extension, a diverse gene pool translating into a high genetic potential and associated organic contaminant degradation potential in hyporheic zones (Posselt *et al.* 2020).

HEF, a function of hydraulic conductivity and sediment morphology (Hester *et al.* 2013), is postulated to promote bacterial diversity and activity as it increases the supply of nutrients and oxygen (Triska *et al.* 1989), especially in downwelling conditions (Peralta-Maraver *et al.* 2018; Galloway *et al.* 2019). However, while bacterial diversity influenced biotransformation of 20 substances, only acesulfame, ibuprofen, sitagliptin and metaxalone were significantly influenced by HEF. This may imply that the latter four substances are particularly sensitive to biodegradation in hyporheic zones. Interestingly, ibuprofen and metaxalone degraded to a lesser extent with the increasing number of bedforms, which contrasts the hypothesis that hyporheic exchange generally increases degradation potential. A common characteristic of acesulfame, ibuprofen and sitagliptin is that they have all been previously reported to be influenced by redox conditions (Burke *et al.* 2018; Henning *et al.* 2019; Jia *et al.* 2020). Little information about the environmental fate of metaxalone is available. Hence, the bedforms might have provided a particular redox environment that favoured or

diminished transformation reactions of those compounds mentioned above. However, the fact that degradation of other redox-sensitive compounds, such as the beta-blockers metoprolol, atenolol and sotalol (Schmidt *et al.* 2017), was not significantly influenced by the number of bedforms highlights the complexity of compound-specific reactions. As discussed previously for acesulfame (Jaeger *et al.* 2019b), the absence of a visible effect of HEF may also be caused by the pronounced effect of the diversity treatment, which ultimately masks the influence of HEF. Some compounds exhibited differences among bedform treatments within the lowest diversity, but this effect is not significant in the overall model because the differences vanish in the higher diversity treatments (e.g. metoprolol, atenolol, bezafibrate, gemfibrozil, valsartan). Alternatively, differences in HEF levels were not sufficient to observe a significant effect on DT50s. Although a numerical model (Betterle *et al.*, 2020 unpublished) shows that the bedform treatments differ in HEF, these differences were diminished by the effects of bedforms on the flow velocities of the overlying water. In future studies, larger differences in HEF would likely result in more distinct dramatic effects of HEF on more compounds. This might be achieved by a numerical model that predicts the highest possible HEF variation for an experimental setup. Still, even if the differences are increased, HEF alone will likely not be a perfect predictor of degradation, as hyporheic travel time distributions and associated redox zonation, as well as variations in microbial communities along flow paths, may differ with HEF and therefore should always be considered (Posselt *et al.* 2020).

6.4.1. Attenuation dynamics of organic micropollutants in the flumes

The degradation of celiprolol exemplified the key role of biodegradation in the attenuation of the micropollutants. This beta-blocker differed markedly from others (atenolol, metoprolol, propranolol and sotalol) with a DT50 an order of magnitude

higher (Table 19), which may be associated with its disubstituted urea moiety that might be less prone to biological hydrolysis than for example the amide or ether side chain in atenolol or metoprolol, respectively. Sorption and photolysis played a minor role compared to biodegradation for dissipation of most TrOCs in the present experimental setup except for irbesartan and some cationic compounds. For anionic and neutral compounds, organic matter is the main potential sorbent (Schaper *et al.* 2019). However, total carbon in the three sediment mixtures was < 0.08% and, thus, dissipation of TrOCs by sorption to organic matter was likely negligible. A sorption test of carbamazepine to the flume sediments further confirmed this. Carbamazepine has one of the highest log D_{OW} (2.77) of the compounds investigated in this study (Only benproperine and irbesartan show higher log D_{OW}). Hence, most of the compounds are less likely to partition into organic matter than carbamazepine. As the test showed no significant sorption of carbamazepine, this probably accounts for all other compounds with lower log D_{OW}. Cationic compounds, in contrast, are particularly prone to sorption by electrostatic interactions with negatively charged binding sites. In sediment-water column tests, compounds of high pK_a previously showed the highest retention by sorption (Schaper *et al.* 2018a). Analysis of the cation-exchange capacity (CEC), however, confirmed that the flume sediments were also poor sorbents for positively charged compounds. Median CEC was 0.6 cmol kg^{-1} (max: 3.6). The reason for this was probably the low content of the sediments in the fine mineral material (particle size < 0.063 mm was below 1%) and the low carbon content (Margot *et al.* 2015). So, sorption was generally of little importance for most compounds. If dissipation of benproperine and irbesartan, which have higher log D_{OW} than carbamazepine, was prone to sorption despite the low content in organic carbon, differences in dissipation between treatments were still caused by biodegradation, as the sediment properties of the different sediment mixtures were very similar. Moreover,

sorption may have affected some compounds (especially those with high log K_{ow}), due to the presence of biofilms. Nevertheless, since overall bacterial abundance was similar between the diversity levels, potential sorption should have a similar impact on all levels.

6.4.2. Microbial communities and taxa associated with the degradation of the test compounds

The enrichment of several taxa in the presence of the test compounds suggests that they might include both some pollutant-degrading species along with pollutant-insensitive species. Some of the enriched genera detected in the present study (Table A8), and previously associated with degradation of organic contaminants in diverse environments included OTUs affiliated with Holophagae and subgroups 6, 17, and 22 in the phylum Acidobacteria which were associated with polychlorinated biphenyl (Nogales *et al.* 1999) and petroleum compound degradation (George *et al.* 2009). Within the phylum Actinobacteria, genera such as *Nocardioides* harbour known ibuprofen degraders (Chen and Rosazza 1994) while *Illumatobacter* is among genera enriched in the presence of organic pollutants such as anilines and phenols, polycyclic aromatic hydrocarbons and organochlorine pesticides (Rodríguez *et al.* 2018). Genera of the phylum Bacteroidetes such as *Terrimonas* and *Flavobacterium* that include benzo[a]pyrene (Song *et al.* 2015) and ibuprofen degrading species were also enriched (Li *et al.* 2016). The dominant phylum Proteobacteria was represented by several genera including *Sphingomonas, Sphingobium* and *Novosphingobium* in the family Sphingomonadaceae that is widely characterized as a family with many prolific aerobic degraders of a wide variety of aromatic compounds (Ghosal *et al.* 2016) as well as Comamonadaceae, also an aerobic degrader of aromatic compounds (Dallinger and Horn 2014). Within the families Xanthomonadaceae and

Pseudomonadaceae, the genera *Arenimonas* and *Pseudomonas* were enriched in response to the 31 test compounds. These genera have previously been linked to biodegradation of polyaromatic compounds such as naphthalene (Ghosal *et al.* 2016). The enriched *Mesorhizobium* is closely related to the metformin-degrader *Aminobacter* (Poursat *et al.* 2019). These genera belong to the family Phyllobacteriaceae whose other members are known for degradation of micropollutants such as dichlorobenzamide (T'Syen *et al.* 2015). Most other enriched operational taxonomic units are affiliated with yet-to-be classified genera and families, which suggests a wide array of taxa potentially involved in the degradation of organic contaminants in the hyporheic sediments and highlights the hyporheic zone as a reservoir of hitherto undetected microbial diversity. In contrast, some genera exhibited $\log_2$ fold change < 0 in the presence of test compounds relative to unamended controls (Table A8) indicating a decrease in their abundance likely due to the potential negative impact of the test compounds. Previous studies (Lawrence *et al.* 2005; Rodríguez *et al.* 2018) have reported such effects of micropollutants on a certain fraction of the indigenous environmental microbiota.

6.5. Conclusions, limitations, and future perspectives

The threat posed to the aquatic environment by an ever-dynamic catalogue of synthetic compounds from households and industry that bypass the conventional wastewater treatment systems remains a matter of concern. The hyporheic zone has, therefore, emerged as the last line of defence against contamination of near-surface aquifers that are important sources of drinking water (Posselt *et al.* 2020). As an ecotone traditionally renowned for robust organic matter decomposition and degradation of nutrients via microbial activity, this dissertation sought to evaluate the response of the resident microbial community to the emerging micropollutants as well as the factors influencing such response.

The potential of the hyporheic zone microbial community to degrade emerging pollutants was evaluated using the model compound ibuprofen that is ubiquitously detected in most receiving rivers due to inefficient removal in the lotic surface water (Kunkel and Radke 2008). The surface area occupied by the sediment particles was hypothesized to host a diverse microbial community capable of ibuprofen degradation. The sedimentary matrix and pore spaces represent ideal microbial habitats ensuring increased contact time with the wastewater-derived pollutants infiltrating into the hyporheic zone. The sediment microcosms amended with ibuprofen efficiently degraded the compound (Figure 8)**.** The primary transformation products detected (Figure 10), were further degraded suggesting potential mineralization of the compound in the hyporheic zone sediments. Refeeding of the microcosms with ibuprofen akin to the recurrent discharge from WWTPs resulted in the enrichment of specific taxa whose relative abundance significantly increased relative to un-amended control setups (Table A1). Moreover, the removal rates of ibuprofen increased with each subsequent refeeding regime suggesting that the microbial community was

adapting to the presence of ibuprofen. The refeeding and corresponding enrichment of ibuprofen-degrading taxa exemplified that the continued supply of TrOCs into the hyporheic zone sediments may eventually result in a shift in the microbial community structure towards specialized degraders of such compounds. Such an evolution is further evidenced by the findings of this dissertation and other recent studies that have reported the biodegradation of acesulfame (Castronovo *et al.* 2017; Kahl *et al.* 2018; Jaeger *et al.* 2019b; Schaper *et al.* 2019), hitherto considered recalcitrant and used as a stable marker in aquatic environment studies (Buerge *et al.* 2009).

The ability of the resident microbial community to degrade ibuprofen in the presence of an easily degradable organic carbon source such as acetate further pointed to the broad diversity of metabolic mechanisms present in the microbial community. While some taxa only degraded acetate, others were shown to degrade both compounds (Table A1), suggesting mixed substrate utilization potential and presence of metabolic and cometabolic degradation mechanisms within the diverse microbial community. Therefore, the results supported Hypothesis 1, on the potential of the hyporheic zone to degrade pollutants courtesy of the inherent potential within its diverse resident microbiota.

Factors such as discharge influence supply of dissolved oxygen, nutrients, and organic matter to the hyporheic zone. Such factors, in turn, impact biogeochemical cycling and associated microbial activity by influencing parameters such as redox potential at the microscale. The distribution of oxygen and associated redox influxes create oxic and anoxic pockets in the hyporheic zone. This, in turn, creates specialized niches for the proliferation of aerobic and anaerobic microorganisms. The evaluation of the effect of redox zonation on the microbial associated degradation of TrOCs using the beta-blocker metoprolol as a model compound revealed specialized taxa and affiliated with

Proteobacteria and Bacteroidetes under oxic conditions (Table A3), and Proteobacteria, Acidobacteria, Chloroflexi, Firmicutes and Gemmatimonadetes under anoxic conditions (Table A5). Moreover, metoprolol transformation in the sediments incubated under oxic and anoxic conditions occurred via variable biodegradation pathways (Figure 39) with different transformation products formed (Figure 22). The results thus supported Hypothesis 2 on the effect of such biogeochemical factors as redox zonation on the microbial community dynamics and coupled processes such as biotransformation of TrOCs.

Additionally, the effect of TOC gradients on microbial community dynamics and coupled processes such as biotransformation of TrOCs evaluated using a set of 13 TrOCs supported Hypothesis 2 by demonstrating that sediments with higher TOC content exhibit higher removal efficiency of some compounds compared to low-TOC sediments. This was linked to the high TOC sediments supporting a higher diverse microbial community relative to low-TOC sediment, which likely influenced the observed degradation patterns (Figure 28). The correlation between TOC content and removal of the micropollutants was, however, not universal and varied among compounds. This indicated that other factors, such as the physicochemical properties of the individual compounds, also played a role in the interaction dynamics with the TOC and microbial communities. Notably, the microbial community in high-TOC sediments was relatively stable against the stressor effects of the micropollutants compared to the low-TOC sediments whose microbial community registered a decline in the relative abundance of most phyla except Proteobacteria. Despite this observation, some lower rank taxa within these phyla still increased in relative abundance in sediment microcosms with compared to those without the TrOCs, suggesting that some taxa within the hyporheic sediment community may be adapted

to degrade micropollutants under oligotrophic conditions. Such taxa belonged to the families Methylophilaceae, Caldilineaceae, Acidimicrobiaceae, Xanthobacteriaceae, Hydrogenophiliaceae, Rhodospirillaceae Gemmatimonadaceae and Rhodocyclaceae.

Sediment topography influences the supply of dissolved oxygen, nutrients, and organic matter to the hyporheic zone at the local scale (Galloway *et al.* 2019). This was hypothesized to promote microbial diversity and activity and the associated removal of organic pollutants. Formulation of bedforms on the sediment surface to influence hyporheic exchange flows was investigated in recirculating flumes. The results, however, showed an increase in HEF did not correlate with an increase in biodiversity or transformation of TrOCs as determined from DT50 values with only four out 31 test compounds correlating with HEF (Table 19). The diversity of the microbial community irrespective of bedform features correlated with 20 out of the 31 compounds tested, suggesting microbial diversity in the sediments plays a critical role in the degradation of TrOCs. External factors such as the formation of algal biofilms in the flumes during the experimental duration may have inhibited hyporheic flow paths through the bedforms, in turn affecting oxygen penetration and nutrient supply. This likely diminished the efficiency of the bedforms in influencing HEFs. Owing to the mentioned limitations, support for hypothesis 3 regarding the influence of HEF on TrOC removal was weak. However, the influence of microbial diversity on TrOC removal was evident as hypothesized.

The effect of microbial diversity on TrOC removal supported the recent findings that have reported the microbial community structure as a significant determinant and potentially an essential predictor of micropollutant degradation capacity in the environment. The correlation between taxonomic diversity indices and degradation of TrOCs may be attributed to the degradation of most emerging micropollutants

seemingly being a rare function where different bacterial taxa produce different enzymes involved in the different steps of the metabolic pathways or targeting different functional groups in the TrOCs. The "collaborative" activity of these microorganisms eventually contributes to the overall degradation of the target compound in a classical "the more, the merrier" modus operandi. While this may be the case for most emerging TrOCs studied thus far, the degradation of other compounds may require specific enzymatic activity found in highly specialized taxa. In such a case, overall low diversity within a community may not adversely affect their degradation. Therefore, the microbial community interaction with specific compounds needs to be considered. Moreover, as bacteria continue to evolve in exposure to these pollutants, as well as through lateral gene transfer, functional redundancy, where different bacteria perform a certain degradation step through the same or different enzyme activity, may eventually arise rendering the correlation between diversity and TrOC degradation invalid.

Across all experimental setups, both stimulatory and stressor effects of the tested compounds were observed among the microbial communities. The decline in alpha diversity indices as observed in the metoprolol-amended anoxic microcosms (Figure 24) for instance suggested the resident microbial community was on the overall negatively impacted by the metoprolol amendment, with the degradation of the compound associated with only a few taxa (Table A5). While this may at first glance be attributed to the use of higher than environmental-relevant concentrations, a similar observation was made in the experimental flume setup using TrOC concentrations similar to those detected in the natural river Erpe sediment (Posselt *et al.* 2020). Many taxa were either enriched or declined in relative abundance in amended relative to unamended samples (Table A8), thus supporting hypothesis 4. Such results have also been previously reported in riverine biofilms exposed to TrOC mixtures and were

attributed to synergistic and additive effects from the interactions among the test compounds (Lawrence *et al.* 2005). With the hyporheic zone continually receiving TrOC cocktails, both nutritive and toxic effects on different fractions of the hyporheic sediment microbial communities can, therefore, be expected.

Though usually occurring in the ng to µg L^{-1} range, the experiments performed in this dissertation used µg L^{-1} to mg L^{-1} due to the need to provide sufficient substrate to stimulate the growth of degraders. Nevertheless, the degradation of high compound concentrations by the hyporheic zone sediment bacterial community in the microcosms was corroborated by the detection of degradation intermediates in river Erpe of some of the compounds including ibuprofen and metoprolol from the *in situ* studies (Posselt *et al.* 2018). Moreover, evidence for the capability of microbes to respond to *in situ* relevant, minute concentrations of organic compounds has been reported from biosensor studies utilizing isolates obtained by enrichments with high, growth supportive substrate concentrations. The biosensor studies suggest that concentrations of organic compounds down to the pg L^{-1} range suffice to induce transcription of catabolic genes associated with the degradation of such compounds, demonstrating that microbes growing on high substrate concentrations also respond to trace quantities of their substrate by consuming it, e.g.(Haque *et al.* 2013). Thus, we predict that the microbes enriched with concentrations higher than usually occurring *in situ* have a high likelihood of being capable of degrading the micropollutants at *in situ* relevant concentrations in the hyporheic zone. However, to sustain biomass, the microorganisms likely rely on easily degradable organic carbon sources as primary substrates, making cometabolic degradation of TrOCs a more significant removal pathway.

Diverse hitherto unknown and known microbes were associated with the degradation of select organic compounds based on correlative data sets of relative abundance values from 16S rRNA gene (whole community) and 16S rRNA ("active") amplicons. By exploiting differential abundance data between unamended controls and amended samples, the taxa contributing significantly to the differences in the microbial community structure were associated positively (enriched) or negatively with the respective micropollutants based on the obtained Log2fold change values. To support this conclusion, a subset of specific taxa identified as enriched by ibuprofen from the relative abundance data was exemplarily analyzed through qPCR through the calculation of the ratio of 16S rRNA to 16S rRNA genes as an indicator of potential specific activity (Foesel *et al.* 2014). It was established that among the select taxa, the 16S rRNA copy numbers were significantly higher in amended relative to unamended samples suggesting transcription activity indicative of protein synthesis potential (Blazewicz *et al.* 2013). The isolation of two ibuprofen degraders (Figure 19) identified as enriched from the relative abundance data, further provided causality for the ibuprofen-enrichment of the two OTUs and their ibuprofen degradation capabilities. Thus, by exploiting complementary data from process studies, 16S rRNA and 16S rRNA gene amplicon sequencing data, the ratio of 16S rRNA to 16S rRNA genes as an indicator of the potential activity of bacterial taxa, and characterization of isolates, we provide evidence for many hitherto unknown ibuprofen degraders. Similar outcomes could, therefore, be anticipated in the other experiments performed in this dissertation. Nevertheless, to capture the functional potential of the actual degraders for the increasingly diverse catalogue of emerging micropollutants, studies using metatranscriptomics and metaproteomic approaches are preferable.

Cumulatively, most taxa associated with the degradation of the TrOCs in this dissertation affiliated with Proteobacteria, Acidobacteria, Actinobacteria, Bacteroidetes, Chloroflexi, Firmicutes and Gemmatimonadetes suggesting the importance of these phyla in the removal of emerging micropollutants in the environment. Further analysis of specific members within these phyla enriched by the different analyzed compounds may provide further insights into the metabolic potential across these phylogenetically diverse taxa. Such candidates may be further isolated to serve as model organisms for elucidating TrOC degradation pathways or for bioaugmentation purposes in polluted environments and WWTPs.

In a dynamic environmental matrix such as the hyporheic zone, the influence of numerous environmental factors makes estimation of persistence or biodegradability of micropollutants challenging to monitor. Using microcosms and mesocosms offers a degree of reliability and reproducibility as different parameters can be controlled accordingly. Extrapolating some findings from the laboratory to the field is, however, at time unreliable. Therefore, to provide a more holistic understanding of how hyporheic processes are linked and how they impact on each other, both lab and field studies cutting across study disciplines are recommended as envisioned within the HypoTRAIN framework.

7. REFERENCES

Abbasian Firouz, Thavamani Palanisami, Mallavarapu Megharaj, Ravi Naidu, Robin Lockington, and Kavitha Ramadass. 2016. Microbial Diversity and Hydrocarbon Degrading Gene Capacity of a Crude Oil Field Soil as Determined by Metagenomics Analysis. *Biotechnology Progress* 32(3): 638–48.

Abromaitis Vytautas, Viktoras Racys, Perry Van Der Marel, and Roel J W Meulepas. 2016. Biodegradation of Persistent Organics Can Overcome Adsorption–Desorption Hysteresis in Biological Activated Carbon Systems. *Chemosphere* 149: 183–89.

Alvarez Analia, Juliana M Saez, Jose S D Costa, Veronica L Colin, Maria S Fuentes, Sergio A Cuozzo, Claudia S Benimeli, Marta A Polti, and Maria J Amoroso. 2017. Actinobacteria: Current Research and Perspectives for Bioremediation of Pesticides and Heavy Metals. *Chemosphere* 166: 41–62.

Arp J Daniel, Chris M Yeager, and Michael R Hyman. 2001. Molecular and Cellular Fundamentals of Aerobic Cometabolism of Trichloroethylene. *Biodegradation* 12(2): 81–103.

Atashgahi Siavash, Rozelin Aydin, Mauricio R Dimitrov, Detmer Sipkema, Kelly Hamonts, Leo Lahti, Farai Maphosa, Thomas Kruse, Edoardo Saccenti, and Dirk Springael. 2015. Impact of a Wastewater Treatment Plant on Microbial Community Composition and Function in a Hyporheic Zone of a Eutrophic River. *Scientific Reports* 5: 17284.

Atashgahi Siavash, Bastian Hornung, Marcelle J Van Der Waals, Ulisses Nunes Da Rocha, Floor Hugenholtz, Bart Nijsse, Douwe Molenaar, Rob Van Spanning, Alfons J M Stams, and Jan Gerritse. 2018. A Benzene-Degrading Nitrate-Reducing Microbial Consortium Displays Aerobic and Anaerobic Benzene Degradation Pathways. *Scientific Reports* 8(1): 1–12.

Balch E William, George E Fox, Linda J Magrum, Carl R Woese, and Ralph S Wolfe. 1979. Methanogens: Reevaluation of a Unique Biological Group. *Microbiological Reviews* 43(2): 260–96.

Balkwill L David, Jim K Fredrickson, and Margaret F Romine. 2003. *Sphingomonas and Related Genera*. Pacific Northwest National Lab.(PNNL), Richland, WA (United States).

Barbosa Junior Fernando, Andres Campiglia, Bruno Rocha, and Daniel Cyr. 2016. Contaminants of Emerging Concern: From the Detection to Their Effects on Human Health. *BioMed Research International*.

Baschien Christiane, Werner Manz, Thomas R Neu, Ludmila Marvanová, and Ulrich Szewzyk. 2008. In Situ Detection of Freshwater Fungi in an Alpine Stream by New Taxon-Specific Fluorescence in Situ Hybridization Probes. *Applied Environmental Microbiology.* 74(20): 6427–36.

Battin J Tom, Louis A Kaplan, Denis J Newbold, Xianhao Cheng, and Claude Hansen. 2003. Effects of Current Velocity on the Nascent Architecture of Stream Microbial Biofilms. *Applied Environmental Microbiology* 69(9): 5443–52.

Battin J Tom, Katharina Besemer, Mia M Bengtsson, Anna M Romani, and Aaron I Packmann. 2016. The Ecology and Biogeochemistry of Stream Biofilms. *Nature Reviews Microbiology* 14(4): 251.

Berkner Silvia, and Claudia Thierbach. 2014. Biodegradability and Transformation of Human Pharmaceutical Active Ingredients in Environmentally Relevant Test Systems. *Environmental Science and Pollution Research* 21(16): 9461–67.

Besemer Katharina, Gabriel Singer, Christopher Quince, Enrico Bertuzzo, William Sloan, and Tom J Battin. 2013. Headwaters Are Critical Reservoirs of Microbial Diversity for Fluvial Networks. *Proceedings of the Royal Society B: Biological Sciences* 280(1771): 20131760.

Besemer Katharina, Gabriel Singer, Iris Hödl, and Tom J Battin. 2009. Bacterial Community Composition of Stream Biofilms in Spatially Variable-Flow Environments. *Applied Environmental Microbiology* 75(22): 7189–95.

Borin Sara, Massimo Marzorati, Lorenzo Brusetti, Mario Zilli, Hanene Cherif, Abdennaceur Hassen, Attilio Converti, Claudia Sorlini, and Daniele Daffonchio. 2006. Microbial Succession in a Compost-Packed Biofilter Treating Benzene-Contaminated Air. *Biodegradation* 17(2): 79–89.

Boulton J Andrew, Stuart Findlay, Pierre Marmonier, Emily H Stanley, and H Maurice Valett. 1998. The Functional Significance of the Hyporheic Zone in Streams and Rivers. *Annual Review of Ecology and Systematics* 29(1): 59–81.

Boxall B A Alistair, Paul Blackwell, Romina Cavallo, Paul Kay, and Johannes Tolls. 2002. The Sorption and Transport of a Sulphonamide Antibiotic in Soil Systems. *Toxicology Letters* 131(1–2): 19–28.

Braga J Kawanishi, Fabrício Motteran, Edson L Silva, and Maria B Amâncio Varesche. 2015. Evaluation of Bacterial Community from Anaerobic Fluidized Bed Reactor for the Removal of Linear Alkylbenzene Sulfonate from Laundry Wastewater by 454-Pyrosequence. *Ecological Engineering* 82: 231–40.

Briceño Gabriela, María S Fuentes, Juliana M Saez, María C Diez, and Claudia S Benimeli. 2018. S Treptomyces Genus as Biotechnological Tool for Pesticide Degradation in Polluted Systems. *Critical Reviews in Environmental Science and Technology* 48(10–12): 773–805.

Brigante Marcello, Marina DellaGreca, Lucio Previtera, Maria Rubino, and Fabio Temussi. 2005. Degradation of Hydrochlorothiazide in Water. *Environmental Chemistry Letters* 2(4): 195–98.

Brooks W Bryan, Kevin C Chambliss, Jacob K Stanley, Alejandro Ramirez, Kenneth E Banks, Robert D Johnson, and Russell J Lewis. 2005. Determination of Select Antidepressants in Fish from an Effluent-dominated Stream. *Environmental Toxicology and Chemistry: An International Journal* 24(2): 464–69.

Brozinski Jenny-Maria, Marja Lahti, Axel Meierjohann, Aimo Oikari, and Leif Kronberg. 2012. The Anti-Inflammatory Drugs Diclofenac, Naproxen and Ibuprofen Are Found in the Bile of Wild Fish Caught Downstream of a Wastewater Treatment Plant. *Environmental Science & Technology* 47(1): 342–48.

Brunke Matthias, and Tom Gonser. 1997. The Ecological Significance of Exchange Processes between Rivers and Groundwater. *Freshwater Biology* 37(1): 1–33.

Bryant A Jessica, Tara M Clemente, Donn A Viviani, Allison A Fong, Kimberley A Thomas, Paul Kemp, David M Karl, Angelicque E White, and Edward F DeLong. 2016. Diversity and Activity of Communities Inhabiting Plastic Debris in the North Pacific Gyre. *MSystems* 1(3): e00024-16.

Brzeszcz Joanna, and Paweł Kaszycki. 2018. Aerobic Bacteria Degrading Both N-Alkanes and Aromatic Hydrocarbons: An Undervalued Strategy for Metabolic Diversity and Flexibility. *Biodegradation* 29(4): 359–407.

Buerge J Ignaz, Hans-Rudolf Buser, Maren Kahle, Markus D Muller, and Thomas Poiger. 2009. Ubiquitous Occurrence of the Artificial Sweetener Acesulfame in the Aquatic Environment: An Ideal Chemical Marker of Domestic Wastewater in Groundwater. *Environmental Science & Technology* 43(12): 4381–85.

Buriánková Iva, Lenka Brablcová, Václav Mach, Petr Dvořák, Prem Prashant Chaudhary, and Martin Rulík. 2013. Identification of Methanogenic Archaea in the Hyporheic Sediment of Sitka Stream. *PLoS One* 8(11).

Burke Victoria, Janek Greskowiak, Tina Asmuß, Rebecca Bremermann, Thomas Taute, and Gudrun Massmann. 2014. Temperature Dependent Redox Zonation and Attenuation of Wastewater-Derived Organic Micropollutants in the Hyporheic Zone. *Science of the Total Environment* 482: 53–61.

Burke Victoria, Laura Schneider, Janek Greskowiak, Patricia Zerball-van Baar, Alexander Sperlich, Uwe Dünnbier, and Gudrun Massmann. 2018. Trace Organic Removal during River Bank Filtration for Two Types of Sediment. *Water* 10(12): 1736.

Carrillo-Pérez Esther, Arturo Ruiz-Manríquez, and Haydée Yeomans-Reina. 2004. Isolation, Identification and Evaluation of a Mixed Culture of Microorganisms for Degradation of DDT. *Revista Internacional de Contaminación Ambiental*: 69–75.

Castronovo Sandro, Arne Wick, Marco Scheurer, Karsten Nödler, Manoj Schulz, and Thomas A Ternes. 2017. Biodegradation of the Artificial Sweetener Acesulfame in Biological Wastewater Treatment and Sandfilters. *Water Research* 110: 342–53.

Cataldo D Anthony, Michael Maroon, Lawrence E Schrader, and Vernon L Youngs. 1975. Rapid Colorimetric Determination of Nitrate in Plant Tissue by Nitration of Salicylic Acid. *Communications in Soil Science and Plant Analysis* 6(1): 71–80.

Chen Yasong, Zheng Zhao, Yuke Peng, Jie Li, Lin Xiao, and Liuyan Yang. 2016. Performance of a Full-Scale Modified Anaerobic/Anoxic/Oxic Process: High-Throughput Sequence Analysis of Its Microbial Structures and Their Community Functions. *Bioresource Technology* 220: 225–32.

Chen Yijun, and John P N Rosazza. 1994. Microbial Transformation of Ibuprofen by a Nocardia Species. *Applied Environmental Microbiology*. 60(4): 1292–96.

Christensen P Bondo, Lars P Nielsen, Jan Sørensen, and Niels P Revsbech. 1990. Denitrification in Nitrate-rich Streams: Diurnal and Seasonal Variation Related to Benthic Oxygen Metabolism. *Limnology and Oceanography* 35(3): 640–51.

Chung E Jin, Tae S Park, Che O Jeon, and Young R Chung. 2012. Chitinophaga Oryziterrae Sp Nov, Isolated from the Rhizosphere Soil of Rice (Oryza Sativa L). *International Journal of Systematic and Evolutionary Microbiology* 62(12): 3030–

35.

Clara Manfred, Birgit Strenn, Oliver Gans, Elena Martinez, Norbert Kreuzinger, and Helmut Kroiss. 2005. Removal of Selected Pharmaceuticals, Fragrances and Endocrine Disrupting Compounds in a Membrane Bioreactor and Conventional Wastewater Treatment Plants. *Water Research* 39(19): 4797–4807.

Clarke K Robert, and Raymond N Gorley. 2001. PRIMER (Plymouth Routines in Multivariate Ecological Research) v5: User Manual/Tutorial. *Primer-E Ltd, Plymouth*: 1–91.

Coll Claudia, Claudia Lindim, Anna Sobek, Michael D Sohn, and Matthew MacLeod. 2019. Prospects for Finding Junge Variability-Lifetime Relationships for Micropollutants in the Danube River. *Environmental Science: Processes & Impacts* 21(9): 1489–97.

Combalbert Sarah, and Guillermina Hernandez-Raquet. 2010. Occurrence, Fate, and Biodegradation of Estrogens in Sewage and Manure. *Applied Microbiology and Biotechnology* 86(6): 1671–92.

Corvini Philippe, Andreas Schäffer, and Dietmar Schlosser. 2006. Microbial Degradation of Nonylphenol and Other Alkylphenols—Our Evolving View. *Applied Microbiology and Biotechnology* 72(2): 223–43.

Cydzik-Kwiatkowska Agnieszka, and Magdalena Zielińska. 2018. Microbial Composition of Biofilm Treating Wastewater Rich in Bisphenol A. *Journal of Environmental Science and Health, Part A* 53(4): 385–92.

Dallinger Anja, and Marcus A Horn. 2014. Agricultural Soil and Drilosphere as Reservoirs of New and Unusual Assimilators of 2, 4-dichlorophenol Carbon. *Environmental Microbiology* 16(1): 84–100.

Daughton G Christian. 2003. Cradle-to-Cradle Stewardship of Drugs for Minimizing Their Environmental Disposition While Promoting Human Health I Rationale for and Avenues toward a Green Pharmacy. *Environmental Health Perspectives* 111(5): 757–74.

Davids Madars, Dita Gudra, Ilze Radovica-Spalvina, Davids Fridmanis, Vadims Bartkevics, and Olga Muter. 2017. The Effects of Ibuprofen on Activated Sludge: Shift in Bacterial Community Structure and Resistance to Ciprofloxacin. *Journal of Hazardous Materials* 340: 291–99.

DeWeerd A Kim, A Saxena, D P Nagle, and Joseph M Suflita. 1988. Metabolism of the 18O-Methoxy Substituent of 3-Methoxybenzoic Acid and Other Unlabeled Methoxybenzoic Acids by Anaerobic Bacteria. *Applied Environmental Microbiology* 54(5): 1237–42.

Dhariwal Achal, Jasmine Chong, Salam Habib, Irah L King, Luis B Agellon, and Jianguo Xia. 2017. MicrobiomeAnalyst: A Web-Based Tool for Comprehensive Statistical, Visual and Meta-Analysis of Microbiome Data. *Nucleic Acids Research* 45(W1): W180–88.

Drury Bradley, Emma Rosi-Marshall, and John J Kelly. 2013. Wastewater Treatment Effluent Reduces the Abundance and Diversity of Benthic Bacterial Communities in Urban and Suburban Rivers. *Applied Environmental Microbiology* 79(6): 1897–1905.

Dzidic Senka, and Vlado Bedeković. 2003. Horizontal Gene Transfer-Emerging Multidrug Resistance in Hospital Bacteria. *Acta Pharmacologica Sinica* 24(6): 519–26.

Elferink Oude, Akkermans-van Vliet, Jaap J Bogte, and Alfons J M Stams. 1999. Desulfobacca Acetoxidans Gen Nov, Sp Nov, a Novel Acetate-Degrading Sulfate Reducer Isolated from Sulfidogenic Granular Sludge. *International Journal of Systematic and Evolutionary Microbiology* 49(2): 345–50.

Engelhardt Irina, Henning Prommer, Catherine Moore, Manoj Schulz, Christoph Schüth, and Thomas A Ternes. 2013. Suitability of Temperature, Hydraulic Heads, and Acesulfame to Quantify Wastewater-related Fluxes in the Hyporheic and Riparian Zone. *Water Resources Research* 49(1): 426–40.

La-Farre Marinel, Sandra Pérez, Lina Kantiani, and Damià Barceló. 2008. Fate and Toxicity of Emerging Pollutants, Their Metabolites and Transformation Products in the Aquatic Environment. *TrAC Trends in Analytical Chemistry* 27(11): 991–1007.

Findlay Stuart, and William V Sobczak. 2000. Streams and Ground Waters. *Microbial Communities in Hyporheic Sediments*. Elsevier Inc.

Findlay Stuart, David Strayer, Cheikh Goumbala, and Kim Gould. 1993. Metabolism of Streamwater Dissolved Organic Carbon in the Shallow Hyporheic Zone. *Limnology and Oceanography* 38(7): 1493–99.

Fisher R Thomas, James D Hagy, and Emma Rochelle-Newall. 1998. Dissolved and Particulate Organic Carbon in Chesapeake Bay. *Estuaries* 21(2): 215–29.

Frank A Jeremy, Claudia I Reich, Shobha Sharma, Jon S Weisbaum, Brenda A Wilson, and Gary J Olsen. 2008. Critical Evaluation of Two Primers Commonly Used for Amplification of Bacterial 16S RRNA Genes. *Applied Environmental Microbiology* 74(8): 2461–70.

Frings Joachim, and Bernhard Schink. 1994. Fermentation of Phenoxyethanol to Phenol and Acetate by a Homoacetogenic Bacterium. *Archives of Microbiology* 162(3): 199–204.

Fujioka Takahiro, Stuart J Khan, James A McDonald, and Long D Nghiem. 2015. Rejection of Trace Organic Chemicals by a Hollow Fibre Cellulose Triacetate Reverse Osmosis Membrane. *Desalination* 368: 69–75.

Galloway Jason, Aryeh Fox, Jörg Lewandowski, and Shai Arnon. 2019. The Effect of Unsteady Streamflow and Stream-Groundwater Interactions on Oxygen Consumption in a Sandy Streambed. *Scientific Reports* 9(1): 1–11.

Gao Han, Jeanne M LaVergne, Corey M G Carpenter, Raj Desai, Xu Zhang, Kimberly Gray, Damian E Helbling, and George F Wells. 2019. Exploring Co-Occurrence Patterns between Organic Micropollutants and Bacterial Community Structure in a Mixed-Use Watershed. *Environmental Science: Processes & Impacts* 21(5): 867–80.

Gargouri Boutheina, Fatma Karray, Najla Mhiri, Fathi Aloui, and Sami Sayadi. 2014. Bioremediation of Petroleum Hydrocarbons-contaminated Soil by Bacterial Consortium Isolated from an Industrial Wastewater Treatment Plant. *Journal of Chemical Technology & Biotechnology* 89(7): 978–87.

George F Isabelle, Mark R Liles, Manuela Hartmann, Wolfgang Ludwig, Robert M Goodman, and Spiros N Agathos. 2009. Changes in Soil Acidobacteria Communities after 2, 4, 6-Trinitrotoluene Contamination. *FEMS Microbiology Letters* 296(2): 159–66.

Ghattas Ann-Kathrin, Ferdinand Fischer, Arne Wick, and Thomas A Ternes. 2017. Anaerobic Biodegradation of (Emerging) Organic Contaminants in the Aquatic Environment. *Water Research* 116: 268–95.

Ghosal Debajyoti, Shreya Ghosh, Tapan K Dutta, and Youngho Ahn. 2016. Current State of Knowledge in Microbial Degradation of Polycyclic Aromatic Hydrocarbons (PAHs): A Review. *Frontiers in Microbiology* 7: 1369.

Gibson Jane, and Caroline S Harwood. 1995. Degradation of Aromatic Compounds by Nonsulfur Purple Bacteria. In *Anoxygenic Photosynthetic Bacteria*, Springer, 991–1003.

Giger Walter, Christian Schaffner, and Hans-Peter E Kohler. 2006. Benzotriazole and Tolyltriazole as Aquatic Contaminants 1 Input and Occurrence in Rivers and Lakes. *Environmental Science & Technology* 40(23): 7186–92.

Gomez-Velez D Jesus, John L Wilson, Bayani Cardenas, and Judson W Harvey. 2017. Flow and Residence Times of Dynamic River Bank Storage and Sinuosity-driven Hyporheic Exchange. *Water Resources Research* 53(10): 8572–95.

Gooseff Michael N. 2010. Defining Hyporheic Zones–Advancing Our Conceptual and Operational Definitions of Where Stream Water and Groundwater Meet. *Geography Compass* 4(8): 945–55.

Griffiths I Robert, Andrew S Whiteley, Anthony G O'Donnell, and Mark J Bailey. 2000. Rapid Method for Coextraction of DNA and RNA from Natural Environments for Analysis of Ribosomal DNA-and RRNA-Based Microbial Community Composition. *Applied Environmental Microbiology* 66(12): 5488–91.

Gu Chuanhui, George M Hornberger, Janet S Herman, and Aaron L Mills. 2008. Effect of Freshets on the Flux of Groundwater Nitrate through Streambed Sediments. *Water Resources Research* 44(5).

Gücker Björn, Mario Brauns, and Martin T Pusch. 2006. Effects of Wastewater Treatment Plant Discharge on Ecosystem Structure and Function of Lowland Streams. *Journal of the North American Benthological Society* 25(2): 313–29.

Ha Hunmoon, Biswanath Mahanty, Soonuk Yoon, and Chang-Gyun Kim. 2016. Degradation of the Long-Resistant Pharmaceutical Compounds Carbamazepine and Diatrizoate Using Mixed Microbial Culture. *Journal of Environmental Science and Health, Part A* 51(6): 467–71.

Hai I Faisal, Nichanan Tadkaew, James A McDonald, Stuart J Khan, and Long D Nghiem. 2011. Is Halogen Content the Most Important Factor in the Removal of Halogenated Trace Organics by MBR Treatment? *Bioresource Technology* 102(10): 6299–6303.

Hai I Faisal, Long D Nghiem, Stuart J Khan, William E Price, and Kazuo Yamamoto. 2014. Wastewater Reuse: Removal of Emerging Trace Organic Contaminants (TrOC).

Hammer Øyvind, David A T Harper, and Paul D Ryan. 2001. PAST: Paleontological Statistics Software Package for Education and Data Analysis. *Palaeontologia Electronica* 4(1): 9.

Hammill B Terry, and Ronald L Crawford. 1996. Degradation of 2-Sec-Butyl-4, 6-Dinitrophenol (Dinoseb) by Clostridium Bifermentans KMR-1. *Applied Environmental Microbiology* 62(5): 1842–46.

Haque Muhammad, Thierry Nadalig, Françoise Bringel, Hubert Schaller, and Stéphane Vuilleumier. 2013. Fluorescence-Based Bacterial Bioreporter for Specific Detection of Methyl Halide Emissions in the Environment. *Applied Environmental Microbiology* 79(21): 6561–67.

Harder Wim, and Lubbert Dijkhuizen. 1982. Strategies of Mixed Substrate Utilization in Microorganisms. *Philosophical Transactions of the Royal Society of London. B, Biological Sciences* 297(1088): 459–80.

Harichová Jana, Edita Karelová, Domenico Pangallo, and Peter Ferianc. 2012. Structure Analysis of Bacterial Community and Their Heavy-Metal Resistance Determinants in the Heavy-Metal-Contaminated Soil Sample. *Biologia* 67(6): 1038–48.

Harvey W Judson, John K Böhlke, Mary A Voytek, Durelle Scott, and Craig R Tobias. 2013. Hyporheic Zone Denitrification: Controls on Effective Reaction Depth and Contribution to Whole-stream Mass Balance. *Water Resources Research* 49(10): 6298–6316.

Hashim N Hazlina, S Shafie, and Stuart J Khan. 2010. Enantiomeric Fraction as an Indicator of Pharmaceutical Biotransformation during Wastewater Treatment and in the Environment–a Review. *Environmental Technology* 31(12): 1349–70.

Hashim N Hazlina, Long D Nghiem, R M Stuetz, and Stuart J Khan. 2011. Enantiospecific Fate of Ibuprofen, Ketoprofen and Naproxen in a Laboratory-Scale Membrane Bioreactor. *Water Research* 45(18): 6249–58.

Hebig H Klaus, Laura G Groza, Michelle J Sabourin, Traugott J Scheytt, and Carol J Ptacek. 2017. Transport Behavior of the Pharmaceutical Compounds Carbamazepine, Sulfamethoxazole, Gemfibrozil, Ibuprofen, and Naproxen, and the Lifestyle Drug Caffeine, in Saturated Laboratory Columns. *Science of The Total Environment* 590: 708–19.

Heider Johann, Maciej Szaleniec, Katharina Suenwoldt, and Matthias Boll. 2016. Ethylbenzene Dehydrogenase and Related Molybdenum Enzymes Involved in Oxygen-Independent Alkyl Chain Hydroxylation. *Journal of Molecular Microbiology and Biotechnology* 26(1–3): 45–62.

Helbling E Damian, David R Johnson, Mark Honti, and Kathrin Fenner. 2012. Micropollutant Biotransformation Kinetics Associate with WWTP Process Parameters and Microbial Community Characteristics. *Environmental Science & Technology* 46(19): 10579–88.

Hemalatha Swarnakaran, and Panchanathan VeeraManikandan. 2011. Characterization of Aromatic Hydrocarbon Rading Bacteria from Petroleum Contaminated Sites. *Journal of Environmental Protection* 2(03): 243.

Henning Nina, Per Falås, Sandro Castronovo, Kevin S Jewell, Kai Bester, Thomas A

Ternes, and Arne Wick. 2019. Biological Transformation of Fexofenadine and Sitagliptin by Carrier-Attached Biomass and Suspended Sludge from a Hybrid Moving Bed Biofilm Reactor. *Water Research* 167: 115034.

Herzog Sarah, Franziska Wemheuer, Bernd Wemheuer, and Rolf Daniel. 2015. Effects of Fertilization and Sampling Time on Composition and Diversity of Entire and Active Bacterial Communities in German Grassland Soils. *PloS one* 10(12): e0145575.

Hester T Erich, Young KI, and Mark A Widdowson. 2013. Mixing of Surface and Groundwater Induced by Riverbed Dunes: Implications for Hyporheic Zone Definitions and Pollutant Reactions. *Water Resources Research* 49(9): 5221–37.

Ho Adrian, Paolo Di Lonardo, and Paul L E Bodelier. 2017. Revisiting Life Strategy Concepts in Environmental Microbial Ecology. *FEMS Microbiology Ecology* 93(3): fix006.

Horn A Marcus, Julian Ihssen, Carola Matthies, Andreas Schramm, Georg Acker, and Harold L Drake. 2005. Dechloromonas Denitrificans Sp Nov, Flavobacterium Denitrificans Sp Nov, Paenibacillus Anaericanus Sp Nov and Paenibacillus Terrae Strain MH72, N2O-Producing Bacteria Isolated from the Gut of the Earthworm Aporrectodea Caliginosa. *International Journal of Systematic and Evolutionary Microbiology* 55(3): 1255–65.

Islam Shahinoor, Yanyan Zhang, Kerry N McPhedran, Yang Liu, and Mohamed Gamal El-Din. 2016. Mechanistic Investigation of Industrial Wastewater Naphthenic Acids Removal Using Granular Activated Carbon (GAC) Biofilm Based Processes. *Science of the Total Environment* 541: 238–46.

Jaeger Anna, Malte Posselt, Andrea Betterle, Jonas Schaper, Jonas Mechelke, Claudia Coll, and Joerg Lewandowski. 2019. Spatial and Temporal Variability in Attenuation of Polar Organic Micropollutants in an Urban Lowland Stream. *Environmental Science & Technology* 53(5): 2383–95.

Jaeger Anna, Claudia Coll, Malte Posselt, Jonas Mechelke, Cyrus Rutere, Andrea Betterle, Muhammad Raza, Anne Mehrtens, Karin Meinikmann, Andrea Portmann, Tanu Singh, Phillip J. Blaen, Stefan Krause, Marcus A. Horn, Juliane Hollender, Jonathan P. Benskin, Anna Sobek, and Joerg Lewandowski. 2019. Using Recirculating Flumes and a Response Surface Model to Investigate the Role of Hyporheic Exchange and Bacterial Diversity on Micropollutant Half-Lives. *Environmental Science: Processes and Impacts*.

Jia Yanyan, Linwan Yin, Samir Kumar Khanal, Huiqun Zhang, Akashdeep Singh Oberoi, and Hui Lu. 2020. Biotransformation of Ibuprofen in Biological Sludge Systems: Investigation of Performance and Mechanisms. *Water Research* 170: 115303.

Jin Decai, Ping Wang, Zhihui Bai, Bo Jin, Zhisheng Yu, Xinxin Wang, Guoqiang Zhuang, and Hongxun Zhang. 2013. Terrimonas Pekingensis Sp Nov, Isolated from Bulking Sludge, and Emended Descriptions of the Genus Terrimonas, Terrimonas Ferruginea, Terrimonas Lutea and Terrimonas Aquatica. *International Journal of Systematic and Evolutionary Microbiology* 63(5): 1658–64.

Johnson R David, Damian E Helbling, Tae Kwon Lee, Joonhong Park, Kathrin Fenner, Hans-Peter E Kohler, and Martin Ackermann. 2015. Association of Biodiversity

with the Rates of Micropollutant Biotransformations among Full-Scale Wastewater Treatment Plant Communities. *Applied Environmental Microbiology* 81(2): 666–75.

Joss Adriano, Sebastian Zabczynski, Anke Göbel, Burkhard Hoffmann, Dirk Löffler, Christa S McArdell, Thomas A Ternes, Angela Thomsen, and Hansruedi Siegrist. 2006. Biological Degradation of Pharmaceuticals in Municipal Wastewater Treatment: Proposing a Classification Scheme. *Water Research* 40(8): 1686–96.

Jung Jaejoon, and Woojun Park. 2015. Acinetobacter Species as Model Microorganisms in Environmental Microbiology: Current State and Perspectives. *Applied Microbiology and Biotechnology* 99(6): 2533–48.

Kahl Stefanie, Sabine Kleinsteuber, Jaime Nivala, Manfred van Afferden, and Thorsten Reemtsma. 2018. Emerging Biodegradation of the Previously Persistent Artificial Sweetener Acesulfame in Biological Wastewater Treatment. *Environmental Science & Technology* 52(5): 2717–25.

Katsura Shinji, Nobuo Yamada, Atsushi Nakashima, Sumihiro Shiraishi, Takayuki Furuishi, and Haruhisa Ueda. 2015. Identification of Furosemide Photodegradation Products in Water–Acetonitrile Mixture. *Chemical and Pharmaceutical Bulletin* 63(8): 617–27.

Kay Paul, Stephen R Hughes, James R Ault, Alison E Ashcroft, and Lee E Brown. 2017. Widespread, Routine Occurrence of Pharmaceuticals in Sewage Effluent, Combined Sewer Overflows and Receiving Waters. *Environmental Pollution* 220: 1447–55.

Kern Susanne, Rebekka Baumgartner, Damian E Helbling, Juliane Hollender, Heinz Singer, Martin J Loos, René P Schwarzenbach, and Kathrin Fenner. 2010. A Tiered Procedure for Assessing the Formation of Biotransformation Products of Pharmaceuticals and Biocides during Activated Sludge Treatment. *Journal of Environmental Monitoring* 12(11): 2100–2111.

Kim Heejung, and Kang-Kun Lee. 2019. Effect of Vertical Flow Exchange on Microbial Community Distributions in Hyporheic Zones. *Episodes Journal of International Geoscience* 42(1): 1–16.

Kleinsteuber Sabine, Kathleen M Schleinitz, Jana Breitfeld, Hauke Harms, Hans H Richnow, and Carsten Vogt. 2008. Molecular Characterization of Bacterial Communities Mineralizing Benzene under Sulfate-Reducing Conditions. *FEMS Microbiology Ecology* 66(1): 143–57.

Knapp Julia, Ricardo González-Pinzón, Jennifer D Drummond, Laurel G Larsen, Olaf A Cirpka, and Judson W Harvey. 2017. Tracer-based Characterization of Hyporheic Exchange and Benthic Biolayers in Streams. *Water Resources Research* 53(2): 1575–94.

Kodešová Radka, Roman Grabic, Martin Kočárek, Aleš Klement, Oksana Golovko, Miroslav Fér, Antonín Nikodem, and Ondřej Jakšík. 2015. Pharmaceuticals' Sorptions Relative to Properties of Thirteen Different Soils. *Science of the Total Environment* 511: 435–43.

Krause Stefan, David M Hannah, Jan H Fleckenstein, Catherine M Heppell, Daniel Kaeser, Roger Pickup, Gilles Pinay, Anne L Robertson, and Paul J Wood. 2011.

Inter-disciplinary Perspectives on Processes in the Hyporheic Zone. *Ecohydrology* 4(4): 481–99.

Krause Stefan, David M Hannah, and Jan H Fleckenstein. 2009. Hyporheic Hydrology: Interactions at the Groundwater-Surface Water Interface. *Hydrological Processes* 23(15): 2103–2263.

Kujala Katharina, Anu Mikkonen, Karita Saravesi, Anna-Kaisa Ronkanen, and Marja Tiirola. 2018. Microbial Diversity along a Gradient in Peatlands Treating Mining-Affected Waters. *FEMS Microbiology Ecology* 94(10): fiy145.

Kumar Sudhir, Glen Stecher, and Koichiro Tamura. 2016. MEGA7: Molecular Evolutionary Genetics Analysis Version 70 for Bigger Datasets. *Molecular Biology and Evolution* 33(7): 1870–74.

Kümmel Steffen, Florian-Alexander Herbst, Arne Bahr, Márcia Duarte, Dietmar H Pieper, Nico Jehmlich, Jana Seifert, Martin von Bergen, Petra Bombach, and Hans H Richnow. 2015. Anaerobic Naphthalene Degradation by Sulfate-Reducing Desulfobacteraceae from Various Anoxic Aquifers. *FEMS Microbiology Ecology* 91(3).

Kunkel Uwe, and Michael Radke. 2008. Biodegradation of Acidic Pharmaceuticals in Bed Sediments: Insight from a Laboratory Experiment. *Environmental Science & Technology* 42(19): 7273–79.

Kuppardt Anke, Sabine Kleinsteuber, Carsten Vogt, Tillmann Lüders, Hauke Harms, and Antonis Chatzinotas. 2014. Phylogenetic and Functional Diversity within Toluene-Degrading, Sulphate-Reducing Consortia Enriched from a Contaminated Aquifer. *Microbial Ecology* 68(2): 222–34.

Lane D Johnson. 1991. 16S/23S RRNA Sequencing. *Nucleic acid Techniques in Bacterial Systematics*: 115–75.

Lapworth J Dan, Daren C Gooddy, and Helen P Jarvie. 2011. Understanding Phosphorus Mobility and Bioavailability in the Hyporheic Zone of a Chalk Stream. *Water, Air, & Soil Pollution* 218(1–4): 213–26.

Lawrence R John, George D W Swerhone, Leonard I Wassenaar, and Thomas R Neu. 2005. Effects of Selected Pharmaceuticals on Riverine Biofilm Communities. *Canadian Journal of Microbiology* 51(8): 655–69.

Lewandowski Jörg, Anke Putschew, David Schwesig, Christiane Neumann, and Michael Radke. 2011. Fate of Organic Micropollutants in the Hyporheic Zone of a Eutrophic Lowland Stream: Results of a Preliminary Field Study. *Science of the Total Environment* 409(10): 1824–35.

Lewandowski Jörg et al. 2019. Is the Hyporheic Zone Relevant beyond the Scientific Community? *Water* 11(11): 1–33.

Li B Fangbai, Xiaomin M Li, Shungui G Zhou, Li Zhuang, Fang Cao, De Y Huang, Wei Xu, Tonxu Liu, and Chunhua Feng. 2010. Enhanced Reductive Dechlorination of DDT in an Anaerobic System of Dissimilatory Iron-Reducing Bacteria and Iron Oxide. *Environmental Pollution* 158(5): 1733–40.

Li Yifei, Bing Wu, Guibing Zhu, Yu Liu, Wun Jern Ng, Adhityan Appan, and Soon Keat Tan. 2016. High-Throughput Pyrosequencing Analysis of Bacteria Relevant to

Cometabolic and Metabolic Degradation of Ibuprofen in Horizontal Subsurface Flow Constructed Wetlands. *Science of the Total Environment* 562: 604–13.

Li Zhe, Michael P Maier, and Michael Radke. 2014. Screening for Pharmaceutical Transformation Products Formed in River Sediment by Combining Ultrahigh Performance Liquid Chromatography/High Resolution Mass Spectrometry with a Rapid Data-Processing Method. *Analytica Chimica Acta* 810: 61–70.

Li Zhe, and Michael S McLachlan. 2019. Biodegradation of Chemicals in Unspiked Surface Waters Downstream of Wastewater Treatment Plants. *Environmental Science & Technology* 53(4): 1884–92.

Liang Xiaoming, Cheryl E Devine, Jennifer Nelson, Barbara Sherwood Lollar, Stephen Zinder, and Elizabeth A Edwards. 2013. Anaerobic Conversion of Chlorobenzene and Benzene to CH4 and CO2 in Bioaugmented Microcosms. *Environmental Science & Technology* 47(5): 2378–85.

Lienert Judit, Karin Güdel, and Beate I Escher. 2007. Screening Method for Ecotoxicological Hazard Assessment of 42 Pharmaceuticals Considering Human Metabolism and Excretory Routes. *Environmental Science & Technology* 41(12): 4471–78.

Liu Fan, Asbjørn Haaning Nielsen, and Jes Vollertsen. 2019. Sorption and Degradation Potential of Pharmaceuticals in Sediments from a Stormwater Retention Pond. *Water* 11(3).

Liu Guangyu, Christoph M Tang, and Rachel M Exley. 2015. Non-Pathogenic Neisseria: Members of an Abundant, Multi-Habitat, Diverse Genus. *Microbiology* 161(7): 1297–1312.

Liu Shi, and Joseph M Suflita. 1993. H2-CO2-Dependent Anaerobic O-Demethylation Activity in Subsurface Sediments and by an Isolated Bacterium. *Applied Environmental Microbiology* 59(5): 1325–31.

Livingstone G Paul, Russell M Morphew, and David E Whitworth. 2017. Myxobacteria Are Able to Prey Broadly upon Clinically-Relevant Pathogens, Exhibiting a Prey Range Which Cannot Be Explained by Phylogeny. *Frontiers in Microbiology* 8: 1593.

Löffler Dirk, Jörg Römbke, Michael Meller, and Thomas A. Ternes. 2005. Environmental Fate of Pharmaceuticals in Water/Sediment Systems. *Environmental Science and Technology* 39(14): 5209–18.

Lorenz G Michael, and Wilfried Wackernagel. 1996. Mechanisms and Consequences of Horizontal Gene Transfer in Natural Bacterial Populations. In *Transgenic Organisms*, Springer, 45–57.

Love I Michael, Wolfgang Huber, and Simon Anders. 2014. Moderated Estimation of Fold Change and Dispersion for RNA-Seq Data with DESeq2. *Genome Biology* 15(12): 550.

Magliozzi Chiara, Philippe Usseglio-Polatera, Albin Meyer, and Robert C Grabowski. 2019. Functional Traits of Hyporheic and Benthic Invertebrates Reveal Importance of Wood-driven Geomorphological Processes in Rivers. *Functional Ecology* 33(9): 1758–70.

Männistö K Minna, Marja A Tiirola, Mirja S Salkinoja-Salonen, Markku S Kulomaa, and Jaakko A Puhakka. 1999. Diversity of Chlorophenol-Degrading Bacteria Isolated from Contaminated Boreal Groundwater. *Archives of Microbiology* 171(3): 189–97.

Marchlewicz Ariel, Urszula Guzik, Wojciech Smułek, and Danuta Wojcieszyńska. 2017. Exploring the Degradation of Ibuprofen by Bacillus Thuringiensis B1 (2015b): The New Pathway and Factors Affecting Degradation. *Molecules* 22(10): 1676.

Marco-Urrea Ernest, Miriam Pérez-Trujillo, Teresa Vicent, and Gloria Caminal. 2009. Ability of White-Rot Fungi to Remove Selected Pharmaceuticals and Identification of Degradation Products of Ibuprofen by Trametes Versicolor. *Chemosphere* 74(6): 765–72.

Margot Jonas, Luca Rossi, David A Barry, and Christof Holliger. 2015. A Review of the Fate of Micropollutants in Wastewater Treatment Plants. *Wiley Interdisciplinary Reviews: Water* 2(5): 457–87.

Marti Romain, Sébastien Ribun, Jean-Baptiste Aubin, Céline Colinon, Stéphanie Petit, Laurence Marjolet, Michèle Gourmelon, Laurent Schmitt, Pascal Breil, and Marylise Cottet. 2017. Human-Driven Microbiological Contamination of Benthic and Hyporheic Sediments of an Intermittent Peri-Urban River Assessed from MST and 16S RRNA Genetic Structure Analyses. *Frontiers in Microbiology* 8: 19.

Martone Ivo, Carlo Gualtieri, and Theodore Endreny. 2020. Characterization of Hyporheic Exchange Drivers and Patterns within a Low-Gradient, First-Order, River Confluence during Low and High Flow. *Water* 12(3): 649.

Marxsen Jürgen. 1996. Measurement of Bacterial Production in Stream-Bed Sediments via Leucine Incorporation. *FEMS Microbiology Ecology* 21(4): 313–25.

Massmann Gudrun, Janek Greskowiak, Uwe Dünnbier, S Zuehlke, A Knappe, and Asaf Pekdeger. 2006. The Impact of Variable Temperatures on the Redox Conditions and the Behaviour of Pharmaceutical Residues during Artificial Recharge. *Journal of Hydrology* 328(1–2): 141–56.

Matozzo Valerio, François Gagné, Maria Gabriella Marin, Francesco Ricciardi, and Christian Blaise. 2008. Vitellogenin as a Biomarker of Exposure to Estrogenic Compounds in Aquatic Invertebrates: A Review. *Environment International* 34(4): 531–45.

Matturro Bruna, Carla Ubaldi, and Simona Rossetti. 2016. Microbiome Dynamics of a Polychlorobiphenyl (PCB) Historically Contaminated Marine Sediment under Conditions Promoting Reductive Dechlorination. *Frontiers in Microbiology* 7: 1502.

Maurer Max, Beate I Escher, P Richle, Christian Schaffner, and Alfredo C Alder. 2007. Elimination of β-Blockers in Sewage Treatment Plants. *Water Research* 41(7): 1614–22.

Mechelke Jonas, Etiënne Vermeirssen, and Juliane Hollender. 2019. Passive Sampling of Organic Contaminants across the Water-Sediment Interface of an Urban Stream. *Water Research* 165.

Messing Joachim. 1983. [2] New M13 Vectors for Cloning. In *Methods in Enzymology*, Elsevier, 20–78.

Miettinen Hanna, Malin Bomberg, Mari Nyyssönen, Anna Reunamo, Kirsten S. Jørgensen, and Minna Vikman. 2019. Oil Degradation Potential of Microbial Communities in Water and Sediment of Baltic Sea Coastal Area. *PLoS ONE.* 14.

Mohatt L Jessica, Lanhua Hu, Kevin T Finneran, and Timothy J Strathmann. 2011. Microbially Mediated Abiotic Transformation of the Antimicrobial Agent Sulfamethoxazole under Iron-Reducing Soil Conditions. *Environmental Science & Technology* 45(11): 4793–4801.

Mohr I Kathrin, Ronald O Garcia, Klaus Gerth, Herbert Irschik, and Rolf Müller. 2012. Sandaracinus Amylolyticus Gen Nov, Sp Nov, a Starch-Degrading Soil Myxobacterium, and Description of Sandaracinaceae Fam Nov. *International Journal of Systematic and Evolutionary Microbiology* 62(5): 1191–98.

Morris E Kathryn, Tancredi Caruso, François Buscot, Markus Fischer, Christine Hancock, Tanja S Maier, Torsten Meiners, Caroline Müller, Elisabeth Obermaier, and Daniel Prati. 2014. Choosing and Using Diversity Indices: Insights for Ecological Applications from the German Biodiversity Exploratories. *Ecology and Evolution* 4(18): 3514–24.

Munz Matthias, Sascha E Oswald, Robin Schäfferling, and Hermann-Josef Lensing. 2019. Temperature-Dependent Redox Zonation, Nitrate Removal and Attenuation of Organic Micropollutants during Bank Filtration. *Water Research* 162: 225–35.

Murdoch W Robert, and Anthony G Hay. 2005. Formation of Catechols via Removal of Acid Side Chains from Ibuprofen and Related Aromatic Acids. *Applied Environmental Microbiology* 71(10): 6121–25.

Murdoch W Robert, and Anthony G Hay. 2013. Genetic and Chemical Characterization of Ibuprofen Degradation by Sphingomonas Ibu-2. *Microbiology* 159(Pt 3): 621.

Murdoch W Robert, and Anthony G Hay. 2015. The Biotransformation of Ibuprofen to Trihydroxyibuprofen in Activated Sludge and by Variovorax Ibu-1. *Biodegradation* 26(2): 105–13.

Muyzer Gerard, Ellen C De Waal, and Andre G Uitterlinden. 1993. Profiling of Complex Microbial Populations by Denaturing Gradient Gel Electrophoresis Analysis of Polymerase Chain Reaction-Amplified Genes Coding for 16S RRNA. *Applied Environmental Microbiology* 59(3): 695–700.

Nasir Najihah, Suhaimi A Talib, Saiyidah Hashim, and Chia C Tay. 2018. Biodegradation of Carbamazepine Using Fungi and Bacteria. *Journal of Fundamental and Applied Sciences* 9(6S): 124.

Nega Marcella, Burga Braun, Sven Künzel, and Ulrich Szewzyk. 2019. Evaluating the Impact Ofwastewater Effluent on Microbial Communities in the Panke, an Urban River. *Water* 11(5): 1–17.

Neu C Harold . 1992. The Crisis in Antibiotic Resistance. *Science* 257(5073): 1064–73.

Nogales Balbina, Edward R B Moore, Wolf-Rainer Abraham, and Kenneth N Timmis. 1999. Identification of the Metabolically Active Members of a Bacterial Community in a Polychlorinated Biphenyl-polluted Moorland Soil. *Environmental Microbiology* 1(3): 199–212.

Onesios M Kathryn, Yu T Jim, and Edward J Bouwer. 2009. Biodegradation and Removal of Pharmaceuticals and Personal Care Products in Treatment Systems: A Review. *Biodegradation* 20(4): 441–66.

Paíga Paula, Manuela Correia, Maria João Fernandes, Ana Silva, Manuela Carvalho, Joana Vieira, Sandra Jorge, Jaime Gabriel Silva, Cristina Freire, and Cristina Delerue-Matos. 2019. Assessment of 83 Pharmaceuticals in WWTP Influent and Effluent Samples by UHPLC-MS/MS: Hourly Variation. *Science of the Total Environment* 648: 582–600.

Pal Amrita, Yiliang He, Martin Jekel, Martin Reinhard, and Karina Yew Hoong Gin. 2014. Emerging Contaminants of Public Health Significance as Water Quality Indicator Compounds in the Urban Water Cycle. *Environment International* 71: 46–62.

Pasternak Zohar, M Njagi, Y Shani, Ryan Chanyi, Or Rotem, Mor N Lurie-Weinberger, Susan Koval, Shmuel Pietrokovski, Uri Gophna, and E Jurkevitch. 2014. In and out: An Analysis of Epibiotic vs Periplasmic Bacterial Predators. *The ISME Journal* 8(3): 625.

Peralta-Maraver Ignacio, Jason Galloway, Malte Posselt, Shai Arnon, Julia Reiss, Jörg Lewandowski, and Anne L Robertson. 2018. Environmental Filtering and Community Delineation in the Streambed Ecotone. *Scientific Reports* 8(1): 1–11.

Peralta-Maraver Ignacio, Malte Posselt, Daniel M Perkins, and Anne L Robertson. 2019. Mapping Micro-Pollutants and Their Impacts on the Size Structure of Streambed Communities. *Water* 11(12): 2610.

Peralta-Maraver Ignacio, Julia Reiss, and Anne L Robertson. 2018. Interplay of Hydrology, Community Ecology and Pollutant Attenuation in the Hyporheic Zone. *Science of the Total Environment* 610: 267–75.

Pérez-Pantoja Danilo, Raúl Donoso, Loreine Agulló, Macarena Córdova, Michael Seeger, Dietmar H Pieper, and Bernardo González. 2012. Genomic Analysis of the Potential for Aromatic Compounds Biodegradation in Burkholderiales. *Environmental Microbiology* 14(5): 1091–1117.

Phan V Hop, Faisal I Hai, Ren Zhang, Jinguo Kang, William E. Price, and Long D. Nghiem. 2016. Bacterial Community Dynamics in an Anoxic-Aerobic Membrane Bioreactor - Impact on Nutrient and Trace Organic Contaminant Removal. *International Biodeterioration and Biodegradation* 109: 61–72.

Pomati Francesco, Sara Castiglioni, Ettore Zuccato, Roberto Fanelli, Davide Vigetti, Carlo Rossetti, and Davide Calamari. 2006. Effects of a Complex Mixture of Therapeutic Drugs at Environmental Levels on Human Embryonic Cells. *Environmental Science & Technology* 40(7): 2442–47.

Posselt Malte, Anna Jaeger, Jonas L Schaper, Michael Radke, and Jonathan P Benskin. 2018. Determination of Polar Organic Micropollutants in Surface and Pore Water by High-Resolution Sampling-Direct Injection-Ultra High Performance Liquid Chromatography-Tandem Mass Spectrometry. *Environmental Science: Processes and Impacts* 20(12): 1716–27.

Posselt Malte, Jonas Mechelke, Cyrus Rutere, Claudia Coll, Anna Jaeger, Muhammad Raza, Karin Meinikmann, Stefan Krause, Anna Sobek, Jörg Lewandowski, Marcus

A Horn, Juliane Hollender, and Jonathan P Benskin. 2020. Bacterial Diversity Controls Transformation of Wastewater-Derived Organic Contaminants in River-Simulating Flumes. *Environmental Science & Technology*.

Poursat AJ Baptiste, Rob JM van Spanning, Martin Braster, Rick Helmus, Pim de Voogt, and John R Parsons. 2019. Biodegradation of Metformin and Its Transformation Product, Guanylurea, by Natural and Exposed Microbial Communities. *Ecotoxicology and Environmental Safety* 182: 109414.

Pruesse Elmar, Jörg Peplies, and Frank Oliver Glöckner. 2012. SINA: Accurate High-Throughput Multiple Sequence Alignment of Ribosomal RNA Genes. *Bioinformatics* 28(14): 1823–29.

Quintana José Benito, Stefan Weiss, and Thorsten Reemtsma. 2005. Pathways and Metabolites of Microbial Degradation of Selected Acidic Pharmaceutical and Their Occurrence in Municipal Wastewater Treated by a Membrane Bioreactor. *Water Research* 39(12): 2654–64.

Rabus Ralf, Matthias Boll, Johann Heider, Rainer U Meckenstock, Wolfgang Buckel, Oliver Einsle, Ulrich Ermler, Bernard T Golding, Robert P Gunsalus, and Peter M H Kroneck. 2016. Anaerobic Microbial Degradation of Hydrocarbons: From Enzymatic Reactions to the Environment. *Journal of Molecular Microbiology and Biotechnology* 26(1–3): 5–28.

Radke Michael, Christoph Lauwigi, Georg Heinkele, Thomas E Mürdter, and Marion Letzel. 2009. Fate of the Antibiotic Sulfamethoxazole and Its Two Major Human Metabolites in a Water Sediment Test. *Environmental Science & Technology* 43(9): 3135–41.

Radke Michael, Hanna Ulrich, Carolin Wurm, and Uwe Kunkel. 2010. Dynamics and Attenuation of Acidic Pharmaceuticals along a River Stretch. *Environmental Science & Technology* 44(8): 2968–74.

Ramil Maria, Tarek El Aref, Guido Fink, Marco Scheurer, and Thomas A Ternes. 2010. Fate of Beta Blockers in Aquatic-Sediment Systems: Sorption and Biotransformation. *Environmental Science & Technology* 44(3): 962–70.

Reemtsma Thorsten, Britta Zywicki, Markus Stueber, Achim Kloepfer, and Martin Jekel. 2002. Removal of Sulfur− Organic Polar Micropollutants in a Membrane Bioreactor Treating Industrial Wastewater. *Environmental Science & Technology* 36(5): 1102–6.

Reichenbach Hans. 2001. Myxobacteria, Producers of Novel Bioactive Substances. *Journal of Industrial Microbiology and Biotechnology* 27(3): 149–56.

Rochman Fauziah, Andriy Sheremet, Ivica Tamas, Alireza Saidi-Mehrabad, Joong Jae Kim, Xiaoli Dong, Christoph W. Sensen, Lisa M. Gieg, and Peter F. Dunfield. 2017. Benzene and Naphthalene Degrading Bacterial Communities in an Oil Sands Tailings Pond. *Frontiers in Microbiology* 8(SEP): 1–12.

Rodríguez Juanjo, Christine Monique Jeanine Gallampois, Sari Timonen, Agneta Andersson, Hanna Sinkko, Peter Haglund, Åsa M M Berglund, Matyas Ripszam, Daniela Figueroa, and Mats Tysklind. 2018. Effects of Organic Pollutants on Bacterial Communities under Future Climate Change Scenarios. *Frontiers in Microbiology* 9: 2926.

Romani Anna, Andrea Butturini, Francesc Sabater, and Sergi Sabater. 1998. Heterotrophic Metabolism in a Forest Stream Sediment: Surface versus Subsurface Zones. *Aquatic Microbial Ecology* 16(2): 143–51.

Rubirola Adria, Marta Llorca, Sara Rodriguez-Mozaz, Nuria Casas, Ignasi Rodriguez-Roda, Daniel Barceló, and Gianluigi Buttiglieri. 2014. Characterization of Metoprolol Biodegradation and Its Transformation Products Generated in Activated Sludge Batch Experiments and in Full Scale WWTPs. *Water Research* 63: 21–32.

Rühmland Sabine, Arne Wick, Thomas A Ternes, and Matthias Barjenbruch. 2015. Fate of Pharmaceuticals in a Subsurface Flow Constructed Wetland and Two Ponds. *Ecological Engineering* 80: 125–39.

Rutere Cyrus, Kirsten Knoop, Malte Posselt, Adrian Ho, and Marcus A Horn. 2020. Ibuprofen Degradation and Associated Bacterial Communities in Hyporheic Zone Sediments. *Microorganisms* 8(8): 1245.

Saiki K Randall, David H Gelfand, Susanne Stoffel, Stephen J Scharf, Russell Higuchi, Glenn T Horn, Kary B Mullis, and Henry A Erlich. 1988. Primer-Directed Enzymatic Amplification of DNA with a Thermostable DNA Polymerase. *Science* 239(4839): 487–91.

Sambrook Joseph, Edward F Fritsch, and Tom Maniatis. 1989. *Molecular Cloning: A Laboratory Manual.* Cold spring harbor laboratory press.

Schaper L Jonas, Wiebke Seher, Gunnar Nützmann, Anke Putschew, Martin Jekel, and Jörg Lewandowski. 2018. The Fate of Polar Trace Organic Compounds in the Hyporheic Zone. *Water Research* 140: 158–66.

Schaper L Jonas, Malte Posselt, Camille Bouchez, Anna Jaeger, Gunnar Nuetzmann, Anke Putschew, Gabriel Singer, and Joerg Lewandowski. 2019. Fate of Trace Organic Compounds in the Hyporheic Zone: Influence of Retardation, the Benthic Biolayer, and Organic Carbon. *Environmental Science and Technology* 53(8): 4224–34.

Schaper L Jonas, Malte Posselt, James L McCallum, Eddie W Banks, Anja Hoehne, Karin Meinikmann, Margaret A Shanafield, Okke Batelaan, and Joerg Lewandowski. 2018. Hyporheic Exchange Controls Fate of Trace Organic Compounds in an Urban Stream. *Environmental Science & Technology* 52(21): 12285–94.

Scheurer Marco, Maria Ramil, Chris D Metcalfe, Stefanie Groh, and Thomas A Ternes. 2010. The Challenge of Analyzing Beta-Blocker Drugs in Sludge and Wastewater. *Analytical and Bioanalytical Chemistry* 396(2): 845–56.

Schindler E John, and David P Krabbenhoft. 1998. The Hyporheic Zone as a Source of Dissolved Organic Carbon and Carbon Gases to a Temperate Forested Stream. *Biogeochemistry* 43(2): 157–74.

Schloss D Patrick, Sarah L Westcott, Thomas Ryabin, Justine R Hall, Martin Hartmann, Emily B Hollister, Ryan A Lesniewski, Brian B Oakley, Donovan H Parks, and Courtney J Robinson. 2009. Introducing Mothur: Open-Source, Platform-Independent, Community-Supported Software for Describing and Comparing Microbial Communities. *Applied Environmental Microbiology* 75(23): 7537–41.

Schmidt K Carsten, Frank T Lange, and Heinz-Jürgen Brauch. 2007. Characteristics and Evaluation of Natural Attenuation Processes for Organic Micropollutant Removal during Riverbank Filtration. *Water Science and Technology: Water Supply* 7(3): 1–7.

Schmidt Natalie, Declan Page, and Andreas Tiehm. 2017. Biodegradation of Pharmaceuticals and Endocrine Disruptors with Oxygen, Nitrate, Manganese (IV), Iron (III) and Sulfate as Electron Acceptors. *Journal of contaminant hydrology* 203: 62–69.

Schwarzenbach René. 1986. Sorption Behavior of Neutral and Ionizable Hydrophobic Organic Compounds. In *Organic Micropollutants in the Aquatic Environment*, Springer, 168–77.

Segata Nicola, Jacques Izard, Levi Waldron, Dirk Gevers, Larisa Miropolsky, Wendy S Garrett, and Curtis Huttenhower. 2011. Metagenomic Biomarker Discovery and Explanation. *Genome biology* 12(6): R60.

Sempéré Richard, Séri C Yoro, France Van Wambeke, and Bruno Charrière. 2000. Microbial Decomposition of Large Organic Particles in the Northwestern Mediterranean Sea: An Experimental Approach. *Marine Ecology Progress Series* 198: 61–72.

Seo Jong-Su, Young-Soo Keum, and Qing X Li. 2009. Bacterial Degradation of Aromatic Compounds. *International journal of environmental research and public health* 6(1): 278–309.

Shahi Aiyoub, Sevcan Aydin, Bahar Ince, and Orhan Ince. 2016. Evaluation of Microbial Population and Functional Genes during the Bioremediation of Petroleum-Contaminated Soil as an Effective Monitoring Approach. *Ecotoxicology and Environmental Safety* 125: 153–60.

Shimada Kohei, Yoshikane Itoh, Kenji Washio, and Masaaki Morikawa. 2012. Efficacy of Forming Biofilms by Naphthalene Degrading Pseudomonas Stutzeri T102 toward Bioremediation Technology and Its Molecular Mechanisms. *Chemosphere* 87(3): 226–33.

Silva S Godinho, Asunción Lago-Lestón, Rodrigo Costa, and Tina Keller-Costa. 2018. Draft Genome Sequence of Sphingorhabdus Sp Strain EL138, a Metabolically Versatile Alphaproteobacterium Isolated from the Gorgonian Coral Eunicella Labiata. *Genome Announcements.* 6(9): e00142-18.

Singh Tanu, Liwen Wu, Jesus D Gomez-Velez, Jörg Lewandowski, David M Hannah, and Stefan Krause. 2019. Dynamic Hyporheic Zones: Exploring the Role of Peak Flow Events on Bedform-Induced Hyporheic Exchange. *Water Resources Research* 55(1): 218–35.

Song Jaeho, and Jang-Cheon Cho. 2007. Methylibium Aquaticum Sp Nov, a Betaproteobacterium Isolated from a Eutrophic Freshwater Pond. *International Journal of Systematic and Evolutionary Microbiology* 57(9): 2125–28.

Song Mengke, Chunling Luo, Longfei Jiang, Dayi Zhang, Yujie Wang, and Gan Zhang. 2015. Identification of Benzo [a] Pyrene-Metabolizing Bacteria in Forest Soils by Using DNA-Based Stable-Isotope Probing. *Applied Environmental Microbiology* 81(21): 7368–76.

Souchier Marine, Dalel Benali-Raclot, Claude Casellas, Valérie Ingrand, and Serge Chiron. 2016. Enantiomeric Fractionation as a Tool for Quantitative Assessment of Biodegradation: The Case of Metoprolol. *Water Research* 95: 19–26.

Stadler B Lauren, Jeseth Delgado Vela, Sunit Jain, Gregory J Dick, and Nancy G Love. 2018. Elucidating the Impact of Microbial Community Biodiversity on Pharmaceutical Biotransformation during Wastewater Treatment. *Microbial Biotechnology* 11(6): 995–1007.

Stams JM Alfons, Caroline M Plugge, Frank AM De Bok, BHGW Van Houten, Piet Lens, H Dijkman, and Jan Weijma. 2005. Metabolic Interactions in Methanogenic and Sulfate-Reducing Bioreactors. *Water Science and Technology* 52(1–2): 13–20.

Stegen C James, Tim Johnson, James K Fredrickson, Michael J Wilkins, Allan E Konopka, William C Nelson, Evan V Arntzen, William B Chrisler, Rosalie K Chu, and Sarah J Fansler. 2018. Influences of Organic Carbon Speciation on Hyporheic Corridor Biogeochemistry and Microbial Ecology. *Nature Communications* 9(1): 1–11.

Storey G Richard, Roberta R Fulthorpe, and Dudley D Williams. 1999. Perspectives and Predictions on the Microbial Ecology of the Hyporheic Zone. *Freshwater Biology* 41(1): 119–30.

Suarez Sonia, Juan M Lema, and Francisco Omil. 2010. Removal of Pharmaceutical and Personal Care Products (PPCPs) under Nitrifying and Denitrifying Conditions. *Water Research* 44(10): 3214–24.

Sundberg Carina, Waleed A Al-Soud, Madeleine Larsson, Erik Alm, Sepehr S Yekta, Bo H Svensson, Søren J Sørensen, and Anna Karlsson. 2013. 454 Pyrosequencing Analyses of Bacterial and Archaeal Richness in 21 Full-Scale Biogas Digesters. *FEMS Microbiology Ecology* 85(3): 612–26.

Svan Alfred, Mikael Hedeland, Torbjörn Arvidsson, Justin T. Jasper, David L. Sedlak, and Curt E. Pettersson. 2016. Identification of Transformation Products from β-Blocking Agents Formed in Wetland Microcosms Using LC-Q-ToF. *Journal of Mass Spectrometry* 51(3): 207–18.

T'Syen Jeroen, Raffaella Tassoni, Lars Hansen, Søren J Sorensen, Baptiste Leroy, Aswini Sekhar, Ruddy Wattiez, René De Mot, and Dirk Springael. 2015. Identification of the Amidase BbdA That Initiates Biodegradation of the Groundwater Micropollutant 2, 6-Dichlorobenzamide (BAM) in Aminobacter Sp MSH1. *Environmental Science & Technology* 49(19): 11703–13.

Tadkaew Nichanan, Faisal I Hai, James A McDonald, Stuart J Khan, and Long D Nghiem. 2011. Removal of Trace Organics by MBR Treatment: The Role of Molecular Properties. *Water Research* 45(8): 2439–51.

Takaichi Shinichi, Takashi Maoka, Kazuto Takasaki, and Satoshi Hanada. 2010. Carotenoids of Gemmatimonas Aurantiaca (Gemmatimonadetes): Identification of a Novel Carotenoid, Deoxyoscillol 2-Rhamnoside, and Proposed Biosynthetic Pathway of Oscillol 2,2′-Dirhamnoside. *Microbiology* 156(3): 757–63.

Táncsics András, Anna Róza Szalay, Milan Farkas, Tibor Benedek, Sándor Szoboszlay, István Szabó, and Tillmann Lueders. 2018. Stable Isotope Probing of

Hypoxic Toluene Degradation at the Siklós Aquifer Reveals Prominent Role of Rhodocyclaceae. *FEMS microbiology ecology* 94(6): fiy088.

Tay Stephen, Harold F Hemond, Martin F Polz, Colleen M Cavanaugh, and Lee R Krumholz. 1999. Importance of Xanthobacter Autotrophicus in Toluene Biodegradation within a Contaminated Stream. *Systematic and Applied Microbiology* 22(1): 113–18.

TeamR Core. 2013. R: A Language and Environment for Statistical Computing.

Thomas François, Jan Hendrik Hehemann, Etienne Rebuffet, Mirjam Czjzek, and Gurvan Michel. 2011. Environmental and Gut Bacteroidetes: The Food Connection. *Frontiers in Microbiology* 2: 1–16.

Tonina Daniele, and John M Buffington. 2009. Hyporheic Exchange in Mountain Rivers I: Mechanics and Environmental Effects. *Geography Compass* 3(3): 1063–86.

Tor M Jason, Caifen Xu, Joseph M Stucki, Michelle M Wander, and Gerald K Sims. 2000. Trifluralin Degradation under Microbiologically Induced Nitrate and Fe (III) Reducing Conditions. *Environmental Science & Technology* 34(15): 3148–52.

Tran N Han, Taro Urase, Huu Hao Ngo, Jiangyong Hu, and Say Leong Ong. 2013. Insight into Metabolic and Cometabolic Activities of Autotrophic and Heterotrophic Microorganisms in the Biodegradation of Emerging Trace Organic Contaminants. *Bioresource Technology* 146: 721–31.

Tran N Han, Martin Reinhard, and Karina Yew-Hoong Gin. 2018. Occurrence and Fate of Emerging Contaminants in Municipal Wastewater Treatment Plants from Different Geographical Regions-a Review. *Water Research* 133: 182–207.

Triska J Frank, Vance C Kennedy, Ronald J Avanzino, Gary W Zellweger, and Kenneth E Bencala. 1989. Retention and Transport of Nutrients in a Third-order Stream in Northwestern California: Hyporheic Processes. *Ecology* 70(6): 1893–1905.

Triska J Frank, John H Duff, and Ronald J Avanzino. 1993. Patterns of Hydrological Exchange and Nutrient Transformation in the Hyporheic Zone of a Gravel-bottom Stream: Examining Terrestrial—Aquatic Linkages. *Freshwater Biology* 29(2): 259–74.

Tülp C Holger, Kathrin Fenner, Rene P Schwarzenbach, and Kai-Uwe Goss. 2009. PH-Dependent Sorption of Acidic Organic Chemicals to Soil Organic Matter. *Environmental Science & Technology* 43(24): 9189–95.

Veetil GP Prajeesh, Anupama V Nadaraja, Arya Bhasi, Sudheer Khan, and Krishnakumar Bhaskaran. 2012. Degradation of Triclosan under Aerobic, Anoxic, and Anaerobic Conditions. *Applied Biochemistry and Biotechnology* 167(6): 1603–12.

Verlicchi Paola, and Elena Zambello. 2014. How Efficient Are Constructed Wetlands in Removing Pharmaceuticals from Untreated and Treated Urban Wastewaters? A Review. *Science of the Total Environment* 470: 1281–1306.

Vervier Philippe, Mike Dobson, and Gilles Pinay. 1993. Role of Interaction Zones between Surface and Ground Waters in DOC Transport and Processing: Considerations for River Restoration. *Freshwater Biology* 29(2): 275–84.

Vivas Astrid, Beatriz Moreno, Coral del Val, Cristina Macci, Grazia Masciandaro, and

Emilio Benitez. 2008. Metabolic and Bacterial Diversity in Soils Historically Contaminated by Heavy Metals and Hydrocarbons. *Journal of Environmental Monitoring* 10(11): 1287–96.

Vogel M Timothy, Craig S Criddle, and Perry L McCarty. 1987. ES&T Critical Reviews: Transformations of Halogenated Aliphatic Compounds. *Environmental Science & Technology* 21(8): 722–36.

Wang Liang, Shixue Zheng, Dan Wang, Lu Wang, and Gejiao Wang. 2014. Thermomonas Carbonis Sp Nov, Isolated from the Soil of a Coal Mine. *International Journal of Systematic and Evolutionary Microbiology* 64(11): 3631–35.

Ward S Adam. 2016. The Evolution and State of Interdisciplinary Hyporheic Research. *Wiley Interdisciplinary Reviews: Water* 3(1): 83–103.

Warnecke Falk, Rudolf Amann, and Jakob Pernthaler. 2004. Actinobacterial 16S RRNA Genes from Freshwater Habitats Cluster in Four Distinct Lineages. *Environmental Microbiology* 6(3): 242–53.

Weisburg William G, Susan M Barns, Dale A Pelletier, and David J Lane. 1991. 16S Ribosomal DNA Amplification for Phylogenetic Study. *Journal of Bacteriology* 173(2): 697–703.

Wellsbury Peter, Rodney A Herbert, and R John Parkes. 1996. Bacterial Activity and Production in Near-Surface Estuarine and Freshwater Sediments. *FEMS Microbiology Ecology* 19(3): 203–14.

White S David, Charles H Elzinga, and Susan P Hendricks. 1987. Temperature Patterns within the Hyporheic Zone of a Northern Michigan River. *Journal of the North American Benthological Society* 6(2): 85–91.

Wilhelm Linda, Gabriel A Singer, Christina Fasching, Tom J Battin, and Katharina Besemer. 2013. Microbial Biodiversity in Glacier-Fed Streams. *The ISME journal* 7(8): 1651–60.

Winkler Marcus, John R Lawrence, and Thomas R Neu. 2001. Selective Degradation of Ibuprofen and Clofibric Acid in Two Model River Biofilm Systems. *Water Research* 35(13): 3197–3205.

Wolff David, Daniel Krah, Andreas Dötsch, Ann Kathrin Ghattas, Arne Wick, and Thomas A. Ternes. 2018. Insights into the Variability of Microbial Community Composition and Micropollutant Degradation in Diverse Biological Wastewater Treatment Systems. *Water Research* 143: 313–24.

Writer Jeffrey H, Ronald C Antweiler, Imma Ferrer, Joseph N Ryan, and E Michael Thurman. 2013. In-Stream Attenuation of Neuro-Active Pharmaceuticals and Their Metabolites. *Environmental Science & Technology* 47(17): 9781–90.

Wroblicky J Gregory, Michael E Campana, H Maurice Valett, and Clifford N Dahm. 1998. Seasonal Variation in Surface-subsurface Water Exchange and Lateral Hyporheic Area of Two Stream-aquifer Systems. *Water Resources Research* 34(3): 317–28.

Wüst P Pia, Marcus A Horn, and Harold L Drake. 2009. Trophic Links between Fermenters and Methanogens in a Moderately Acidic Fen Soil. *Environmental*

Microbiology 11(6): 1395–1409.

Xu Jian, Laosheng Wu, and Andrew C Chang. 2009. Degradation and Adsorption of Selected Pharmaceuticals and Personal Care Products (PPCPs) in Agricultural Soils. *Chemosphere* 77(10): 1299–1305.

Xu Jinlan, Haixin Deng, Tinglin Huang, and Shaohua Song. 2014. Enhanced Biodegradation of Crude Oil in Contaminated Soil by Inoculation of Hydrocarbon-Degraders. *Desalination and Water Treatment* 52(25–27): 5126–35.

Xu Xingjian, Wenming Liu, Shuhua Tian, Wei Wang, Qige Qi, Pan Jiang, Xinmei Gao, Fengjiao Li, Haiyan Li, and Hongwen Yu. 2018. Petroleum Hydrocarbon-Degrading Bacteria for the Remediation of Oil Pollution Under Aerobic Conditions: A Perspective Analysis. *Frontiers in Microbiology* 9(December): 1–11.

Yagi Naomi, Harumi Kenmotsu, Hitoshi Sekikawa, and Masahiko Takada. 1991. Studies on the Photolysis and Hydrolysis of Furosemide in Aqueous Solution. *Chemical and Pharmaceutical Bulletin* 39(2): 454–57.

Yarza Pablo, Michael Richter, Jörg Peplies, Jean Euzeby, Rudolf Amann, Karl-Heinz Schleifer, Wolfgang Ludwig, Frank Oliver Glöckner, and Ramon Rosselló-Móra. 2008. The All-Species Living Tree Project: A 16S RRNA-Based Phylogenetic Tree of All Sequenced Type Strains. *Systematic and Applied Microbiology* 31(4): 241–50.

Ye Jian, George Coulouris, Irena Zaretskaya, Ioana Cutcutache, Steve Rozen, and Thomas L Madden. 2012. Primer-BLAST: A Tool to Design Target-Specific Primers for Polymerase Chain Reaction. *BMC Bioinformatics* 13(1): 134.

Yu C Chun, Ting C Chang, Chien S Liao, and Yi T Chang. 2019. A Comparison of the Microbial Community and Functional Genes Present in Free-Living and Soil Particle-Attached Bacteria from an Aerobic Bioslurry Reactor Treating High-Molecular-Weight PAHs. *Sustainability (Switzerland)* 11(4): 1–18.

Zarnetske P Jay, Roy Haggerty, Steven M Wondzell, and Michelle A Baker. 2011a. Dynamics of Nitrate Production and Removal as a Function of Residence Time in the Hyporheic Zone. *Journal of Geophysical Research: Biogeosciences* 116(G1).

Zarnetske P Jay, Roy Haggerty, Steven M Wondzell, Michelle A Baker. 2011b. Labile Dissolved Organic Carbon Supply Limits Hyporheic Denitrification. *Journal of Geophysical Research: Biogeosciences* 116(G4).

Zhang Bo, Quanwei Yu, Guoqi Yan, Hubo Zhu, Xiang yang Xu, and Liang Zhu. 2018. Seasonal Bacterial Community Succession in Four Typical Wastewater Treatment Plants: Correlations between Core Microbes and Process Performance. *Scientific Reports* 8(1): 1–11.

Zhang De Chao, Christoph Mörtelmaier, and Rosa Margesin. 2012. Characterization of the Bacterial Archaeal Diversity in Hydrocarbon-Contaminated Soil. *Science of the Total Environment* 421–422: 184–96.

Zhang Hui, Yuji Sekiguchi, Satoshi Hanada, Philip Hugenholtz, Hongik Kim, Yoichi Kamagata, and Kazunori Nakamura. 2003. Gemmatimonas Aurantiaca Gen Nov, Sp Nov, a Gram-Negative, Aerobic, Polyphosphate-Accumulating Micro-Organism, the First Cultured Representative of the New Bacterial Phylum Gemmatimonadetes Phyl Nov. *International Journal of Systematic and*

Evolutionary Microbiology 53(4): 1155–63.

Zhang Shuangfei, Zhong Hu, and Hui Wang. 2019. Metagenomic Analysis Exhibited the Co-Metabolism of Polycyclic Aromatic Hydrocarbons by Bacterial Community from Estuarine Sediment. *Environment International* 129: 308–19.

Zhang Shuying, Qingfeng Wang, and Shuguang Xie. 2012. Stable Isotope Probing Identifies Anthracene Degraders under Methanogenic Conditions. *Biodegradation* 23(2): 221–30.

Zhao Jianguo, Xiurong Chen, Linlin Bao, Zheng Bao, Yixuan He, Yuying Zhang, and Jiahui Li. 2016. Correlation between Microbial Diversity and Toxicity of Sludge Treating Synthetic Wastewater Containing 4-Chlorophenol in Sequencing Batch Reactors. *Chemosphere* 153: 138–45.

Żur Joanna, Artur Piński, Ariel Marchlewicz, Katarzyna Hupert-Kocurek, Danuta Wojcieszyńska, and Urszula Guzik. 2018. Organic Micropollutants Paracetamol and Ibuprofen—Toxicity, Biodegradation, and Genetic Background of Their Utilization by Bacteria. *Environmental Science and Pollution Research* 25(22): 21498–524.

Zwiener Christian, S Seeger, Thomas Glauner, and Fritz Frimmel. 2002. Metabolites from the Biodegradation of Pharmaceutical Residues of Ibuprofen in Biofilm Reactors and Batch Experiments. *Analytical and bioanalytical chemistry* 372(4): 569–75.

8. ACKNOWLEDGEMENTS

I wish to express my sincere gratitude to Prof. Dr. Marcus A. Horn, my supervisor, for the opportunity and guidance as I undertook this project.

Special thanks to my family, friends and colleagues from the HypoTRAIN Innovative Training Network, Department of Ecological Microbiology - University of Bayreuth and the Institute of Microbiology - Leibniz University Hannover for support.

Funding of the project by the European Union's Framework Programme for Research and Innovation Horizon 2020 through the Marie Sklodowska-Curie fellowship and the Leibniz University of Hannover is gratefully acknowledged.

All glory to the Almighty God.

9. PUBLICATIONS AND CONFERENCE PRESENTATIONS

Some of the data and textual content in this dissertation is from published articles and manuscripts listed below:

Rutere, C., Knoop, K., Posselt, M., Ho, A., and Horn, M. A. (2020). Ibuprofen degradation and associated bacterial communities in hyporheic zone sediments. *Microorganisms*, 8(8): 1245.

Rutere, C.*, Posselt, M.*, Mechelke, J.*, Coll, C., Jaeger, A., Raza, M., Meinikmann, K., Krause, S., Sobek, A., Lewandowski, J., Horn, M. A., Hollender, J., Benskin, J. P. (2020). Bacterial diversity controls transformation of wastewater-derived organic contaminants in river-simulating flumes. *Environmental Science & Technology*, 54(9): 5467-5479.

** shared first authorship*

Jaeger, A., Coll, C., Posselt, M., Mechelke, J., **Rutere, C**., Betterle, A., Raza, M., Mehrtens, A., Meinikmann, K., Portmann, A., Singh, T., Blaen, P., Krause, S., Horn, M. A., Hollender, J., Benskin, J.P, Sobek, A., Lewandowski, J. (2019). Using recirculating flumes and a response surface model to investigate the role of hyporheic exchange and bacterial diversity on micropollutant half-lives. *Environmental Science: Processes & Impacts*, 21(12): 2093-2108.

Lewandowski, J., Arnon, S., Banks, E., Batelaan, O., Betterle, A., Broecker, T., Coll, C., Drummond, J. D., Garcia, J. G., Galloway, J., Gomez-Velez, J., Grabowski, R. C., Herzog, S. P., Hinkelmann, R., Höhne, A., Hollender, J., Horn, M. A., Jaeger, A., Krause, S., Löchner Prats, A., Magliozzi, C., Meinikmann, K.,

Mojarrad, B. B., Mueller, B. M., Peralta-Maraver, I., Popp, A. L., Posselt, M., Putschew, A., Radke, M., Raza, M., Riml, J., Robertson, A., **Rutere, C**., Schaper, J. L., Schirmer, M., Schulz, H., Shanafield, M., Singh, T., Ward, A. S., Wolke, P., Wörman, A., Wu, L. (2019). Is the hyporheic zone relevant beyond the scientific community?, *Water*, 11 (11): 2230.

Manuscripts

Rutere, C., Posselt, M., Ho, A., and Horn, M.A. (2020). Bacterial communities associated with biodegradation of metoprolol in oxic and anoxic hyporheic zone sediments. *Applied Microbiology and Biotechnology*.

Rutere, C., Posselt, M., and Horn, M. A. (2020). Organic carbon content influence on the microbial and sorptive removal of organic micropollutants in hyporheic zone sediments. *Water*.

Manuscripts not related to this dissertation

Peralta-Maraver, I., Reiss, J., **Rutere, C**., Horn, M. A., and Robertson, A. (2020). Nutrients and predators control the biodegradation of emerging organic contaminants by bacteria.

Posselt, M., Schaper, J. L., Jaeger, A., **Rutere, C**., Mechelke, J., Kusebauch, B., Gergs, R., Portmann, A., Herzog, S., Galloway,J., Lewandowski, J., Hollender, J., Horn, M. A, and Benskin, J. P. (2020). Spatial and temporal variability of metformin transformation in a large-scale flume study.

Jaeger, A., Posselt, M., Schaper, J.L., Betterle, A., **Rutere, C**., Coll, C., Mechelke, J., Raza, M., Meinikmann, K., Portmann, A., Blaen, P.J., Krause, S., Horn, M.A., and Lewandowski, J. (2020). Transformation of organic micropollutants along horizontal hyporheic flowpaths in a river-simulating flume experiment.

Portmann, A., Posselt, M., Jaeger, A., Herzog, S., **Rutere**, C., Moradi, A., Abdi, A., Gergs, R., Higgins, C., McCray, J. (2020). Engineering hyporheic zones for the attenuation of metformin in urban waters.

Conference Presentations

Talks

Rutere, C., and Horn, M. A. (2018). Microbial Removal of Organic Micropollutants in the Hyporheic zone. *2nd European Hyporheic Forum*. London, UK.

Rutere, C., and Horn, M. A. (2018). Microbial removal of pharmaceutical residues in the hyporheic zone. *The joint conference of the 7th European Bioremediation Conference (EBC-VII) and the 11th International Society for Environmental Biotechnology Conference (ISEB).* Chania (Crete), Greece.

Peralta-Maraver, I., Reiss, J., **Rutere, C**., Horn, M. A., and Robertson, A. (2018). Mechanistic understanding of an ecosystem service: Efficiency of emergent pollutant biodegradation in the hyporheic zone. *2nd European Hyporheic Forum*. London, UK.

Posselt, M., Gergs, R., Jaeger, A., Schaper, J., **Rutere, C**., Galloway, J., Benskin, J. P. (2018).Transformation of the antidiabetic drug metformin in mesocosm and river systems. *2nd European Hyporheic Forum*. London, UK.

Portmann, A., Posselt, M., Jaeger, A., Herzog, S., **Rutere, C**., Moradi, A., Abdi, A., Gergs, R., Higgins, C., McCray, J. (2020). Engineering Hyporheic Zones for the Attenuation of Metformin in urban streams. *American Chemical Society Fall 2020 National Meeting & Expo*. San Franscisco, US.

Posters

Rutere, C., Muhammad, R., Posselt, M, Paramjothy, S., Mechelke, J., Jaeger, A. (2016). Occurence and fate of organic pollutants in River Erpe; A joint field study. *1st European Hyporheic Forum*. Berlin, Germany.

Rutere, C., Posselt, M., and Horn, M. A. (2017). Microbial degradation of Ibuprofen in the hyporheic zone of a lowland stream. *69th Annual Meeting of the German Society for Hygiene and Microbiology (DGHM) & Annual Meeting of the Association for General and Applied Microbiology (VAAM)*. Wurzbug, Germany.

Rutere, C., Posselt, M., and Horn, M. A. (2017). New microbes as causative agents of ibuprofen degradation capabilities in the hyporheic zone of a lowland stream. *European Geosciencies Union-General Assembly 2017*. Vienna, Austria.

Rutere, C., and Horn, M. A. (2017). Hyporheic zone: A harbor for novel bacterial micropollutant degraders.*7th Congress of European Microbiologists (FEMS).* Valencia, Spain.

Rutere, C., Posselt, M., Ho, A., and Horn, M.A. (2018). Effect of oxygen on microbial removal of metoprolol in the hyporheic zone. *17th International Symposium on Microbial Ecology (ISME)*. Leipzig, Germany.

Posselt, M., Coll, C., Mechelke, J., Jaeger, A., **Rutere, C**.*, Raza, M., Betterle, A., Singh, T., Krause, S., Hollender, J., Sobek, A., Lewandowski, J., Horn, M. A., Meinikmann, K., Benskin, J. P. (2019). Impacts of Bacterial Diversity and Hyporheic Exchange Flows on the Fate of Wastewater-derived Polar Organic Micropollutants: A Central Composite Face Designed Flume Study. *29th Annual Meeting of the Society of Environmental Toxicology and Chemistry (SETAC).* Helsinki, Finland.

Coll, C., Posselt, M., **Rutere, C**., Jaeger, A., Mechelke, J., Benskin, J.P., Lewandowski, J., Hollender, J., Sobek, A. (2020). Dissipation of acesulfame and carbamazepine in recirculating flumes and bottle incubations with different levels of bacterial diversity. *30th Annual Meeting of the Society of Environmental Toxicology and Chemistry (SETAC).* Dublin, Ireland.

Posselt, M., Schaper, J., Jaeger, A., **Rutere, C**., Kusebauch, B., Portman, A., Herzog, H., Gergs, R., Mechelke, J., Li, Z., Lewandowski, J., Benskin, J.P. (2020). Spatial and Temporal Variability of Metformin Transformation in a Flume Study. 30*th Annual Meeting of the Society of Environmental Toxicology and Chemistry (SETAC).* Dublin, Ireland.

10. APPENDIX

Table A1. Classification of bacterial OTUs enriched by ibuprofen relative to unamended controls sampled at the same time point, and closest cultured relatives of OTU representative 16S rRNA gene sequences. Significant (p-adj < 0.05) Log2-fold change > 0 are reported as determined by Deseq2. IBU40 and IBU400, ibuprofen amendment with 40 and 400 µM ibuprofen, respectively. IBA40 and IBA400, ibuprofen amendment with 40 and 400 µM ibuprofen, respectively, together with 1 mM acetate.Table used with permission from Rutere *et al.* (2020).

Phylum/Subphylum-level	Genus-level (OTU No.)	Closest cultured relative	Acc. No. [a]	[%] [b]	Log2-fold change									
					16S rRNA genes					16S RNA				
					- Acetate			+ Acetate		- Acetate			+ Acetate	
					IBU40	IBU400		IBA40	IBA400	IBU40	IBU400		IBA40	IBA400
Acidobacteria	*Bryobacter* (144)	*Bryobacter aggregatus*	AM 887762	92	2.1	-- [c]		--	--	2.1	2.3		1.8	--
	Bryobacter (61)*d	*Paludibaculum fermentans*	NR_134120	93	--	--		--	--	1	2.0		1.8	1.4
	Bryobacter (115)	*Bryobacter aggregatus*	AM887762	90	--	--		--	--	2.1	--		1.5	--
	Bryobacter (562)	*Bryobacter aggregatus*	AM887762	90	--	--		--	--	--	2.5		--	2.5
	Uncultured subgroup_3 (901)	*Paludibaculum fermentans*	NR_134120	93	--	--		--	--	--	3.3		2.7	3.8
	Uncultured subgroup_3 (55)	*Paludibaculum fermentans*	NR_134120	94	--	--		--	--	--	1.5		--	3.3
	Uncultured subgroup_3 (516)	*Paludibaculum fermentans*	NR_134120	93	--	--		--	--	--	2.2		--	1.5
	Blastocatella (126)	*Blastocatella fastidiosa*	NR_118350	95	1.3	--		--	--	--	--		--	--
	Uncultured subgroup_6 (85)	*Vicinamibacter silvestris*	CP011998	87	3.9	--		2.6	--	--	4.4		--	--
	Uncultured subgroup_6 (10)	*Vicinamibacter silvestris*	NR_151905	92	1.9	--		--	--	2.6	2.1		--	--
	Uncultured subgroup_6 (212)	*Vicinamibacter silvestris*	NR_151905	90	--	--		--	--	3.6	3.7		3	2.5
	Uncultured subgroup_6 (304)	*Luteitalea pratensis*	NR_156918	91	2.6	--		--	--	2.9	--		--	--

	Uncultured subgroup_6 (401)	*Luteitalea pratensis*	NR_156918	93	--	--		--	--		2.8	2.9		--	--
	Uncultured subgroup_6 (581)	*Vicinamibacter silvestris*	NR_151905	93	--	--		--	--		--	2.9		--	2.7
	Uncultured subgroup_6 (412)	*Vicinamibacter silvestris*	NR_151905	91	--	--		--	--		3.1	2.7		--	--
	Uncultured subgroup_6 (147)*	*Ralstonia solanacearum*	CP011998	90	1.9	2.0		--	--		--	--		--	--
	Uncultured subgroup_6 (85)*	*Ralstonia solanacearum*	CP011998	90	--	--		--	--		--	4.4		--	--
	Uncultured subgroup_17 (39)	*Vicinamibacter silvestris*	NR_151905	88	3.1	2.2		2.6	1.7		1.7	2		1.6	--
	Uncultured subgroup_22 (329)	*Anaeromyxobacter dehalogenans*	NR_074927	86	3.3	--		--	--		4.4	2.8		3.9	--
	Uncultured subgroup_22 (340)	*Thermaerobacter marianensis*	NR_074944	86	--	--		--	--		3.1	--		--	2
	Uncultured subgroup_22 (57)	*Vicinamibacter silvestris*	NR_151905	85	1.8	2		--	--		2.2	3.2		2.6	2.2
Actinobacteria	Uncultured Sva0996_marine_group (83)	*Acidimicrobium ferrooxidans*	NR_074390	92	2.1	--		--	--		2.6	--		2.2	2
	Aeromicrobium (332)	*Aeromicrobium panaciterrae*	NR_041382	100	4	--		--	--		--	--		--	--
	Marmoricola (69)	*Marmoricola pocheonensis*	NR_108597	99	1.9	--		--	--		--	--		--	--
	Nocardioides (372)	*Nocardioides intraradicalis*	NR_152019	97	2.6	2.9		2.5	--		--	--		--	--
	Nocardioides (210)	*Nocardioides sediminis*	NR_044228	100	1.9	--		--	--		2.9	--		--	--
	Nocardioides (102)	*Nocardioides islandensis*	NR_044235	96	--	1.7		1.6	1.8		--	--		--	--
	Uncultured MB-A2-108 (94)	*Kitasatospora kazusensis*	NR_041539	92	--	--		--	--		--	3.7		3.3	2.9

	Iamia (188)	*Aquihabitans daechungensis*	NR_132289	99	--	2.7		2.8	2.9		2.5	3.7		3	3.7
	Iamia (362)	*Iamia majanohamensis*	NR_041634	94	--	--		--	--		3.3	--		--	--
	Uncultured Acidimicrobiales (1265)	*Aciditerrimonas ferrireducens*	NR_112972	94	--	--		--	4.2		--	--		--	4.8
	Uncultured 480-2(627)	*Solirubrobacter phytolaccae*	NR_133858	90	--	--		--	--		3.6	--		3.5	--
	Solirubrobacter (29)	*Solirubrobacter ginsenosidimutans*	NR_108192	99	--	--		--	--		2.8	--		--	--
	Sva0996_marine_group(441)	*Acidimicrobium ferrooxidans*	NR_074390	91	--	--		--	--		2.9	--		--	--
	Flavobacterium (633)	*Flavobacterium cheniae*	NR_044198	97	--	5.3		5.4	6.7		--	--		--	--
	Flavobacterium (2394)	*Flavobacterium cheonhonense*	NR_125552	100	--	4.9		--	4.7		--	--		--	--
	Uncultured NS9_marine_group (438)	*Vicingus serpentipes*	NR_159281	87	--	3.1		--	3.6		--	--		--	4.1
	Uncultured NS9_marine_group (277)	*Phaeocystidibacter marisrubri*	NR_136475	86	--	3.2		--	3.6		--	3.1		--	3.5
	Rhodococcus (459)	*Rhodococcus koreensis*	LT838098	100	--	4.4		--	4.5		4.3	4.3		3.7	5.4
	Fodinicola (15)	*Streptomyces aomiensis*	NR_112998	97	--	1.4		--	1		1.3	1.8		1.8	1.6

	Nocardioides (405)	*Nocardioides opuntiae*	NR_133796	97	--	3.9		3.8	3.4		--	--		--	--
	Uncultured Acidimicrobiales (612)	*Ilumatobacter nonamiensis*	NR_112713	92	--	--		4.1	--		--	--		3.7	3.7
	Uncultured Actinobacteria (359)	*Longivirga aurantiaca*	NR_159886	91	--	2.8		--	2.9		--	--		--	--
	Uncultured MB-A2-108 (137)	*Streptacidiphilus hamsterleyensis*	NR_133867	90	1.7	1.8		--	--		3.3	4		3.2	--
	CL500-29_marine_group (28)	*Ilumatobacter nonamiensis*	NR_112713	92	--	--		--	2.2		--	--		1.9	2.1
	Uncultured Acidimicrobiales (569)	*Aciditerrimonas ferrireducens*	NR_112972	94	--	--		--	--		--	--		3.2	3.5
	Uncultured intrasporangiaceae (19)*	*Knoellia flava*	MG205530	99	--	--		1.3	1.3		--	--		--	--
	Gaiella (45)*	*Gaiella occulta*	NR_118138	97	--	--		--	--		1.7	--		--	--
Armatimonadetes	Uncultured Armatimonadetes (371)	*Fimbriimonas ginsengisoli*	NR_121726	88	4.7	--		--	--		--	--		--	--
Bacteroidetes	*Chryseolinea* (165)	*Chryseolinea serpens*	NR_108511	96	4.3	4		5	4.4		--	3.4		3.6	--
	Chryseolinea (483)	*Chryseolinea serpens*	NR_108511	93	3.4	4.1		4.4	--		--	--		--	--
	Chryseolinea (231)	*Chryseolinea serpens*	NR_108511	92	2.6	2.9		3.3	2.5		--	--		--	--
	Chryseolinea (1195)				3.8	--		4.1	--		--	--		--	--
	Uncultured Rhodothermaceae (363)	*Natronotalea proteilytica*	NR_158101	88	4.5	--		--	--		5.1	--		--	--
	Ferruginibacter (499)	*Ferruginibacter lapsinanis*	NR_044589	96	3.9	5.5		5.4	6.9		--	--		--	--

	Ferruginibacter (378)	*Ferruginibacter yonginensis*	NR_133743	96	--	3.1		--	--		--	--		--	--
	Flavobacterium (2394)	*Flavobacterium cheonhonense*	NR_125552	100	--	6.5		--	--		--	--		--	--
	Flavobacterium (376)	*Flavobacterium inkyongense*	NR_156036	99	4.9	--		--	5.6		--	--		--	--
	Uncultured Cytophagaceae (451)	*Chryseolinea serpens*	NR_108511	91	4.4	--		4.5	--		--	--		--	--
	Ferruginibacter (256)	*Ferruginibacter alkalilentus*	NR_044588	97	2.5	2.6		3	3.1		--	--		--	--
	Uncultured Saprospiraceae (380)	*Phaeodactylibacter luteus*	NR_136808	88	--	2.9		--	3.2		--	2.3		--	--
	Uncultured Saprospiraceae (383)	*Portibacter lacus*	NR_113569	90	4.4	3.7		--	3.8		--	--		--	--
	Uncultured Saprospiraceae (472)	*Phaeodactylibacter xiamenensis*	NR_134132	88	--	4.5		3.6	3.9		--	--		--	--
	Uncultured Sphingobacteriales (711)	*Ferruginibacter profundus*	NR_148259	90	--	5.9		4.7	6.5		--	--		--	--
	Uncultured env.OPS_17 (726)	*Lentimicrobium saccharophilum*	NR_149795	87	--	6.6		--	7		--	--		--	5.7
	Uncultured env.OPS_17 (876)	*Mucilaginibacter terrae*	NR_158094	85	--	5.7		5.1	--		--	--		--	--
	Uncultured env.OPS_17 (548)	*Anseongella ginsenosidimutans*	NR_148803	85	4.1	--		--	--		4.3	--		--	--
	Uncultured KD3-93 (46)	*Geofilum rhodophaeum*	NR_158091	89	--	7.5		--	--		--	7.8		--	5.4
	Uncultured NS11-12_marine_group (616)	*Ekhidna lutea*	NR_115061	89	--	5.3		4	4.9		--	--		--	--
	PHOS-HE51 (1186)	*Owenweeksia hongkongensis*	NR_074100	88	--	5		--	5.3		--	--		--	--

	Uncultured Sphingobacteriales (409)	*Ferruginibacter profundus*	NR_148259	88	3.7	--		2.8	--		5.1	--		--	--
	Terrimonas (139)	*Terrimonas lutea*	NR_041250	98	2.7	3.5		4.3	4.6		--	--		--	--
	Terrimonas (149)	*Terrimonas soli*	NR_159891	98	--	--		4.2	4.3		--	--		--	--
	Terrimonas (253)	*Terrimonas arctica*	NR_134213	98	--	2.4		2.7	2.4		--	--		--	--
					--	--		--	--						
Cand_div_BRC1	Uncultured Candidate_div_BRC1 (542)	*Desulfomonile limimaris*	NR_025079	81	--	--		--	--		6.4	--		--	--
	Uncultured Candidate_div_BRC1 (1346)	*Desulfosalsimonas propionicica*	NR_115678	80	--	--		--	--		5.5	--		--	--
Gemmatimonadetes	Uncultured Gemmatimonadaceae (124)	*Gemmatimonas phototrophica*	NR_136770	91	3	3.9		3.8	3.8		4.3	4.6		4.4	3.7
	Uncultured Gemmatimonadaceae (32)	*Gemmatimonas phototrophica*	NR_136770	86	2.8	1.7		1.5	1.5		3.3	3.2		2.6	2.1
	Uncultured Gemmatimonadaceae (52)	*Gemmatimonas phototrophica*	NR_136770	85	2.2	--		--	--		2.9	2.7		2.2	1.8
	Uncultured Gemmatimonadaceae (251)	*Gemmatimonas aurantiaca*	NR_074708	85	4.3	4		--	--		3.9	4.5		3.2	2.7
	Uncultured Gemmatimonadaceae (269)	*Gemmatimonas phototrophica*	NR_136770	91	3	--		--	3.3		5	5.6		5.2	4.6
	Uncultured Gemmatimonadaceae (299)	*Gemmatimonas aurantiaca*	NR_074708	85	2.5	--		--	--		3.5	--		2.8	2.6
	Uncultured Gemmatimonadaceae (388)	*Gemmatirosa kalamazoonesis*	NR_132675	89	--	--		--	--		3	2.7		2.3	--

Chlorobi	Uncultured BSV26 (580)	*Ignavibacterium album*	NR_074698	86	4.6	--		--	--		--	--		--	--
	Uncultured BSV26 (93)	*Ignavibacterium album*	NR_074698	82	--	2.1		2.6	2		--	--		2.7	2.5
	Uncultured BSV26 (413)	*Ignavibacterium album*	NR_074698	82	--	4.2		3.6	3.9		--	--		--	--
	Uncultured OPB56 (740)	*Hippea maritima*	NR_119289	81	--	--		--	4.9		--	4.9		4.5	5.2
	Uncultured SJA-28 (284)	*Melioribacter roseus*	NR_074796	83	1.9	--		--	--		--	--		--	--
Chloroflexi	Uncultured Caldilineaceae (110)	*Litorilinea aerophila*	NR_132330	88	--	--		--	--		3.5	--		--	--
	Uncultured KD4-96 (27)	*Dehalogenimonas alkenigignens*	NR_109657	86	1.5	--		--	--		1.6	1.8		--	--
	Uncultured Anaerolineaceae (233)	*Thermanaerothrix daxensis*	NR_117865	88	2.7	--		--	--		3.9	--		2.8	2.5
	Uncultured Anaerolineaceae (611)	*Thermomicrobium roseum*	NR_044678	84	4.3	--		4.8	4.8		4.5	--		3.9	--
	Uncultured Anaerolineaceae (628)	*Bellilinea caldifistulae*	NR_041354	84	3.4	--		--	--		3.1	--		--	--
	Unclassified Gitt-GS-136 (127)	*Hydrogenispora ethanolica*	NR_125455	85	1.8	--		--	--		2.4	--		--	--
	Uncultured KD4-96 (96)	*Hydrogenispora ethanolica*	NR_125455	85	1.6	--		--	--		2.3	2.1		--	--
	Unclassified JG30-KF-CM45 (145)	*Sphaerobacter thermophilus*	NR_074379	88	2.1	2		--	2.2		2.8	--		--	--
	Uncultured KD4-96* (8)	*Dehalogenimonas lykanthroporepellens*	NR_074337	86	--	--		--	--		--	1.5		--	--

	Uncultured KD4-96* (16)	*Dehalogenimonas alkenigignens*	JQ994267	86	--	--		--	--		1.2	1.3		--	1.3
Latescibacteria	Uncultured Latescibacteria (95)	*Desulfonatronum thiosulfatophilum*	NR_116694	81	1.8	2.3		--	--		5	4.6		4.1	3.3
	Uncultured Latescibacteria (154)	*Acidicapsa acidisoli*	NR_148580	88	--	4.6		4.8	4.3		4.8	5.4		4.8	4.3
	Uncultured Latescibacteria (308)	*Syntrophorhabdus aromaticivorans*	NR_041306	84	2.6	--		--	--		2.6	--		--	--
	Uncultured Latescibacteria (326)	*Desulfopila inferna*	NR_115066	83	--	--		--	--		4.2	4.1		3.9	3.3
	Uncultured Latescibacteria (342)	*Desulfobulbus mediterraneus*	NR_025150	84	--	--		--	--		2.1	--		2.3	--
	Uncultured Latescibacteria (453)	*Desulfobulbus oligotrophicus*	NR_156089	85	--	--		--	--		3	2.8		2.4	--
	Uncultured Latescibacteria (503)	*Pseudomaricurvus alkylphenolicus*	NR_114390	81	--	--		--	--		3.9	4.2		4	3.5
	Uncultured Latescibacteria (534)	*Thermoanaerobaculum aquaticum*	NR_109681	83	--	--		--	--		4.4	--		3	--
	Uncultured Latescibacteria (706)	*Desulfotalea psychrophila*	NR_028729	83	--	--		--	--		3.1	3.8		3.6	3.3
	Uncultured Latescibacteria (732)	*Syntrophus gentianae*	NR_029295	82	--	--		--	--		4.3	3.9		4.5	3.9
	Uncultured Latescibacteria (864)	*Desulfobulbus oligotrophicus*	NR_156089	85	--	--		--	--		4.1	3.6		3.9	
	Uncultured Latescibacteria (422)	*Desulfotalea psychrophile*	NR_028729	82	--	--		--	--		3.7	3.9		3.2	3.2
	Uncultured Latescibacteria (1054)	*Desulfotalea psychrophila*	NR_028729	83	--	--		--	--		5.5	--		--	--
Nitrospirae	*Nitrospira* (7)	*Nitrospira moscoviensis*	NR_029287	98	1.4	2.7		1.9	2.4		1.4	2		--	1.6

	Nitrospira (23)	*Nitrospira moscoviensis*	NR_029287	94	--	2.3		2.3	2.1		1.6	--		--	--
	Nitrospira (26)	*Nitrospira lenta*	NR_148573	100	--	--		2.4	2.4		--	--		--	--
Proteobacteria															
Alphaproteobacteria	*Sphingobium* (17)	*Sphingobium czechense*	NR_118306	99	3.7	--		--	--		--	--		--	5.4
	Hyphomicrobium (60)	*Hyphomicrobium facile*	NR_027610	98	1.6	1.8		--	2		--	--		--	--
	Hyphomicrobium (347)	*Hyphomicrobium facile*	NR_027610	96	--	--		--	--		5.2	4.8		4	4.9
	Hirschia (62)	*Asprobacter aquaticus*	NR_159164		2.4	2.9		2.1	2.5		--	--		--	--
	Novosphingobium (64)	*Novosphingobium fuchskuhlense*	NR_118270	99	6.1	--		6.1	3.3		4.4	--		4.3	--
	Pedomicrobium (84)	*Pedomicrobium manganicum*	NR_104841	96	1.7	1.8		--	2		--	--		--	2.3
	Uncultured Rhizobiales (335)	*Blastochloris viridis*	NR_117911	95	2.1	2.6		--	2.9		--	--		--	--
	Defluviimonas (202)	*Defluviimonas aestuarii*	NR_118305	98	2.2	2.8		2.8	2.6		--	--		--	--
	Hyphomicrobium (129)	*Hyphomicrobium aestuarii*	NR_104954	96	2.1	--		--	--		2.5	--		--	1.7
	Uncultured AKYH478 (645)	*Lacibacterium aquatile*	NR_125556	94	--	--		--	--		--	5		--	--
	Uncultured F0723 (1059)	*Phreatobacter stygius*	NR_158009	98	--	--		--	--		--	6.2		--	--
	Uncultured MNG7 (35)	*Nordella oligomobilis*	NR_114615	96		2.2		2	2.3		--	--		--	--
	Uncultured Phyllobacteriaceae (87)	*Carbophilus carboxidus*	NR_104931	91	--	--		5.9	--		--	3.4		--	--
	Uncultured Sphingomonadaceae (1)	*Novosphingobium chloroacetimidivorans*	NR_134105	99	--	--		4.6	6		--	5.1		3.3	6.1
	Uncultured Sphingomonadaceae (119)	*Sphingorhabdus wooponensis*	NR_109148	99	3.7	4.7		5.2	4.4		--	--		--	--
	Sphingopyxis (553)	*Sphingopyxis fribergensis*	NR_137271	100	--	4		4.2	5		--	--		--	--
	Woodsholea (181)	*Aquidulcibacter paucihalophilus*	NR_156862	91	5.2	5.4		5.4	6.1		2.9	--		--	2.3
	Woodsholea (183)	*Roseitalea porphyridii*	NR_156092	91	3	3.2		3.3	3.6		--	--		--	--

	Woodsholea (615)				--	3.2		--	3.1		--	--		--	--
	Uncultured Rhizobiaceae (100)	*Rhizobium azooxidifex*	NR_144599	99	--	3.5		3	2.7		--	--		--	--
	Uncultured AKYH478 (645)	*Lacibacterium aquatile*	NR_125556	94	--	4		--	4.2		--	4.9		--	--
	Defluviimonas (202)*	*Defluviimonas aestuarii*	NR_118305	99	2.2	2.8		2.8	2.6		--	--		--	--
Deltaproteobacteria	*Bdellovibrio* (63)	*Bdellovibrio exovorus*	NR_102876	98	4.7	--		6.9	--		5.6	7.9		6.6	--
	Haliangium (479)	*Haliangium tepidum*	NR_024781	91	--	--		--	--		3.9	--		4	3.3
	Haliangium (248)	*Kofleria flava*	NR_041981	92	5	--		--	--		6.2	--		3.3	--
	Haliangium (457)	*Kofleria flava*	NR_041981	93	3.9	--		--	--		5	3.7		4.4	4.7
	Haliangium (739)	*Kofleria flava*	NR_041981	90	--	--		--	--		3.8	4		4.1	4.6
	OM27-Clade (166)	*Rhodomicrobium vannielii*	NR_074186	97	--	6.3		4.6	--		--	4.6		--	6.4
	Anaeromyxobacter (220)	*Anaeromyxobacter dehalogenans*	NR_074927	92	--	--		3.2	--		1.9	1.6		1.5	--
	Anaeromyxobacter (82)*	*Anaeromyxobacter dehalogenans*	FJ190057	95	--	--		--	--		1.2	1.6		--	--
	Sandaracinus (260)	*Sandaracinus amylolyticus*	NR_118001	94	--	--		--	--		7.8	--		7.1	--
	Sandaracinus (382)	*Sandaracinus amylolyticus*	NR_118001	95	--	--		--	4.8		--	3.4		5.6	5
	Sorangium (709)	*Chondromyces lanuginosus*	NR_025345	95	--	--		--	--		4.9	3.6		4.5	4.9
	Sorangium (1348)	*Labilithrix luteola*	NR_126182	95	--	--		--	--		6.1	--		6.4	--
	Sorangium (352)	*Labilithrix luteola*	NR_126182	96	--	--		3.4	--		--	3.2		--	--
	Uncultured Cystobacteraceae (203)	*Vitiosangium cumulatum*	NR_156939	94	--	--		3.9	4.6		--	2.5		--	2.6
	Uncultured Sandaracinaceae (33)	*Sandaracinus amylolyticus*	NR_118001	91	6.3	5.8		6.8	6.5		8.3	6.6		8.4	7.8

	Uncultured Sandaracinaceae (404)	*Sandaracinus amylolyticus*	NR_118001	92	--	--		--	--		4.2	--		5.9	4.4
	Uncultured Sandaracinaceae (686)	*Sandaracinus amylolyticus*	NR_118001	89	--	--		--	--		--	3.7		3.9	4.8
	Uncultured Sandaracinaceae (240)	*Sandaracinus amylolyticus*	NR_118001	90	4.3	5.5		4.3	6		5.2	4.3		4.6	4.8
	Uncultured Sandaracinaceae (764)	*Sandaracinus amylolyticus*	NR_118001	88	--	--		--	--		6.2	--		6	--
	Uncultured Sh765B-TzT-29 (414)	*Desulfonatronum parangueonense*	NR_159236	91	--	--		--	--		4.1	--		3.9	4.3
	Uncultured δ-bacteria (105)	*Anaeromyxobacter dehalogenans*	NR_074927	89	--	--		5.5	--		--	7.5		--	--
	Uncultured δ-bacteria (54)	*Phaselicystis flava*	NR_044523	89	--	--		--	--		5.0	5.0		--	4.5
	Phaselicystis (163)*	*Jahnella thaxteri*	NR_117461	95	--	--		--	--		--	--		--	8.2
Gammaproteobacteria (Betaproteobacterales)	*Hydrogenophaga* (9)	*Hydrogenophaga defluvii*	NR_029024	99	4.2	4.2		4.3	5.8		6	4.8		5.5	6.7
	Leeia (513)	*Annwoodia aquaesulis*	NR_044793	98	--	5		--	--			--		2.1	--
	Piscinibacter (14)	*Piscinibacter aquaticus*	NR_043921	99	2.5	3.5		3.1	3.5		3.7	2.3		2.4	2.8
	Rhizobacter (123)	*Rhizobacter profundi*	NR_149234	98	--	5.7		--	5.3		3	4.4		2.9	4.7
	Uncultured Comamonadaceae (4)	*Kinneretia asaccharophila*	NR_115151	99	1.4	2.6		2.3	3		2.2	1.8		1.8	2.7
	Uncultured Comamonadaceae (36)	*Azohydromonas lata*	NR_114103	98	3.1	4		3.4	4.1		4.6	4.3		3.3	4.4
	Uncultured Comamonadaceae (113)	*Variovorax boronicumulans*	NR_114214	98	3.1	--		4.4	5.8		--	--		--	--
	Uncultured Comamonadaceae (152)	*Azohydromonas lata*	NR_114103	98	--	--		--	--		2.9	2.5		2.1	2.8
	Uncultured Comamonadaceae (1113)	*Rhodoferax antarcticus*	NR_104835	97	3.8	--		--	5.1		--	4		--	4.1

	Uncultured Comamonadaceae (12)*	*Aquincola tertiaricarbonis*	MH844953	99	--	1.3		--	1.6		--	1.0		--	1.0
	Azohydromonas (43)	*Zhizhongheella caldifontis*	NR_134232	98	--	2.7		--	3.1		1.8	2.1		1.9	2.8
	Uncultured Gallionellaceae (320)	*Sideroxydans lithotrophicus*	NR_074731	95	--	2.4		2.4	2.2		--	--		--	--
	Uncultured Nitrosomonadaceae (20)	*Collimonas fungivorans*	NR_028007	93	--	1.8		1.3	2		--	--		--	--
	Uncultured Nitrosomonadaceae (350)	*Herbaspirillum chlorophenolicum*	NR_114143	91	--	3.7		2.8	3.8		--	--		--	--
	Uncultured Nitrosomonadaceae (92)*	*Nitrosospira multiformis*	NR_074736	92	--	--		1.1	--		--	--		--	--
	Uncultured Oxalobacteraceae (215)	*Herbaspirillum autotrophicum*	NR_113747	98	--	4		5.8	6.1		--	--		5.4	5.1
	Vogesella (44)	*Vogesella indigofera*	NR_040800	100	--	--		4.7	5.7		--	--		3.5	4.3
	Dechloromonas (138)	*Dechloromonas hortensis*	NR_042819	98	--	--		3.1	3.3		--	--			1.9
	Thauera (40)	*Thauera humireducens*	NR_109534	99	--	--			5.3		--	--		2.7	4.8
	Uncultured SC-I-84 (89)	*Robbsia andropogonis*	NR_104960	91	--	--			1.4		--	2.7		2.3	3.4
	Uncultured SC-I-84 (354)	*Tepidimonas thermarum*	NR_042418	91	--	--			2		--	--		--	4.1
	Uncultured β-proteobacteria (66)	*Derxia gummosa*	NR_114127	93	--	--			2		--	--		--	2.6
	Zoogloea (266)*	*Zoogloea ramigera*	MK138653	100	--	--		--	--		--	--		--	3.1
	Acidiferrobacter (67)	*Sulfuricaulis limicola*	NR_147747	93		1.8		1.4	1.4		--	--		--	--

	Arenimonas (520)	*Arenimonas subflava*	NR_135888	97	5.3	--		4.7	4.7		4.5	4.7		4.1	4.1
	Arenimonas (357)	*Arenimonas subflava*	NR_135888	99		5.6		4.4	--		4.8	--		3.9	4.5
	Pseudomonas (24)	*Pseudomonas migulae*	NR_114223	99	4.5	6.2		6.8	--		3	3.1		4.6	5.4
	Unclutured Pseudomonadaceae (3)*	*Pseudomonas linyingensis*	MG576046	100	--	--		5.0	6.6		--	--		3.4	7.8
	Thermomonas (58)	*Thermomonas carbonis*	NR_134219	97	2.5	3.6		3.4	4		--	--		--	--
	Uncultured Xanthomonadaceae (70)	*Dyella marensis*	NR_042691	94	--	--		2.8	1.8		--	--		--	--
	Uncultured γ-proteobacteria (452)	*Permianibacter aggregans*	NR_134131	96	--	4.7		4.2	4.5		4.5	4.4		5.6	3.9
	Uncultured γ-proteobacteria (541)	*Permianibacter aggregans*	NR_134131	93	--	--		5.3	--		5.1	--		5.9	--
	Uncultured γ-proteobacteria (505)	*Steroidobacter denitrificans*	NR_044309	90	--	4.4		3.4	3.7		--	--		--	--
	Uncultured γ-proteobacteria (715)	*Pseudomonas reidholzensis*	NR_157777	91	6.3	--		--	5.1			4.4		5.2	4.7
	Uncultured γ-proteobacteria (1758)	*Sulfuriflexus mobilis*	NR_152000	90	6.3	--		--	--		--	--		--	--
	Acidiferrobacter (196)	*Acidiferrobacter thiooxydans*	NR_114629	90	1.6	2		--	1.7		--	--		--	--
Saccharibacteria	Uncultured Saccharibacteria (980)	*Alkaliphilus metalliredigens*	NR_074633	81	4.1	--		4.9	--		--	--		--	--
					--	--		--	--		--	--		--	--
Verrucomicrobia	*Prosthecobacter* (162)	*Prosthecobacter vanneervenii*	NR_026022	97	3.5	6.8		--	6		--	3.8		--	2.9
	Verrucomicrobium (903)	*Verrucomicrobium spinosum*	NR_026266	87	--	4.3		--	--		--	3.8		--	--
	Uncultured DEV007 (1517)	*Roseibacillus ponti*	NR_041622	88	--	--		5.5			--	--		--	--

Unclassified	Uncultured bacterium (315)*	*Thiomonas islandica*	NR_116394	80	6.5	--		5.1	--		--	--		--	--
	Uncultured bacterium (255)*	*Negadavirga shengliensis*	NR_136439	81	--	--		--	--		4.1	6.2		--	3.7

[a] Gene bank accession number.

[b] Similarity of OTU representative 16S rRNA gene sequence to that of closest cultured relative.

[c] Non-significant differential abundance between treatment and unamended controls.

[d] Significant (p-adj < 0.1) Log2-fold change > 0 are reported as determined by Deseq2.

Table A2. Relative abundance of bacterial OTUs from the original microbial community enriched by 40 and 400 µM ibuprofen treatments at DNA and RNA levels under oxic conditions after incubation. 0, represents unamended samples and 40 and 400 correspond to samples amended with 40 and 400 µM ibuprofen, respectively. 0', 3', and 5' correspond to samples obtained at the start of the incubation, and after the third and fifth refeeding, respectively. Data represents the mean of triplicate samples in % of total rarified reads (uniform sequencing depth of 10,767 per sample) ± standard error of mean (SEM). Table used with permission from Rutere *et al.* (2020).

Phylum/Subphylum-level	Genus-level (OTU No.)	**DNA**						
		0_0'	0_3'	0_5'	40_3'	40_5'	400_3'	400_5'
Acidobacteria	*Bryobacter* (144)	0.28 ± 0.05	0.04 ± 0.00	0.12 ± 0.02	0.15 ± 0.02	0.17 ± 0.02	0.10 ± 0.02	0.09 ± 0.03
	Bryobacter (61)	0.07 ± 0.03	0.05 ± 0.00	0.11 ± 0.01	0.1 ± 0.02	0.09 ± 0.00	0.12 ± 0.01	0.17 ± 0.04
	Bryobacter (115)	0.25 ± 0.06	0.03 ± 0.01	0.23 ± 0.02	0.06 ± 0.01	0.09 ± 0.02	0.07 ± 0.00	0.09 ± 0.01
	Bryobacter (562)	0.01 ± 0.00	0.01 ± 0.01	0.01 ± 0.00	0.01 ± 0.00	0.02 ± 0.01	0.01 ± 0.01	0.05 ± 0.02
	Uncultured subgroup_3 (901)	0.03 ± 0.00	0.01 ± 0.00	0.01 ± 0.00	0.01 ± 0.00	0.01 ± 0.01	0.00 ± 0.00	0.02 ± 0.01
	Uncultured subgroup_3 (55)	0.00 ± 0.00	0.11 ± 0.01	0.26 ± 0.05	0.07 ± 0.02	0.14 ± 0.03	0.08 ± 0.02	0.18 ± 0.02
	Uncultured subgroup_3 (516)	0.01 ± 0.01	0.01 ± 0.00	0.03 ± 0.01	0.01 ± 0.00	0.03 ± 0.01	0.01 ± 0.00	0.02 ± 0.00
	Blastocatella (126)	0.16 ± 0.02	0.17 ± 0.00	0.27 ± 0.01	0.16 ± 0.01	0.45 ± 0.04	0.19 ± 0.01	0.61 ± 0.12
	Uncultured subgroup_6 (85)	0.05 ± 0.01	0.02 ± 0.01	0.05 ± 0.01	0.13 ± 0.02	0.34 ± 0.12	0.09 ± 0.03	1.09 ± 0.43
	Uncultured subgroup_6 (10)	0.01 ± 0.00	0.23 ± 0.05	0.86 ± 0.12	0.48 ± 0.03	0.92 ± 0.04	0.52 ± 0.01	1.39 ± 0.22
	Uncultured subgroup_6 (212)	0.21 ± 0.03	0.03 ± 0.01	0.11 ± 0.01	0.09 ± 0.01	0.11 ± 0.02	0.06 ± 0.00	0.11 ± 0.01
	Uncultured subgroup_6 (304)	0.00 ± 0.00	0.01 ± 0.00	0.04 ± 0.00	0.08 ± 0.00	0.10 ± 0.01	0.05 ± 0.02	0.08 ± 0.01
	Uncultured subgroup_6 (401)	0.01 ± 0.01	0.04 ± 0.01	0.04 ± 0.00	0.07 ± 0.02	0.07 ± 0.02	0.09 ± 0.02	0.12 ± 0.02
	Uncultured subgroup_6 (581)	0.03 ± 0.01	0.03 ± 0.00	0.1 ± 0.02	0.02 ± 0.01	0.05 ± 0.01	0.01 ± 0.00	0.03 ± 0.00
	Uncultured subgroup_6 (412)	0.02 ± 0.00	0.04 ± 0.01	0.09 ± 0.03	0.08 ± 0.02	0.15 ± 0.02	0.08 ± 0.02	0.05 ± 0.02
	Uncultured subgroup_6 (147)	0.04 ± 0.00	0.06 ± 0.01	0.05 ± 0.01	0.11 ± 0.02	0.23 ± 0.05	0.10 ± 0.01	0.17 ± 0.02
	Uncultured subgroup_6 (85)	0.05 ± 0.01	0.02 ± 0.01	0.05 ± 0.01	0.13 ± 0.02	0.34 ± 0.12	0.09 ± 0.03	1.09 ± 0.43
	Uncultured subgroup_17 (39)	0.00 ± 0.00	0.09 ± 0.02	0.70 ± 0.06	0.54 ± 0.07	0.89 ± 0.09	0.42 ± 0.02	0.60 ± 0.17
	Uncultured subgroup_22 (329)	0.01 ± 0.01	0.01 ± 0.02	0.06 ± 0.01	0.06 ± 0.01	0.11 ± 0.01	0.04 ± 0.02	0.03 ± 0.01
	Uncultured subgroup_22 (340)	0.01 ± 0.01	0.01 ± 0.01	0.13 ± 0.01	0.03 ± 0.01	0.05 ± 0.00	0.04 ± 0.00	0.02 ± 0.01

	Uncultured subgroup_22 (57)	0.34 ± 0.03	0.04 ± 0.00	0.35 ± 0.06	0.17 ± 0.03	0.17 ± 0.05	0.17 ± 0.01	0.25 ± 0.04
Actinobacteria	Uncultured Sva0996_marine_group (83)	0.12 ± 0.01	0.1 ± 0.00	0.20 ± 0.02	0.24 ± 0.05	0.46 ± 0.03	0.22 ± 0.05	0.38 ± 0.06
	Aeromicrobium (332)	0.04 ± 0.01	0.00 ± 0.00	0.02 ± 0.01	0.01 ± 0.00	0.11 ± 0.07	0.01 ± 0.01	0.25 ± 0.13
	Marmoricola (69)	0.31 ± 0.09	0.05 ± 0.01	0.04 ± 0.02	0.20 ± 0.02	0.22 ± 0.05	0.14 ± 0.04	0.20 ± 0.10
	Nocardioides (372)	0.00 ± 0.00	0.02 ± 0.00	0.05 ± 0.02	0.09 ± 0.01	0.13 ± 0.02	0.14 ± 0.01	0.10 ± 0.02
	Nocardioides (210)	0.07 ± 0.02	0.04 ± 0.01	0.02 ± 0.00	0.15 ± 0.02	0.15 ± 0.03	0.14 ± 0.05	0.16 ± 0.09
	Nocardioides (102)	0.07 ± 0.01	0.15 ± 0.01	0.23 ± 0.00	0.39 ± 0.02	0.21 ± 0.01	0.46 ± 0.01	0.28 ± 0.09
	Uncultured MB-A2-108 (94)	0.22 ± 0.03	0.24 ± 0.07	0.39 ± 0.03	0.36 ± 0.01	0.41 ± 0.02	0.30 ± 0.04	0.21 ± 0.00
	Iamia (188)	0.15 ± 0.03	0.03 ± 0.01	0.05 ± 0.01	0.10 ± 0.01	0.08 ± 0.01	0.18 ± 0.03	0.15 ± 0.02
	Iamia (362)	0.06 ± 0.00	0.04 ± 0.01	0.02 ± 0.00	0.06 ± 0.02	0.13 ± 0.04	0.04 ± 0.01	0.08 ± 0.01
	Uncultured Acidimicrobiales (1265)	0.05 ± 0.01	0.00 ± 0.00	0.00 ± 0.00	0.02 ± 0.01	0.00 ± 0.00	0.03 ± 0.01	0.01 ± 0.00
	Uncultured 480-2(627)	0.00 ± 0.00	0.03 ± 0.01	0.03 ± 0.01	0.04 ± 0.01	0.07 ± 0.01	0.03 ± 0.00	0.05 ± 0.01
	Solirubrobacter (29)	0.05 ± 0.02	0.04 ± 0.02	0.03 ± 0.01	0.03 ± 0.01	0.04 ± 0.01	0.03 ± 0.00	0.04 ± 0.00
	Sva0996_marine_group(441)	0.00 ± 0.00	0.00 ± 0.00	0.04 ± 0.00	0.04 ± 0.01	0.04 ± 0.01	0.03 ± 0.01	0.04 ± 0.00
	Flavobacterium (633)	0.02 ± 0.01	0.00 ± 0.00	0.00 ± 0.00	0.11 ± 0.04	0.01 ± 0.00	0.18 ± 0.14	0.00 ± 0.00
	Flavobacterium (2394)	0.01 ± 0.00	0.00 ± 0.00	0.00 ± 0.00	0.00 ± 0.00	0.00 ± 0.01	0.12 ± 0.09	0.00 ± 0.00
	Uncultured NS9_marine_group (438)	0.06 ± 0.01	0.03 ± 0.01	0.05 ± 0.01	0.06 ± 0.03	0.01 ± 0.00	0.23 ± 0.07	0.08 ± 0.04
	Uncultured NS9_marine_group (277)	0.02 ± 0.00	0.02 ± 0.01	0.04 ± 0.02	0.08 ± 0.01	0.06 ± 0.00	0.24 ± 0.09	0.13 ± 0.03
	Rhodococcus (459)	0.00 ± 0.00	0.00 ± 0.00	0.08 ± 0.01	0.01 ± 0.01	0.04 ± 0.02	0.04 ± 0.01	0.04 ± 0.01
	Fodinicola (15)	0.06 ± 0.02	0.52 ± 0.08	1.25 ± 0.07	1.26 ± 0.17	0.97 ± 0.07	1.31 ± 0.18	0.76 ± 0.11
	Nocardioides (405)	0.00 ± 0.00	0.01 ± 0.00	0.10 ± 0.02	0.12 ± 0.04	0.06 ± 0.01	0.13 ± 0.01	0.12 ± 0.01
	Uncultured Acidimicrobiales (612)	0.00 ± 0.00	0.00 ± 0.00	0.05 ± 0.01	0.03 ± 0.01	0.03 ± 0.01	0.03 ± 0.00	0.04 ± 0.01
	Uncultured Actinobacteria (359)	0.00 ± 0.00	0.01 ± 0.01	0.07 ± 0.01	0.13 ± 0.02	0.05 ± 0.01	0.11 ± 0.01	0.08 ± 0.01
	Uncultured MB-A2-108 (137)	0.11 ± 0.02	0.09 ± 0.01	0.41 ± 0.06	0.24 ± 0.01	0.32 ± 0.02	0.31 ± 0.05	0.20 ± 0.03
	CL500-29_marine_group (28)	0.26 ± 0.04	0.04 ± 0.01	0.07 ± 0.03	0.07 ± 0.02	0.09 ± 0.01	0.09 ± 0.01	0.57 ± 0.04
	Uncultured Acidimicrobiales (569)	0.04 ± 0.00	0.05 ± 0.00	0.01 ± 0.00	0.08 ± 0.03	0.02 ± 0.00	0.02 ± 0.01	0.01 ± 0.01
	Uncultured *Intrasporangiaceae* (19)	0.47 ± 0.03	0.12 ± 0.01	0.18 ± 0.02	0.24 ± 0.03	0.22 ± 0.02	0.24 ± 0.03	0.22 ± 0.06
	Gaiella (45)	0.00 ± 0.00	0.45 ± 0.07	0.30 ± 0.02	0.26 ± 0.01	0.47 ± 0.02	0.22 ± 0.01	0.29 ± 0.02
Armatimonadetes	Uncultured Armatimonadetes (371)	0.17 ± 0.06	0.00 ± 0.00	0.00 ± 0.00	0.01 ± 0.01	0.07 ± 0.03	0.01 ± 0.00	0.33 ± 0.08
Bacteroidetes	*Chryseolinea* (165)	0.10 ± 0.02	0.01 ± 0.00	0.08 ± 0.03	0.45 ± 0.07	0.26 ± 0.04	0.18 ± 0.05	0.17 ± 0.04

	Chryseolinea (483)	0.05 ± 0.02	0.00 ± 0.00	0.03 ± 0.01	0.15 ± 0.07	0.07 ± 0.02	0.09 ± 0.01	0.07 ± 0.03
	Chryseolinea (231)	0.21 ± 0.02	0.03 ± 0.01	0.13 ± 0.01	0.32 ± 0.06	0.19 ± 0.02	0.20 ± 0.04	0.13 ± 0.04
	Chryseolinea (1195)	0.02 ± 0.00	0.00 ± 0.00	0.02 ± 0.00	0.04 ± 0.01	0.04 ± 0.01	0.02 ± 0.01	0.02 ± 0.01
	Uncultured *Rhodothermaceae* (363)	0.02 ± 0.01	0.00 ± 0.00	0.00 ± 0.00	0.02 ± 0.00	0.10 ± 0.01	0.01 ± 0.01	0.04 ± 0.03
	Ferruginibacter (499)	0.09 ± 0.01	0.00 ± 0.00	0.01 ± 0.01	0.04 ± 0.00	0.04 ± 0.01	0.09 ± 0.00	0.15 ± 0.05
	Ferruginibacter (378)	0.02 ± 0.01	0.02. ± 0.01	0.05 ± 0.02	0.11 ± 0.04	0.06 ± 0.01	0.09 ± 0.01	0.16 ± 0.04
	Flavobacterium (2394)	0.01 ± 0.00	0.00 ± 0.00	0.00 ± 0.00	0.00 ± 0.00	0.00 ± 0.00	0.12 ± 0.09	0.00 ± 0.00
	Flavobacterium (376)	0.02 ± 0.01	0.00 ± 0.00	0.00 ± 0.00	0.20 ± 0.07	0.08 ± 0.02	0.04 ± 0.01	0.00 ± 0.00
	Uncultured *Cytophagaceae* (451)	0.11 ± 0.02	0.00 ± 0.00	0.02 ± 0.01	0.10 ± 0.04	0.09 ± 0.04	0.03 ± 0.01	0.10 ± 0.04
	Ferruginibacter (256)	0.00 ± 0.00	0.02 ± 0.01	0.06 ± 0.01	0.19 ± 0.08	0.14 ± 0.01	0.13 ± 0.02	0.21 ± 0.07
	Uncultured *Saprospiraceae* (380)	0.00 ± 0.00	0.02 ± 0.01	0.04 ± 0.02	0.05 ± 0.01	0.03 ± 0.01	0.13 ± 0.05	0.16 ± 0.04
	Uncultured *Saprospiraceae* (383)	0.00 ± 0.00	0.01 ± 0.00	0.02 ± 0.00	0.04 ± 0.01	0.18 ± 0.08	0.09 ± 0.02	0.13 ± 0.01
	Uncultured *Saprospiraceae* (472)	0.04 ± 0.01	0.00 ± 0.00	0.01 ± 0.01	0.02 ± 0.01	0.02 ± 0.01	0.14 ± 0.07	0.29 ± 0.14
	Uncultured Sphingobacteriales (711)	0.02 ± 0.01	0.00 ± 0.00	0.02 ± 0.01	0.08 ± 0.02	0.02 ± 0.00	0.12 ± 0.01	0.04 ± 0.02
	Uncultured env.OPS_17 (726)	0.01 ± 0.00	0.00 ± 0.00	0.00 ± 0.00	0.02 ± 0.01	0.00 ± 0.00	0.20 ± 0.08	0.00 ± 0.00
	Uncultured env.OPS_17 (876)	0.01 ± 0.00	0.00 ± 0.00	0.02 ± 0.01	0.05 ± 0.02	0.01 ± 0.00	0.11 ± 0.03	0.01 ± 0.01
	Uncultured env.OPS_17 (548)	0.01 ± 0.01	0.00 ± 0.00	0.00 ± 0.00	0.00 ± 0.00	0.05 ± 0.00	0.01 ± 0.01	0.09 ± 0.09
	Uncultured KD3-93 (46)	0.33 ± 0.06	0.00 ± 0.00	0.00 ± 0.00	0.17 ± 0.00	0.02 ± 0.01	0.61 ± 0.26	0.09 ± 0.06
	NS11-12_marine_group (616)	0.01 ± 0.01	0.00 ± 0.00	0.00 ± 0.00	0.09 ± 0.02	0.03 ± 0.01	0.14 ± 0.03	0.03 ± 0.02
	PHOS-HE51 (1186)	0.00 ± 0.00	0.00 ± 0.00	0.00 ± 0.00	0.02 ± 0.01	0.01 ± 0.00	0.07 ± 0.03	0.04 ± 0.01
	Uncultured Sphingobacteriales (409)	0.23 ± 0.09	0.00 ± 0.00	0.00 ± 0.00	0.00 ± 0.00	0.04 ± 0.01	0.00 ± 0.00	0.09 ± 0.03
	Terrimonas (139)	0.02 ± 0.00	0.02 ± 0.01	0.03 ± 0.01	0.22 ± 0.05	0.14 ± 0.03	0.21 ± 0.05	0.72 ± 0.21
	Terrimonas (149)	0.04 ± 0.00	0.03 ± 0.01	0.07 ± 0.01	0.36 ± 0.27	0.06 ± 0.01	0.15 ± 0.07	0.12 ± 0.05
	Terrimonas (253)	0.03 ± 0.01	0.03 ± 0.00	0.12 ± 0.02	0.17 ± 0.02	0.10 ± 0.01	0.15 ± 0.02	0.11 ± 0.03
Cand_div_BRC1	Uncultured Candidate_div_BRC1 (542)	0.00 ± 0.00	0.00 ± 0.00	0.02 ± 0.01	0.02 ± 0.01	0.01± 0.00	0.00 ± 0.00	0.01 ± 0.01
	Uncultured Candidate_div_BRC1 (1346)	0.01 ± 0.00	0.00 ± 0.00	0.00 ± 0.00	0.00 ± 0.00	0.00 ± 0.00	0.00 ± 0.00	0.00 ± 0.00
Gemmatimonadetes	Uncultured *Gemmatimonadaceae* (124)	0.00 ± 0.00	0.01 ± 0.01	0.08 ± 0.03	0.13 ± 0.01	0.10 ± 0.01	0.17 ± 0.01	0.13 ± 0.01
	Uncultured *Gemmatimonadaceae* (32)	0.51 ± 0.07	0.14 ± 0.04	0.41 ± 0.04	0.62 ± 0.08	1.06 ± 0.07	0.41 ± 0.04	0.48 ± 0.08
	Uncultured *Gemmatimonadaceae* (52)	0.31 ± 0.05	0.09 ± 0.02	0.28 ± 0.05	0.30 ± 0.08	0.42 ± 0.05	0.21 ± 0.05	0.26 ± 0.05
	Uncultured *Gemmatimonadaceae* (251)	0.00 ± 0.00	0.00 ± 0.00	0.06 ± 0.00	0.06 ± 0.03	0.09 ± 0.00	0.05 ± 0.02	0.08 ± 0.01

	Uncultured *Gemmatimonadaceae* (269)	0.09 ± 0.05	0.01 ± 0.00	0.04 ± 0.01	0.10 ± 0.01	0.07 ± 0.01	0.06 ± 0.02	0.06 ± 0.01
	Uncultured *Gemmatimonadaceae* (299)	0.01 ± 0.01	0.03 ± 0.00	0.02 ± 0.00	0.06 ± 0.00	0.17 ± 0.01	0.07 ± 0.03	0.13 ± 0.07
	Uncultured *Gemmatimonadaceae* (388)	0.06 ± 0.02	0.05 ± 0.01	0.07 ± 0.02	0.08 ± 0.01	0.08 ± 0.01	0.04 ± 0.01	0.03 ± 0.01
Chlorobi	Uncultured BSV26 (580)	0.02 ± 0.01	0.00 ± 0.00	0.02 ± 0.01	0.06 ± 0.01	0.02 ± 0.01	0.04 ± 0.00	0.01 ± 0.01
	Uncultured BSV26 (93)	0.20 ± 0.01	0.11 ± 0.04	0.33 ± 0.13	0.63 ± 0.04	0.24 ± 0.01	0.45 ± 0.09	0.18 ± 0.02
	Uncultured BSV26 (413)	0.05 ± 0.01	0.01 ± 0.00	0.06 ± 0.01	0.10 ± 0.03	0.05 ± 0.01	0.13 ± 0.03	0.05 ± 0.01
	Uncultured OPB56 (740)	0.00 ± 0.00	0.00 ± 0.00	0.01 ± 0.00	0.02 ± 0.00	0.00 ± 0.00	0.04 ± 0.03	0.01 ± 0.00
	Uncultured SJA-28 (284)	0.07 ± 0.00	0.07 ± 0.00	0.21 ± 0.02	0.26 ± 0.04	0.12 ± 0.01	0.10 ± 0.01	0.11 ± 0.01
Chloroflexi	Uncultured *Caldilineaceae* (110)	0.14 ± 0.02	0.09 ± 0.00	0.76 ± 0.07	0.27 ± 0.05	0.38 ± 0.09	0.21 ± 0.06	0.38 ± 0.11
	Uncultured KD4-96 (27)	0.08 ± 0.02	0.31 ± 0.10	0.56 ± 0.02	0.56 ± 0.04	0.97 ± 0.08	0.47 ± 0.06	0.93 ± 0.09
	Uncultured *Anaerolineaceae* (233)	0.10 ± 0.02	0.02 ± 0.01	0.15 ± 0.01	0.09 ± 0.01	0.19 ± 0.01	0.11 ± 0.03	0.12 ± 0.03
	Uncultured *Anaerolineaceae* (611)	0.04 ± 0.01	0.00 ± 0.00	0.00 ± 0.00	0.04 ± 0.01	0.05 ± 0.02	0.03 ± 0.02	0.13 ± 0.04
	Uncultured *Anaerolineaceae* (628)	0.04 ± 0.01	0.00 ± 0.00	0.03 ± 0.01	0.04 ± 0.02	0.07 ± 0.01	0.03 ± 0.02	0.04 ± 0.01
	Unclassified Gitt-GS-136 (127)	0.14 ± 0.02	0.11 ± 0.10	0.13 ± 0.02	0.17 ± 0.03	0.42 ± 0.02	0.10 ± 0.01	0.30 ± 0.05
	Uncultured KD4-96 (96)	0.12 ± 0.03	0.20 ± 0.03	0.16 ± 0.03	0.20 ± 0.03	0.66 ± 0.05	0.14 ± 0.04	0.20 ± 0.04
	Unclassified JG30-KF-CM45 (145)	0.05 ± 0.00	0.05 ± 0.01	0.13 ± 0.02	0.13 ± 0.01	0.24 ± 0.03	0.18 ± 0.03	0.43 ± 0.08
	Uncultured KD4-96 (8)	0.12 ± 0.05	1.59 ± 0.47	1.33 ± 0.04	1.18 ± 0.02	1.06 ± 0.03	1.08 ± 0.11	1.18 ± 0.06
	Uncultured KD4-96 (16)	0.38 ± 0.04	0.83 ± 0.20	0.43 ± 0.07	0.74 ± 0.05	1.09 ± 0.05	0.48 ± 0.05	1.04 ± 0.10
Latescibacteria	Uncultured Latescibacteria (95)	0.21 ± 0.01	0.04 ± 0.01	0.07 ± 0.01	0.18 ± 0.02	0.15 ± 0.02	0.18 ± 0.01	0.08 ± 0.03
	Uncultured Latescibacteria (154)	0.14 ± 0.01	0.00 ± 0.00	0.06 ± 0.03	0.12 ± 0.01	0.02 ± 0.01	0.08 ± 0.03	0.06 ± 0.02
	Uncultured Latescibacteria (308)	0.01 ± 0.00	0.01 ± 0.01	0.01 ± 0.01	0.01 ± 0.01	0.10 ± 0.02	0.01 ± 0.01	0.15 ± 0.05
	Uncultured Latescibacteria (326)	0.08 ± 0.00	0.02 ± 0.01	0.04 ± 0.02	0.08 ± 0.02	0.04 ± 0.01	0.07 ± 0.02	0.04 ± 0.01
	Uncultured Latescibacteria (342)	0.06 ± 0.00	0.02 ± 0.01	0.07 ± 0.01	0.05 ± 0.02	0.05 ± 0.01	0.03 ± 0.01	0.04 ± 0.00
	Uncultured Latescibacteria (453)	0.00 ± 0.00	0.02 ± 0.01	0.06 ± 0.01	0.03 ± 0.01	0.06 ± 0.00	0.03 ± 0.01	0.04 ± 0.00
	Uncultured Latescibacteria (503)	0.03 ± 0.00	0.00 ± 0.00	0.02 ± 0.01	0.06 ± 0.01	0.02 ± 0.00	0.03 ± 0.01	0.01 ± 0.01
	Uncultured Latescibacteria (534)	0.02 ± 0.00	0.02 ± 0.00	0.04 ± 0.01	0.06 ± 0.01	0.08 ± 0.02	0.03 ± 0.00	0.03 ± 0.01
	Uncultured Latescibacteria (706)	0.01 ± 0.01	0.01 ± 0.00	0.12 ± 0.03	0.02 ± 0.00	0.03 ± 0.01	0.01 ± 0.01	0.01± 0.00
	Uncultured Latescibacteria (732)	0.01 ± 0.00	0.00 ± 0.00	0.02 ± 0.00	0.02 ± 0.01	0 .00 ± 0.00	0.01 ± 0.00	0.01 ± 0.00
	Uncultured Latescibacteria (864)	0.01 ± 0.01	0.00 ± 0.00	0.01 ± 0.01	0.01 ± 0.00	0.02 ± 0.01	0.01 ± 0.01	0.02 ± 0.01
	Uncultured Latescibacteria (422)	0.07 ± 0.01	0.05 ± 0.02	0.25 ± 0.04	0.10 ± 0.01	0.06 ± 0.01	0.05 ± 0.01	0.04 ± 0.00

	Uncultured Latescibacteria (1054)	0.00 ± 0.00	0.00 ± 0.00	0.01 ± 0.00	0.01 ± 0.01	0.02 ± 0.01	0.01 ± 0.01	0.01 ± 0.01
Nitrospirae	*Nitrospira* (7)	0.85 ± 0.14	0.1 ± 0.01	0.22 ± 0.03	0.36 ± 0.03	0.29 ± 0.04	0.62 ± 0.06	0.29 ± 0.08
	Nitrospira (23)	1.12 ± 0.20	0.09 ± 0.02	0.36 ± 0.08	0.48 ± 0.14	0.15 ± 0.02	0.41 ± 0.08	0.20 ± 0.03
	Nitrospira (26)	0.70 ± 0.09	0.04 ± 0.01	0.32 ± 0.06	0.28 ± 0.03	0.13 ± 0.01	0.19 ± 0.09	0.06 ± 0.03
Alphaproteobacteria	*Sphingobium* (17)	0.61 ± 0.07	0.00 ± 0.00	0.00 ± 0.00	0.30 ± 0.28	0.08 ± 0.02	0.04 ± 0.02	0.04 ± 0.02
	Hyphomicrobium (60)	0.35 ± 0.07	0.09 ± 0.02	0.30 ± 0.04	0.23 ± 0.02	0.29 ± 0.03	0.29 ± 0.00	0.23 ± 0.03
	Hyphomicrobium (347)	0.06 ± 0.02	0.02 ± 0.00	0.04 ± 0.04	0.00 ± 0.00	0.08 ± 0.01	0.02 ± 0.02	0.07 ± 0.01
	Hirschia (62)	0.07 ± 0.02	0.05 ± 0.01	0.27 ± 0.04	0.25 ± 0.04	0.30 ± 0.03	0.36 ± 0.04	0.45 ± 0.20
	Novosphingobium (64)	0.00 ± 0.00	0.02 ± 0.00	0.01 ± 0.01	0.05 ± 0.01	2.04 ± 0.78	0.51 ± 0.48	0.03 ± 0.02
	Pedomicrobium (84)	0.07 ± 0.01	0.08 ± 0.01	0.22 ± 0.02	0.15 ± 0.02	0.28 ± 0.03	0.26 ± 0.01	0.38 ± 0.06
	Uncultured Rhizobiales (335)	0.16 ± 0.03	0.03 ± 0.01	0.10 ± 0.04	0.04 ± 0.01	0.13 ± 0.03	0.17 ± 0.04	0.15 ± 0.06
	Defluviimonas (202)	0.00 ± 0.00	0.03 ± 0.00	0.10 ± 0.01	0.23 ± 0.03	0.15 ± 0.01	0.20 ± 0.03	0.13 ± 0.01
	Hyphomicrobium (129)	0.09 ± 0.02	0.05 ± 0.00	0.16 ± 0.03	0.12 ± 0.01	0.26 ± 0.02	0.13 ± 0.00	0.19 ± 0.03
	Uncultured AKYH478 (645)	0.01 ± 0.00	0.00 ± 0.00	0.02 ± 0.01	0.03 ± 0.02	0.04 ± 0.00	0.06 ± 0.01	0.19 ± 0.06
	Uncultured F0723 (1059)	0.04 ± 0.01	0.01 ± 0.00	0.01 ± 0.00	0.00 ± 0.00	0.01 ± 0.00	0.03 ± 0.02	0.09 ± 0.03
	Uncultured MNG7 (35)	0.00 ± 0.00	0.20 ± 0.04	0.66 ± 0.11	0.75 ± 0.03	0.43 ± 0.02	0.89 ± 0.08	0.83 ± 0.13
	Uncultured *Phyllobacteriaceae* (87)	0.14 ± 0.02	0.04 ± 0.01	0.04 ± 0.01	0.04 ± 0.01	0.05 ± 0.01	0.16 ± 0.05	0.39 ± 0.12
	Uncultured *Sphingomonadaceae* (1)	0.00 ± 0.00	0.13 ± 0.02	0.15 ± 0.03	1.30 ± 0.16	0.28 ± 0.02	6.16 ± 4.93	4.14 ± 1.16
	Uncultured *Sphingomonadaceae* (119)	0.00 ± 0.00	0.01 ± 0.01	0.05 ± 0.01	0.27 ± 0.02	0.18 ± 0.04	0.29 ± 0.01	0.26 ± 0.09
	Sphingopyxis (553)	0.02 ± 0.00	0.00 ± 0.00	0.09 ± 0.02	0.08 ± 0.01	0.01 ± 0.01	0.08 ± 0.00	0.01 ± 0.00
	Woodsholea (181)	0.07 ± 0.01	0.00 ± 0.00	0.11 ± 0.01	0.22 ± 0.03	0.25 ± 0.07	0.23 ± 0.04	0.09 ± 0.02
	Woodsholea (183)	0.01 ± 0.00	0.02 ± 0.00	0.16 ± 0.01	0.21 ± 0.03	0.15 ± 0.03	0.15 ± 0.02	0.10 ± 0.01
	Woodsholea (615)	0.04 ± 0.01	0.01 ± 0.00	0.05 ± 0.01	0.04 ± 0.01	0.04 ± 0.01	0.10 ± 0.02	0.02 ± 0.00
	Uncultured *Rhizobiaceae* (100)	0.46 ± 0.10	0.02 ± 0.01	0.07 ± 0.02	0.19 ± 0.01	0.09 ± 0.02	0.21 ± 0.03	0.32 ± 0.19
	Uncultured AKYH478 (645)	0.01 ± 0.00	0.00 ± 0.00	0.02 ± 0.01	0.03 ± 0.02	0.04 ± 0.00	0.06 ± 0.01	0.19 ± 0.06
	Defluviimonas (202)	0.00 ± 0.00	0.03 ± 0.00	0.10 ± 0.01	0.23 ± 0.03	0.15 ± 0.01	0.20 ± 0.03	0.13 ± 0.01
Deltaproteobacteria	*Bdellovibrio* (63)	0.05 ± 0.00	0.00 ± 0.00	0.00 ± 0.00	0.46 ± 0.11	0.00 ± 0.01	0.08 ± 0.00	0.11 ± 0.07
	Haliangium (479)	0.01 ± 0.00	0.00 ± 0.00	0.02 ± 0.00	0.04 ± 0.02	0.04 ± 0.01	0.01 ± 0.00	0.02 ± 0.00
	Haliangium (248)	0.00 ± 0.00	0.00 ± 0.00	0.00 ± 0.00	0.01 ± 0.00	0.08 ± 0.04	0.00 ± 0.00	0.12 ± 0.06
	Haliangium (457)	0.10 ± 0.02	0.00 ± 0.00	0.01 ± 0.00	0.02 ± 0.00	0.06 ± 0.01	0.01 ± 0.01	0.03 ± 0.02

	Haliangium (739)	0.00 ± 0.00	0.00 ± 0.00	0.01 ± 0.00	0.02 ± 0.01	0.02 ± 0.01	0.02 ± 0.01	0.02 ± 0.01
	OM27-Clade (166)	0.01 ± 0.00	0.00 ± 0.00	0.00 ± 0.00	0.01 ± 0.00	0.00 ± 0.00	0.11 ± 0.05	0.08 ± 0.07
	Anaeromyxobacter (220)	0.15 ± 0.02	0.01 ± 0.00	0.02 ± 0.01	0.05 ± 0.02	0.05 ± 0.00	0.06 ± 0.01	0.06 ± 0.02
	Anaeromyxobacter (82)	0.24 ± 0.02	0.16 ± 0.01	0.16 ± 0.01	0.17 ± 0.03	0.16 ± 0.01	0.14 ± 0.03	0.06 ± 0.02
	Sandaracinus (260)	0.05 ± 0.01	0.00 ± 0.00	0.01 ± 0.00	0.05 ± 0.03	0.02 ± 0.01	0.02 ± 0.01	0.03 ± 0.02
	Sandaracinus (382)	0.00 ± 0.00	0.00 ± 0.00	0.01 ± 0.01	0.04 ± 0.02	0.01 ± 0.00	0.02 ± 0.01	0.01 ± 0.00
	Sorangium (709)	0.01 ± 0.01	0.00 ± 0.00	0.03 ± 0.00	0.01 ± 0.01	0.01 ± 0.00	0.02 ± 0.00	0.00 ± 0.00
	Sorangium (1348)	0.00 ± 0.00	0.00 ± 0.00	0.01 ± 0.00	0.00 ± 0.00	0.01 ± 0.00	0.00 ± 0.00	0.00 ± 0.00
	Sorangium (352)	0.00 ± 0.00	0.01 ± 0.00	0.01 ± 0.00	0.00 ± 0.00	0.05 ± 0.02	0.00 ± 0.00	0.04 ± 0.02
	Uncultured *Cystobacteraceae* (203)	0.02 ± 0.00	0.00 ± 0.00	0.05 ± 0.01	0.02 ± 0.00	0.02 ± 0.00	0.05 ± 0.01	0.06 ± 0.02
	Uncultured *Sandaracinaceae* (33)	0.16 ± 0.01	0.00 ± 0.00	0.11 ± 0.02	0.24 ± 0.05	0.21 ± 0.05	0.12 ± 0.04	0.04 ± 0.01
	Uncultured *Sandaracinaceae* (404)	0.04 ± 0.01	0.00 ± 0.00	0.01 ± 0.00	0.05 ± 0.01	0.02 ± 0.00	0.01 ± 0.01	0.00 ± 0.00
	Uncultured *Sandaracinaceae* (686)	0.07 ± 0.01	0.00 ± 0.00	0.00 ± 0.00	0.04 ± 0.01	0.00 ± 0.00	0.02 ± 0.01	0.00 ± 0.00
	Uncultured *Sandaracinaceae* (240)	0.1 ± 0.03	0.00 ± 0.00	0.02 ± 0.01	0.06 ± 0.02	0.05 ± 0.02	0.09 ± 0.00	0.04 ± 0.01
	Uncultured *Sandaracinaceae* (764)	0.01 ± 0.01	0.00 ± 0.00	0.00 ± 0.00	0.00 ± 0.00	0.01 ± 0.01	0.00 ± 0.00	0.00 ± 0.00
	Uncultured Sh765B-TzT-29 (414)	0.05 ± 0.02	0.02 ± 0.01	0.10 ± 0.01	0.10 ± 0.01	0.06 ± 0.01	0.07 ± 0.02	0.09 ± 0.01
	Uncultured δ-bacteria (105)	0.18 ± 0.02	0.00 ± 0.00	0.00 ± 0.00	0.00 ± 0.00	0.00 ± 0.00	0.00 ± 0.00	0.07 ± 0.05
	Uncultured δ-bacteria (54)	0.37 ± 0.04	0.00 ± 0.00	0.00 ± 0.00	0.00 ± 0.00	0.04 ± 0.03	0.00 ± 0.00	0.02 ± 0.02
	Phaselicystis (163)	0.02 ± 0.01	0.00 ± 0.00	0.00 ± 0.00	0.00 ± 0.00	0.00 ± 0.00	0.00 ± 0.00	0.12 ± 0.01
Gammaproteobacteria (Betaproteobacteriales)	*Hydrogenophaga* (9)	1.15 ± 0.17	0.02 ± 0.00	0.11 ± 0.02	0.21 ± 0.03	0.35 ± 0.08	0.32 ± 0.13	1.29 ± 0.13
	Leeia (513)	0.05 ± 0.02	0.00 ± 0.00	0.01 ± 0.01	0.10 ± 0.03	0.03 ± 0.01	0.01 ± 0.00	0.00 ± 0.00
	Piscinibacter (14)	0.16 ± 0.01	0.03 ± 0.00	0.13 ± 0.01	0.27 ± 0.04	0.17 ± 0.01	0.29 ± 0.02	0.76 ± 0.12
	Rhizobacter (123)	0.33 ± 0.03	0.00 ± 0.00	0.07 ± 0.01	0.04 ± 0.01	0.01 ± 0.00	0.20 ± 0.09	0.05 ± 0.02
	Uncultured *Comamonadaceae* (4)	0.00 ± 0.00	0.10 ± 0.02	0.28 ± 0.05	0.40 ± 0.03	0.28 ± 0.01	0.58 ± 0.14	1.29 ± 0.26
	Uncultured *Comamonadaceae* (36)	0.24 ± 0.04	0.02 ± 0.00	0.07 ± 0.01	0.19 ± 0.05	0.16 ± 0.03	0.26 ± 0.06	0.70 ± 0.16
	Uncultured *Comamonadaceae* (113)	0.05 ± 0.01	0.01 ± 0.00	0.00 ± 0.00	0.11 ± 0.06	0.08 ± 0.05	0.45 ± 0.25	0.28 ± 0.14
	Uncultured *Comamonadaceae* (152)	0.02 ± 0.00	0.02 ± 0.01	0.01 ± 0.00	0.05 ± 0.01	0.03 ± 0.00	0.07 ± 0.01	0.34 ± 0.24
	Uncultured *Comamonadaceae* (1113)	0.04 ± 0.01	0.00 ± 0.00	0.00 ± 0.00	0.01 ± 0.01	0.04 ± 0.02	0.04 ± 0.02	0.02 ± 0.01
	Uncultured *Comamonadaceae* (12)	0.46 ± 0.12	0.17 ± 0.03	0.35 ± 0.04	0.32 ± 0.02	0.17 ± 0.01	0.40 ± 0.07	0.52 ± 0.08
	Azohydromonas (43)	0.53 ± 0.10	0.02 ± 0.01	0.06 ± 0.02	0.05 ± 0.02	0.05 ± 0.01	0.11 ± 0.02	0.16 ± 0.04

	Uncultured *Gallionellaceae* (320)	0.10 ± 0.00	0.02 ± 0.01	0.06 ± 0.03	0.16 ± 0.02	0.05 ± 0.01	0.13 ± 0.02	0.06 ± 0.03
	Uncultured *Nitrosomonadaceae* (20)	0.11 ± 0.00	0.35 ± 0.04	0.65 ± 0.08	0.81 ± 0.03	0.70 ± 0.12	1.18 ± 0.04	1.33 ± 0.30
	Uncultured *Nitrosomonadaceae* (350)	0.05 ± 0.01	0.01 ± 0.01	0.05 ± 0.02	0.13 ± 0.02	0.03 ± 0.02	0.19 ± 0.02	0.34 ± 0.19
	Uncultured *Nitrosomonadaceae* (92)	0.07 ± 0.01	0.21 ± 0.04	0.24 ± 0.04	0.39 ± 0.05	0.27 ± 0.05	0.30 ± 0.02	0.23 ± 0.03
	Uncultured *Oxalobacteraceae* (215)	0.14 ± 0.04	0.01 ± 0.00	0.00 ± 0.00	0.15 ± 0.04	0.04 ± 0.01	0.11 ± 0.01	0.03 ± 0.01
	Vogesella (44)	0.03 ± 0.01	0.00 ± 0.00	0.00 ± 0.00	0.00 ± 0.00	0.00 ± 0.00	0.00 ± 0.00	0.00 ± 0.00
	Dechloromonas (138)	0.11 ± 0.01	0.01 ± 0.00	0.01 ± 0.01	0.01 ± 0.01	0.00 ± 0.00	0.03 ± 0.01	0.01 ± 0.00
	Thauera (40)	0.13 ± 0.01	0.00 ± 0.00	0.00 ± 0.00	0.01 ± 0.01	0.01 ± 0.00	0.02 ± 0.01	0.01 ± 0.00
	Uncultured SC-I-84 (89)	0.20 ± 0.04	0.21 ± 0.03	0.24 ± 0.02	0.29 ± 0.04	0.26 ± 0.03	0.44 ± 0.11	0.35 ± 0.12
	Uncultured SC-I-84 (354)	0.07 ± 0.00	0.05 ± 0.00	0.07 ± 0.01	0.08 ± 0.03	0.07 ± 0.01	0.16 ± 0.05	0.15 ± 0.03
	Uncultured β-proteobacteria (66)	0.14 ± 0.00	0.15 ± 0.01	0.10 ± 0.02	0.16 ± 0.05	0.19 ± 0.05	0.34 ± 0.03	0.83 ± 0.25
	Zoogloea (266)	0.00 ± 0.00	0.00 ± 0.00	0.00 ± 0.00	0.00 ± 0.00	0.00 ± 0.00	0.00 ± 0.00	0.00 ± 0.00
	Acidiferrobacter (67)	0.17 ± 0.03	0.16 ± 0.01	0.13 ± 0.05	0.48 ± 0.04	0.20 ± 0.05	0.53 ± 0.04	0.19 ± 0.06
	Arenimonas (520)	0.02 ± 0.01	0.00 ± 0.00	0.01 ± 0.00	0.06 ± 0.01	0.10 ± 0.01	0.03 ± 0.00	0.02 ± 0.01
	Arenimonas (357)	0.00 ± 0.00	0.00 ± 0.00	0.02 ± 0.01	0.25 ± 0.05	0.06 ± 0.01	0.25 ± 0.06	0.03 ± 0.01
	Pseudomonas (24)	0.09 ± 0.02	0.00 ± 0.00	0.08 ± 0.01	0.50 ± 0.12	0.15 ± 0.03	0.41 ± 0.06	0.08 ± 0.03
	Unclutured *Pseudomonadaceae* (3)	0.00 ± 0.00	0.00 ± 0.00	0.00 ± 0.00	0.00 ± 0.00	0.00 ± 0.00	0.00 ± 0.00	0.00 ± 0.00
	Thermomonas (58)	0.07 ± 0.01	0.05 ± 0.01	0.06 ± 0.01	0.43 ± 0.14	0.32 ± 0.08	0.59 ± 0.07	0.37 ± 0.12
	Uncultured *Xanthomonadaceae* (70)	0.05 ± 0.01	0.11 ± 0.04	0.41 ± 0.01	0.75 ± 0.07	0.21 ± 0.01	0.31 ± 0.02	0.47 ± 0.15
	Uncultured γ-proteobacteria (452)	0.00 ± 0.00	0.00 ± 0.00	0.01 ± 0.00	0.08 ± 0.02	0.02 ± 0.00	0.05 ± 0.02	0.01 ± 0.00
	Uncultured γ-proteobacteria (541)	0.02 ± 0.00	0.00 ± 0.00	0.00 ± 0.00	0.05 ± 0.01	0.02 ± 0.01	0.00 ± 0.00	0.00 ± 0.00
	Uncultured γ-proteobacteria (505)	0.04 ± 0.01	0.00 ± 0.00	0.03 ± 0.02	0.09 ± 0.03	0.01 ± 0.01	0.11 ± 0.01	0.02 ± 0.01
	Uncultured γ-proteobacteria (715)	0.01 ± 0.01	0.00 ± 0.00	0.02 ± 0.01	0.06 ± 0.02	0.02 ± 0.01	0.03 ± 0.01	0.00 ± 0.00
	Uncultured γ-proteobacteria (1758)	0.00 ± 0.00	0.00 ± 0.00	0.00 ± 0.00	0.08 ± 0.06	0.04 ± 0.01	0.00 ± 0.00	0.00 ± 0.00
	Acidiferrobacter (196)	0.02 ± 0.01	0.06 ± 0.01	0.08 ± 0.02	0.21 ± 0.03	0.21 ± 0.01	0.24 ± 0.02	0.15 ± 0.02
Saccharibacteria	Uncultured Saccharibacteria (980)	0.01 ± 0.00	0.00 ± 0.00	0.00 ± 0.00	0.13 ± 0.05	0.05 ± 0.01	0.05 ± 0.03	0.02 ± 0.01
Verrucomicrobia	*Prosthecobacter* (162)	0.20 ± 0.04	0.00 ± 0.00	0.02 ± 0.01	0.04 ± 0.02	0.05 ± 0.01	0.40 ± 0.02	0.10 ± 0.03
	Verrucomicrobium (903)	0.01 ± 0.01	0.00 ± 0.00	0.00 ± 0.00	0.01 ± 0.01	0.01 ± 0.00	0.11 ± 0.03	0.20 ± 0.05
	Uncultured DEV007 (1517)	0.00 ± 0.00	0.00 ± 0.00	0.00 ± 0.00	0.00 ± 0.00	0.00 ± 0.00	0.00 ± 0.00	0.10 ± 0.03
Unclassified	Uncultured bacterium (315)	0.01 ± 0.00	0.00 ± 0.00	0.01 ± 0.01	0.11 ± 0.04	0.42 ± 0.09	0.00 ± 0.00	0.00 ± 0.00

	Uncultured bacterium (255)	0.19 ± 0.02	0.00 ± 0.00	0.00 ± 0.00	0.01 ± 0.00	0.05 ± 0.02	0.03 ± 0.01	0.06 ± 0.05
						RNA		
Phylum/Subphylum-level	Genus-level (OTU No.)	0_0‘	0_3‘	0_5‘	40_3‘	40_5‘	400_3‘	400_5‘
Acidobacteria	*Bryobacter* (144)	0.06 ± 0.02	0.04 ± 0.01	0.15 ± 0.02	0.21 ± 0.01	0.21 ± 0.06	0.26 ± 0.02	0.12 ± 0.01
	Bryobacter (61)	0.27 ± 0.05	0.14 ± 0.06	0.51 ± 0.08	0.62 ± 0.03	0.33 ± 0.03	0.63 ± 0.01	0.52 ± 0.10
	Bryobacter (115)	0.11 ± 0.03	0.06 ± 0.03	0.55 ± 0.11	0.16 ± 0.02	0.29 ± 0.09	0.15 ± 0.06	0.28 ± 0.04
	Bryobacter (562)	0.01 ± 0.00	0.01 ± 0.00	0.03 ± 0.01	0.04 ± 0.01	0.04 ± 0.00	0.08 ± 0.02	0.13 ± 0.03
	Uncultured subgroup_3 (901)	0.02 ± 0.01	0.00 ± 0.00	0.03 ± 0.00	0.04 ± 0.01	0.02 ± 0.01	0.07 ± 0.02	0.04 ± 0.01
	Uncultured subgroup_3 (55)	0.47 ± 0.04	0.20 ± 0.13	0.81 ± 0.01	0.39 ± 0.03	0.33 ± 0.08	0.66 ± 0.05	0.65 ± 0.14
	Uncultured subgroup_3 (516)	0.04 ± 0.00	0.01 ± 0.01	0.06 ± 0.01	0.09 ± 0.01	0.04 ± 0.01	0.09 ± 0.00	0.08 ± 0.01
	Blastocatella (126)	0.03 ± 0.01	0.03 ± 0.01	0.05 ± 0.01	0.03 ± 0.01	0.05 ± 0.02	0.05 ± 0.02	0.12 ± 0.02
	Uncultured subgroup_6 (85)	0.00 ± 0.01	0.02 ± 0.00	0.02 ± 0.01	0.07 ± 0.02	0.06 ± 0.01	0.06 ± 0.03	0.47 ± 0.16
	Uncultured subgroup_6 (10)	0.14 ± 0.02	0.18 ± 0.04	1.21 ± 0.27	0.79 ± 0.07	1.34 ± 0.18	0.94 ± 0.24	1.56 ± 0.44
	Uncultured subgroup_6 (212)	0.03 ± 0.01	0.01 ± 0.00	0.15 ± 0.02	0.21 ± 0.05	0.23 ± 0.01	0.25 ± 0.10	0.14 ± 0.05
	Uncultured subgroup_6 (304)	0.01 ± 0.00	0.02 ± 0.00	0.06 ± 0.00	0.15 ± 0.03	0.19 ± 0.05	0.09 ± 0.01	0.12 ± 0.04
	Uncultured subgroup_6 (401)	0.01 ± 0.00	0.01 ± 0.00	0.04 ± 0.02	0.06 ± 0.01	0.06 ± 0.01	0.07 ± 0.03	0.06 ± 0.01
	Uncultured subgroup_6 (581)	0.03 ± 0.02	0.00 ± 0.00	0.17 ± 0.05	0.08 ± 0.02	0.04 ± 0.01	0.05 ± 0.00	0.04 ± 0.01
	Uncultured subgroup_6 (412)	0.01 ± 0.00	0.01 ± 0.00	0.06 ± 0.01	0.04 ± 0.01	0.08 ± 0.00	0.06 ± 0.00	0.03 ± 0.01
	Uncultured subgroup_6 (147)	0.01 ± 0.00	0.06 ± 0.02	0.01 ± 0.00	0.06 ± 0.02	0.15 ± 0.04	0.09 ± 0.01	0.08 ± 0.02
	Uncultured subgroup_6 (85)	0.00 ± 0.00	0.02 ± 0.00	0.02 ± 0.01	0.07 ± 0.02	0.06 ± 0.01	0.06 ± 0.03	0.47 ± 0.16
	Uncultured subgroup_17 (39)	0.07 ± 0.00	0.07 ± 0.03	0.41 ± 0.03	0.39 ± 0.05	0.34 ± 0.01	0.41 ± 0.09	0.30 ± 0.11
	Uncultured subgroup_22 (329)	0.03 ± 0.00	0.01 ± 0.00	0.10 ± 0.03	0.12 ± 0.03	0.21 ± 0.01	0.06 ± 0.01	0.06 ± 0.02
	Uncultured subgroup_22 (340)	0.03 ± 0.00	0.02 ± 0.02	0.24 ± 0.07	0.13 ± 0.03	0.10 ± 0.00	0.11 ± 0.02	0.05 ± 0.02
	Uncultured subgroup_22 (57)	0.10 ± 0.05	0.07 ± 0.03	0.47 ± 0.09	0.71 ± 0.25	0.43 ± 0.05	0.89 ± 0.18	0.54 ± 0.02
Actinobacteria	Uncultured Sva0996_marine_group (83)	0.01 ± 0.00	0.01 ± 0.00	0.05 ± 0.02	0.05 ± 0.01	0.12 ± 0.03	0.07 ± 0.02	0.09 ± 0.08
	Aeromicrobium (332)	0.00 ± 0.00	0.00 ± 0.00	0.00 ± 0.00	0.00 ± 0.00	0.01 ± 0.00	0.00 ± 0.00	0.04 ± 0.02
	Marmoricola (69)	0.04 ± 0.01	0.04 ± 0.01	0.03 ± 0.00	0.13 ± 0.02	0.13 ± 0.00	0.04 ± 0.00	0.12 ± 0.06
	Nocardioides (372)	0.01 ± 0.00	0.00 ± 0.01	0.00 ± 0.00	0.00 ± 0.00	0.00 ± 0.00	0.01 ± 0.00	0.01 ± 0.01
	Nocardioides (210)	0.00 ± 0.00	0.01 ± 0.00	0.01 ± 0.00	0.05 ± 0.01	0.09 ± 0.02	0.01 ± 0.01	0.08 ± 0.04
	Nocardioides (102)	0.03 ± 0.00	0.02 ± 0.01	0.03 ± 0.01	0.06 ± 0.02	0.02 ± 0.01	0.03 ± 0.01	0.04 ± 0.01

	Uncultured MB-A2-108 (94)	0.02 ± 0.00	0.01 ± 0.00	0.10 ± 0.01	0.17 ± 0.02	0.10 ± 0.01	0.14 ± 0.04	0.07 ± 0.02
	Iamia (188)	0.01 ± 0.00	0.01 ± 0.01	0.02 ± 0.01	0.12 ± 0.01	0.06 ± 0.01	0.14 ± 0.05	0.06 ± 0.01
	Iamia (362)	0.01 ± 0.00	0.00 ± 0.00	0.01 ± 0.00	0.02 ± 0.00	0.04 ± 0.01	0.00 ± 0.00	0.03 ± 0.01
	Uncultured Acidimicrobiales (1265)	0.00 ± 0.00	0.00 ± 0.00	0.00 ± 0.00	0.03 ± 0.01	0.00 ± 0.00	0.02 ± 0.02	0.00 ± 0.00
	Uncultured 480-2(627)	0.01 ± 0.01	0.00 ± 0.00	0.00 ± 0.00	0.02 ± 0.01	0.03 ± 0.01	0.01 ± 0.00	0.00 ± 0.00
	Solirubrobacter (29)	0.02 ± 0.01	0.01 ± 0.00	0.02 ± 0.01	0.07 ± 0.02	0.08 ± 0.00	0.03 ± 0.00	0.04 ± 0.01
	Sva0996_marine_group(441)	0.01 ± 0.00	0.01 ± 0.01	0.06 ± 0.02	0.12 ± 0.02	0.09 ± 0.02	0.15 ± 0.08	0.11 ± 0.03
	Flavobacterium (633)	0.00 ± 0.00	0.00 ± 0.00	0.00 ± 0.00	0.02 ± 0.00	0.00 ± 0.00	0.04 ± 0.02	0.00 ± 0.00
	Flavobacterium (2394)	0.00 ± 0.00	0.00 ± 0.00	0.00 ± 0.00	0.00 ± 0.00	0.00 ± 0.00	0.02 ± 0.02	0.00 ± 0.00
	Uncultured NS9_marine_group (438)	0.01 ± 0.01	0.01 ± 0.01	0.05 ± 0.02	0.03 ± 0.02	0.01 ± 0.00	0.13 ± 0.10	0.10 ± 0.06
	Uncultured NS9_marine_group (277)	0.03 ± 0.01	0.02 ± 0.01	0.04 ± 0.01	0.04 ± 0.01	0.03 ± 0.01	0.21 ± 0.17	0.09 ± 0.03
	Rhodococcus (459)	0.00 ± 0.00	0.00 ± 0.00	0.07 ± 0.01	0.05 ± 0.04	0.08 ± 0.03	0.08 ± 0.02	0.10 ± 0.04
	Fodinicola (15)	0.13 ± 0.04	0.13 ± 0.06	0.28 ± 0.02	0.59 ± 0.02	0.38 ± 0.06	0.55 ± 0.01	0.19 ± 0.05
	Nocardioides (405)	0.01 ± 0.00	0.01 ± 0.00	0.02 ± 0.01	0.01 ± 0.00	0.01 ± 0.00	0.01 ± 0.01	0.02 ± 0.01
	Uncultured Acidimicrobiales (612)	0.01 ± 0.00	0.00 ± 0.00	0.07 ± 0.02	0.07 ± 0.01	0.02 ± 0.01	0.03 ± 0.01	0.03 ± 0.01
	Uncultured Actinobacteria (359)	0.01 ± 0.01	0.01 ± 0.00	0.02 ± 0.01	0.07 ± 0.01	0.01 ± 0.01	0.05 ± 0.01	0.02 ± 0.02
	Uncultured MB-A2-108 (137)	0.03 ± 0.01	0.01 ± 0.01	0.12 ± 0.01	0.23 ± 0.03	0.13 ± 0.03	0.22 ± 0.03	0.06 ± 0.01
	CL500-29_marine_group (28)	0.02 ± 0.01	0.05 ± 0.01	0.04 ± 0.01	0.10 ± 0.01	0.12 ± 0.00	0.13 ± 0.01	1.34 ± 0.14
	Uncultured Acidimicrobiales (569)	0.01 ± 0.00	0.01 ± 0.00	0.00 ± 0.00	0.07 ± 0.01	0.03 ± 0.01	0.04 ± 0.02	0.00 ± 0.00
	Uncultured *Intrasporangiaceae* (19)	0.07 ± 0.02	0.17 ± 0.03	0.06 ± 0.01	0.19 ± 0.02	0.15 ± 0.01	0.16 ± 0.01	0.10 ± 0.02
	Gaiella (45)	0.05 ± 0.01	0.11 ± 0.06	0.13 ± 0.01	0.24 ± 0.02	0.43 ± 0.02	0.16 ± 0.01	0.19 ± 0.04
Armatimonadetes	Uncultured Armatimonadetes (371)	0.00 ± 0.00	0.00 ± 0.00	0.00 ± 0.00	0.00 ± 0.00	0.03 ± 0.02	0.00 ± 0.00	0.18 ± 0.01
Bacteroidetes	*Chryseolinea* (165)	0.01 ± 0.00	0.00 ± 0.00	0.02 ± 0.01	0.05 ± 0.01	0.02 ± 0.01	0.03 ± 0.01	0.03 ± 0.00
	Chryseolinea (483)	0.01 ± 0.00	0.01 ± 0.01	0.00 ± 0.00	0.02 ± 0.00	0.02 ± 0.01	0.02 ± 0.00	0.01 ± 0.01
	Chryseolinea (231)	0.04 ± 0.01	0.02 ± 0.01	0.01 ± 0.00	0.06 ± 0.01	0.03 ± 0.01	0.05 ± 0.02	0.03 ± 0.00
	Chryseolinea (1195)	0.02 ± 0.01	0.00 ± 0.00	0.01 ± 0.00	0.01 ± 0.01	0.00 ± 0.00	0.01 ± 0.00	0.00 ± 0.00
	Uncultured *Rhodothermaceae* (363)	0.00 ± 0.00	0.00 ± 0.00	0.00 ± 0.00	0.01 ± 0.00	0.12 ± 0.02	0.02 ± 0.01	0.09 ± 0.07
	Ferruginibacter (499)	0.00 ± 0.00	0.01 ± 0.01	0.00 ± 0.00	0.02 ± 0.01	0.01 ± 0.01	0.04 ± 0.02	0.06 ± 0.02
	Ferruginibacter (378)	0.01 ± 0.01	0.00 ± 0.00	0.00 ± 0.00	0.02 ± 0.00	0.01 ± 0.00	0.02 ± 0.01	0.04 ± 0.02
	Flavobacterium (2394)	0.00 ± 0.00	0.00 ± 0.00	0.00 ± 0.00	0.00 ± 0.00	0.00 ± 0.00	0.02 ± 0.02	0.00 ± 0.00

	Flavobacterium (376)	0.00 ± 0.00	0.00 ± 0.00	0.00 ± 0.00	0.04 ± 0.01	0.01 ± 0.01	0.01 ± 0.00	0.00 ± 0.00
	Uncultured *Cytophagaceae* (451)	0.00 ± 0.00	0.01 ± 0.00	0.01 ± 0.00	0.01 ± 0.01	0.00 ± 0.00	0.00 ± 0.00	0.01 ± 0.00
	Ferruginibacter (256)	0.01 ± 0.00	0.02 ± 0.01	0.01 ± 0.00	0.03 ± 0.01	0.02 ± 0.00	0.02 ± 0.00	0.06 ± 0.02
	Uncultured *Saprospiraceae* (380)	0.00 ± 0.00	0.01 ± 0.01	0.03 ± 0.02	0.03 ± 0.00	0.04 ± 0.02	0.09 ± 0.04	0.12 ± 0.04
	Uncultured *Saprospiraceae* (383)	0.00 ± 0.00	0.00 ± 0.00	0.00 ± 0.00	0.01 ± 0.00	0.02 ± 0.01	0.01 ± 0.01	0.01 ± 0.00
	Uncultured *Saprospiraceae* (472)	0.00 ± 0.00	0.00 ± 0.00	0.00 ± 0.00	0.01 ± 0.00	0.01 ± 0.00	0.03 ± 0.02	0.10 ± 0.05
	Uncultured Sphingobacteriales (711)	0.00 ± 0.00	0.00 ± 0.00	0.00 ± 0.00	0.00 ± 0.00	0.00 ± 0.00	0.01 ± 0.01	0.01 ± 0.01
	Uncultured env.OPS_17 (726)	0.00 ± 0.00	0.00 ± 0.00	0.00 ± 0.00	0.01 ± 0.00	0.00 ± 0.00	0.05 ± 0.01	0.00 ± 0.00
	Uncultured env.OPS_17 (876)	0.00 ± 0.00	0.00 ± 0.00	0.00 ± 0.00	0.02 ± 0.00	0.00 ± 0.00	0.02 ± 0.00	0.00 ± 0.00
	Uncultured env.OPS_17 (548)	0.03 ± 0.01	0.00 ± 0.00	0.02 ± 0.00	0.01 ± 0.00	0.20 ± 0.00	0.00 ± 0.00	0.55 ± 0.51
	Uncultured KD3-93 (46)	0.00 ± 0.00	0.00 ± 0.00	0.01 ± 0.01	0.69 ± 0.15	0.05 ± 0.00	2.92 ± 1.93	0.32 ± 0.16
	NS11-12_marine_group (616)	0.00 ± 0.00	0.00 ± 0.00	0.00 ± 0.00	0.01 ± 0.00	0.01 ± 0.00	0.02 ± 0.01	0.01 ± 0.01
	PHOS-HE51 (1186)	0.00 ± 0.00	0.00 ± 0.00	0.00 ± 0.00	0.00 ± 0.00	0.00 ± 0.00	0.03 ± 0.02	0.05 ± 0.01
	Uncultured Sphingobacteriales (409)	0.00 ± 0.00	0.00 ± 0.00	0.00 ± 0.00	0.00 ± 0.00	0.12 ± 0.07	0.02 ± 0.01	0.41 ± 0.16
	Terrimonas (139)	0.01 ± 0.00	0.01 ± 0.00	0.00 ± 0.00	0.02 ± 0.01	0.01 ± 0.00	0.02 ± 0.01	0.06 ± 0.03
	Terrimonas (149)	0.01 ± 0.00	0.01 ± 0.00	0.01 ± 0.01	0.02 ± 0.01	0.00 ± 0.00	0.03 ± 0.01	0.02 ± 0.01
	Terrimonas (253)	0.02 ± 0.01	0.02 ± 0.00	0.03 ± 0.01	0.03 ± 0.01	0.02 ± 0.01	0.03 ± 0.01	0.01 ± 0.01
Cand_div_BRC1	Uncultured Candidate_div_BRC1 (542)	0.01 ± 0.00	0.00 ± 0.00	0.13 ± 0.08	0.22 ± 0.10	0.03 ± 0.01	0.05 ± 0.03	0.01 ± 0.00
	Uncultured Candidate_div_BRC1 (1346)	0.00 ± 0.00	0.00 ± 0.00	0.04 ± 0.02	0.09 ± 0.04	0.00 ± 0.00	0.02 ± 0.01	0.03 ± 0.02
Gemmatimonadetes	Uncultured *Gemmatimonadaceae* (124)	0.01 ± 0.01	0.01 ± 0.01	0.14 ± 0.03	0.32 ± 0.06	0.23 ± 0.05	0.29 ± 0.03	0.26 ± 0.05
	Uncultured *Gemmatimonadaceae* (32)	0.03 ± 0.01	0.06 ± 0.05	0.21 ± 0.03	0.77 ± 0.17	0.67 ± 0.12	0.64 ± 0.07	0.14 ± 0.03
	Uncultured *Gemmatimonadaceae* (52)	0.02 ± 0.00	0.06 ± 0.04	0.28 ± 0.03	0.57 ± 0.10	0.56 ± 0.05	0.46 ± 0.09	0.37 ± 0.04
	Uncultured *Gemmatimonadaceae* (251)	0.01 ± 0.01	0.01 ± 0.00	0.07 ± 0.02	0.22 ± 0.05	0.18 ± 0.04	0.28 ± 0.07	0.08 ± 0.01
	Uncultured *Gemmatimonadaceae* (269)	0.02 ± 0.00	0.00 ± 0.00	0.09 ± 0.02	0.15 ± 0.03	0.11 ± 0.01	0.17 ± 0.03	0.12 ± 0.03
	Uncultured *Gemmatimonadaceae* (299)	0.00 ± 0.00	0.01 ± 0.00	0.01 ± 0.00	0.05 ± 0.01	0.15 ± 0.02	0.09 ± 0.07	0.10 ± 0.08
	Uncultured *Gemmatimonadaceae* (388)	0.02 ± 0.00	0.01 ± 0.01	0.06 ± 0.03	0.09 ± 0.00	0.11 ± 0.00	0.09 ± 0.02	0.05 ± 0.04
Chlorobi	Uncultured BSV26 (580)	0.05 ± 0.02	0.01 ± 0.01	0.06 ± 0.01	0.06 ± 0.02	0.04 ± 0.02	0.05 ± 0.00	0.02 ± 0.01
	Uncultured BSV26 (93)	0.02 ± 0.01	0.01 ± 0.00	0.05 ± 0.01	0.06 ± 0.01	0.04 ± 0.02	0.04 ± 0.00	0.03 ± 0.01
	Uncultured BSV26 (413)	0.03 ± 0.02	0.02 ± 0.01	0.02 ± 0.01	0.06 ± 0.01	0.05 ± 0.00	0.08 ± 0.00	0.06 ± 0.01
	Uncultured OPB56 (740)	0.02 ± 0.01	0.00 ± 0.00	0.05 ± 0.02	0.12 ± 0.02	0.01 ± 0.00	0.13 ± 0.11	0.03 ± 0.01

	Uncultured SJA-28 (284)	0.02 ± 0.00	0.02 ± 0.01	0.03 ± 0.01	0.01 ± 0.00	0.01 ± 0.00	0.00 ± 0.00	0.02 ± 0.01
Chloroflexi	Uncultured *Caldilineaceae* (110)	0.01 ± 0.00	0.01 ± 0.00	0.22 ± 0.05	0.12 ± 0.01	0.03 ± 0.02	0.05 ± 0.02	0.10 ± 0.02
	Uncultured KD4-96 (27)	0.05 ± 0.01	0.07 ± 0.02	0.16 ± 0.04	0.39 ± 0.05	0.26 ± 0.02	0.30 ± 0.04	0.39 ± 0.00
	Uncultured *Anaerolineaceae* (233)	0.02 ± 0.01	0.01 ± 0.01	0.08 ± 0.03	0.06 ± 0.02	0.21 ± 0.00	0.05 ± 0.00	0.14 ± 0.03
	Uncultured *Anaerolineaceae* (611)	0.00 ± 0.00	0.00 ± 0.00	0.01 ± 0.00	0.01 ± 0.00	0.06 ± 0.02	0.00 ± 0.00	0.12 ± 0.03
	Uncultured *Anaerolineaceae* (628)	0.00 ± 0.00	0.01 ± 0.00	0.02 ± 0.01	0.02 ± 0.00	0.11 ± 0.00	0.00 ± 0.00	0.06 ± 0.03
	Unclassified Gitt-GS-136 (127)	0.01 ± 0.00	0.02 ± 0.01	0.05 ± 0.01	0.08 ± 0.02	0.14 ± 0.05	0.04 ± 0.01	0.10 ± 0.04
	Uncultured KD4-96 (96)	0.04 ± 0.00	0.02 ± 0.01	0.06 ± 0.02	0.11 ± 0.01	0.14 ± 0.02	0.12 ± 0.02	0.08 ± 0.01
	Unclassified JG30-KF-CM45 (145)	0.01 ± 0.01	0.02 ± 0.01	0.08 ± 0.02	0.10 ± 0.01	0.16 ± 0.01	0.24 ± 0.16	0.27 ± 0.11
	Uncultured KD4-96 (8)	0.26 ± 0.05	0.32 ± 0.12	0.48 ± 0.12	1.35 ± 0.08	0.45 ± 0.00	1.13 ± 0.08	0.47 ± 0.06
	Uncultured KD4-96 (16)	0.11 ± 0.03	0.16 ± 0.02	0.16 ± 0.07	0.62 ± 0.05	0.48 ± 0.08	0.49 ± 0.08	0.54 ± 0.02
Latescibacteria	Uncultured Latescibacteria (95)	0.06 ± 0.03	0.01 ± 0.00	0.51 ± 0.15	0.57 ± 0.11	0.27 ± 0.03	0.49 ± 0.06	0.25 ± 0.11
	Uncultured Latescibacteria (154)	0.01 ± 0.00	0.00 ± 0.00	0.35 ± 0.12	0.40 ± 0.05	0.23 ± 0.08	0.35 ± 0.03	0.31 ± 0.15
	Uncultured Latescibacteria (308)	0.01 ± 0.00	0.01 ± 0.01	0.01 ± 0.01	0.04 ± 0.01	0.12 ± 0.05	0.03 ± 0.01	0.20 ± 0.07
	Uncultured Latescibacteria (326)	0.02 ± 0.01	0.00 ± 0.00	0.11 ± 0.03	0.18 ± 0.02	0.14 ± 0.06	0.13 ± 0.00	0.08 ± 0.03
	Uncultured Latescibacteria (342)	0.04 ± 0.02	0.02 ± 0.01	0.08 ± 0.01	0.13 ± 0.05	0.11 ± 0.01	0.04 ± 0.00	0.07 ± 0.02
	Uncultured Latescibacteria (453)	0.00 ± 0.00	0.01 ± 0.00	0.13 ± 0.01	0.09 ± 0.02	0.09 ± 0.01	0.08 ± 0.01	0.07 ± 0.02
	Uncultured Latescibacteria (503)	0.02 ± 0.01	0.00 ± 0.00	0.11 ± 0.03	0.13 ± 0.03	0.08 ± 0.00	0.10 ± 0.02	0.06 ± 0.03
	Uncultured Latescibacteria (534)	0.01 ± 0.00	0.00 ± 0.00	0.04 ± 0.01	0.05 ± 0.01	0.16 ± 0.05	0.01 ± 0.01	0.03 ± 0.02
	Uncultured Latescibacteria (706)	0.02 ± 0.01	0.00 ± 0.00	0.19 ± 0.01	0.07 ± 0.01	0.02 ± 0.00	0.04 ± 0.01	0.02 ± 0.00
	Uncultured Latescibacteria (732)	0.00 ± 0.00	0.00 ± 0.00	0.09 ± 0.02	0.10 ± 0.03	0.06 ± 0.03	0.04 ± 0.00	0.02 ± 0.01
	Uncultured Latescibacteria (864)	0.02 ± 0.00	0.00 ± 0.00	0.02 ± 0.00	0.05 ± 0.01	0.09 ± 0.02	0.06 ± 0.01	0.05 ± 0.01
	Uncultured Latescibacteria (422)	0.01 ± 0.00	0.00 ± 0.00	0.28 ± 0.06	0.10 ± 0.02	0.06 ± 0.00	0.07 ± 0.01	0.04 ± 0.02
	Uncultured Latescibacteria (1054)	0.00 ± 0.00	0.00 ± 0.00	0.04 ± 0.01	0.05 ± 0.01	0.04 ± 0.00	0.02 ± 0.01	0.02 ± 0.01
Nitrospirae	*Nitrospira* (7)	0.79 ± 0.18	0.47 ± 0.09	1.02 ± 0.09	0.89 ± 0.12	1.57 ± 0.20	2.32 ± 0.61	1.44 ± 0.22
	Nitrospira (23)	0.49 ± 0.04	0.39 ± 0.08	1.86 ± 0.58	0.77 ± 0.12	1.51 ± 0.17	0.74 ± 0.07	0.80 ± 0.20
	Nitrospira (26)	0.52 ± 0.02	0.61 ± 0.03	1.36 ± 0.13	1.16 ± 0.16	0.73 ± 0.12	0.91 ± 0.38	0.42 ± 0.21
Alphaproteobacteria	*Sphingobium* (17)	0.00 ± 0.00	0.00 ± 0.00	0.00 ± 0.00	0.12 ± 0.11	0.05 ± 0.00	0.03 ± 0.02	0.02 ± 0.01
	Hyphomicrobium (60)	0.22 ± 0.04	0.23 ± 0.02	0.44 ± 0.08	0.27 ± 0.06	0.38 ± 0.06	0.22 ± 0.02	0.59 ± 0.10
	Hyphomicrobium (347)	0.00 ± 0.00	0.00 ± 0.00	0.16 ± 0.04	0.08 ± 0.01	0.13 ± 0.06	0.09 ± 0.01	0.19 ± 0.06

	Hirschia (62)	0.09 ± 0.01	0.16 ± 0.06	0.34 ± 0.11	0.15 ± 0.00	0.55 ± 0.01	0.14 ± 0.01	1.18 ± 0.76
	Novosphingobium (64)	0.01 ± 0.01	0.01 ± 0.00	0.01 ± 0.00	0.01 ± 0.00	0.62 ± 0.10	0.14 ± 0.01	0.03 ± 0.02
	Pedomicrobium (84)	0.09 ± 0.02	0.07 ± 0.02	0.15 ± 0.03	0.21 ± 0.03	0.08 ± 0.00	0.30 ± 0.00	0.48 ± 0.22
	Uncultured Rhizobiales (335)	0.01 ± 0.00	0.02 ± 0.01	0.03 ± 0.01	0.01 ± 0.00	0.03 ± 0.02	0.01 ± 0.01	0.04 ± 0.04
	Defluviimonas (202)	0.06 ± 0.01	0.05 ± 0.01	0.09 ± 0.02	0.07 ± 0.01	0.04 ± 0.01	0.03 ± 0.01	0.11 ± 0.04
	Hyphomicrobium (129)	0.11 ± 0.01	0.06 ± 0.01	0.15 ± 0.02	0.22 ± 0.02	0.14 ± 0.01	0.23 ± 0.01	0.22 ± 0.14
	Uncultured AKYH478 (645)	0.01 ± 0.00	0.01 ± 0.01	0.00 ± 0.00	0.01 ± 0.01	0.01 ± 0.01	0.03 ± 0.00	0.12 ± 0.05
	Uncultured F0723 (1059)	0.03 ± 0.00	0.02 ± 0.00	0.00 ± 0.00	0.00 ± 0.00	0.00 ± 0.00	0.03 ± 0.01	0.09 ± 0.04
	Uncultured MNG7 (35)	0.15 ± 0.01	0.17 ± 0.02	0.12 ± 0.01	0.11 ± 0.01	0.09 ± 0.02	0.13 ± 0.01	0.24 ± 0.07
	Uncultured *Phyllobacteriaceae* (87)	0.09 ± 0.01	0.20 ± 0.04	0.05 ± 0.00	0.02 ± 0.01	0.05 ± 0.03	0.09 ± 0.06	0.48 ± 0.13
	Uncultured *Sphingomonadaceae* (1)	0.09 ± 0.02	0.10 ± 0.01	0.06 ± 0.02	3.26 ± 0.56	0.28 ± 0.01	7.71 ± 4.09	4.41 ± 0.57
	Uncultured *Sphingomonadaceae* (119)	0.00 ± 0.00	0.01 ± 0.00	0.01 ± 0.00	0.03 ± 0.01	0.08 ± 0.06	0.02 ± 0.01	0.08 ± 0.01
	Sphingopyxis (553)	0.02 ± 0.00	0.04 ± 0.01	0.02 ± 0.00	0.02 ± 0.01	0.00 ± 0.00	0.01 ± 0.01	0.01 ± 0.01
	Woodsholea (181)	0.03 ± 0.00	0.02 ± 0.01	0.09 ± 0.02	0.07 ± 0.00	0.22 ± 0.05	0.06 ± 0.00	0.06 ± 0.03
	Woodsholea (183)	0.02 ± 0.01	0.07 ± 0.01	0.10 ± 0.02	0.08 ± 0.02	0.11 ± 0.03	0.05 ± 0.02	0.12 ± 0.05
	Woodsholea (615)	0.02 ± 0.01	0.02 ± 0.01	0.05 ± 0.02	0.02 ± 0.00	0.02 ± 0.01	0.02 ± 0.00	0.02 ± 0.02
	Uncultured *Rhizobiaceae* (100)	0.04 ± 0.03	0.07 ± 0.01	0.03 ± 0.01	0.08 ± 0.02	0.10 ± 0.05	0.02 ± 0.00	0.26 ± 0.20
	Uncultured AKYH478 (645)	0.01 ± 0.00	0.01 ± 0.01	0.00 ± 0.00	0.01 ± 0.01	0.01 ± 0.01	0.03 ± 0.00	0.12 ± 0.05
	Defluviimonas (202)	0.06 ± 0.01	0.05 ± 0.01	0.09 ± 0.02	0.07 ± 0.01	0.04 ± 0.01	0.03 ± 0.01	0.11 ± 0.04
Deltaproteobacteria	*Bdellovibrio* (63)	0.01 ± 0.00	0.00 ± 0.00	0.00 ± 0.00	0.98 ± 0.42	0.01 ± 0.00	0.16 ± 0.04	0.26 ± 0.19
	Haliangium (479)	0.01 ± 0.00	0.00 ± 0.00	0.07 ± 0.01	0.07 ± 0.01	0.07 ± 0.02	0.02 ± 0.01	0.02 ± 0.00
	Haliangium (248)	0.00 ± 0.00	0.00 ± 0.00	0.00 ± 0.00	0.05 ± 0.01	0.27 ± 0.12	0.02 ± 0.01	0.39 ± 0.19
	Haliangium (457)	0.00 ± 0.00	0.00 ± 0.00	0.04 ± 0.02	0.08 ± 0.02	0.13 ± 0.00	0.05 ± 0.03	0.03 ± 0.02
	Haliangium (739)	0.01 ± 0.00	0.00 ± 0.00	0.04 ± 0.02	0.07 ± 0.01	0.04 ± 0.02	0.05 ± 0.02	0.03 ± 0.01
	OM27-Clade (166)	0.02 ± 0.00	0.02 ± 0.01	0.02 ± 0.00	0.11 ± 0.02	0.01 ± 0.01	0.61 ± 0.46	0.47 ± 0.37
	Anaeromyxobacter (220)	0.05 ± 0.01	0.05 ± 0.01	0.12 ± 0.03	0.20 ± 0.04	0.24 ± 0.07	0.18 ± 0.01	0.18 ± 0.01
	Anaeromyxobacter (82)	0.16 ± 0.00	0.15 ± 0.05	0.29 ± 0.08	0.53 ± 0.09	0.45 ± 0.06	0.59 ± 0.07	0.17 ± 0.06
	Sandaracinus (260)	0.01 ± 0.00	0.00 ± 0.00	0.07 ± 0.01	0.25 ± 0.08	0.16 ± 0.01	0.07 ± 0.06	0.18 ± 0.13
	Sandaracinus (382)	0.01 ± 0.00	0.00 ± 0.00	0.09 ± 0.01	0.26 ± 0.06	0.01 ± 0.00	0.06 ± 0.04	0.02 ± 0.02
	Sorangium (709)	0.00 ± 0.00	0.00 ± 0.00	0.17 ± 0.02	0.10 ± 0.02	0.10 ± 0.04	0.04 ± 0.01	0.01 ± 0.01

	Sorangium (1348)	0.00 ± 0.00	0.00 ± 0.00	0.06 ± 0.02	0.06 ± 0.01	0.01 ± 0.00	0.00 ± 0.00	0.00 ± 0.00
	Sorangium (352)	0.00 ± 0.00	0.00 ± 0.00	0.03 ± 0.01	0.03 ± 0.00	0.36 ± 0.10	0.00 ± 0.00	0.26 ± 0.12
	Uncultured *Cystobacteraceae* (203)	0.05 ± 0.00	0.03 ± 0.00	0.21 ± 0.03	0.12 ± 0.04	0.05 ± 0.01	0.21 ± 0.04	0.27 ± 0.09
	Uncultured *Sandaracinaceae* (33)	0.01 ± 0.01	0.00 ± 0.00	0.73 ± 0.08	1.20 ± 0.17	1.50 ± 0.17	0.44 ± 0.14	0.21 ± 0.04
	Uncultured *Sandaracinaceae* (404)	0.00 ± 0.00	0.00 ± 0.00	0.07 ± 0.01	0.21 ± 0.05	0.09 ± 0.01	0.02 ± 0.00	0.01 ± 0.00
	Uncultured *Sandaracinaceae* (686)	0.00 ± 0.00	0.00 ± 0.00	0.00 ± 0.00	0.11 ± 0.03	0.00 ± 0.01	0.04 ± 0.02	0.00 ± 0.00
	Uncultured *Sandaracinaceae* (240)	0.00 ± 0.00	0.00 ± 0.00	0.07 ± 0.02	0.18 ± 0.04	0.28 ± 0.01	0.14 ± 0.00	0.11 ± 0.04
	Uncultured *Sandaracinaceae* (764)	0.00 ± 0.00	0.00 ± 0.00	0.01 ± 0.00	0.03 ± 0.01	0.13 ± 0.03	0.00 ± 0.00	0.00 ± 0.00
	Uncultured Sh765B-TzT-29 (414)	0.00 ± 0.00	0.00 ± 0.00	0.03 ± 0.00	0.02 ± 0.01	0.05 ± 0.01	0.02 ± 0.00	0.05 ± 0.01
	Uncultured δ-bacteria (105)	0.00 ± 0.00	0.00 ± 0.00	0.00 ± 0.00	0.00 ± 0.01	0.00 ± 0.00	0.00 ± 0.00	0.21 ± 0.15
	Uncultured δ-bacteria (54)	0.00 ± 0.00	0.00 ± 0.00	0.00 ± 0.00	0.01 ± 0.00	0.28 ± 0.21	0.00 ± 0.00	0.18 ± 0.11
	Phaselicystis (163)	0.00 ± 0.00	0.00 ± 0.00	0.00 ± 0.00	0.00 ± 0.00	0.00 ± 0.00	0.00 ± 0.00	0.30 ± 0.28
Gammaproteobacteria (Betaproteobacterales)	*Hydrogenophaga* (9)	0.01 ± 0.00	0.01 ± 0.00	0.10 ± 0.01	0.24 ± 0.02	0.61 ± 0.01	0.24 ± 0.14	1.11 ± 0.14
	Leeia (513)	0.05 ± 0.01	0.02 ± 0.01	0.03 ± 0.01	0.15 ± 0.06	0.05 ± 0.03	0.02 ± 0.00	0.01 ± 0.01
	Piscinibacter (14)	0.17 ± 0.02	0.07 ± 0.03	0.65 ± 0.23	0.48 ± 0.06	1.27 ± 0.19	0.46 ± 0.01	1.76 ± 0.44
	Rhizobacter (123)	0.01 ± 0.00	0.01 ± 0.00	0.20 ± 0.07	0.12 ± 0.03	0.09 ± 0.02	0.26 ± 0.11	0.17 ± 0.06
	Uncultured *Comamonadaceae* (4)	0.28 ± 0.06	0.23 ± 0.03	0.90 ± 0.18	0.71 ± 0.11	1.35 ± 0.21	1.03 ± 0.01	2.70 ± 0.48
	Uncultured *Comamonadaceae* (36)	0.03 ± 0.02	0.02 ± 0.00	0.29 ± 0.09	0.25 ± 0.05	0.64 ± 0.10	0.49 ± 0.13	1.98 ± 0.36
	Uncultured *Comamonadaceae* (113)	0.01 ± 0.00	0.01 ± 0.00	0.00 ± 0.00	0.09 ± 0.05	0.09 ± 0.05	0.38 ± 0.31	0.30 ± 0.15
	Uncultured *Comamonadaceae* (152)	0.06 ± 0.02	0.02 ± 0.01	0.14 ± 0.04	0.13 ± 0.02	0.26 ± 0.01	0.18 ± 0.01	0.65 ± 0.23
	Uncultured *Comamonadaceae* (1113)	0.01 ± 0.00	0.00 ± 0.00	0.00 ± 0.00	0.01 ± 0.00	0.03 ± 0.03	0.13 ± 0.01	0.01 ± 0.01
	Uncultured *Comamonadaceae* (12)	0.6 ± 0.07	0.51 ± 0.07	0.91 ± 0.21	0.51 ± 0.03	1.01 ± 0.14	0.65 ± 0.11	1.58 ± 0.34
	Azohydromonas (43)	0.07 ± 0.02	0.03 ± 0.01	0.16 ± 0.04	0.11 ± 0.01	0.11 ± 0.03	0.14 ± 0.00	0.47 ± 0.09
	Uncultured *Gallionellaceae* (320)	0.06 ± 0.03	0.10 ± 0.01	0.07 ± 0.02	0.08 ± 0.01	0.03 ± 0.00	0.05 ± 0.02	0.02 ± 0.01
	Uncultured *Nitrosomonadaceae* (20)	0.07 ± 0.03	0.05 ± 0.02	0.06 ± 0.01	0.09 ± 0.02	0.13 ± 0.04	0.14 ± 0.01	0.21 ± 0.06
	Uncultured *Nitrosomonadaceae* (350)	0.01 ± 0.01	0.03 ± 0.02	0.01 ± 0.00	0.01 ± 0.01	0.01 ± 0.01	0.00 ± 0.00	0.04 ± 0.03
	Uncultured *Nitrosomonadaceae* (92)	0.04 ± 0.03	0.04 ± 0.01	0.03 ± 0.02	0.03 ± 0.01	0.04 ± 0.00	0.03 ± 0.01	0.05 ± 0.02
	Uncultured *Oxalobacteraceae* (215)	0.00 ± 0.00	0.00 ± 0.00	0.00 ± 0.00	0.07 ± 0.05	0.03 ± 0.01	0.03 ± 0.01	0.01 ± 0.00
	Vogesella (44)	0.00 ± 0.00	0.00 ± 0.00	0.00 ± 0.00	0.00 ± 0.00	0.00 ± 0.00	0.00 ± 0.00	0.00 ± 0.00
	Dechloromonas (138)	0.05 ± 0.00	0.04 ± 0.01	0.04 ± 0.00	0.03 ± 0.00	0.01 ± 0.00	0.04 ± 0.00	0.02 ± 0.01

	Thauera (40)	0.01 ± 0.00	0.01 ± 0.01	0.02 ± 0.00	0.02 ± 0.01	0.00 ± 0.00	0.04 ± 0.00	0.02 ± 0.01
	Uncultured SC-I-84 (89)	0.05 ± 0.01	0.02 ± 0.02	0.06 ± 0.01	0.09 ± 0.01	0.04 ± 0.01	0.19 ± 0.05	0.13 ± 0.03
	Uncultured SC-I-84 (354)	0.01 ± 0.01	0.00 ± 0.00	0.01 ± 0.00	0.02 ± 0.01	0.01 ± 0.00	0.03 ± 0.02	0.03 ± 0.01
	Uncultured β-proteobacteria (66)	0.13 ± 0.07	0.07 ± 0.00	0.05 ± 0.00	0.19 ± 0.05	0.15 ± 0.00	0.30 ± 0.00	0.57 ± 0.10
	Zoogloea (266)	0.00 ± 0.00	0.00 ± 0.00	0.00 ± 0.00	0.00 ± 0.00	0.00 ± 0.00	0.00 ± 0.00	0.00 ± 0.00
	Acidiferrobacter (67)	0.36 ± 0.12	0.41 ± 0.10	0.18 ± 0.02	0.31 ± 0.03	0.23 ± 0.05	0.26 ± 0.04	0.10 ± 0.02
	Arenimonas (520)	0.00 ± 0.00	0.00 ± 0.00	0.01 ± 0.00	0.08 ± 0.01	0.07 ± 0.02	0.08 ± 0.00	0.01 ± 0.00
	Arenimonas (357)	0.00 ± 0.00	0.00 ± 0.00	0.01 ± 0.00	0.07 ± 0.01	0.00 ± 0.00	0.09 ± 0.03	0.02 ± 0.01
	Pseudomonas (24)	0.00 ± 0.00	0.02 ± 0.01	0.08 ± 0.01	0.33 ± 0.12	0.19 ± 0.02	0.21 ± 0.04	0.06 ± 0.01
	Unclutured *Pseudomonadaceae* (3)	0.00 ± 0.00	0.02 ± 0.01	0.00 ± 0.00	0.00 ± 0.00	0.00 ± 0.00	0.00 ± 0.00	0.00 ± 0.00
	Thermomonas (58)	0.02 ± 0.01	0.06 ± 0.02	0.05 ± 0.01	0.12 ± 0.03	0.19 ± 0.09	0.15 ± 0.03	0.09 ± 0.03
	Uncultured *Xanthomonadaceae* (70)	0.02 ± 0.00	0.07 ± 0.03	0.07 ± 0.02	0.14 ± 0.01	0.05 ± 0.02	0.03 ± 0.00	0.11 ± 0.03
	Uncultured γ-proteobacteria (452)	0.00 ± 0.00	0.00 ± 0.00	0.07 ± 0.02	0.14 ± 0.03	0.07 ± 0.03	0.06 ± 0.02	0.02 ± 0.01
	Uncultured γ-proteobacteria (541)	0.00 ± 0.00	0.00 ± 0.00	0.00 ± 0.00	0.13 ± 0.01	0.10 ± 0.01	0.00 ± 0.00	0.00 ± 0.00
	Uncultured γ-proteobacteria (505)	0.02 ± 0.02	0.04 ± 0.01	0.05 ± 0.02	0.05 ± 0.02	0.04 ± 0.01	0.07 ± 0.02	0.05 ± 0.01
	Uncultured γ-proteobacteria (715)	0.00 ± 0.00	0.00 ± 0.00	0.01 ± 0.01	0.05 ± 0.01	0.01 ± 0.00	0.07 ± 0.05	0.00 ± 0.00
	Uncultured γ-proteobacteria (1758)	0.00 ± 0.00	0.00 ± 0.00	0.00 ± 0.00	0.01 ± 0.01	0.00 ± 0.00	0.00 ± 0.00	0.00 ± 0.00
	Acidiferrobacter (196)	0.13 ± 0.06	0.13 ± 0.05	0.05 ± 0.02	0.07 ± 0.01	0.05 ± 0.00	0.06 ± 0.02	0.03 ± 0.00
Saccharibacteria	Uncultured Saccharibacteria (980)	0.00 ± 0.00	0.00 ± 0.00	0.00 ± 0.00	0.01 ± 0.00	0.01 ± 0.00	0.00 ± 0.00	0.00 ± 0.00
Verrucomicrobia	*Prosthecobacter* (162)	0.03 ± 0.01	0.02 ± 0.01	0.03 ± 0.00	0.10 ± 0.02	0.07 ± 0.04	0.57 ± 0.04	0.09 ± 0.02
	Verrucomicrobium (903)	0.00 ± 0.00	0.00 ± 0.00	0.00 ± 0.00	0.01 ± 0.01	0.01 ± 0.01	0.11 ± 0.04	0.13 ± 0.02
	Uncultured DEV007 (1517)	0.00 ± 0.00	0.00 ± 0.00	0.00 ± 0.00	0.00 ± 0.00	0.00 ± 0.00	0.00 ± 0.00	0.10 ± 0.03
Unclassified	Uncultured bacterium (315)	0.00 ± 0.00	0.00 ± 0.00	0.00 ± 0.00	0.02 ± 0.00	0.16 ± 0.01	0.00 ± 0.00	0.00 ± 0.00
	Uncultured bacterium (255)	0.00 ± 0.00	0.00 ± 0.00	0.00 ± 0.00	0.01 ± 0.00	0.06 ± 0.04	0.02 ± 0.02	0.24 ± 0.21

Table A3. Bacterial OTUs enriched by metoprolol relative to unamended controls sampled simultaneously from samples incubated under oxic conditions, and closest cultured relatives of OTU representative 16S rRNA gene sequences. Significant (p-adj < 0.05) Log2-fold changes > 0 are reported as determined by Deseq2. 15 µM and 150 µM indicate metoprolol concentration.

Phylum/Subphylum-level	Genus-level (OTU No.)	Closest cultured relative	Acc. No[a]	[%][b]	Log2-fold Change	
					16S rRNA	
					15 µM	150 µM
Proteobacteria						
	Phenylobacterium (155)	*Phenylobacterium koreense*	NR_114055	97	6[c]	7
	Caulobacter (581)	*Caulobacter segnis*	LC500798	100	--[d]	5
	Sphingopyxis (913)	*Sphingopyxis chilensis*	MN684303	100	4	5
	Sphingomonas (90)	*Sphingomonas panni*	MH930068	100	3	4
	Sphingobium (486)	*Sphingobium xenophagum*	MK456509	100	--	3
Gammaproteobacteria	*Acinetobacter* (4)	*Acinetobacter guillouiae*	MH379731	100	--	12
	Pseudomonas (8)	*Pseudomonas stutzeri*	MN733041	100	--	3
	Rheinheimera (2462)	*Rheinheimera tilapiae*	NR_117918	97	--	5
	Aquabacterium (6)	*Aquabacterium olei*	CP029210	97	11	12
	Limnobacter (55)	*Limnobacter thiooxidans*	MF193773	100	8	9
	Ralstonia (122)	*Ralstonia pickettii*	MK231010	100	7	9
	Pelomonas (41)	*Pelomonas puraquae*	KF817703	100	6	7
	Albidiferax (189)	*Rhodoferax antarcticus*	CP019240	99	5	--
	Aquabacterium (206)	*Aquabacterium citratiphilum*	MN684290	100	3	5
	Thiomonas (246)	*Thiomonas intermedia*	CP002021	99	--	5
	Unc. Gammaproteobacteria (2279)	*Acinetobacter guillouiae*	MH379731	92	--	4
Bacteroidetes	*Flavobacterium* (265)	*Flavobacterium limicola*	NR_118473	98	--	3
	Flavobacterium (591)	*Flavobacterium terrigena*	NR_044006	99	6	6
	Hydrotalea (406)	*Hydrotalea flava*	JN999927	97	5	7

Table A4. Relative abundance of bacterial OTUs from the original microbial community enriched by different metoprolol treatments relative to unamended controls under oxic conditions. Only genera with a relative abundance > 0.01% are shown. Data represents the mean of triplicate samples in % of total rarified reads (uniform sequencing depth of 11,435 per sample) ± standard error of mean (SEM).

		16S rRNA gene						
Phylum/Subphylum	**Genus**	**0_0**	**0_65**	**0_120**	**15_65**	**15_120**	**150_65**	**150_120**
Alphaproteobacteria	*Phenylobacterium* (155)	0.00 ± 0.00	0.07 ± 0.02	0.07 ± 0.06	0.06 ± 0.03	0.06 ± 0.03	0.04 ± 0.02	0.06 ± 0.02
	Caulobacter (581)	0.01 ± 0.01	0.01 ± 0.01	0.01 ± 0.01	0.01 ± 0.01	0.02 ± 0.02	0.01 ± 0.01	0.01 ± 0.01
	Sphingopyxis (913)	0.01 ± 0.01	0.00 ± 0.00	0.01 ± 0.01	0.00 ± 0.00	0.01 ± 0.01	0.01 ± 0.00	0.00 ± 0.00
	Sphingomonas (90)	0.06 ± 0.02	0.14 ± 0.05	0.01 ± 0.01	0.04 ± 0.02	0.06 ± 0.04	0.05 ± 0.02	0.09 ± 0.01
	Sphingobium (486)	0.01 ± 0.01	0.01 ± 0.01	0.01 ± 0.01	0.01 ± 0.01	0.02 ± 0.01	0.01 ± 0.01	0.03 ± 0.01
Gammaproteobacteria	*Acinetobacter* (4)	12.62 ± 7.76	14.28 ± 1.37	14.16 ± 10.3	15.28 ± 1.29	22.53 ± 5.71	7.85 ± 4.10	19.12 ± 2.63
	Pseudomonas (8)	2.51 ± 1.46	4.88 ± 0.53	3.21 ± 0.18	7.04 ± 2.88	4.71 ± 0.63	1.91 ± 1.03	4.26 ± 0.17
	Rheinheimera (2462)	0.00 ± 0.00	0.00 ± 0.00	0.01 ± 0.01	0.00 ± 0.00	0.01 ± 0.01	0.00 ± 0.00	0.00 ± 0.00
	Aquabacterium (6)	2.94 ± 1.03	6.70 ± 0.72	6.31 ± 0.92	5.93 ± 0.11	9.62 ± 2.96	3.58 ± 1.97	5.50 ± 0.23
	Limnobacter (55)	0.08 ± 0.02	0.17 ± 0.02	0.07 ± 0.06	0.09 ± 0.05	0.23 ± 0.06	0.07 ± 0.04	0.18 ± 0.05
	Ralstonia (122)	0.01 ± 0.01	0.00 ± 0.00	0.09 ± 0.05	2.42 ± 2.39	0.21 ± 0.16	0.03 ± 0.02	0.05 ± 0.02
	Pelomonas (41)	0.01 ± 0.01	0.05 ± 0.02	0.19 ± 0.10	1.55 ± 1.47	0.22 ± 0.09	0.03 ± 0.01	0.09 ± 0.02
	Albidiferax (189)	0.03 ± 0.01	0.00 ± 0.00	0.00 ± 0.00	0.00 ± 0.00	0.00 ± 0.00	0.00 ± 0.00	0.00 ± 0.00
	Aquabacterium (206)	0.03 ± 0.01	0.05 ± 0.02	0.04 ± 0.01	0.03 ± 0.02	0.01 ± 0.01	0.02 ± 0.01	0.06 ± 0.02
	Thiomonas (246)	0.00 ± 0.00	0.00 ± 0.00	0.00 ± 0.00	0.00 ± 0.00	0.00 ± 0.00	0.00 ± 0.00	0.00 ± 0.00
	Unc. Gammaprot (2279)	0.00 ± 0.00	0.00 ± 0.00	0.00 ± 0.00	0.00 ± 0.00	0.00 ± 0.00	0.01 ± 0.01	0.00 ± 0.00
Bacteroidetes	*Flavobacterium* (265)	0.02 ± 0.01	0.04 ± 0.01	0.01 ± 0.01	0.02 ± 0.01	0.02 ± 0.01	0.03 ± 0.02	0.08 ± 0.04
	Flavobacterium (591)	0.01 ± 0.01	0.01 ± 0.01	0.02 ± 0.01	0.01 ± 0.01	0.01 ± 0.01	0.01 ± 0.01	0.01 ± 0.01
	Hydrotalea (406)	0.00 ± 0.00	0.03 ± 0.01	0.01 ± 0.01	0.01 ± 0.01	0.02 ± 0.01	0.01 ± 0.01	0.01 ± 0.01
		16S rRNA						
Alphaproteobacteria	*Phenylobacterium* (155)	0.00 ± 0.00	0.08 ± 0.00	0.08 ± 0.06	0.01 ± 0.01	0.09± 0.02	0.08 ± 0.01	0.13 ± 0.03
	Caulobacter (581)	0.01 ± 0.01	0.01 ± 0.01	0.01 ± 0.01	0.00 ± 0.00	0.00 ± 0.00	0.01 ± 0.01	0.03 ± 0.02
	Sphingopyxis (913)	0.00 ± 0.00	0.00 ± 0.00	0.00 ± 0.00	0.00 ± 0.00	0.03 ± 0.00	0.02 ± 0.01	0.00 ± 0.00
	Sphingomonas (90)	0.06 ± 0.03	0.13 ± 0.01	0.07 ± 0.05	0.04 ± 0.03	0.14 ± 0.06	0.14 ± 0.01	0.09 ± 0.01
	Sphingobium (486)	0.02 ± 0.02	0.01 ± 0.01	0.03 ± 0.01	0.00 ± 0.00	0.01 ± 0.01	0.02 ± 0.00	0.03 ± 0.02
Gammaproteobacteria	*Acinetobacter* (4)	10.57 ± 6.61	15.81 ± 1.82	21.54 ± 0.66	6.42 ± 5.20	19.62 ± 1.39	16.05 ± 2.89	18.97 ± 1.52
	Pseudomonas (8)	1.82 ± 0.95	3.22 ± 0.08	2.98 ± 0.08	1.18 ± 0.96	2.83 ± 0.18	3.77 ± 0.33	2.61 ± 0.25
	Rheinheimera (2462)	0.00 ± 0.00	0.00 ± 0.00	0.00 ± 0.00	0.00 ± 0.00	0.00 ± 0.00	0.00 ± 0.00	0.01 ± 0.01
	Aquabacterium (6)	4.76 ± 1.42	9.35 ± 2.10	6.52 ± 0.06	2.51 ± 2.19	6.50 ± 0.31	6.51 ± 0.38	6.03 ± 0.55
	Limnobacter (55)	0.34 ± 0.18	0.20 ± 0.01	0.14 ± 0.08	0.10 ± 0.09	0.27 ± 0.03	0.26 ± 0.04	0.18 ± 0.04
	Ralstonia (122)	0.14 ± 0.12	0.19 ± 0.08	0.07 ± 0.01	0.02 ± 0.02	0.11 ± 0.04	0.08 ± 0.03	0.14 ± 0.03
	Pelomonas (41)	0.28 ± 0.24	0.06 ± 0.00	0.41 ± 0.16	0.10 ± 0.06	0.21 ± 0.05	0.21 ± 0.11	0.26 ± 0.04
	Albidiferax (189)	0.02 ± 0.02	0.00 ± 0.00	0.00 ± 0.00	0.14 ± 0.09	0.01 ± 0.01	0.00 ± 0.00	0.01 ± 0.00
	Aquabacterium (206)	0.11 ± 0.06	0.01 ± 0.01	0.08 ± 0.02	0.01 ± 0.01	0.06 ± 0.03	0.09 ± 0.02	0.04 ± 0.01
	Thiomonas (246)	0.04 ± 0.04	0.01 ± 0.01	0.00 ± 0.00	0.17 ± 0.09	0.00 ± 0.00	0.01 ± 0.00	0.01 ± 0.01

	Unc. Gammaprot (2279)	0.00 ± 0.00	0.00 ± 0.00	0.00 ± 0.00	0.00 ± 0.00	0.00 ± 0.00	0.00 ± 0.00	0.01 ± 0.01
Bacteroidetes	*Flavobacterium* (265)	0.02 ± 0.01	0.02 ± 0.01	0.04 ± 0.01	0.02 ± 0.01	0.05 ± 0.02	0.03 ± 0.01	0.05 ± 0.02
	Flavobacterium (591)	0.00 ± 0.00	0.01 ± 0.01	0.02 ± 0.01	0.01 ± 0.01	0.04 ± 0.02	0.01 ± 0.00	0.02 ± 0.01
	Hydrotalea (406)	0.02 ± 0.02	0.01 ± 0.01	0.05 ± 0.04	0.00 ± 0.00	0.03 ± 0.02	0.05 ± 0.02	0.02 ± 0.01

Table A5. Bacterial OTUs enriched by metoprolol relative to unamended controls sampled simultaneously from samples incubated under anoxic conditions, and closest cultured relatives of OTU representative 16S rRNA gene sequences. Significant (p-adj < 0.05) Log2-fold changes > 0 are reported as determined by Deseq2. 15 µM and 150 µM indicate metoprolol concentration

Phylum/Subphylum-level	Genus-level (OTU)	Closest cultured relative	Acc. No.	[%]	Log2FoldChange 16S rRNA gene	
					15 µM	150 µM
Proteobacteria Alphaproteobacteria						
	Rhodomicrobium (25)	*Rhodomicrobium vannielii*	AM691111	96	10	10
	Pedomicrobium (28)	*Pedomicrobium americanum*	NR_104908	97	10	10
	Rhodobium (56)	*Rhodobium orientis*	LC110383	95	8	9
	unc. DB1-14 (78)	*Rhodospirillum photometricum*	HE663493	89	8	10
	unc. Rhodospirillaceae (105)	*Fodinicurvata halophila*	NR_134730	92	7	8
	unc. Rhizobiales (30)	*Pseudorhodoplanes sinuspersici*	CP021112	96	7	--
	unc. A0839 (127)	*Azospirillum amazonense*	AB568112	90	7	--
	Rhodoplanes (145)	*Rhodoplanes roseus*	D25313	96	8	8
Deltaproteobacteria	unc. GR-WP33-30 (33)	*Desulfuromonas acetexigens*	NR_044770	87	9	9
	OM27_clade (42)	*Taonella mepensis*	MN602464	84	9	9
	Byssovorax (86)	*Byssovorax cruenta*	NR_042341	97	8	9
	unc. Myxococcales (86)	*Racemicystis persica*	NR_156102	93	8	8
	unc. Deltaproteobacteria (119)	*Cystobacter fuscus*	KM978086	89	7	8
	unc. Myxococcales (62)	*Racemicystis persica*	NR_156102	94	9	--
	Desulfobacca (173)	*Desulfobacca acetoxidans*	NR_074955	90	6	--
	Sandaracinus (190)	*Sandaracinus amylolyticus*	KP306728	93	7	--
	Sorangium (295)	*Sorangium cellulosum*	CP012673	94	7	--
	unc. Cystobacteraceae (104)	*Archangium violaceum*	NR_043943	94	9	9
	unc. Myxococcales (159)	*Chondromyces robustus*	AJ233942	93	8	8
	unc. Deltaproteobacteria (170)	*Anaeromyxobacter dehalogenans*	KF952438	90	8	8

Gammaproteobacteria	Acidiferrobacter (7)	*Acidiferrobacter thiooxydans*	NR_114629	89	6	7
	unc. Gammaproteobacteria (11)	*Thioprofundum lithotrophicum*	NR_112620	91	10	9
	unc. Gammaproteobacteria (15)	*Sulfurivermis fontis*	AP018724	90	11	11
	unc. Gammaproteobacteria (16)	*Thiosocius teredinicola*	MG097873	92	10	10
	unc. Gammaproteobacteria (18)	*Thioprofundum hispidum*	NR_112620	92	7	8
	unc. Gammaproteobacteria (40)	*Thioalbus denitrificans*	NR_122087	92	8	10
	unc. Gammaproteobacteria (48)	*Thioprofundum hispidum*	NR_112620	92	8	10
	unc. Gammaproteobacteria (58)	*Sulfuricaulis limicola*	NR_147747	92	8	8
	unc. Gammaproteobacteria (59)	*Thiohalobacter thiocyanaticus*	AP018052	92	7	8
	Escherichia (1)	*Escherichia coli*	CP020495	100	10	--
	Enhydrobacter (49)	*Enhydrobacter aerosaccus*	LR215098	100	6	--
	unc. Gammaproteobacteria (103)	*Sulfuricaulis limicola*	AP014879	89	7	--
	unc. Gammaproteobacteria (114)	*Thiohalocapsa halophila*	NR_028863	90	7	--
	unc. Gammaproteobacteria (255)	*Thioprofundum hispidum*	NR_112620	93	8	--
Unclassified Proteobacteria	unc. Proteobacteria (72)	*Thiorhodococcus minor*	NR_116948	89	8	8
	unc. Proteobacteria (14)	*Thiosocius teredinicola*	MG097873	96	11	--
	unc. Proteobacteria (108)	*Thiohalobacter thiocyanaticus*	AP018052	93	8	--
Acidobacteria	unc. Subgroup_6 (93)	*Anaeromyxobacter dehalogenans*	EU_331409	86	8	--
	unc. Subgroup_6 (37)	*Vicinamibacter silvestris*	NR_151905	87	10	8
	unc. Subgroup_6 (195)	*Vicinamibacter silvestris*	NR_151905	86	7	--
	unc. Subgroup_6 (212)	*Vicinamibacter silvestris*	NR_151905	87	7	--
	unc. Subgroup_6 (278)	*Luteitalea pratensis*	CP015136	92	8	8
	unc. Subgroup_6 (314)	*Vicinamibacter silvestris*	NR_151905	91	7	--
	unc. Subgroup_9 (193)	*Luteitalea pratensis*	NR_156918	93	7	--
	unc. ABS-19 (124)	*Luteitalea pratensis*	NR_156918	92	7	--
	unc. Subgroup-17 (31)	*Ralstonia solanacearum*	CP011998	91	7	--
	unc. Subgroup_17 (211)	*Vicinamibacter silvestris*	NR_151905	92	7	--
	unc. Subgroup_17 (311)	*Luteitalea pratensis*	NR_156918	84	8	--
Chloroflexi	unc. KD4-96 (64)	*Dehalogenimonas alkeniggnens*	JQ994267	86	7	8
	unc. S085 (137)	*Thermomarinilinea lacunifontana*	NR_132293	87	7	7

	unc. KD4-96 (79)	*Dehalogenimonas alkenigignens*	JQ994267	87	7	--
	unc. Anaerolineaceae (227)	*Thermomarinilinea lacunifontana*	NR_132293	84	7	--
	unc. Ardenticatenia (238)	*Flexilinea flocculi*	NR_148566	85	7	--
	unc. Anaerolineaceae (256)	*Thermanaerothrix daxensis*	NR_117865	84	8	--
Firmicutes	*Bacillus* (160)	*Bacillus longiquaesitum*	AM747042	100	7	8
Gemmatimonadetes	unc. Gemmatimonadaceae (29)	*Gemmatimonas aurantiaca*	KF228166	91	7	8

Table A6. Relative abundance of bacterial OTUs from the original microbial community enriched by different metoprolol treatments relative to unamended controls under anoxic conditions. Only genera with a relative abundance > 0.01% are shown. Data represents the mean of triplicate samples in % of total rarified reads (uniform sequencing depth of 14,063 per sample) ± standard error of mean (SEM).

		16S rRNA gene						
Phylum/Subphylum	**Genus**	**0_0**	**0_65**	**0_120**	**15_65**	**15_120**	**150_65**	**150_120**
Alphaproteobacteria	*Rhodomicrobium* (25)	0.00 ± 0.00	0.36 ± 0.18	1.64 ± 0.90	1.30 ± 0.44	0.22 ± 0.05	0.43 ± 0.09	0.06 ± 0.02
	Pedomicrobium (28)	0.01 ± 0.01	0.29 ± 0.05	0.72 ± 0.17	0.85 ± 0.13	0.26 ± 0.04	0.57 ± 0.02	0.00 ± 0.00
	Rhodobium (56)	0.01 ± 0.01	0.13 ± 0.02	0.15 ± 0.02	0.17 ± 0.06	0.12 ± 0.02	0.32 ± 0.03	0.00 ± 0.00
	unc. DB1-14 (78)	0.00 ± 0.00	0.09 ± 0.01	0.19 ± 0.01	0.21 ± 0.01	0.22 ± 0.05	0.42 ± 0.08	0.00 ± 0.00
	unc. Rhodospirillaceae (105)	0.00 ± 0.00	0.09 ± 0.01	0.22 ± 0.04	0.15 ± 0.06	0.18 ± 0.03	0.18 ± 0.01	0.00 ± 0.00
	unc. Rhizobiales (30)	0.04 ± 0.04	0.29 ± 0.05	0.50 ± 0.07	0.50 ± 0.08	0.30 ± 0.02	0.59 ± 0.06	0.00 ± 0.00
	unc. A0839 (127)	0.01 ± 0.01	0.10 ± 0.03	0.10 ± 0.02	0.10 ± 0.01	0.10 ± 0.02	0.11 ± 0.01	0.00 ± 0.00
	Rhodoplanes (145)	0.00 ± 0.00	0.06 ± 0.01	0.19 ± 0.05	0.24 ± 0.05	0.02 ± 0.01	0.13 ± 0.02	0.00 ± 0.00
Deltaproteobacteria	unc. GR-WP33-30 (33)	0.03 ± 0.03	0.36 ± 0.08	0.66 ± 0.09	0.54 ± 0.08	0.56 ± 0.05	0.50 ± 0.09	0.00 ± 0.00
	OM27_clade (42)	0.00 ± 0.00	0.32 ± 0.03	0.86 ± 0.31	0.41 ± 0.12	0.33 ± 0.01	0.31 ± 0.06	0.00 ± 0.00
	Byssovorax (86)	0.00 ± 0.00	0.24 ± 0.02	0.25 ± 0.04	0.37 ± 0.07	0.06 ± 0.02	0.22 ± 0.08	0.00 ± 0.00
	unc. Deltaproteobacteria (119)	0.00 ± 0.00	0.32 ± 0.03	0.16 ± 0.07	0.17 ± 0.03	0.10 ± 0.02	0.16 ± 0.03	0.00 ± 0.00
	unc. Myxococcales (62)	0.03 ± 0.03	0.18 ± 0.09	0.55 ± 0.14	0.64 ± 0.01	0.12 ± 0.05	0.16 ± 0.05	0.00 ± 0.00
	Desulfobacca (173)	0.00 ± 0.00	0.11 ± 0.03	0.12 ± 0.03	0.09 ± 0.03	0.13 ± 0.02	0.10 ± 0.02	0.00 ± 0.00
	Sandaracinus (190)	0.00 ± 0.00	0.11 ± 0.02	0.22 ± 0.05	0.13 ± 0.01	0.04 ± 0.01	0.07 ± 0.01	0.00 ± 0.00
	Sorangium (295)	0.00 ± 0.00	0.03 ± 0.02	0.06 ± 0.01	0.08 ± 0.02	0.15 ± 0.01	0.14 ± 0.06	0.00 ± 0.00
	unc. Cystobacteraceae (104)	0.00 ± 0.00	0.24 ± 0.03	0.18 ± 0.06	0.10 ± 0.02	0.06 ± 0.03	0.31 ± 0.02	0.00 ± 0.00
	unc. Myxococcales (159)	0.00 ± 0.00	0.20 ± 0.02	0.18 ± 0.04	0.11 ± 0.03	0.05 ± 0.02	0.15 ± 0.02	0.00 ± 0.00
	unc. Deltaproteobacteria (170)	0.00 ± 0.00	0.09 ± 0.01	0.10 ± 0.08	0.07 ± 0.03	0.06 ± 0.02	0.30 ± 0.08	0.00 ± 0.00
Gammaproteobacteria	Acidiferrobacter (7)	0.11 ± 0.11	9.51 ± 0.84	8.43 ± 1.15	6.76 ± 0.53	5.75 ± 0.13	10.33 ± 0.88	0.02 ± 0.02
	unc. Gammaproteobacteria (11)	0.04 ± 0.04	5.02 ± 1.07	2.60 ± 0.61	3.37 ± 0.22	4.02 ± 0.56	2.89 ± 0.10	0.00 ± 0.00
	unc. Gammaproteobacteria (15)	0.03 ± 0.03	2.14 ± 0.33	1.85 ± 0.33	2.17 ± 0.58	3.24 ± 0.62	2.03 ± 0.19	0.00 ± 0.00
	unc. Gammaproteobacteria (16)	0.02 ± 0.01	2.31 ± 0.38	2.20 ± 0.16	1.01 ± 0.16	3.32 ± 0.58	1.50 ± 0.66	0.00 ± 0.00
	unc. Gammaproteobacteria (18)	0.01 ± 0.01	1.66 ± 0.08	1.32 ± 0.20	1.17 ± 0.32	1.51 ± 0.04	2.05 ± 0.18	0.00 ± 0.00
	unc. Gammaproteobacteria (40)	0.01 ± 0.01	0.23 ± 0.04	0.55 ± 0.19	0.34 ± 0.11	0.41 ± 0.08	0.48 ± 0.10	0.00 ± 0.00
	unc. Gammaproteobacteria (48)	0.01 ± 0.01	0.27 ± 0.02	0.38 ± 0.08	0.22 ± 0.11	0.22 ± 0.06	0.54 ± 0.08	0.00 ± 0.00
	unc. Gammaproteobacteria (58)	0.01 ± 0.01	0.31 ± 0.04	0.24 ± 0.01	0.20 ± 0.02	0.13 ± 0.01	0.24 ± 0.03	0.00 ± 0.00
	unc. Gammaproteobacteria (59)	0.00 ± 0.00	0.43 ± 0.06	0.41 ± 0.03	0.20 ± 0.02	0.65 ± 0.09	0.29 ± 0.14	0.00 ± 0.00
	Escherichia (1)	83.87 ± 14.9	0.06 ± 0.05	0.98 ± 0.42	0.89 ± 0.36	6.35 ± 0.06	0.03 ± 0.02	97.42 ± 0.74
	Enhydrobacter (49)	0.06 ± 0.05	0.01 ± 0.01	1.06 ± 0.98	0.12 ± 0.07	0.70 ± 0.24	0.00 ± 0.00	0.03 ± 0.01
	unc. Gammaproteobacteria (103)	0.00 ± 0.00	0.28 ± 0.03	0.21 ± 0.03	0.14 ± 0.03	0.10 ± 0.04	0.17 ± 0.05	0.00 ± 0.00
	unc. Gammaproteobacteria (114)	0.00 ± 0.00	0.11 ± 0.01	0.40 ± 0.03	0.15 ± 0.03	0.05 ± 0.02	0.17 ± 0.01	0.00 ± 0.00
	unc. Gammaproteobacteria (255)	0.00 ± 0.00	0.01 ± 0.01	0.04 ± 0.01	0.04 ± 0.02	1.21 ± 0.48	0.00 ± 0.00	0.00 ± 0.00
Unclassified Proteobacteria	unc. Proteobacteria (72)	0.01 ± 0.01	0.18 ± 0.02	0.31 ± 0.08	0.31 ± 0.12	0.13 ± 0.08	0.21 ± 0.02	0.00 ± 0.00
	unc. Proteobacteria (14)	0.01 ± 0.01	1.69 ± 0.12	2.05 ± 0.18	1.59 ± 0.16	2.52 ± 0.14	2.42 ± 0.24	0.01 ± 0.01

	unc. Proteobacteria (108)	0.00 ± 0.00	0.38 ± 0.04	0.04 ± 0.01	0.22 ± 0.09	0.14 ± 0.01	0.16 ± 0.06	0.00 ± 0.00
Acidobacteria	unc. Subgroup_6 (93)	0.01 ± 0.01	0.29 ± 0.06	0.20 ± 0.02	0.27 ± 0.05	0.13 ± 0.02	0.19 ± 0.03	0.00 ± 0.00
	unc. Subgroup_6 (37)	0.01 ± 0.01	0.08 ± 0.02	0.84 ± 0.23	0.21 ± 0.02	3.15 ± 0.59	0.06 ± 0.03	0.01 ± 0.01
	unc. Subgroup_6 (195)	0.01 ± 0.01	0.10 ± 0.01	0.11 ± 0.03	0.19 ± 0.03	0.03 ± 0.01	0.06 ± 0.01	0.00 ± 0.00
	unc. Subgroup_6 (212)	0.01 ± 0.01	0.05 ± 0.01	0.10 ± 0.03	0.16 ± 0.07	0.08 ± 0.01	0.07 ± 0.03	0.00 ± 0.00
	unc. Subgroup_6 (278)	0.00 ± 0.0	0.03 ± 0.01	0.15 ± 0.06	0.05 ± 0.02	0.37 ± 0.11	0.03 ± 0.01	0.00 ± 0.00
	unc. Subgroup_6 (314)	0.00 ± 0.00	0.05 ± 0.02	0.04 ± 0.01	0.13 ± 0.06	0.09 ± 0.03	0.07 ± 0.02	0.00 ± 0.00
	unc. Subgroup_9 (193)	0.00 ± 0.0	0.04 ± 0.01	0.09 ± 0.01	0.17 ± 0.05	0.19 ± 0.00	0.06 ± 0.01	0.00 ± 0.00
	unc. ABS-19 (124)	0.00 ± 0.00	0.04 ± 0.01	0.13 ± 0.01	0.12 ± 0.02	0.66 ± 0.22	0.15 ± 0.06	0.00 ± 0.00
	unc. Subgroup-17 (31)	0.00 ± 0.0	0.11 ± 0.03	0.90 ± 0.08	0.22 ± 0.02	3.76 ± 0.65	0.16 ± 0.05	0.00 ± 0.00
	unc. Subgroup_17 (211)	0.00 ± 0.00	0.09 ± 0.01	0.13 ± 0.01	0.06 ± 0.01	0.31 ± 0.02	0.08 ± 0.02	0.00 ± 0.00
	unc. Subgroup_17 (311)	0.00 ± 0.00	0.02 ± 0.01	0.07 ± 0.02	0.15 ± 0.03	0.06 ± 0.02	0.03 ± 0.01	0.00 ± 0.00
Chloroflexi	unc. KD4-96 (64)	0.02 ± 0.01	0.15 ± 0.05	0.16 ± 0.03	0.16 ± 0.02	0.08 ± 0.01	0.20 ± 0.05	0.00 ± 0.00
	unc. S085 (137)	0.05 ± 0.05	0.12 ± 0.05	0.13 ± 0.08	0.14 ± 0.04	0.12 ± 0.03	0.10 ± 0.02	0.00 ± 0.00
	unc. KD4-96 (79)	0.00 ± 0.00	0.11 ± 0.03	0.14 ± 0.03	0.10 ± 0.01	0.22 ± 0.01	0.14 ± 0.04	0.00 ± 0.00
	unc. Anaerolineaceae (227)	0.00 ± 0.00	0.11 ± 0.05	0.08 ± 0.04	0.14 ± 0.04	0.08 ± 0.02	0.06 ± 0.02	0.00 ± 0.00
	unc. Ardenticatenia (238)	0.00 ± 0.00	0.04 ± 0.02	0.09 ± 0.02	0.13 ± 0.03	0.08 ± 0.01	0.02 ± 0.01	0.00 ± 0.00
	unc. Anaerolineaceae (256)	0.00 ± 0.00	0.01 ± 0.01	0.06 ± 0.01	0.22 ± 0.16	0.11 ± 0.02	0.01 ± 0.01	0.00 ± 0.00
Firmicutes	*Bacillus* (160)	0.02 ± 0.01	0.12 ± 0.02	0.06 ± 0.02	0.11 ± 0.03	0.11 ± 0.01	0.16 ± 0.03	0.00 ± 0.00
Gemmatimonadetes	unc. Gemmatimonadaceae (29)	0.03 ± 0.01	0.37 ± 0.03	0.28 ± 0.05	0.48 ± 0.02	0.25 ± 0.01	0.73 ± 0.13	0.00 ± 0.00
		16S rRNA						
Alphaproteobacteria	*Rhodomicrobium* (25)	0.08 ± 0.05	0.00 ± 0.00	0.00 ± 0.00	0.00 ± 0.00	0.00 ± 0.00	0.00 ± 0.00	0.13 ± 0.03
	Pedomicrobium (28)	0.07 ± 0.04	0.00 ± 0.00	0.00 ± 0.00	0.00 ± 0.00	0.00 ± 0.00	0.00 ± 0.00	0.00 ± 0.00
	Rhodobium (56)	0.29 ± 0.16	0.01 ± 0.00	0.01 ± 0.01	0.00 ± 0.00	0.00 ± 0.00	0.00 ± 0.00	0.00 ± 0.00
	unc. DB1-14 (78)	0.01 ± 0.01	0.00 ± 0.00	0.00 ± 0.00	0.00 ± 0.00	0.00 ± 0.00	0.00 ± 0.00	0.00 ± 0.00
	unc. Rhodospirillaceae (105)	0.12 ± 0.07	0.03 ± 0.01	0.03 ± 0.01	0.00 ± 0.00	0.00 ± 0.00	0.00 ± 0.00	0.00 ± 0.00
	unc. Rhizobiales (30)	0.29 ± 0.08	0.00 ± 0.00	0.00 ± 0.00	0.01 ± 0.01	0.00 ± 0.00	0.00 ± 0.00	0.00 ± 0.00
	unc. A0839 (127)	0.06 ± 0.03	0.01 ± 0.01	0.01 ± 0.00	0.00 ± 0.00	0.00 ± 0.00	0.00 ± 0.00	0.00 ± 0.00
	Rhodoplanes (145)	0.01 ± 0.01	0.00 ± 0.00	0.00 ± 0.00	0.00 ± 0.00	0.00 ± 0.00	0.00 ± 0.00	0.00 ± 0.00
Deltaproteobacteria	unc. GR-WP33-30 (33)	0.05 ± 0.02	0.00 ± 0.00	0.00 ± 0.00	0.00 ± 0.00	0.00 ± 0.00	0.00 ± 0.00	0.00 ± 0.00
	OM27_clade (42)	0.00 ± 0.00	0.00 ± 0.00	0.00 ± 0.00	0.00 ± 0.00	0.00 ± 0.00	0.00 ± 0.00	0.00 ± 0.00
	Byssovorax (86)	0.01 ± 0.00	0.00 ± 0.00	0.00 ± 0.00	0.00 ± 0.00	0.00 ± 0.00	0.00 ± 0.00	0.00 ± 0.00
	unc. Deltaproteobacteria (119)	0.01 ± 0.00	0.00 ± 0.00	0.00 ± 0.00	0.00 ± 0.00	0.00 ± 0.00	0.00 ± 0.00	0.00 ± 0.00
	unc. Myxococcales (62)	0.01 ± 0.00	0.00 ± 0.00	0.00 ± 0.00	0.00 ± 0.00	0.00 ± 0.00	0.00 ± 0.00	0.00 ± 0.00
	Desulfobacca (173)	0.03 ± 0.01	0.07 ± 0.03	0.07 ± 0.03	0.01 ± 0.01	0.00 ± 0.00	0.01 ± 0.01	0.00 ± 0.00
	Sandaracinus (190)	0.01 ± 0.01	0.00 ± 0.00	0.00 ± 0.00	0.00 ± 0.00	0.00 ± 0.00	0.00 ± 0.00	0.00 ± 0.00
	Sorangium (295)	0.00 ± 0.00	0.00 ± 0.00	0.00 ± 0.00	0.00 ± 0.00	0.00 ± 0.00	0.00 ± 0.00	0.00 ± 0.00
	unc. Cystobacteraceae (104)	0.00 ± 0.00	0.00 ± 0.00	0.00 ± 0.00	0.00 ± 0.00	0.00 ± 0.00	0.00 ± 0.00	0.00 ± 0.00
	unc. Myxococcales (159)	0.00 ± 0.00	0.00 ± 0.00	0.00 ± 0.00	0.00 ± 0.00	0.00 ± 0.00	0.00 ± 0.00	0.00 ± 0.00
	unc. Deltaproteobacteria (170)	0.02 ± 0.01	0.00 ± 0.00	0.00 ± 0.00	0.00 ± 0.00	0.00 ± 0.00	0.00 ± 0.00	0.00 ± 0.00
Gammaproteobacteria	Acidiferrobacter (7)	1.92 ± 0.05	0.32 ± 0.13	0.32 ± 0.13	0.05 ± 0.03	0.01 ± 0.01	0.03 ± 0.02	0.01 ± 0.01
	unc. Gammaproteobacteria (11)	0.26 ± 0.14	0.06 ± 0.02	0.06 ± 0.02	0.02 ± 0.01	0.02 ± 0.01	0.03 ± 0.03	0.01 ± 0.00
	unc. Gammaproteobacteria (15)	0.03 ± 0.01	0.00 ± 0.00	0.00 ± 0.00	0.00 ± 0.00	0.00 ± 0.00	0.00 ± 0.00	0.00 ± 0.00
	unc. Gammaproteobacteria (16)	0.08 ± 0.04	0.00 ± 0.00	0.00 ± 0.00	0.00 ± 0.00	0.00 ± 0.00	0.00 ± 0.00	0.00 ± 0.00
	unc. Gammaproteobacteria (18)	0.23 ± 0.11	0.03 ± 0.02	0.03 ± 0.02	0.01 ± 0.01	0.00 ± 0.00	0.02 ± 0.02	0.00 ± 0.00
	unc. Gammaproteobacteria (40)	0.08 ± 0.04	0.00 ± 0.00	0.00 ± 0.00	0.00 ± 0.00	0.00 ± 0.00	0.00 ± 0.00	0.00 ± 0.00
	unc. Gammaproteobacteria (48)	0.05 ± 0.03	0.00 ± 0.00	0.00 ± 0.00	0.00 ± 0.00	0.00 ± 0.00	0.00 ± 0.00	0.00 ± 0.00
	unc. Gammaproteobacteria (58)	0.38 ± 0.04	0.02 ± 0.01	0.02 ± 0.01	0.01 ± 0.01	0.00 ± 0.00	0.00 ± 0.00	0.00 ± 0.00

	unc. Gammaproteobacteria (59)	0.01 ± 0.01	0.00 ± 0.00	0.00 ± 0.00	0.00 ± 0.00	0.00 ± 0.00	0.00 ± 0.00	0.00 ± 0.00
	Escherichia (1)	25.38 ± 14.6	17.04 ± 4.82	17.04 ± 14.8	55.87 ± 28.5	94.33 ± 1.71	90.26 ± 6.36	97.91 ± 0.59
	Enhydrobacter (49)	0.00 ± 0.00	0.03 ± 0.02	0.03 ± 0.02	0.06 ± 0.03	0.03 ± 0.02	0.02 ± 0.00	0.04 ± 0.01
	unc. Gammaproteobacteria (103)	0.00 ± 0.00	0.00 ± 0.00	0.00 ± 0.00	0.00 ± 0.00	0.00 ± 0.00	0.00 ± 0.00	0.00 ± 0.00
	unc. Gammaproteobacteria (114)	0.00 ± 0.00	0.00 ± 0.00	0.00 ± 0.00	0.00 ± 0.00	0.00 ± 0.00	0.00 ± 0.00	0.00 ± 0.00
	unc. Gammaproteobacteria (255)	0.00 ± 0.00	0.00 ± 0.00	0.00 ± 0.00	0.00 ± 0.00	0.00 ± 0.00	0.00 ± 0.00	0.00 ± 0.00
Unclassified Proteobacteria	unc. Proteobacteria (72)	0.06 ± 0.03	0.00 ± 0.00	0.00 ± 0.00	0.00 ± 0.00	0.00 ± 0.00	0.00 ± 0.00	0.00 ± 0.00
	unc. Proteobacteria (14)	0.02 ± 0.01	0.00 ± 0.00	0.00 ± 0.00	0.00 ± 0.00	0.00 ± 0.00	0.00 ± 0.00	0.00 ± 0.00
	unc. Proteobacteria (108)	0.07 ± 0.04	0.00 ± 0.00	0.00 ± 0.00	0.00 ± 0.00	0.00 ± 0.00	0.00 ± 0.00	0.00 ± 0.00
Acidobacteria	unc. Subgroup_6 (93)	0.00 ± 0.00	0.00 ± 0.00	0.00 ± 0.00	0.00 ± 0.00	0.00 ± 0.00	0.00 ± 0.00	0.00 ± 0.00
	unc. Subgroup_6 (37)	0.05 ± 0.02	0.02 ± 0.02	0.02 ± 0.00	0.01 ± 0.01	0.00 ± 0.00	0.00 ± 0.00	0.00 ± 0.00
	unc. Subgroup_6 (195)	0.01 ± 0.01	0.00 ± 0.00	0.00 ± 0.00	0.00 ± 0.00	0.00 ± 0.00	0.00 ± 0.00	0.00 ± 0.00
	unc. Subgroup_6 (212)	0.06 ± 0.03	0.01 ± 0.01	0.01 ± 0.00	0.00 ± 0.00	0.00 ± 0.00	0.00 ± 0.00	0.00 ± 0.00
	unc. Subgroup_6 (278)	0.00 ± 0.00	0.00 ± 0.00	0.00 ± 0.00	0.00 ± 0.00	0.00 ± 0.00	0.00 ± 0.00	0.00 ± 0.00
	unc. Subgroup_6 (314)	0.00 ± 0.00	0.00 ± 0.00	0.00 ± 0.00	0.00 ± 0.00	0.00 ± 0.00	0.00 ± 0.00	0.00 ± 0.00
	unc. Subgroup_9 (193)	0.04 ± 0.02	0.00 ± 0.00	0.00 ± 0.00	0.00 ± 0.00	0.00 ± 0.00	0.00 ± 0.00	0.00 ± 0.00
	unc. ABS-19 (124)	0.01 ± 0.01	0.00 ± 0.00	0.00 ± 0.00	0.00 ± 0.00	0.00 ± 0.00	0.00 ± 0.00	0.00 ± 0.00
	unc. Subgroup-17 (31)	0.02 ± 0.01	0.01 ± 0.01	0.01 ± 0.01	0.00 ± 0.00	0.00 ± 0.00	0.00 ± 0.00	0.00 ± 0.00
	unc. Subgroup_17 (211)	0.00 ± 0.00	0.00 ± 0.00	0.00 ± 0.00	0.00 ± 0.00	0.00 ± 0.00	0.00 ± 0.00	0.00 ± 0.00
	unc. Subgroup_17 (311)	0.01 ± 0.01	0.00 ± 0.00	0.00 ± 0.00	0.00 ± 0.00	0.00 ± 0.00	0.00 ± 0.00	0.00 ± 0.00
Chloroflexi	unc. KD4-96 (64)	0.28 ± 0.16	0.00 ± 0.00	0.00 ± 0.00	0.00 ± 0.00	0.00 ± 0.00	0.00 ± 0.00	0.00 ± 0.00
	unc. S085 (137)	0.06 ± 0.02	0.02 ± 0.01	0.02 ± 0.01	0.00 ± 0.00	0.00 ± 0.00	0.00 ± 0.00	0.00 ± 0.00
	unc. KD4-96 (79)	0.16 ± 0.08	0.02 ± 0.01	0.02 ± 0.01	0.01 ± 0.01	0.00 ± 0.00	0.00 ± 0.00	0.00 ± 0.00
	unc. Anaerolineaceae (227)	0.01 ± 0.01	0.00 ± 0.00	0.02 ± 0.01	0.01 ± 0.01	0.00 ± 0.00	0.00 ± 0.00	0.00 ± 0.00
	unc. Ardenticatenia (238)	0.02 ± 0.01	0.00 ± 0.00	0.00 ± 0.00	0.00 ± 0.00	0.00 ± 0.00	0.00 ± 0.00	0.00 ± 0.00
	unc. Anaerolineaceae (256)	0.00 ± 0.00	0.00 ± 0.00	0.00 ± 0.00	0.00 ± 0.00	0.00 ± 0.00	0.00 ± 0.00	0.00 ± 0.00
Firmicutes	*Bacillus* (160)	0.03 ± 0.02	0.00 ± 0.00	0.00 ± 0.00	0.00 ± 0.00	0.00 ± 0.00	0.00 ± 0.00	0.00 ± 0.00
Gemmatimonadetes	unc. Gemmatimonadaceae (29)	0.24 ± 0.12	0.03 ± 0.02	0.03 ± 0.02	0.00 ± 0.00	0.00 ± 0.00	0.00 ± 0.00	0.00 ± 0.00

Table A7. Bacterial OTUs enriched in micropollutant-amended subsurface sediments relative to unamended controls sampled simultaneously from samples incubated under oxic conditions, and closest cultured relatives of OTU representative 16S rRNA gene sequences. Significant (p-adj < 0.05) Log2-fold changes > 0 are reported as determined by Deseq2.

Phylum/Sub-phylum	Genus-level (OTU No.)	Closest cultured relative	Acc.No[a]	[%][b]	Log2Fold Change	
					16S rRNA gene	16S rRNA
Proteobacteria Alphaproteobacteria	*Xanthobacter* (75)	*Xanthobacter agilis*	MK402058	99	5[c]	4
	Hyphomicrobium (21)	*Hyphomicrobium vulgare*	KC447318	99	2	--
	Magnetospirillum (510)	*Magnetospirillum magneticum*	AB983194	100	--[d]	4
	Novosphingobium (120)	*Novosphingobium aromaticivorans*	KU924009	100	--	4
	Reyranella (439)	*Reyranella aquatilis*	NR_158037	100	--	3
	Rhizobium (546)	*Rhizobium selenitireducens*	MH665748	100	--	2
	Prosthecomicrobium (388)	*Prosthecomicrobium hirschii*	NR_104906	100	--	2
Deltaproteobacteria	unc. Myxococcales (1467)	*Vulgatibacter incomptus*	CP012332	92	5	3
	Phaselicystis (462)	*Phaselicystis flava*	NR_044523	91	4	--
	Geothermobacter (241)	*Geothermobacter ehrlichii*	NR_042754	94	--	2
Gammaproteobacteria	Neisseriaceae (1382)	*Annwoodia aquaesulis*	NR_044793	95	3	--
	Ferritrophicum (36)	*Ferritrophicum radinicola*	DQ386273	94	2	--
	unc. Betaproteobacteriales (56)	*Piscinibacter aquaticus*	LC430085	93	2	--
	Nitrosomonadaceae (77)	*Collimonas fungivorans*	KM604833	93	1	--
	Crenothrix (268)	*Crenothrix polyspora*	DQ295898	96	--	5
Bacteroidetes Sphingobacteriia	unc. KD3-93 (2443)	*Owenweeksia hongkongensis*	CP003156	90	--	6
	unc. env.OPS_17 (2106)	*Sphingobacterium tabacisoli*	NR_159136	89	--	5
	unc. env.OPS_17 (818)	*Anseongella ginsenosidimutans*	CP042432	85	--	4
	Terrimonas (370)	*Terrimonas soli*	NR_159891	98	2	--
Cytophagia	Rhodothermaceae (1646)	*Rhodothermus marinus*	Y14143	90	--	2

Table A8. Bacterial OTUs enriched or inhibited by the micropollutant-amendment in the flumes relative to unamended controls. Closest cultured relatives of OTU representative 16S rRNA gene sequences. Significant (p-adj < 0.05) Log2-fold changes are reported as determined by Deseq2. Table used with permission from Posselt *et al.* (2020).

Phylum/Sub-phylum	Genus-level (OTU No.)	Closest cultured relative	Acc.No[a]	[%][b]	Log2Fold Change
Acidobacteria	*Geothrix* (58)	*Geothrix fermentans*	HF559181	97	-9,2
Actinobacteria	Candidatus_Microthrix (137)	*Iamia majanohamensis*	JQ899225	92	5,7
	Nocardioides (144)	*Nocardioides sediminis*	NR_044228	100	-3,7
Bacteroidetes	*Ferruginibacter* (92)	*Ferruginibacter lapsinanis*	NR_044589	96	7,6
	Haliscomenobacter (156)	*Haliscomenobacter hydrossis*	NR_074420	99	7,3
	Flavobacterium (115)	*Flavobacterium cheonhonense*	MF592269	100	7,1
	Lewinella (105)	*Lewinella cohaerens*	NR_115012	93	6,7
	unclassified saprospiraceae (316)	*Phaeodactylibacter luteus*	MN867941	89	5,9
	Runella (223)	*Runella slithyformis*	NR_074339	99	5,6
	unclassified saprospiraceae (453)	*Lewinella nigricans*	EU371936	86	5,5
	Leadbetterella (79)	*Leadbetterella byssophila*	NR_074303	90	5
	Flavobacterium (143)	*Flavobacterium caeni*	NR_114264	96	4,9
	Flavobacterium (131)	*Flavobacterium myungsuense*	NR_108537	98	4,7
	unclassified NS11-12_marine_group (302)	*Phaeodactylibacter luteus*	NR_132329	89	3,9
	unclassified NS9_marine_group (138)	*Lentimicrobium saccharophilum*	MG264237	87	3,2
	Flavobacterium (4)	*Flavobacterium granuli*	MF592284	100	-3
	unclassified Cytophagaceae (361)	*Chryseolinea*	NR_165708	93	-5,1
	unclassified WCHB1-32 (181)	*Sunxiuqinia rutila*	NR_134207	91	-6,3
	Paludibacter (104)	*Paludibacter propionicigenes*	AB910740	98	-8,2
Candidate_division_BRC1	unclassified Candidate_division_BRC1 (78)	*Desulfobulbus alkaliphilus*	NR_117882	82	2,2
Chloroflexi	unclassified Thermomicrobia (301)	*Sphaerobacter thermophilus*	AJ871226	88	6,7
	unclassified Caldilineaceae (224)	*Litorilinea aerophila*	NR_132330	91	5,4
	unclassified Caldilineaceae (232)	*Litorilinea aerophila*	NR_132330	91	4,8
	unclassified Thermomicrobia (305)	*Burkholderia tropica*	KM974662	90	4,7
	unclassified Thermomicrobia (100)	*Sphaerobacter thermophilus*	AJ871226	92	3,7

	unclassified Caldilineaceae (73)	*Litorilinea aerophila*	NR_132330	91	2,9
Cyanobacteria	unclassified ML635J-21 (68)	*Heliorestis acidaminivorans*	NR_132700	86	5,5
	Nostoc (106)	*Nostoc calcicola*	MG596755	100	-6,4
	unclassified FamilyI (397)	*Chroakolemma pellucida*	MF685894	95	-8,5
Firmicutes	*Youngiibacter* (135)	*Youngiibacter multivorans*	AB910755	99	-6,7
	Erysipelothrix (120)	*Erysipelothrix rhusiopathiae*	AB055909	93	-7,7
	Anaerovorax (195)	*Anaerovorax odorimutans*	NR_028911	97	-7,8
	Erysipelothrix (90)	*Erysipelothrix rhusiopathiae*	AB055909	93	-9,7
	Fusibacter (19)	*Fusibacter tunisiensis*	MG264211	99	-10,7
Planctomycetes	Candidatus_Nostocoida (877)	*Tundrisphaera lichenicola*	NR_158050	88	5,1
Proteobacteria (Alpha)	*Defluviimonas* (243)	*Defluviimonas pyrenivorans*	NR_159922	98	7,5
	Sphingobium (129)	*Sphingobium scionense*	KM978212	99	6,3
	Candidatus_Odyssella (506)	*Trajonella thessalonices*	AF069496	93	5,3
	Woodsholea (435)	*Woodsholea maritima*	FM886859	96	5,2
	unclassified Alphaproteobacteria (155)	*Bacterium Ellin6506*	HM748654	97	5
	Paracoccus (235)	*Paracoccus limosus*	MH915458	100	4,4
	Hyphomicrobium (178)	*Hyphomicrobium fecile*	Y14312	97	4
	Prosthecomicrobium (455)	*Prosthecomicrobium hirschii*	NR_104906	100	3,4
	Woodsholea (35)	*Woodsholea maritima*	FM886859	100	3,2
	Pedomicrobium (164)	*Pedomicrobium manganicum*	X97691	96	3
	unclassified A0839 (101)	*Rhizomicrobium electricum*	NR_108115	89	2,7
	unclassified A0839 (216)	*Azospirillum amazonese*	AB568112	90	2,7
	unclassified MNG7 (116)	*Aestuariivirga litoralis*	MH371374	96	2,4
	Brevundimonas (47)	*Brevundimonas alba*	MF101127	100	2
	Pseudoxanthobacter (109)	*Pseudoxanthobacter soli*	KX082828	98	-2,8
	unclassified I-10 (469)	*Lacibacterium aquatile*	KY077145	98	-4,9
	Methylobacterium (678)	*Methylobacterium adhaesivum*	MK138652	100	-5,6
	Azospirillum (752)	*Azospirillum lipoferum*	MK542987	99	-7,1
	unclassified 7B-8 (944)	*Sphingoaurantiacus polygranulatus*	NR_147725	100	-7,5
Proteobacteria (Delta)	*Bdellovibrio* (582)	*Bdellovibrio bacteriovorus*	AF148941	94	5,6
	Bdellovibrio (146)	*Bdellovibrio bacteriovorus*	MK779947	96	4,6
	Desulfovibrio (540)	*Desulfovibrio putealis*	NR_029118	100	-6,2
	unclassified BVA18 (194)	*Geobacter psychrophilus*	NR_043075	97	-7,8

Proteobacteria (Gamma)	*Thermomonas* (191)	*Thermomonas fusca*	MG897133	97	6,3
	Arenimonas (25)	*Arenimonas maotaiensis*	MK396579	100	6,2
	Dokdonella (161)	*Dokdonella immobilis*	NR_108377	98	6
(Betaproteobacteriales)	*Lysobacter* (151)	*Lysobacter ginsengisoli*	NR_112563	100	4,5
	Arenimonas (97)	*Arenimonas oryziterrae*	NR_116294	99	2,9
	Arenimonas (124)	*Arenimonas subflava*	KY012256	100	2,5
	Buttiauxella (6)	*Buttiauxella agrestis*	MN513216	100	-4,1
	Tolumonas (11)	*Tolumonas auensis*	MN646993	100	-4,9
	Sphaerotilus (394)	*Sphaerotilus hippei*	NR_117539	100	5,2
	Albidiferax (55)	*Albidiferax ferrireducens*	KC855480	98	4,2
	Methylibium (171)	*Methylibium petroleiphilum*	KP099963	100	3,7
	Methylotenera (54)	*Methylotenera versatilis*	NR_074693	98	3,5
	unclassified Comamonadaceae (91)	*Gemmobacter aquatilis*	MK425674	99	-2
	Vogesella (10)	*Vogesella indigofera*	NR_040800	100	-2,2
	Dechloromonas (71)	*Dechloromonas hortensis*	MK138646	100	-2,6
	Methyloversatilis (66)	*Methyloversatilis discipulorum*	KY284088	99	-3,3
	unclassified Comamonadaceae (177)	*Acidovorax cattleyae*	MH209630	100	-3,3
	Azoarcus (668)	*Azoarcus evansii*	MN646997	100	-6
Verrucomicrobia	*Verrucomicrobium* (389)	*Verrucomicrobium spinosum*	NR_026266	97	6,4
	unclassified Verrucomicrobia (444)	*Verrucomicrobium spinosum*	MN684281	92	6,3
	Haloferula (60)	*Haloferula*	NR_041673	95	6,2
	unclassified Verrucomicrobiae (170)	*Verrucomicrobium spinosum*	MN684281	92	5,8
	unclassified Verrucomicrobiae (395)	*Luteolibacter cuticulihirudinis*	NR_109603	89	5,6
	unclassified Verrucomicrobiaceae (471)	*Verrucomicrobium spinosum*	MN684281	96	4,9
	Chthoniobacter (300)	*Chthoniobacter flavus*	NR_115225	91	3,3
	Prosthecobacter (99)	*Prosthecobacter dejongeli*	NR_026021	99	-3,9

[a] Gene bank accession number.

[b] Similarity of OTU representative 16S rRNA gene sequence to that of closest cultured relative.

[c] Significant (p-adj < 0.05) Log2-fold change > 0 and < 0 are reported as determined by Deseq2.

[d] Non-significant differential abundance between treatment and unamended controls.

11. (EIDESSTATTLICHE) VERSICHERUNGEN UND ERKLÄRUNGEN

(§ 8 Satz 2 Nr. 3 PromO Fakultät)

Hiermit versichere ich eidesstattlich, dass ich die Arbeit selbstständig verfasst und keine anderen als die von mir angegebenen Quellen und Hilfsmittel benutzt habe (vgl. Art. 64 Abs. 1 Satz 6 BayHSchG).

(§ 8 Satz 2 Nr. 3 PromO Fakultät)

Hiermit erkläre ich, dass ich die Dissertation nicht bereits zur Erlangung eines akademischen Grades eingereicht habe und dass ich nicht bereits diese oder eine gleichartige Doktorprüfung endgültig nicht bestanden habe.

(§ 8 Satz 2 Nr. 4 PromO Fakultät)

Hiermit erkläre ich, dass ich Hilfe von gewerblichen Promotionsberatern bzw. –vermittlern oder ähnlichen Dienstleistern weder bisher in Anspruch genommen habe noch künftig in Anspruch nehmen werde.

(§ 8 Satz 2 Nr. 7 PromO Fakultät)

Hiermit erkläre ich mein Einverständnis, dass die elektronische Fassung der Dissertation unter Wahrung meiner Urheberrechte und des Datenschutzes einer gesonderten Überprüfung unterzogen werden kann.

(§ 8 Satz 2 Nr. 8 PromO Fakultät)

Hiermit erkläre ich mein Einverständnis, dass bei Verdacht wissenschaftlichen Fehlverhaltens Ermittlungen durch universitätsinterne Organe der wissenschaftlichen Selbstkontrolle stattfinden können.

……

Ort, Datum, Unterschrift